Novel chemistry and applications of polythiazyl

King, Roberto S.P.. 2019. “Novel Chemistry and Applications of Polythiazyl”. figshare.
https://hdl.handle.net/2134/12571.

NOVEL CHEMISTRY AND APPLICATIONS OF POLYTHIAZYL

by

Roberto S.P. King

A Doctoral Thesis

Submitted in partial fulfilment of the requirements for the award of
Doctor of Philosophy of Loughborough University

Department of Chemistry
Loughborough University
Loughborough
Leicestershire
LE11 3TU

Abstract

Diverse investigations into the synthesis, formation, reactivity and stability of disulfur dinitride, S_2N_2, enabled through the fabrication of custom-made apparatus and tailored reaction conditions, are reported. The polymerisation process of the former to the (super)conductive polythiazyl material has also been explored by means of both single crystal X-ray diffraction and *in situ* reaction chemistry.

The introduction of the volatile S_2N_2 moiety to microporous materials has been thoroughly examined and occlusion of the reactive nitride is achievable providing host pore aperture diameters in the range of *ca.* 4-6 Å. Subsequent polymerisation of S_2N_2 occurs rapidly, in most cases, owing to the spatial constraints and increased intimacy of adjacent monomeric units within the porous voids. Thorough characterisation has been conducted on an array of zeolite, sodalite and lamellar solids, with particular focus on Na-ZSM-5, silica sodalite and kaolinite, respectively. Optimised loading of the conductive $(SN)_x$ polymer was calculated at > 70% by weight for the Na-ZSM-5-$(SN)_x$ system, as determined *via* mass change experimental data.

The interaction of S_2N_2 with latent fingerprint residues on glass sample holders, observed during microporous occlusion reactions, invoked exploration of the potential forensic utilisation and application of polythiazyl. Preliminary findings have indicated that exposure of fingerprints to S_2N_2 vapour results in the prints being visually imaged by polymeric $(SN)_x$ on an unprecedented range of surface media, including materials that, hitherto, have eluded forensic fingerprint identification capabilities (fabrics, spent gun casings and organic/aqueous wetted samples). Direct fingerprint enhancement on various media have also been investigated directly from $(SN)_x$, using novel sublimation techniques, and have provided comparable results. In addition, the use of $(NSCl)_3$ as a fingerprint development material has provided some evidence of favourable enhancement across more 'routine' surface types (papers and metals).

Reaction chemistry of $(SN)_x$ has been investigated, with attempted co-ordination reactions to various transition metal complexes. A new synthetic route to $(SN)_x$ has been identified, through reaction of $[S_3N_2Cl]Cl$ with liquid NH_3 and subsequent vacuum treatment.

Studies relating to the isolation of both the reactive NSCl monomer and other thiazyl moieties within zeolite matrices have also provided some potentially useful products, with interesting (photo)chromic properties. Although characterisation is limited, UV/vis, XRD and Raman investigations have all helped provide some insight into the host-guest systems.

The synthesis, full characterisation and utilisation of template-free silica sodalite, $Si_{12}O_{24}$, has also been developed. This material, essentially a novel polymorph of silica, is readily prepared by subjecting ethylene glycol silica sodalite to sustained heat (680°C) under a nitrogen atmosphere, successfully removing the templating agent to give cubic silica sodalite, which, upon consequent heating under an oxygen atmosphere transforms, in the solid state, into a rhombohedral form of the empty sodalite; constituting the first experimental example of a stable, isolable, room temperature, rhombohedral sodalite material. Moreover, subsequent exposure of this material to S_2N_2 vapour also results in successful occlusion of $(SN)_x$ within the β-cage system of silica sodalite.

Acknowledgements

There are so many people that I owe a great deal of thanks to for their input, both academically and personally, over the duration of my studies. I'd like to start by thanking my supervisors, Dr Paul Kelly and Prof. Roger Mortimer: your help, guidance, knowledge and faith have been truly invaluable and I am eternally grateful for the opportunity you have given to me. As well as great supervisors, you have become good friends, and it's that relationship that has been so important during the course of this work.

I would also like to take this opportunity to thank all other members of the Inorganic section at Loughborough University. A particular mention must go to Dr Sandie Dann for all her help with powder XRD and solid state Chemistry in general, Dr Mark Elsegood for taking the time to help with single crystal structure characterisation, Dr Martin Smith for some great ideas along the way and Mrs Pauline King (no relation) for her superb assistance with elemental analysis and general laboratory issues. Praise must also go to Mr John Spray for his outstanding glassblowing skills that have enabled me to develop and use apparatus that otherwise would never have happened. To you all, thank you!

Of course, there has to be a large thankyou to all my peers and collegues within the section and department over the past few years. One way or another, each and every one of you has provided me with the support, guidance, amusement, and frustration required to bring me out of the lows and keep me in check so the highs never became so unappreciable. A specific mention to those who've made an impact on me over the years: Stanny, Gav, Lee, Andy, Chris, Raf, Russell and Stuart. Thank you all for your support!!

Last, but certainly not least, I would like to take this opportunity to thank the people closest to me; my family. Mum/Dad, words cannot portray how much I am endebted to you for all your support (financially as well as emotionally!!), encouragement and help over all these years. You have been there for me when

I needed it the most and I am truly grateful! I never thought I could get this far and it's through your motivation that I've achieved things that have far exceeded my expectations. Andrew, Daniel and Natalie, again, thank you for being great brothers and a sister to me! I know we've had our moments, but it makes us who we are and I wish you all the best in your futures!! To my grandparents, 'grazie per tutto ciò che avete fatto per me nel corso degli anni. Sono eternamente grato!' Leanne, the lady in my life, how can I thank you enough?! You've not only had to put up with me, but you've had to sit there and endure reading through vast parts of my thesis! You've been a true God-send and a wonderful person to have in my life. Thank you!

To everyone above, and anyone I've forgotten to mention (sorry), thank you once again and I hope that in some way I've been able to re-pay you all for everything you have done for me!!

Table of Contents

List of Figures

List of Equations

List of Tables

Abbreviations and Glossary of Terms

Å	Angström unit, 10^{-10} m
Atm	atmospheres
av.	average
b	broad
Bu	butyl, $(CH_2)_3CH_3$
ca.	circa
$CHCl_3$	chloroform
CH_2Cl_2	dichloromethane, *see also* DCM
C H N	Carbon, Hydrogen, Nitrogen; elemental analysis
cm^{-1}	wavenumber
cm^3	cubic centimetres, volume
cod	cycloocta-1,5-diene
d	days (in method)/doublet (in NMR data)
DC	direct current
dd	doublet of doublets
d.p.	decimal place
DEPT	Distortionless Enhancement by Polarisation Transfer
DCM	dichloromethane, *see also* CH_2Cl_2
EDX	Energy Dispersive X-ray Spectroscopy
EGS-SOD	ethylene glycol silica sodalite
EI	Electron Impact
ES	Electrospray
Et	ethyl, CH_2CH_3
Et_2O	diethyl ether
EtOH	ethanol
FAB	Fast Atom Bombardment
g	grams
h	hours
Hz	Hertz
IR	Infra-red spectroscopy

K	temperature, in Kelvin
m	multiplet
m	meta
med	medium
Me	methyl, CH_3
MeCN	acetonitrile
MeOH	methanol
MFI	Mobil Five (zeolite)
min	minutes
MS	Mass Spectrometry
NMR	Nuclear Magnetic Resonance spectroscopy
o	ortho
p	para
ppm	parts per million
ppsn	powdered poly(sulfur nitride)
RBF	round-bottomed flask
r.t.	room temperature
s	strong
SEM	Scanning Electron Microscopy
sh	sharp
S-SOD	silica sodalite
^{t}Bu	tertiary-butyl, $C(CH_3)_3$
THF	tetrahydrofuran
TPA	tetrapropylammonium
vb	very broad
w	weak
XRD	X-ray diffraction
ZSM-5	Zeolite Socony Mobil #5
°	degrees
°C	temperature, in degrees centigrade
θ	Theta, degrees Theta for XRD
~	Tilde, up to (an amount), range
α	alpha
β	beta

γ	gamma
δ	chemical shift (in NMR)
υ	chemical shift (in IR)
>	greater than
<	less than
μm	micrometre
Ω	Omega, ohm, unit of electrical resistance

1. Introduction

1.1. *Sulfur-Nitrogen Chemistry*

The diverse reaction chemistry and unusual structures and properties of sulfur-nitrogen species have stimulated tremendous interest over recent decades. Aside from structural characterisation studies involving X-ray crystallography, spectroscopic measurements and nuclear magnetic resonance (NMR), theoretical chemists have also focussed their attention on these intriguing systems. Sulfur-nitrogen research has produced an array of materials with unique properties (magnetic, conductive, chromic, *etc.*) that have the potential to bridge the gap between materials and chemical research, and be utilised within functional systems. Although further developments within the last several years have concentrated on other isovalent chalcogen-nitrogen systems (primarily selenium and tellurium), it is the sulfur derivatives that become pertinent to this work.

The broad collection of S-N compounds fall, primarily, into one of six subgroups that can be summarised as illustrated in Figure 1. Generally, such compounds exist as either neutral, charged (cationic or anionic), nitrogen-rich, sulfur-rich, or sulfur/nitrogen equal, species. Accordingly, it becomes difficult to succinctly summarise all areas of S-N chemistry and a focus, in this instance, towards the binary S_xN_y systems becomes germane.

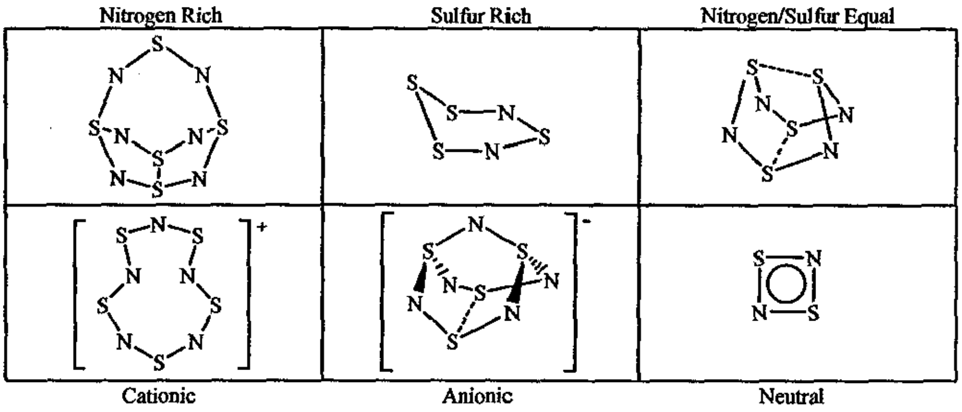

Figure 1 – *The six different types of sulfur-nitrogen compounds.*

Perhaps one of the most appropriate and fundamental sulfur-nitrogen starting reagents is tetrasulfur tetranitride, S_4N_4, first prepared, in an impure form, by William Gregory in 1835.[1] Purification of the binary sulfur nitride occurred several years later and it was not until the mid twentieth century that its unusual structure was elucidated.[2, 3] S_4N_4 is a pernicious contact explosive that crystallises as vibrant orange coloured needles. Crystalline S_4N_4 is thermochromic, adopting a pale yellow colour at low temperatures (77 K), orange at room temperature, and dark red at increased temperatures (373 K).[4] The molecule itself adopts an extreme cradle formation that is best viewed as an eight-membered ring consisting of alternating sulfur and nitrogen atoms. Owing to weak transannular sulfur-sulfur interactions, a cage-like structure results, which, in essence, produces two fused S_3N_2 five-membered rings (see Figure 2). Delocalised bonding is believed to be present within this ring system, accounting for the similarity in bond distances between neighbouring sulfur and nitrogen heteroatoms.

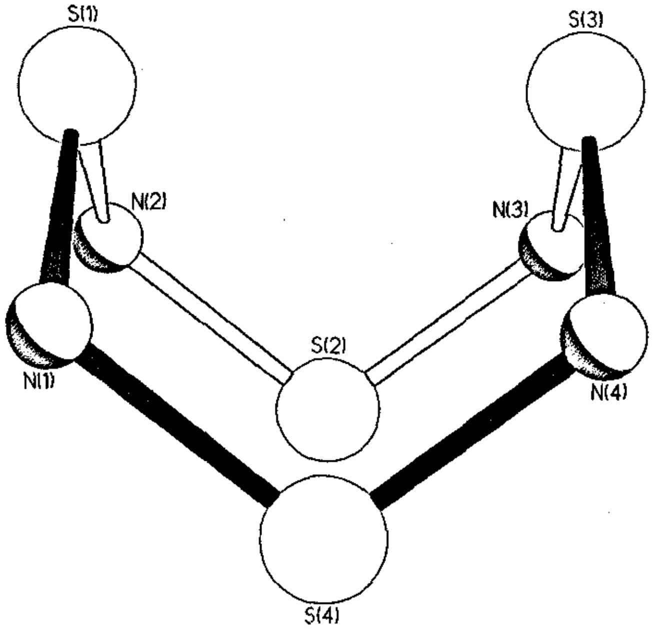

Figure 2 – ***Crystal structure of tetrasulfur tetranitride.***

Kinetically, S_4N_4 is stable in air, although in a thermodynamic sense, it is an unstable molecule owing to a positive heat of formation ($\Delta H^{\circ}_f = +460$ kJ mol^{-1}). Such a property is not uncommon amongst many compounds, yet for systems as simple as tetrasulfur tetranitride, it is most surprising.

Although several routes to preparing S_4N_4 exist,[5-8] the most widely employed is the large scale preparation *via* ammination of sulfur dichloride, SCl_2, in carbon tetrachloride (see Equation 1).[5] This synthetic route has been optimised somewhat from its initial discovery, nearly two centuries ago. The continuous passage of ammonia gas into a luke-warm solution of SCl_2 in carbon tetrachloride, yields a mixture which experiences several colour changes and a number of reaction products: S_4N_4, S_8, S_7NH, $S_6(NH)_2$, S_4N_3Cl and NH_4Cl. However, by changing reaction conditions so that the amount of ammonia used is in excess, and by maintaining a constant temperature range between 20°C and 50°C, the reaction favours the production of S_4N_4.[9] Yields as high as 60-70% are known for the gaseous ammonia route, compared to other syntheses such as the heating of NH_4Cl with S_2Cl_2 (*ca.* 30%).

$$6\,SCl_2 + 16\,NH_3 \xrightarrow{20-50°C} S_4N_4 + 2\,S + 12\,NH_4Cl$$

Equation 1 – ***Traditional synthesis of tetrasulfur tetranitride.***

Historically, following isolation of the crude product *via* filtration and washing with water to remove ammonium chloride, the pure target material is obtained through soxhlet extraction with refluxing dioxane, followed by recrystallisation from hot benzene.[5, 9] In the pure form, care must be taken when handling S_4N_4, as excessive mechanical shock or percussion can lead to spontaneous disassembly of the nitride. Although sensitive to rapid heat exposure (> 100°C), S_4N_4 can be sublimed under vacuum, allowing purification of small quantities to be achieved.

Reaction chemistry utilising S_4N_4 is both extensive and diverse, and still of great interest today. Four general reaction types exist: reactions with ring conservation, reactions with ring expansion, reactions with ring contraction and reactions with ring cleavage (see Figure 3 for an example of each). It is, however, the latter of these which is pertinent to the formation of the four-membered ring system, disulfur dinitride, S_2N_2.

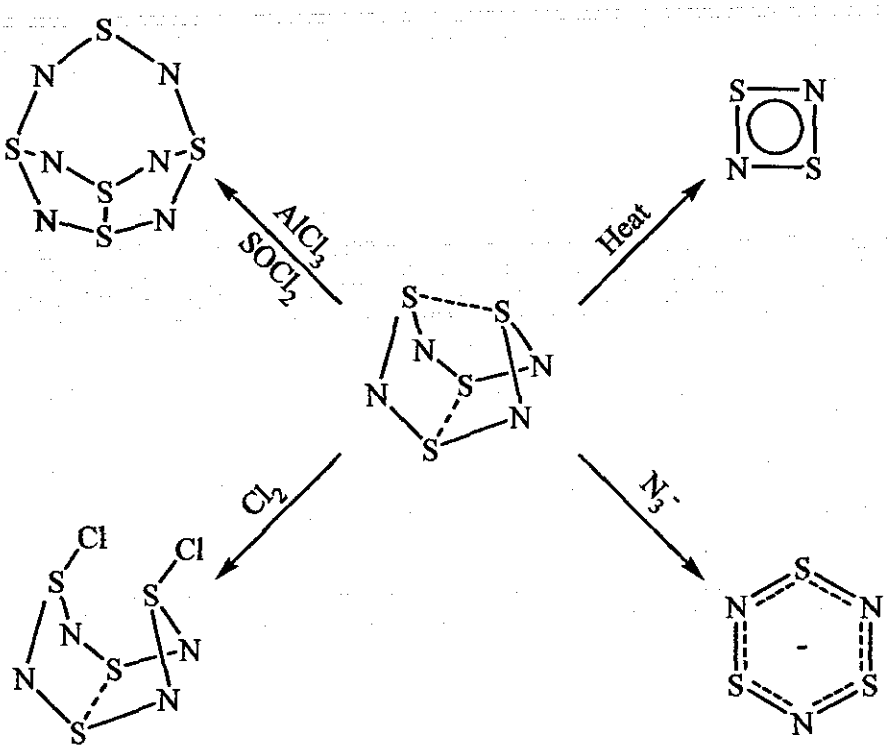

Figure 3 – *The four types of reaction associated with tetrasulfur tetranitride.*

The *in situ* vacuum pyrolysis (thermal cracking) of S_4N_4 vapour through heated silver wool (*ca.* 300°C) yields the colourless, or pale white, crystalline S_2N_2 product, which must be collected using either a cold trap or cold finger, usually cooled with liquid nitrogen.[5, 9, 10] Commonly, there is a small proportion of side-products that can form in the collection vessel and isolation/purification of S_2N_2 is usually achieved either through gentle warming and further condensation with liquid nitrogen in a separate trap, or *via* ether extraction and recrystallisation.

S_2N_2 is a square planar molecule that has a bond length which approximates to the average of single and double S-N bonds, and is therefore consistent with a partial aromatic state. In its purest form, crystals are insoluble in both water and acids, but readily dissolve with decomposition in basic solutions. Conversely, in many organic solvents, such as ether, acetone and dioxane, solubility is plausible. In the solid state, S_2N_2 is an extremely volatile compound, especially under reduced pressure and at temperatures greater than approximately 20°C , it sublimes rapidly. Although purity dependent, temperatures nearing 30°C have been known to cause explosive detonation of S_2N_2, to its elements.[11] Additionally, to a greater extent than that of S_4N_4, crystals of S_2N_2 are extremely sensitive to mechanical shock, percussion and friction and can explode violently; they have also been known to detonate spontaneously at room temperature. Interestingly however, there has not been any reports of detonation from S_2N_2 crystals isolated from the solid state, through the warming and re-condensation method previously described.[12] Perhaps this is a coincidental occurrence, or potentially the presence of trace amounts of organic solvent in recrystallised samples, may catalyse such decomposition.

Although there are many compounds and complexes that consist of the S_2N_2 moiety, either as a terminal group[13, 14] or as a bridging linker unit,[15] very few reactions have actually been reported using S_2N_2 itself.[12, 16] Largely, this is the result of difficult handling protocols and the short stability period for the nitride. Some reaction products, for example, from reactions involving S_4N_4 or $S_3N_3Cl_3$, produce the monomeric S_2N_2 unit,[17, 18] and this is often the preferred method of synthesising complexes containing the latter.

Primarily, the inherent instability and explosive nature of S_2N_2 limits the amount of work plausible in many synthetic approaches. However, the observation that upon standing under vacuum, S_2N_2 undergoes spontaneous polymerisation to poly(sulfur nitride), $(SN)_x$, is one of the most interesting discoveries within sulfur-nitrogen chemistry, to date.

Selenium and tellurium analogues sharing the X_2N_2 formula unit have eluded experimental isolation and characterisation. The properties associated with such molecules may be considered to be of great interest, especially if identical polymerisation processes occur. The eight-membered ring system, tetraselenium tetranitride, Se_4N_4, is well known[19-21] and its sensitivity to friction is much greater than that of its sulfur analogue. It would therefore be reasonable to assume similar, if not more hazardous, properties be associated with an Se_2N_2 or Te_2N_2 compound. The thermolysis of Se_4N_4, under vacuum, yields only elemental selenium and dinitrogen.[22] Despite no definitive isolation as the free ligand, both main group and transition metal halide adducts containing Se_2N_2 have been characterised,[23, 24] commonly through reaction of the Se_4N_4 parent species. Such complications in obtaining monomeric Se_2N_2 has probed *ab initio* calculations and theoretical studies into predicted conformation and spectroscopic data pertaining to the selenium nitride.[25] Recent investigation into such systems, however, by Kelly *et al.* has provided the first example of a 'free' Se_2N_2 unit.[26] Despite not being isolable or indeed polymerisable, attempts to do so resulting only in dimerisation back to Se_4N_4, its presence as a free ligand can be confirmed through co-ordination reaction with $[Pt(\mu\text{-}Cl)Cl(PMe_2Ph)]_2$. Good similarity can be seen between proposed and experimental spectroscopic data.

Tellurium systems do not appear to follow in a homologous nature to their sulfur and selenium counterparts. The first tellurium nitride was observed over a century ago following the reaction of tellurium tetrabromide, $TeBr_4$, with liquid ammonia. The resulting yellow product, whose empirical formula was initially defined as TeN, is highly insoluble and explosive in nature. Since then, investigation has determined a more accurate composition to be Te_3N_4, thereby requiring Te to be in a tetravalent state. Accordingly, no observation of a $(TeN)_x$ polymeric system has been reported.

1.1.1. Poly(sulfur nitride), $(SN)_x$

Poly(sulfur nitride), also commonly known as polythiazyl, thiazyl polymer, or $(SN)_x$ (hereinafter referred to as $(SN)_x$), was first discovered almost 100 years ago by F.P. Burt.[10] This novel material, at the time, was overlooked somewhat in relation to inherent properties, and it was not until the late 60's and 70's that it was recognised as being the first example of a polymeric metal; despite being composed solely of two non-metallic elements: sulfur and nitrogen respectively. Although its physical properties are now universally agreed, conflicting reports have been identified relating to its stability and conductivity characteristics.

Typically, $(SN)_x$ can be prepared in both crystalline and powdered forms. The first synthetic route to $(SN)_x$ yielded well-formed crystals that were bright golden and lustrous to the naked eye with reflectivity from individual crystal facets being highly anisotropic (directionally dependent). In single crystal form, $(SN)_x$ consists of highly orientated parallel fibre bundles, incorporating a repeating S-N backbone. Remarkably, the fibre bundle tips themselves are noticeably blue-black in appearance.[27] The reaction scheme outlined in Equation 2 depicts the traditional route to $(SN)_x$ crystals; the thermal cracking of the explosive precursor, S_4N_4, through silver wool, onto a cold finger, yields S_2N_2 crystals which polymerise in the solid state to produce $(SN)_x$ crystals that are typically several millimetres in diameter.[10] The presence of silver wool primarily limits the formation of tetrasulfur dinitride impurities, S_4N_2 (reaction of excess sulfur with either S_4N_4 or S_2N_2 affords S_4N_2). This is achieved by reaction of residual elemental sulfur traces with the silver to afford a silver sulfide, AgS, side product. Although substitution of the silver, with copper or silver-plated quartz wool, does induce formation of S_2N_2 and in turn $(SN)_x$, yields are significantly decreased and S_4N_2 contamination is excessive.[9]

$$S_4N_4 + 8\,Ag \longrightarrow 4\,Ag_2S + 2\,N_2$$

$$S_4N_4 \xrightarrow{Ag_2S} 2\,S_2N_2 \xrightarrow{\textit{Solid State Polymerisation}} (SN)_x$$

Equation 2 – ***Reaction scheme showing the synthesis of $(SN)_x$.***

Following numerous electron paramagnetic resonance spectroscopy studies (EPR), the polymerisation process was traditionally believed to follow a two-stepped mechanism, that involved the formation of an S_2N_2 diradical intermediate species. The inherent reactive nature of the diradical synthon is then able to facilitate spontaneous polymerisation to form $(SN)_x$ (see Figure 4).

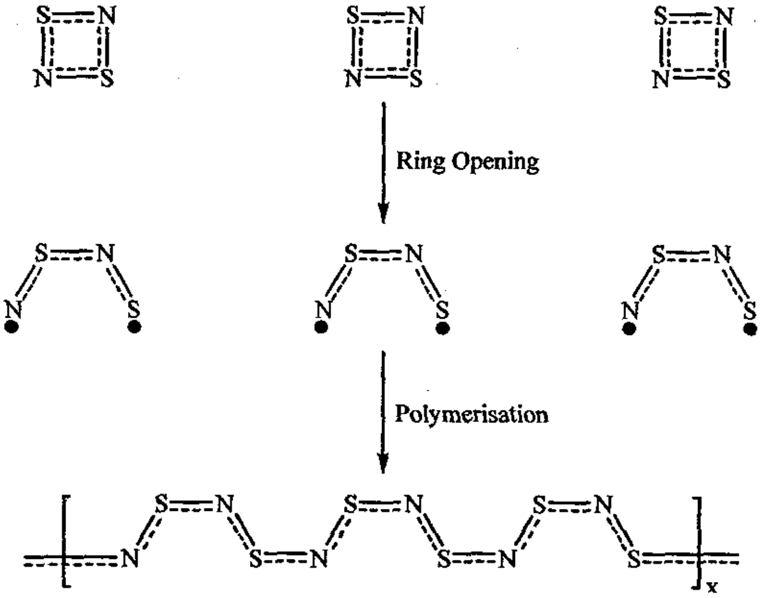

Figure 4 – ***Proposed reaction mechanism for the solid-state conversion of S_2N_2 to $(SN)_x$.***

Suggested by Mikulski et al.[28, 29]

More recent investigations, however, concerning both S_2N_2 and $(SN)_x$, have actually attempted to prove/disprove the initially suggested conversion mechanism, using advanced computational modelling.[30, 31] Although largely correct, it is suggested that the generally accepted mechanism (Figure 4) may require modification to include complex 'triplet state' intermediate S_2N_2 moieties.

A powdered variant of $(SN)_x$, first prepared by Passmore *et al.*,[32] is also known, and exists as a dark blue-black finely divided, static, amorphous powder. The preparation of powdered poly(sulfur nitride) (ppsn) arguably utilises a much more facile preparative route (see Equation 3), without the need to handle or generate inherently sensitive compounds, namely S_2N_2 and S_4N_4.

$$(NSCl)_3 + 3\ Me_3SiN_3 \longrightarrow 9/2\ N_2 + 3\ Me_3SiCl + 3/x\ (SN)_x$$

Equation 3 – ***Conventional preparation of powdered poly(sulfur nitride).***

Essentially, the fundamental property of $(SN)_x$ is its tremendous ability to act as a highly anisotropic conducting polymer at room temperature, with the capacity to become superconductive at temperatures below that of liquid helium ($T_c = 0.26$ K).[33] The critical temperature, or T_c, represents the temperature at which a material's resistance becomes zero. Amongst undoped polymers (where there is no addition of either a positive or negative charge carrier source), this property is very much unique.

Literature discussions, spanning the last 50 years, regarding the conductivity of crystalline $(SN)_x$ samples, often depict mixed results. In many cases however, such differing observations are likely to be the result of variations in sample purity. It has been suggested that these variations may be due to extrinsic effects on conductivity arising from the interaction of the conduction electrons with localised spins on chain breaks and defects (known as the Kondo effect).[34-36]

Generally speaking however, room temperature conductivity data, acquired from direct current (DC) four-point probe measurements, for $(SN)_x$ single crystals, is in the range of 1-4 x $10^3\ \Omega^{-1}\ cm^{-1}$. Additionally, a linear correlation exists between decreasing temperature and increasing conductivity, along the parallel S-N fibres.

With temperatures as low as 4.2 K, conductivity has been shown to increase by a factor of 10^2.[4, 37] Conversely, ppsn produced from the reaction between $(NSCl)_3$ and trimethylsilyl azide, in acetonitrile, yields $(SN)_x$ with a conductivity of *ca.* 5 Ω^{-1} cm^{-1}; three orders of magnitude lower than the crystalline material.[32]

The intrinsic perpendicular conductivity of $(SN)_x$, again determined through DC probe methods, is not facilitated due to the fibrous structure of the polymer. Kaneto *et al.*[38] found that by using microwave techniques, that are less affected by the perpendicular barriers, a perpendicular conductivity value of approximately 40 Ω^{-1} cm^{-1} at room temperature was achieved. The main reason for the remarkable difference between parallel and perpendicular conductivities in crystalline $(SN)_x$ (two orders of magnitude) is the result of weak S---S interactions (3.48 Å) between adjacent S-N chains. The anisotropy ratio is reported to be approximately 50:1 at room temperature and pressure, and 1000:1 at 40 K.[4, 39]

Pressure effects on $(SN)_x$ and its conductivity have also been extensively focused upon over the last three decades. Research has found that the parallel and perpendicular conductivities/resistivities have similar pressure dependencies. These similarly increase/decrease, respectively, with increasing pressure, to approximately 20-30 kbar, before plateauing.[40, 41] Interestingly, additional pressure increases up to 400 kbar show a monotonic decrease/increase.[42] The critical temperature of the $(SN)_x$ was also found to increase linearly with pressure, to 3 K at *ca.* 9 kbar, before decreasing again.[40, 42, 43] Such observations are initially, perhaps, to be expected, as increased pressure would inevitably lead to greater point-point intimacy and compression of the perpendicular fibres towards each other. Similarly, increasing the pressure further (in this case to 400 kbar) would maintain, or indeed, strengthen such physical changes, thereby facilitating, at the very least, no net change in conductivity/resistivity. It is surprising, therefore, that conductivity appears to decrease upon extensive pressure loading.

Although it is apparent that the effect of pressure significantly alters the conductivity and critical temperature characteristics of the polymer, a conclusive explanation into the mechanism accounting for these trends has not been definitively postulated. Theories including band structure change, defect interference, fibre coupling and phase transitions have all been proposed. However, more recently, Jones and Bardo have suggested the possibility in the exothermic, intra-molecular rearrangement of $(SN)_x$ to $(SNNS)_x$ at high pressure (a 6-membered ring polymer, fused at N-N bonds).[44] As a consequence, the S---S distances would be reduced, causing a higher transition temperature in longer chains; shorter $(SNNS)_x$ chains (more insulating) would conversely decrease the conductivity at these higher pressures, in turn displaying the observed trends.

More recently, X-ray diffraction studies have been used to identify the presence of two polymorphs of $(SN)_x$ within bulk samples. The less prevalent (10%) α-$(SN)_x$, is orthorhombic with its counterpart, β-$(SN)_x$ (90%), adopting a monoclinic unit cell.[45] It is thought that the reason for the two polymorphs of $(SN)_x$ is due to martensitic (displacive, diffusionless solid-state transformation) transitions in which the S_2N_2 structure approaches that of $(SN)_x$ before undergoing ring cleavage and polymerisation.[46] The beta form of $(SN)_x$ is commonly talked about in literature, with the alpha form predominantly existing in epitaxial films of $(SN)_x$. Larger percentage conversion to α-$(SN)_x$ can be achieved by careful grinding of β-$(SN)_x$, although full conversion is unlikely.

The crystal structure of $(SN)_x$, first solved by Boudelle in 1975,[47] depicts a *cis, trans* polymer that is almost completely planar. The adjacent S-N bond lengths have been found to be 1.63 Å and 1.59 Å, which is intermediate between single and double S-N, bonds and therefore reinforces the proposed delocalised structure.[48] Furthermore, the S-N-S bond angle was found to be approximately 120° with the N-S-N angle being slightly more acute, at approximately 106°.[48] An example of the crystal structure and packing within the molecular lattice can be seen in Figure 5.

The ability of $(SN)_x$ to act as a 'metallic' compound can be further explained by consideration of the π-bonding within the polymer. S_2N_2 can be considered as an electron-rich system, based on the Huckel $(4n + 2)$ analogy, where each sulfur atom contributes one pair of 3p electrons and each nitrogen contributes one 2p electron to the 6π-electron delocalised system.

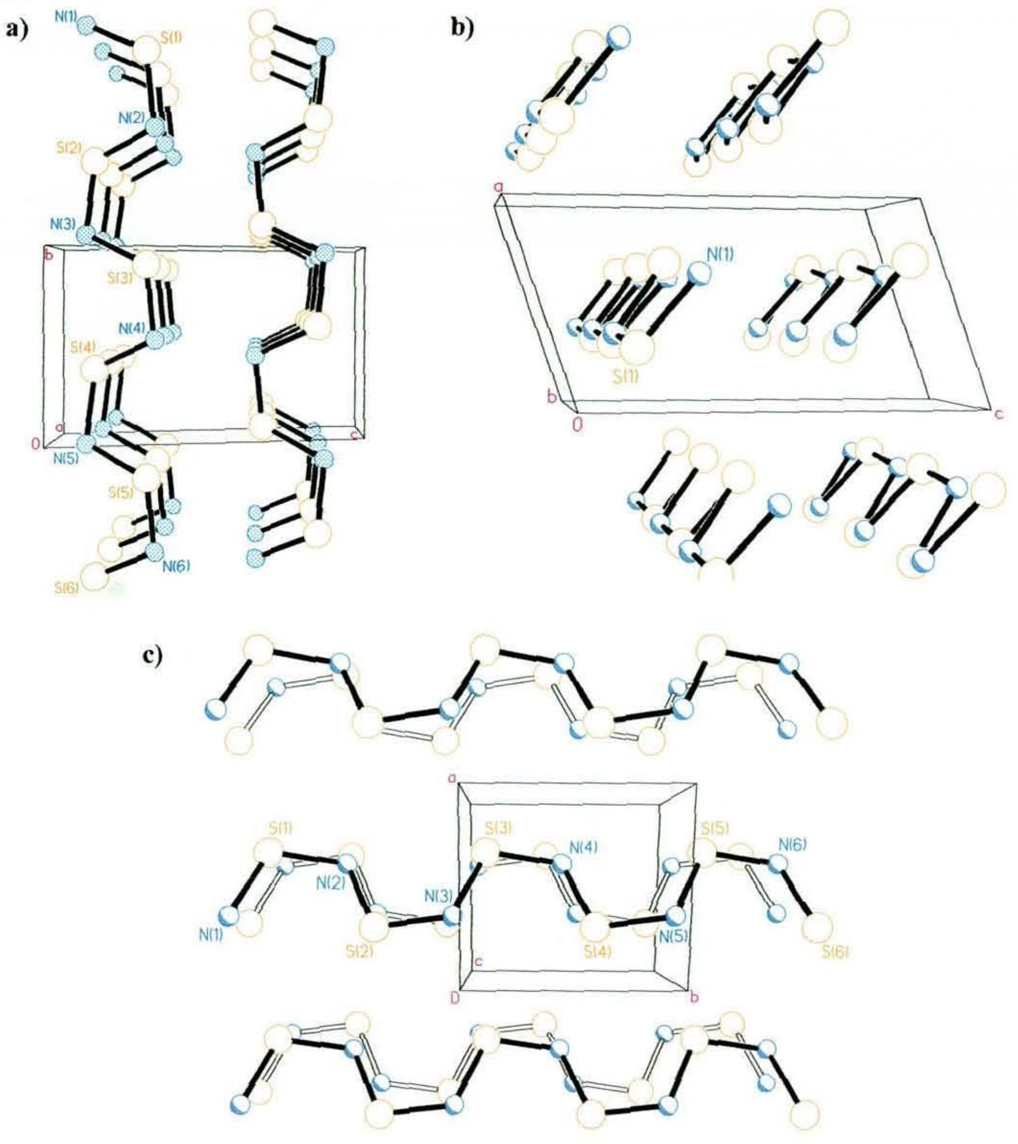

Figure 5 – *Crystal structure and packing diagrams of $(SN)_x$ as viewed along the (a) a-axis, (b) b-axis and (c) c-axis.*

This, essentially, results in three doubly occupied molecular orbitals. If, in the case of $(SN)_x$, we consider the repeat unit to be S_2N_2, then one antibonding orbital remains vacant. Thus, based on the fact that these monomeric S_2N_2 units combine to form polymeric chains of infinite length, a filled valence band and half-filled conduction band arise, as illustrated in Figure 6.

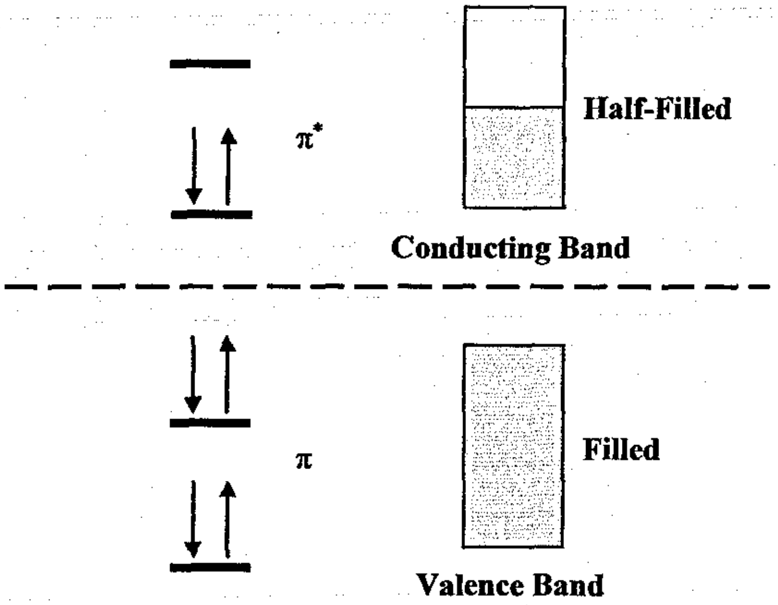

Figure 6 – ***Band structure of a repeat S_2N_2 unit within $(SN)_x$.***

With the introduction of an applied potential (V), the electrons occupying the partially filled conduction band are able to move, and hence conductivity occurs along the chain itself.[49] Banister and Gorrell[39] noted that the so-called Peierls distortion, is inhibited within $(SN)_x$. In a one-dimensional solid, the spacing of the atoms is determined by the distribution of the electrons and thus, there is no certainty that the lowest energy state occurs through regular lattice spacing. In the case of anisotropic solids, such as $(SN)_x$, at T = 0 K, a distortion will typically exist in which a lower energy is present than in a perfectly regular solid, through the result of a 'long and short bond' effect. This trait has the net consequence of trapping the electrons near the Fermi surface from travelling through the solid. The Peierls distortion introduces a band gap in the centre of the original conducting band and thus, the filled orbitals are now separated from the empty orbitals. As a direct result, the distortion results in semiconductor or insulator behaviour rather than that solely of a metallic conductor. Consequently, a superconductor has zero electrical resistance below a critical temperature, a metallic conductor is a substance with an electrical conductivity that decreases with increasing temperature and a semiconductor is a substance with an electrical conductivity that increases with temperature.

However, in the case of $(SN)_x$, the presence of weak S-S and S-N inter-chain interactions (S•••S = 3.47-3.70 Å, S•••N = 3.26-3.38 Å)[39] inhibit such a phenomenon, meaning that $(SN)_x$ does not adopt semi-conductive properties, as with many other polymeric compounds.[50]

The chemical stability of $(SN)_x$ is much debated amongst the literature. It is universally acknowledged that the polymer is completely insoluble[4, 27, 39] and thus, reaction chemistry has been extremely limited. High purity crystals of $(SN)_x$ have been found to typically contain a hydride content of 5-10%, suggesting a hydrolytic reaction with water/moisture traces.[51] Conversely, Mikulski *et al.*[52] found that hydride formation is not present for at least seven days after pure, polymerised $(SN)_x$ crystal formation; whereas tarnishing of incompletely polymerised crystals is evident. Additionally, cyclic voltammetry (CV) studies, using $(SN)_x$ as an electrode medium in aqueous solution, confirmed its stability in the presence of water.[53] $(SN)_x$ has also been found to readily decompose in alkaline solutions.[39]

It is clear that physical perfection of crystals is important when considering the characteristics and physical properties of the SN polymer. Evidently, in some syntheses, impurities within the $(SN)_x$ crystal are present, in the form of free S_2N_2 and small oligomers of the polymer. Thus, it still remains unclear whether formation of purer $(SN)_x$ is more favoured through slow polymerisation of large or small crystals of the S_2N_2 precursor.[4]

The stability of poly(sulfur nitride) to air has also been much discussed and, similarly, observations suggest the initial purity of the sample is essential. Labes and co-workers[36] noted predominant oxygen contamination to air exposure, which differs from the findings of Greene *et al.*,[27] who found there to be no significant change in the microanalysis. The Temple group, however, obtained evidence[4] suggesting that $(SN)_x$ is not air stable, by comparing the percentage composition (S, N, O, C and H) of unexposed crystals, exposed crystals and exposed films of $(SN)_x$, to air, at ambient temperatures. The study showed that exposed $(SN)_x$ developed oxygen concentrations of between 4-8% and small concentrations of carbon and hydrogen (typically sub 1%). Similarly, Mikulski *et al.* believe this trend to be associated with trace quantities of unpolymerised S_2N_2, physical imperfection and the presence of other chemical impurities.[52]

The thermal stability of $(SN)_x$ is poor. Atmospheric heating of the polymer to *ca.* 240°C leads to explosive decomposition.[27] Heating in an inert gaseous atmosphere also causes an explosive reaction, preceded by decomposition *via* sublimation.[27] It is possible to sublime $(SN)_x$ crystals, and thus deposit them on varying deposition media, by gradual heating to approximately 135°C under dynamic vacuum.[4, 54]

To date, numerous patents have been secured for the use of $(SN)_x$: cathode materials in batteries,[55] electroconductive resins,[56] explosive initiators,[57] to name but a few. A $(SN)_x$-GaAs solar cell has been fabricated[58] with an efficiency of 6.2% and an open-circuit voltage of 43% higher than that of the Au-GaAs analogue. Although $(SN)_x$ electrodes are known, their instability to atmospheric conditions and their inability to better other commercially available electrodes, renders them obsolete. Since poly(sulfur nitride) may have a degree of moisture and air sensitivity, any industrial uses are limited, as anhydrous, anaerobic conditions would be required. For all this interest, however, and despite the intensity of the initial work prompted by the first observations of superconductivity, practical applications of the polymerisation process, and utilisation of the polymer, have largely remained elusive.

Since the isolation of $(SN)_x$, much work has gone into devising a synthetic route to the polymer which is both facile, safe and uses inexpensive precursors. To date, only Passmore and co-workers have been able to successfully accomplish this;[32] although the formation of the $(NSCl)_3$ starting material could be argued to be slightly arduous. Although other synthetic routes to the polymer are known, most of these only provide small quantities of the target material.[39] Additionally, it is believed that less time-consuming routes to $(SN)_x$ may stimulate a new surge of work into its reaction chemistry, with the plausibility to modify the conducting chain and promote an application base for the polymer.

1.1.2. Poly(thiazyl bromide), $(SNBr_{0.4})_x$

The modification of $(SN)_x$, *via* halogenation, has also generated considerable interest. The original literature findings of Clever and Muthmann,[59] spanning back over 100 years, reports the initial synthesis and characterisation of a $(BrS{=}N)_x$ polymer. More recently however, Bernard *et al.*,[60] Street *et al.*,[61] and MacDiarmid *et al.*,[62] have provided conclusive evidence of the formation of poly(thiazyl bromide), $(SNBr_{0.4})_x$, as well as other halogenated analogues.

Currently, three main preparative routes are known for the formation of $(SNBr_{0.4})_x$. The addition of bromine to $(SN)_x$ yields $(SNBr_{0.4})_x$; exposure of $(SN)_x$ crystals to the vapour pressure of dry bromine, at room temperature and pressure for 24 hours, yields fibrous blue/black crystals, known to be $(SNBr_{0.5})_x$. Further treatment of these crystals under high dynamic vacuum for half an hour, at ambient temperature, results in $(SNBr_{0.4})_x$.[61] Secondly, in 1986, Dehnicke and Demant[63] proposed a new synthetic pathway to the brominated polymer, involving the reaction between $(NSCl)_3$ and Me_3SiBr in dry methylene chloride at -60°C. The resulting product was a dark blue/black, loose, amorphous powder, characterised as being identical in nature to that obtained through direct bromination. Perhaps the most facile synthesis of bromine substituted $(SN)_x$ results from direct Br_2 vapour exposure of S_4N_4 crystals, followed by pumping at varying temperatures to afford $(SNBr_{0.25})_x$.

It is clear, however, that air and moisture sensitivity is much greater in this halogenated polymer than for poly(sulfur nitride) itself;[62, 63] visible surface tarnishing is evident within minutes of air exposure, although mass change is negligible. Stringent anaerobic conditions must be ensured for storage and handling of any prepared samples.

$(SNBr_{0.4})_x$ crystals adopt an expanded geometry, approximately 50% greater in volume than the original $(SN)_x$ parent crystals. The increase in volume is seen to be in directions that are perpendicular to the $(SN)_x$ backbone.[61] Initial confusion into the location and form of bromine in this polymer was evident, and it was not until Iqbal and co-workers used a combination of Raman scattering and X-ray diffraction studies of the brominated polymer, that a conclusion was reached; interpretation of their findings suggest that bromine is present within interfibrillar regions as Br_3^-, and as Br_2 within the $(SN)_x$ lattice itself.[64] Additionally, it is interesting to note that observed fibre widths of $(SNBr_{0.4})_x$ are approximately half of that attributed to $(SN)_x$: 30 Å and 50-70 Å, respectively.[61] This finding further re-enforces the theory that the bromine resides between the S-N chains, as an intercalated moiety.

DC conductivity data for the brominated polymer is an order of magnitude greater than that of $(SN)_x$. At room temperature and pressure, $(SNBr_{0.4})_x$ crystals exhibit a conductivity of approximately $2 \times 10^4\ \Omega^{-1}\ cm^{-1}$.[65] Similarly, with respect to $(SN)_x$, the conductivity of $(SNBr_{0.4})_x$ also increases linearly, with decreasing temperature, and a critical temperature is reached at 0.31 K; $(SNBr_{0.4})_x$ can therefore be classified as super-conductive. Unsurprisingly, the T_c does not differ much from that of $(SN)_x$ and thereby helps provide further proof of the unchanged S-N backbone present within $(SNBr_{0.4})_x$.

It is clear that the doping of $(SN)_x$ with bromine yields a polymer with similar properties, yet slightly more conductive. Other halogen substituted variants of $(SN)_x$ can be prepared by reaction of S_4N_4 with I_2, IBr and ICl respectively. In such cases, conductivity has been found to increase significantly, often greater than 10 orders of magnitude compared to $(SN)_x$. In light of these findings, it is plausible that numerous other superconducting derivatives of $(SN)_x$ may exist and adaptation with appropriate intercalators could help stabilise the system. It appears that, possibly due to air sensitivity and restrictive solubility issues, very little work concerning reaction chemistry of $(SNBr_{0.4})_x$ has been undertaken, both in the solid state or using solvated environments.

1.2. Microporous Materials

In the general sense, microporous materials are substances containing a pore system, with a pore aperture, or diameter, of less than 20 Å. The term microporous material, is broad, and is an umbrella classification for many minerals, clays and molecular sieves. Materials comprised of pore networks with a diameter exceeding 20 Å are classified as either mesoporous (> 20 Å) or macroporous (> 500 Å).[66]

1.2.1. Minerals

Although often able to be chemically synthesised, a mineral is best defined as a naturally occurring substance that is formed through geological processes and has a characteristic general formula (illite, for example, adopting the general formula $(K,H)Al_2(Si,Al)_4O_{10}(OH)_2 \cdot xH_2O$). Minerals can vary tremendously in their composition, from pure elements and simple salts, to complicated silicates. Typically, minerals are characterised based on their:

- crystal structure and habit (often powder X-ray diffraction is used)
- hardness, according to the Mohs Scale.
- colour and iridescence
- streak
- cleavage
- fracture
- specific gravity
- other specific properties, such as piezoelectricity, fluorescence, magnetism, *etc.*

Comfortably, the most abundant group of minerals belong to the silicate family, which are composed of mainly silicon and oxygen atoms, alongside cations such as magnesium and calcium. Aluminosilicate minerals have the basic $AlSiO_4$ repeat unit as their building block. It is the hydrated aluminosilicates that are given the term, 'zeolite', and these are commonly used for both gas and liquid phase adsorption.

1.2.2. Molecular Sieves

Molecular sieves are crystalline aluminosilicates that have an open type structure with apertures of molecular proportions. Their name is derived through the observation that these compounds only absorb molecules that are smaller than the aperture itself, and can therefore be used to selectively separate molecules of varying sizes. A traditional application of such function is the selective removal of ethanol from aqueous mixtures by Ca-A (calcium zeolite A), used commonly within the brewing industry.[67, 68] The molecular sieve cages are highly regular and of accurate size and are thus able to selectively include/exclude hosts to a greater extent than many high surface area solids, such as silica gel.

Substances comprising of an aluminosilicate framework containing trapped cations, typically from Group 1 or 2, within the channels or cages, are known as zeolites. In addition to their use as a molecular sieve, zeolites are also able to undergo metathesis type reactions with ion containing solutions. The actual name zeolite derives from the Greek translation, *zein*, "to boil"; *lithos*, "a stone". The general formula for a zeolite follows that of:

$$(M^{n+})_{nx/m}(Si_{1-x}Al_x)_nO_{2n}$$

where M is usually an alkali, or alkali earth metal

Some zeolites may also be used in shape-selective heterogeneous catalysis. One of the most common, widespread, and mainstream examples of this is the molecular sieve ZSM-5,[69] developed by Mobil Oil. Here, the zeolite is used in the catalytic synthesis of para-xylene (*p*-xylene), for use as an octane booster additive in the petrochemical industry. The ortho and meta substituted xylenes are not produced in the aforementioned reaction due to the restraining factors invoked by the size and shape of the zeolite channels and cages. For similar reasons, zeolites, particularly zeolite A, are commonly used as drying agents in the laboratory.[70] Furthermore, the addition of certain guest molecules has been widely exploited to induce pigmentation properties for use in pigments and dispersants.[71-74] Their application in gaseous processes is also important, where they are commonly used to purify a mixture of gasses and trap impurities, using size selective inclusion/exclusion principles.[70]

The aperture diameters, despite exact values being known, are conventionally discussed in terms of constituent ring size. Terminology such as '8-ring' and '10-ring', or 8 T and 10 T respectively, relates to the closed loop that is built from 8 (or 10) tetrahedrally coordinated Si or Al atoms, and 8 (or 10) oxygen atoms. Although numerous zeolites may be comprised of the same ring system (8 T, for example) it does not strictly mean that exact aperture diameters will be identical. Often, bond strain and steric hindrance throughout the framework matrix, or framework coordination to charged ions within the channels, results in slight aperture asymmetry, where a perfectly flat pore opening is prohibited.[75, 76]

ZSM-5 is an aluminosilicate zeolite of the MFI framework type, usually with a high silica and low aluminium content. Although many zeolite structures are cubic, and their channels the same in all three lattice directions, ZSM-5 has a more complex structure. Within the MFI framework, the channels, which run parallel to the axes, have different sizes. Larger channels, that run parallel to the *b*-axis, intersect smaller channels that run in the other two directions, thereby creating a zig-zag arrangement when viewed along certain orientations (see Figure 7). This characteristic structure differs significantly from the more familiar orthodox arrangement seen in many large and small pore zeolites, such as faujasite and Linde Type A (LTA), respectively.[77]

ZSM-5 has reasonably large cavities that are initially formed around the tetra-*n*-propylammonium, $N(C_3H_7)_4^+$, ion, that serves as a templating agent during hydrothermal synthesis. Within the framework matrix, the aluminium sites are very acidic and the substitution of Al^{3+} in place of the tetrahedral Si^{4+} silica requires the presence of an added positive charge. Typically, this conversion utilises either Na^+ or H^+, though other cationic variants are known.[78-80] The unit cell formula for Na-ZSM-5 is that of $Na_nAl_nSi_{96-n},O_{192}$ (where n = ~ 3). It has an orthorhombic symmetry, as determined by computer based molecular modelling, single crystal X-ray diffraction (XRD) and powder XRD. The channel bottleneck diameter in ZSM-5 is approximately 5.5 Å.[77]

The zeolite family is vast, and a wide array of compounds exist with differing pore apertures and repeat building units. Such a diverse range allows function specific selection to be achieved, based on the intended application and physical constraints required.

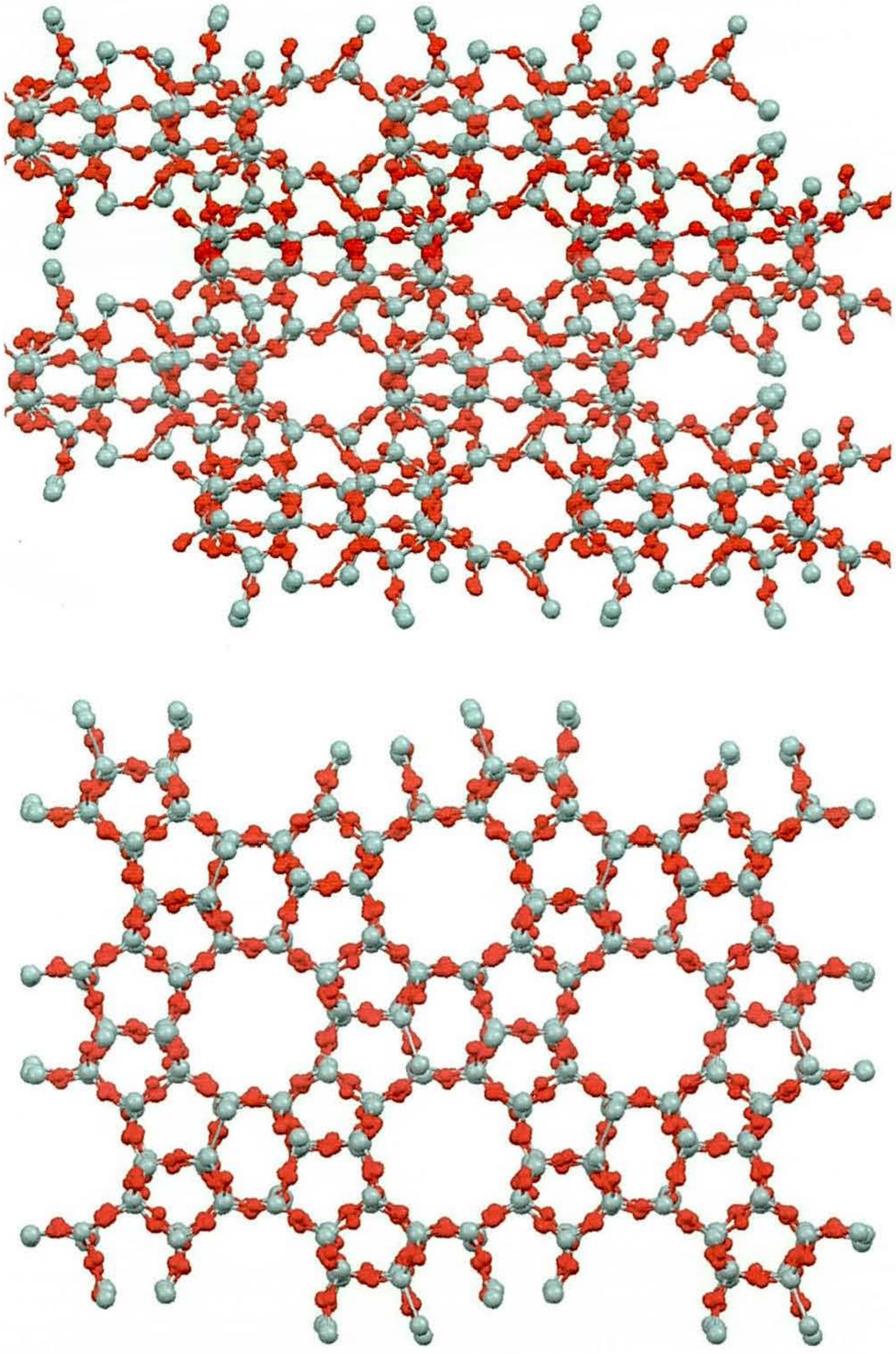

Figure 7 – ***MFI framework structure of ZSM-5 showing the bilateral 'zig-zag' channel network (upper) and large 10T pore aperture (lower).***

Aside from pure zeolite systems however, another fundamentally important family of solid state materials exist; the sodalites. The sodalite group of compounds are physically the smallest (in terms of their building units), and compositionally the most diverse, members of the zeolite family, with general formula $M_8[TT'O_4]_6[X]_y$, comprising of both naturally occurring members (e.g. lapis lazuli)[81] and numerous synthetic examples.[76, 81-87] Their structural diversity and importance results not only in the nature of the framework elements themselves, but also from the nature of the occluded species.

Typically, during hydrothermal syntheses, the TO_4 tetrahedra link together to form a framework structure within which the guest molecules (X) are incorporated by tilting the tetrahedra out of their normal planes and deviation of the perfect tetrahedral geometry around T(T') results. Whilst, by far, the most numerous subgroup of the sodalite genus are the aluminosilicates, pure aluminate[88] and silicate versions have also been synthesised.[89-92]

In the majority of sodalites the framework is charged, and the occluded cations and anions perform a charge-balancing role, meaning that the cage is largely filled and it is impossible to remove these ion clusters without total collapse of the framework (a property classifying sodalites as clathrates). Such physical deterioration means that, in contrast to many of the larger zeolite systems, it has not been possible, thus far, to utilise the sodalite framework for shape selective catalysis,[93] or indeed in the simple modelling of the guest-host relationship (as a result of the ionic interactions that exist). For these reasons, filled silica sodalites of general formula $Si_{12}O_{24}\cdot X$ (wherein X = ethylene glycol, ethylene diamine, ethanolamine, 1,3-dioxolane, or 1,3,5-trioxane)[89-92] have attracted much interest, as both the framework, and template, are neutral, allowing the modelling of interaction energies between both moieties to be achieved.[94-98] Such modelling studies have also been extended to predicting high temperature and template free modifications, including a putative rhombohedral form of sodalite.[99] While many past attempts have been made to produce a template free silica sodalite (with authors often alluding to the desirability of such a system)[100] none have thus far been successful.

As a rule, sodalites have minimum diameter channel voids of 2.5 Å and are therefore defined as microporous materials. Commonly, however, the sodalite pore apertures are in the range of 4-5 Å. The structural combination and linking of pores to form a channel network framework, affords cage-like structures within the matrix (see

Figure 8). It is for this reason that the frequently used term, sodalite cages, or β-cages, is used in conjunction with sodalites; their entire construction being based upon arrangement of β-cages, connected through common 4 T ring windows along the cubic <100>, and 6 T ring windows along the cubic <111> direction.[101]

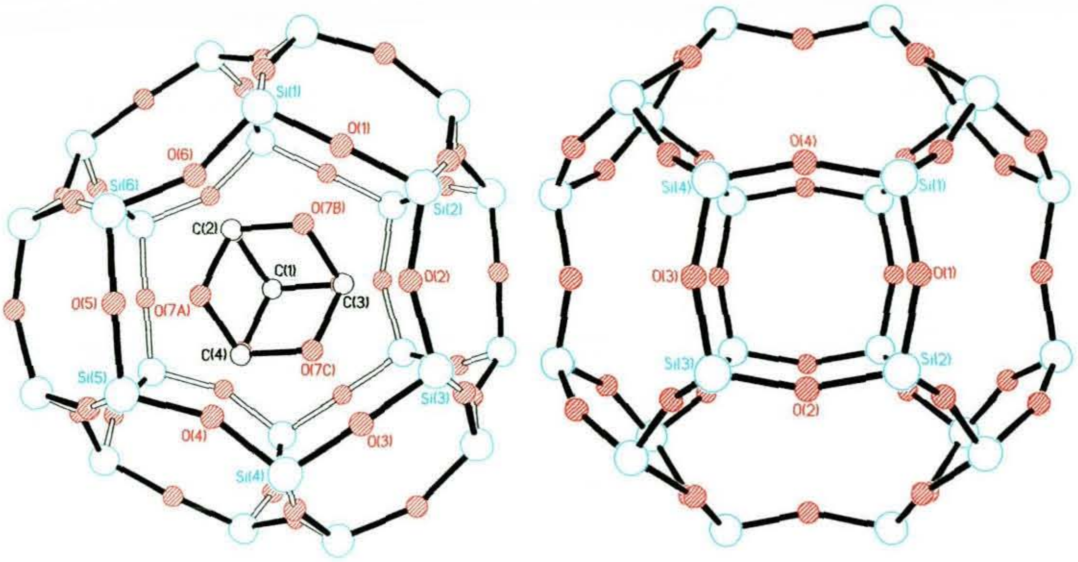

Figure 8 – The ***sodalite cage, or β-cage, within a typical sodalite framework. Individual cage viewed down the 6-ring window, showing the occluded template (left) and down the 4-ring window with the template deleted for clarity (right).***

The three dimensional sodalite framework is perhaps well defined by the individual sodalite cage itself. The former is an identical representation of the walls of the β-cages and on such basis, a definition pertaining to the structure of the sodalite framework becomes divided: either a rigid framework of corner-connected tetrahedra that enclose the β-cages, or as an arrangement of individual cages that are separated by the thin walled tetrahedral framework.[76] The compact arrangement of the sodalite framework is determining in its physical and chemical properties. The narrow channel apertures permit strong interaction between framework and guest atoms, due to decreased interatomic distances. Additionally, the rigid nature (and charge, in the case of alumina containing sodalites) of the host system means that any templating host molecule has distinct conformational restraints that it must match in order to be viably accepted into the framework. Therefore, the number of feasible host and guest combinations becomes limited, even more so when considering pure silica sodalites, as deviation away from a cubic geometry is largely unfavourable. Of the 213 sodalite structures currently deposited in the Inorganic Crystal Structural Database (ICSD) at the time of print, 201 have cubic cell parameters.

The regular structure of the sodalite host-guest system is largely the result of weak, but important, interactions between the framework and the guest molecules. These interactions are rather easily broken upon heating, allowing the guest molecules to acquire kinetic energy and permit movement. Their mobility, however, is restricted as a result of the small aperture width of the β-cages and thus, migration out of the sodalite is prohibited meaning the guest remains trapped within the framework (as in the case of nitrate sodalite,[83, 102] for example). The resulting guest movement at elevated temperatures can often result in a slight variation of positional occupancy of the guest species, but such observations depend largely on the available space within the β-cages and any steric constraints the guest molecule may incur.[76] As an aside to this trend, partial ion exchange has been found to occur at high temperatures, with very little, or indeed no, reaction at room temperature.[103, 104]

Notwithstanding diverse theoretical applications sodalite materials may possess, their primary uses are as clathrate and zeolite systems. In the case of the former, the sodalite framework composition ensures a matrix isolation effect is readily achieved, meaning that individual guest molecules are located in adjacent β-cages and are essentially isolated from each other.[85] In doing so, some physiochemical properties of the guest, compared to that of the bulk material in its native state, are affected and thus the behaviour of individual molecules may be observed. The pigment, ultramarine, takes advantage of this property through isolation of radical anions, in the form of S_2^- or S_3^-, within the β-cages, which would otherwise readily dimerise in any other environment.[72, 74] As briefly mentioned earlier, there is evidence to suggest zeolite type behaviour amongst some sodalites at augmented temperatures.[76, 103, 105] Sodium hydrosodalite, $Na_6[AlSiO_4]_6.8H_2O$, can undergo ion exchange, under reflux, with $LiNO_3$ and result in good conversion (*ca.* 80%) to the lithium hydrosodalite analogue, $Li_6[AlSiO_4]_6.8H_2O$. Additionally, studies have also shown that the water molecules can be progressively lost from this system, affording a fully dehydrated derivative of general formula $X_6[AlSiO_4]_6$ (where X = Na or Li).[103]

There is little doubt that novel synthetic routes will facilitate the growth of a broader family of sodalite materials, with perhaps even more interesting properties than those commonly understood. Advancement in this field should, in turn, lend itself to the development of highly desired host-guest clathrates for potential application in a wide range of environments. The sodalite family, as a whole, has the potential to bridge the gap between purely open type zeolitic systems, with that of dense, closely packed compounds,[82, 106] and facilitate interesting developmental solid state chemistry for the future.

More recently, many zeolite systems have stimulated renewed interest, as the desire for small scale, molecular innovation is becoming more and more of a niche. With technology constantly developing, and miniaturisation seeming to be the next generations' advancement, structures such as "Insulated Molecular Wires", IMW's, are growing in stature.[107] Furthermore, the aspiration to prepare simple, convenient, solid state hydrogen storage materials, has enabled in depth analysis and structural tailoring of many microporous materials, that otherwise may have been overlooked.[108-112]

The ability to encapsulate property specific compounds in an inert zeolite matrix bodes much interest, not only from a theoretical and scientific perspective, but also from a property adaptation and modification point of view. The question arises as to whether a compound that has a certain function on the macroscopic scale in the laboratory, is able to display this, to a greater or lesser extent, if, and when, encapsulated within certain host systems.

Consequently, with cross-reference to $(SN)_x$, although partial success at incorporating the polymer into functional systems has been achieved, examples of chemical derivatisation of the polymer, or growth of the polymer within new environments have been limited. On the first front, and as mentioned earlier, partially oxidised materials, such as $(SNBr_{0.4})_x$, have been prepared.[60-62] Shortly following the discovery of the properties associated with $(SN)_x$, efforts were also made to incorporate the polymer into both clathrate and zeolite systems.[113] During the latter work, Love *et al.* observed a filamental type growth of, presumably, $(SN)_x$, along the fibre axis of perhydrotriphenylene (PHTP) crystals, that resulted from its prolonged exposure to a tetrahydrofuran, thf, solution of S_2N_2. Additionally, the same research group observed interactions with both benzophenone and thiourea matrices, though attempts to induce polymerisation within the channels of a crystal of the natural zeolite, mordenite, proved apparently unrewarding. In this case some yellow colouration was observed when the crystal was exposed to S_2N_2 vapour, and after a few days dark filaments were noted "along the needle axis".[113] It is not clear, however, that this was indicative of polymer formation within the zeolitic channels. More recently, and perhaps more definitively, Hulliger and co-workers reported that similar investigations into the reaction of S_2N_2 with PHTP and other analogous host systems to those initially attempted, had proved fruitless.[75]

Given the advances within zeolite chemistry since these initial attempts, and in light of the intense current interest in so-called insulated molecular wires,[107] reconsideration of the ability of S_2N_2 to polymerise within porous systems becomes germane, especially given that other conducting materials, such as polyacetylene, have been successfully incorporated into zeolite hosts.[114] Introducing the intrinsically conducting $(SN)_x$ wire into such a host is a conceptually obvious modification that thus far has proven to be synthetically impractical.

1.3. Fingerprint Development Techniques

The skin is a vitally important organ of the human body, serving as both an insulator and a barrier to ambient surroundings, as well as aiding with temperature regulation, sensation and synthesis of essential vitamins. The epidermal (outermost) layer of skin is of particular importance when considering fingerprint structure, as it is host to a series of friction ridges, unique to each individual. The fingerprint itself, is best defined as an impression of the friction ridges of all, or any part, of the finger onto a particular surface. A friction ridge, or dermal ridge/papillae, is a raised portion of the epidermis on the palm or fingers, consisting of one or more connected ridge units of friction ridge skin and it is suggested that the principal function of friction ridge skin, for evolutionary purposes, is to increase grip; yet it serves a crucially different, but pertinent, role in the forensic sense.

Figure 9 – ***Illustration of friction ridge skin.***

The latent fingermark, or print, is considered one of the most commonly occurring, fundamental pieces of evidence found in and around crime scene investigation scenarios. Currently, more positive identifications occur, per annum, as a result of fingerprint detection and suspect comparison, than that of DNA analysis itself.[115] Typically however, latent print detection through natural observation is restricted, as the fingermark itself is usually invisible (*latent* meaning "present and capable of becoming though not now visible, obvious, or active" or from Latin, *latent-, lateens,* present participle of *latere*, to lie hidden)[116] thus implying detection and enhancement techniques are required to facilitate visibility. Patent and/or plastic fingermarks, where the print is visible to the naked eye, although important, do not relate to work exploring latent print enhancement and will therefore be disregarded.

The deposited latent fingermark, is a random, complex mixture of natural secretions and contaminants from the surrounding environment and can vary significantly from individual to individual and with an individual from day to day, minute to minute. Of the three types of gland found across the human body; apocrine, eccrine and sebaceous, it is the eccrine gland secretions that are unique to the palms of the hands and soles of the feet. Typically, such glands secrete >98% water, through sweat evolution, and contain a mixture of aqueous soluble inorganic and organic constituents, known as the Water Soluble Deposit (WSD) (See Table 1). The exclusive coating of the friction ridges of the hands by eccrine glands, means that some amount of eccrine gland secretion must be initially present within each and every latent fingermark. That is not to say that no other secretion component may be present within the deposited material; in fact, contamination *via* sebaceous gland secretions (such as waxes and fats, known as Non-Water Soluble Deposits (NWSD)) is frequent, and often the result of touching parts of the body and hair.

Source	**Location**	**Inorganic Constituent**	**Organic Constituent**
Eccrine Glands	Most of the body but exclusive to the palms of the hands and soles of the feet.	Water (>98%) Chloride Metal ions (Na^+, K^+) Sulfate Phosphate Bicarbonate Ammonia	Amino acids Proteins Urea Uric acid Lactic acid Sugars Creatinine Choline
Appocrine Glands	In the groin and armpits. Associated with hair follicles around the genitals and mammary glands.	Water (>98%) Iron	Proteins Carbohydrates Sterols
Sebaceous Glands	Most of the body except on the palms of the hands and the soles of the feet. Highest concentration is on the forehead and back; associated with hair roots.	–	Glycerides (30-40%) Fatty acids (15-25%) Wax esters (20-25%) Squalene (10-12%) Sterol esters (2-3%) Sterols (1-3%)

Table 1 – ***Table showing the major chemical constituents of the natural gland secretions in the human body.***

Adapted from Lee et al.[117]

From the late 19th century to the present day, various fingerprint detection techniques have evolved, often through chance, facilitating the plausible detection and enhancement of latent residues from a broad array of surface types and environments. The surface media to which a latent print is 'adhered' drastically affects the detection method chosen for print enhancement. Although few studies initially considered the interaction between fingerprint ridges and the surface that they touch, work in the mid-to-late nineties by Bobev[118] showed that surface phenomena play important roles in fingerprint retrieval. Henceforth, all surfaces can be subdivided into three categories: porous, semi-porous, and non-porous (see Table 2).

Type of Surfaces		
Porous	**Semi-porous**	**Non-porous**
- Absorbs WSD very quickly, following deposition. - The NWSD remains on the surface for longer (*ca.* 12-24 hrs). - A small amount of the NWSD stays on the surface for a significant period.	- Absorbs WSD slowly after deposition (minutes to hours). - The NWSD remains on the surface much longer (several days). - A small amount of the NWSD stays on the surface for a significant period.	- No absorption of any part of the latent fingerprint deposit. - The WSD and NWSD remains on the surface for extended period of time, as an emulsion mixture. - Latent deposits remain on the surface and are very fragile.
Typical examples: Paper Cardboard Fabrics (e.g cotton) Untreated wood	**Typical examples:** Some plastics Waxed surfaces Varnished wood Wall paints	**Typical examples:** Some plastics Glass Metals Glazed ceramics

Table 2 – ***Types of surface and their interaction with the latent fingerprint deposit.***
Adapted from Champod et al.[116]

1.3.1. Porous

Porous surface types are commonly understood to be those that readily, and quickly, absorb the latent fingerprint deposit; common examples include papers, wood and fabrics, such as cotton. Typically, the WSD is absorbed into the outermost layers of the surface within seconds, often leaving an array of residues behind (NaCl, amino acids, *etc.*), following evaporation of the aqueous component. The depth to which the fingermark deposit penetrates into the porous surface largely depends on environmental factors, such as humidity and temperature. Following stabilisation and 'fixation' of the WSD within the porous material, its conservation to mechanical interference is high, although water interaction is likely to lead to washing away of the WSD.

With time, and depending on environmental conditions, several deposited components can show varying degrees of mobility on the porous surface. Salts, for example, tend to diffuse continuously throughout the substrate and such a process is often humidity driven (higher humidity leads to increased diffusion rates). NWSD's, on the other hand, remain intact on the surface itself for extended periods of time, and only slight diffusion is noticed when ambient temperatures exceed 30°C. Typically, under 'normal' conditions, a small proportion of the NWSD can remain on the sample surface for several years.

1.3.2. Non-Porous

In contrast to porous surfaces, the non-porous substrate inhibits absorption of any component of the latent fingerprint deposit; common examples of such surfaces include plastics, glass and metals. In such scenarios, an emulsion mixture containing both WSD and NWSD forms an adsorbate on the sample surface and remain intact for extended periods of time (years) unless it is removed through mechanical action, degradation caused by ageing, or organic solvent interaction. Consequently, fingermark contaminated samples in the laboratory, on non-porous surfaces, must be handled with increased care and attention, due to the susceptibility of print deformation and removal.

1.3.3. Semi-Porous

As its name suggests, semi-porous surfaces exhibit intermediate characteristics compared with porous and non-porous substrates; common examples of semi-porous surfaces include varnished woods, some plastics and polymer coated paper. When contaminated with a latent fingermark, these surfaces absorb the WSD, but over a longer time-scale compared to porous surfaces. Additionally, the NWSD remains on the surface for longer than it would on a porous surface, but not as long as it would on a non-porous medium.

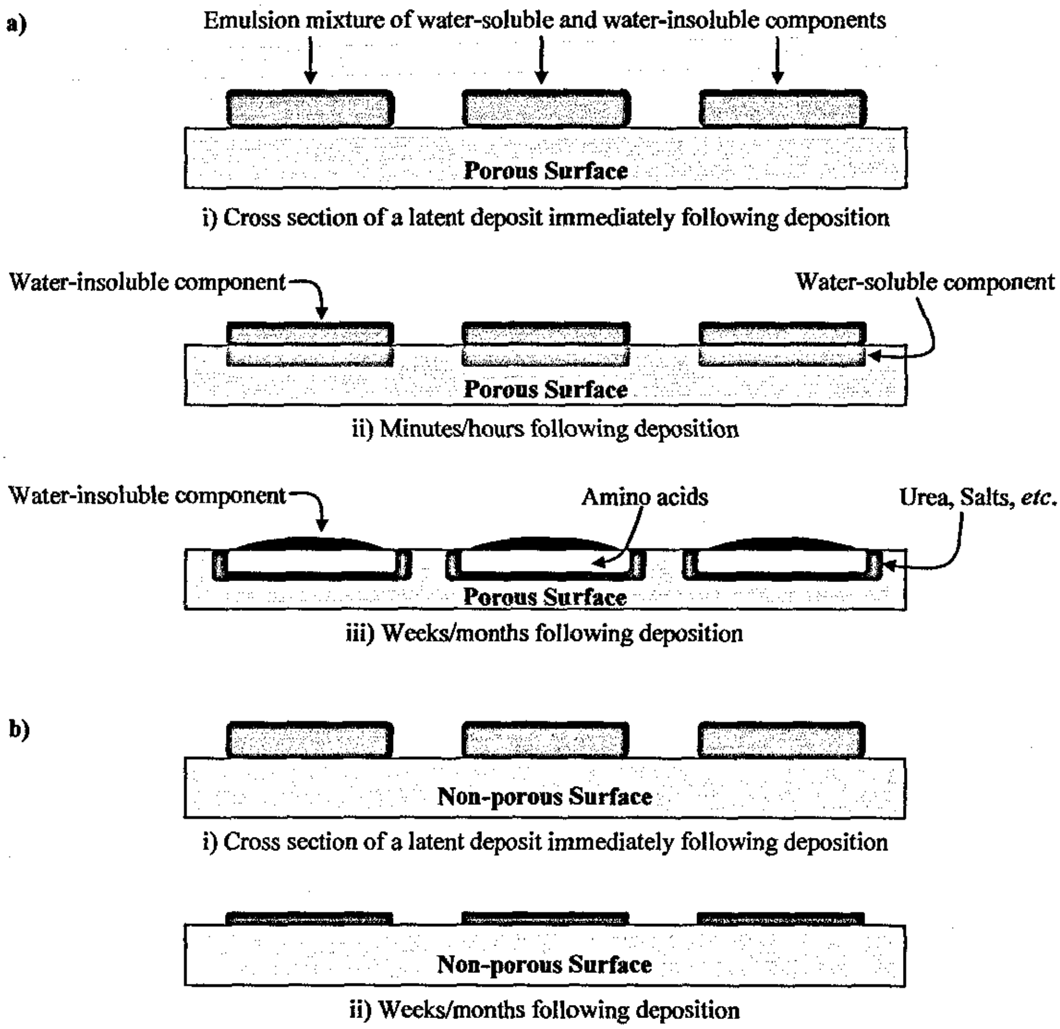

Figure 10 – ***Schematic representation showing the ageing of a latent fingermark on a porous surface (a) and non-porous surface (b).***

Adapted from Champod et al. [116]

1.3.4. Detection Techniques

As discussed earlier in this Chapter, the constituents of the latent fingerprint can, and do, vary dramatically. This issue, along with the fact the deposit is invisible to the naked eye, mean that detection techniques must be broad, and provide the user with the potential to detect prints on a wide variety of surfaces, in a mixture of different environments and with maximum ease. The presence of a specific chemical in a fingerprint depends not only on the constituents of the original print, but also the nature of the surface, storage conditions and elapsed time. Furthermore, air, light, heat and moisture exposure have the potential to alter both the physical and chemical nature of the latent deposit, thus further complicating detection protocols.

Characteristically, as the aqueous component (water) is the first to be lost from the fingerprint, samples older than several days are not suitable for detection processes that primarily rely on the presence (and detection) of water. In such instances, fingerprint enhancement success is augmented by the utilisation of processes that are sensitive to fatty components.

This said, it immediately becomes evident that fingerprint detection is far from straightforward and it becomes almost impossible to predict the most suitable and effective process to develop latent fingerprints. Considering the exact nature of a fingerprint is unknown prior to examination, it is quite common that two or more individual processes may be used sequentially to increase the chance of success.

Currently, three main types of detection techniques exist in order to help visualise a latent fingermark: optical, chemical and physical. Although an extensive range of techniques are currently at the disposal of the forensic scientist, some are considered much more useful and important than others and will therefore be outlined in more detail below.

1.3.4.1. Optical Detection

Optical detection techniques are non-destructive and especially favourable if other analyses are to be conducted on the sample in question (DNA screening, age identification, *etc.*). Thus, optical enhancement always precludes any secondary fingerprint development technique and is often also used following other techniques with the aim to improve resolution and clarity of the enhanced print.

In the simplest case, observation of the 'contaminated' area under plane polarised white light, can occasionally show a fingermark that is then able to be photographed and need no additional treatment. In situations where there may be trace amounts of coloured contaminants on the fingers (such as blood), absorption imaging may be used. The advantage with such a technique is that illumination of the sample can be adjusted and fine-tuned so that absorption peak of the contaminant is in strong contrast to the sample surface, thus facilitating visualisation. Blood, for example, has a sharp absorption peak at 415 nm and is often easily detectable on most surfaces, using appropriate interference filters.[119, 120]

Research by Dalrymple *et al.*[121] indicated the premise of laser interaction with latent fingermark deposits on non-luminescent substrates. Although more recent attempts have proven successful to some extent, the lack of a high success rate and the cost of the laser units themselves, does question their functionality in modern forensic scenarios. Nonetheless, fingerprint contamination from naturally occurring luminescent materials does allow such techniques to yield positive, identifiable results.

Another optical property of latent fingermarks is their ability to diffusely reflect light; this is most easily observed on smooth, shiny, non-porous surfaces, such as glass. In such instances, the use of oblique lighting (similar to the episcopic coaxial illumination setup)[122] can occasionally reveal latent fingerprint deposits and often can further enhance those already developed by alternative processes.

The last main optical detection technique is that of Ultraviolet (UV) imaging. This technique is based solely on the UV absorption difference between the surface and the fingerprint. Typically, surfaces will absorb or reflect UV light whereas the latent print may exhibit a mixture of diffuse reflectance and absorbance. The result of such UV exposure is an image where the print ridges appear light, with a contrasting dark background, or *vice versa*. To help justify such observations, Johnson[123] and Fraval[124] found that the amino acids, tyrosine and tryptophan, are responsible for most UV luminescence from finger sweat residues. Owing to its low cost and ease of use, UV imaging is commonly employed in some forensic laboratories, however its main limitation is the time required to search an exhibit because it is not a 'self-imaging' technique; often several hours are spent on just a small sample.

1.3.4.2. Detection Techniques for Porous Surfaces

Following optical examination, the use of further development methods will depend whether the sample has been wet (wetted). In such cases, the WSD will have been removed and the analysis process limited to the use of Physical Developer. Physical Developer (PD) is a silver based aqueous reagent that reacts with sebaceous residues, forming a dark grey silver metal deposit along the fingerprint ridges. The process was developed in the 1970s by the Atomic Weapons Research Establishment (AWRE),[125] and is one of the most commonly used fingerprint development techniques in the world; typically on paper type samples. Although there is still a lack of understanding as to why the PD can selectively develop latent fingermark deposits from porous media,[116] there is a clear explanation pertaining to the reaction mechanism involved in generating the silver metal atoms (see Equation 4). The PD solution comprises a mixture of Ag ions, a ferro/ferri redox system, a citric acid buffer, and a cationic surfactant.

$$Fe^{2+}_{(aq)} + Ag^{+}_{(aq)} \rightleftharpoons Fe^{3+}_{(aq)} + Ag^{0}$$

Equation 4 – ***The redox reaction involved during the Physical Developer process.***

The first stage of the reaction involves reduction of Ag^{+} to Ag^{0} through oxidation of Fe^{2+} to Fe^{3+}. As a low pH is required, the citric acid is required to complex with ferric (Fe^{3+}) ions. The necessity for a surfactant is to regulate and limit the amount of Ag^0 agglomeration and premature deposition. Thus, Ag^0 particles are 'trapped' within positively charged surfactant micelles, and are able to repel any further Ag^+ ions in solution.

The use of PD on previously wetted samples means it is of tremendous use in many circumstances, however its application is limited solely to porous surfaces. Additionally, developing times can exceed periods of one hour and the solutions themselves are delicate and time-consuming to prepare, as well as being quite expensive. Its major drawback, however, is that the detection process is considered destructive, as documentation evidence is permanently stained. Furthermore, typed or written text can often suffer from ink running, and no further fingermark treatment is possible. Regardless, PD enhancement is still the only choice for wetted porous samples, and its reasonably high sensitivity makes it more suitable than other techniques, often discovering some latent marks where other techniques (ninhydrin, DFO) have failed.

Perhaps the most universally well known detection technique for paper surfaces, however, is ninhydrin. Ninhydrin, discovered in 1954,[126] is a chemical reagent that readily reacts with amino acids, proteins and peptides (as found in the eccrine component of latent fingerprints) to yield a deep purple coloured product, referred to as Ruheman's Purple (see Figure 11). As ninhydrin is a non-specific amino acid reagent, it is able to cumulatively react with all primary and secondary amine components within the latent residue and thereby 'build' the Ruheman's Purple deposit along the print ridges.

Ninhydrin formulations are solvent based and treatment generally involves dipping the items of interest in ninhydrin 'baths' and leaving the prints to develop for 24-48 hours. The developing time can be decreased through the use of a humidity chamber, but even then, some prints can take up to several weeks to fully materialise. Problems arise during the use of ninhydrin because of its need for a carrier solvent. Similarly to PD, it often becomes a destructive technique when dealing with typed/written documentation where ink running becomes a problem, and it is also known to interfere with samples requiring indentation analysis (ESDA).

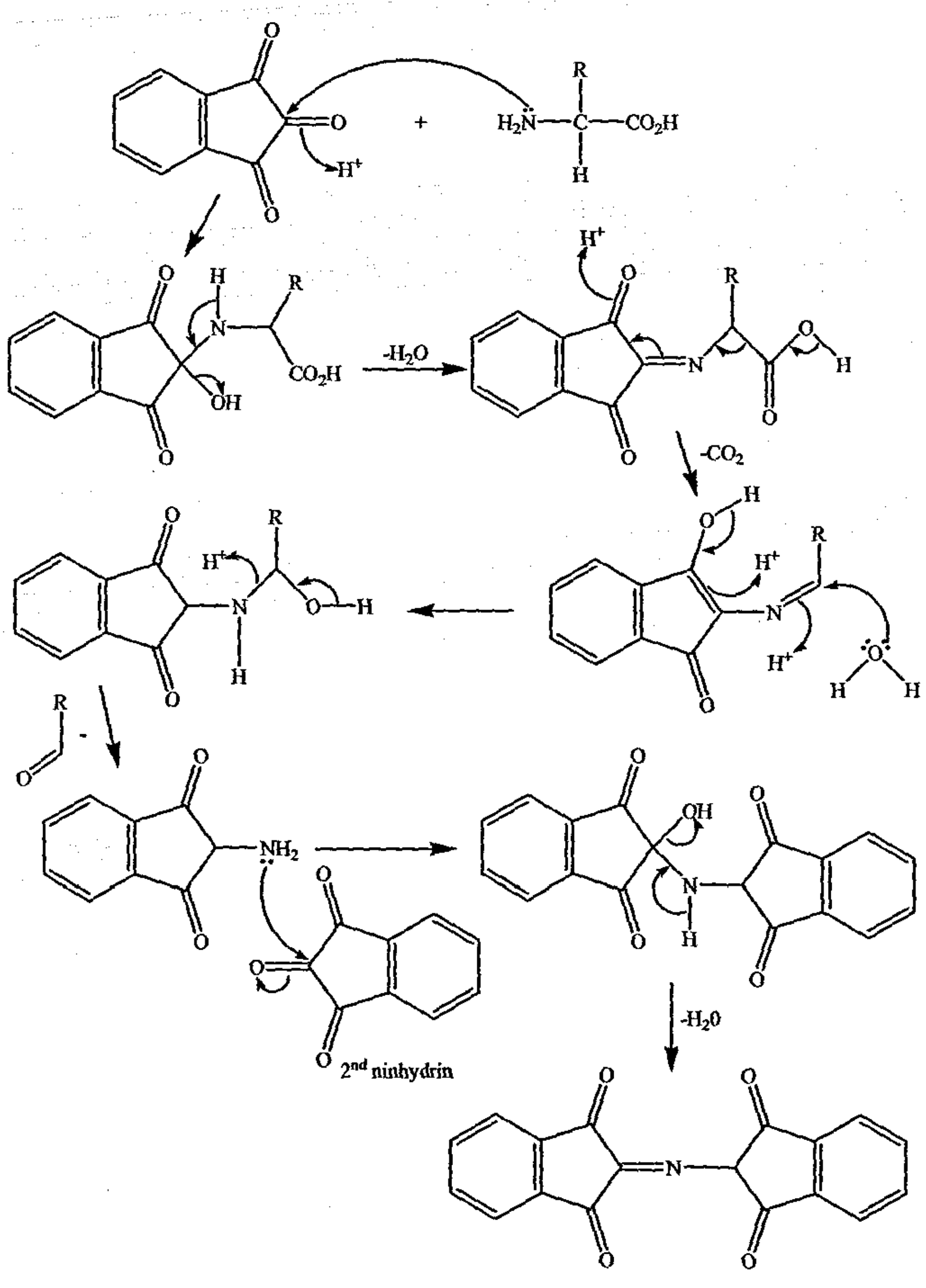

Figure 11 – ***Mechanism for the reaction of ninhydrin with an amino acid.***

Although some suitable solvents have been proposed and used successfully in the past, namely 1,1,2-trichlorotrifluoroethane[127] (generically Arklone P and Freon 113) and dichlorofluoroethane[128, 129] (generically Genesolv 2020 and Genesolv 2000), the harmful ozone depleting effects have rendered them obsolete. Current convention has suggested hydrofluoroether (HFE), 1-methoxynonafluorobutane (HFE7100) and 1,1,1,2,3,4,4,5,5,5-decafluoropentane as suitable alternatives to the CFC and HCFC based solvents, with research suggesting equally good, if not better, results.[130, 131]

Unfortunately, the only limitation of such solvents is their high cost and this can often restrict their use in some laboratories.

Treatment of ninhydrin enhanced fingermarks with a secondary metal salt, typically zinc or cadmium, leads to further enhancement of the print. The coordination complex that forms results in a colour change and provides a print that can appear luminescent under appropriate conditions.

More recently, ninhydrin analogues have become an important focal point, with the aim to produce compounds that improve fingermark detection through having a good initial colour, a wide solubility range, superior luminescence properties and a low cost.[132] Whilst there are a wide variety of new ninhydrin analogues (benzoninhydrin and 5-methoxyninhydrin, for example) that have been developed, and currently undergoing operational testing,[133] ninhydrin itself is still the preferred method across the forensic community.

In a similar manner to ninhydrin, the compound 1,8-diazafluoren-9-one, or DFO (see Figure 12), was developed and has since become a very effective fingerprint detection reagent for paper and other porous surfaces. DFO is very sensitive to amines and reacts with amino acids in a similar manner to ninhydrin, producing a pale purple product along the fingerprint ridges, that can only be developed with the presence of heat. The developed print has a superior property to its ninhydrin sister in that it is highly luminescent at room temperature without any additional treatment.[134] The development process itself requires the exhibit to be dipped in DFO solution (similar carrier solvents to ninhydrin), dried, and heated at temperatures between 100 and 160°C, until the print develops (between 30 seconds and 30 minutes).[135] Again, the use of solvent based systems does impede on the variety of samples suitable for DFO treatment and work involving a 'solid state' application of DFO ("DFO-dry") has proved promising.[136]

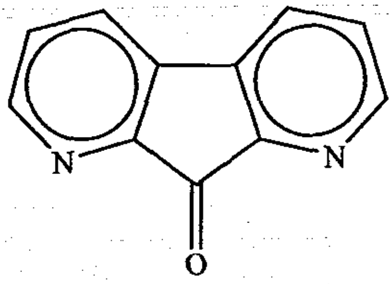

Figure 12 – ***Structure of 1,8-diazafluoren-9-one, DFO.***

It is believed that the sensitivity of DFO over ninhydrin can, in some situations, reach as high as three times that of the latter. That said, the expense of DFO solutions, the inability to obtain fingerprint contrast from fluorescent backgrounds (as fluorescent imaging is required) and the fact that prints can often develop if samples are handled following DFO exposure, mean that there are still disadvantages that need to be overcome.

Another technique that provided promise upon its discovery in 1989 is multi-metal deposition, or MMD.[137] MMD is a two-step procedure that initially involves the sample being soaked in an anionic colloidal gold suspension, that initiates Au adhesion to any cationic organic moieties within the fingermark deposit. Although, at this stage, any visual enhancement is minimal, further treatment with Modified Physical Developer (MPD) solution allows elemental silver to precipitate over the gold nano-particles, resulting in a deep grey/black coloured fingerprint. Owing to the high expense of the consumable reagents and other disadvantages comparable to PD, MMD treatment is often dismissed, with preference to PD at the end of the detection sequence.

There is a small variety of other detection techniques available for porous type surfaces, and indeed those that have some success on both porous and non-porous substrates; however, those discussed above are by far the most commonplace and effective.

There are often small variations on the global scale relating to the proposed detection sequence, or process selection chart, for porous surfaces. A typical example, however, of a simplified guide is summarised in Figure 13.

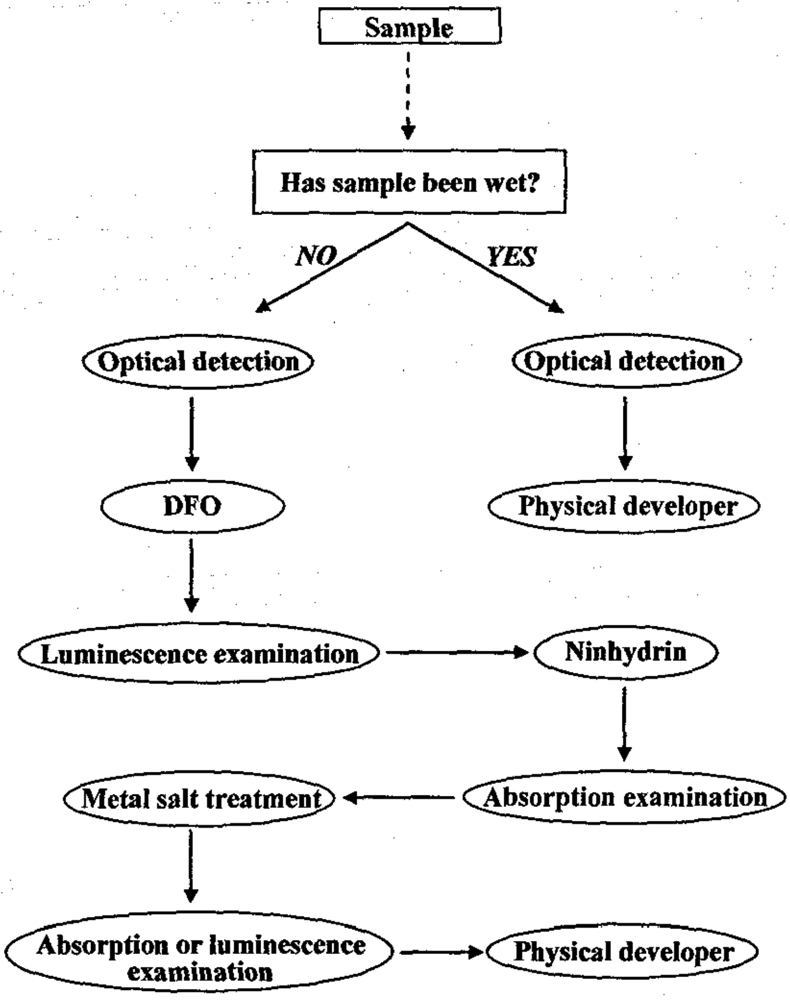

Figure 13 – ***Recommended detection sequence/process selection chart for fingerprint contaminated porous surfaces.***
Derived from Champod et al.[116] *and PSDB*[120]

1.3.4.3. Detection Techniques for Non-Porous Surfaces

Following optical examination, in a similar manner to those described previously (Section 1.3.4.1 and 1.3.4.2), there are certain non-porous substrate specific fingerprint detection techniques available to the forensic examiner. Largely, such methodologies depend on the texture of the non-porous surface that the latent print is believed to be adhered to; smooth surfaces often requiring different primary treatment to rough surfaces.

In general, the most mainstream method used, especially for fixed surfaces at the crime scene itself, is powdering. Fingerprint powders have been used in fingerprint detection since the early 20th century[117] and although their formulations and composition have been widely explored, 'argentoratum'[138, 139] (aluminium powder with a suitable binder) is the preferred choice. Indeed, comparison testing examining various different powders concluded that the former was the most effective medium for detecting latent deposits on non-porous surfaces.[140] It has been suggested, however, that the selection of the fingerprint powder for each individual use must ensure there is no chemical reaction, or high natural affinity, between the powder and the surface itself.[117]

The powdering process relies primarily on the adhesion properties of the powder to the 'wet' components of the latent residue (often sebaceous constituents) and hence can only be considered if the sample is dry. Powder is applied using a fine brush that is swept over the surface, eventually resulting in visualisation of the fingerprint itself. The development of suitable adhesive tapes and gels has meant that powder developed fingerprints can be 'lifted' from the site of their initial deposit and taken back to the laboratory for data storage and further analysis.

Unfortunately, in spite of the relatively low cost and ease of use regarding fingerprint powders, their function has low sensitivity and often only fresh, recently deposited fingermarks can be detected due to drying out of the sticky residues that form the adhesion centre for the powder. Additionally, the actual act of applying the powders in the conventional manner can sometimes lead to partial, or total, destruction of the fragile latent residue, through mechanical friction, that often leads to difficulty in print identification.[141, 142] To overcome this, more recent developments have concentrated on magnetic powders that do not require any physical contact during application. Here, the powders have a coarse iron particle content that serves as a carrier for the non-magnetic matrix (kaolin, for example) thereby mimicking a 'brush'. The introduction and withdrawal of a magnetised steel rod helps control the deposition and removal of the charged powder and thus enables prints to be developed with greater operator control.

Luminescent powders have recently become an important advancement, as they aid with fingerprint detection on multicoloured or highly reflective surfaces, where more conventional formulations may struggle. Such powders are composed in a typical manner, but contain a small percentage of natural or synthetic compounds that fluoresce or phosphoresce when exposed to UV light or laser. Menzel *et al.*[143, 144] have since developed complexed lanthanide containing powders, instead of the organic derivatives, that offer increased luminescent life-spans and much narrower emissions. Additionally, such powders have proved to have some degree of functionality across more problematic surfaces, such as wood and polythene.

On similar principles to fingerprint powders, a wet suspension method is currently in place that is able to develop prints, with reasonable success, on rough and smooth, non-porous surfaces. Small particle reagent, as it is known, is commonly a fine suspension (nearing a colloid) of molybdenum disulfide, MoS_2, that reacts chemically with fatty, sebaceous residues of the latent fingermark, and results in the formation of a grey coloured deposit that defines the ridge pattern of the fingerprint.[145] Although it is a quick and simple, sensitive technique, it performs best on samples that have not aged. In a similar manner to ninhydrin and DFO, the method requires dipping of the sample in a molybdenum disulfide solution, and this can lead to problems analogous to those discussed previously; although a spray application is available, its sensitivity is significantly reduced. Small particle reagent is advantageous as it can be applied to wetted samples; something that is uncommon to many fingerprint detection techniques.

On darker backgrounds, MoS_2 deposits are often hard to detect, failing the use of luminescent additives to the original mixture.[146] The suggestion of a white coloured zinc carbonate small particle reagent mixture does allow dark surfaces to be studied with higher resolution and clarity, and is used when circumstances permit.

Unfortunately, enhanced prints obtained from small particle reagent exposure are easily damaged and must be lifted or photographed immediately for longevity. The application of the reagent mixture as an aerosol or spray is extremely messy and often unfavourable in certain scenarios. The solvent based nature of the reagent means that it is considered a destructive technique where written or printed documentation is concerned, and therefore must be conducted after any other analysis has been performed.

Aside from powdering procedures, the most commonly practiced fingerprint development technique on non-porous surfaces is that of cyanoacrylate fuming, or "Superglue" fuming. Alkyl-2-cyanoacrylate ester (see Figure 14) is a colourless, monomeric liquid that is able to sublime when heated to temperatures of *ca.* 120°C. It is believed that the vapour selectively reacts with sebaceous and eccrine components of the latent ridge deposit, inducing a polymerisation process that affords a hard, white, polymeric solid: polycyanoacrylate. No reaction occurs within the fingerprint furrows, and thus a clearly visible ridge pattern results.

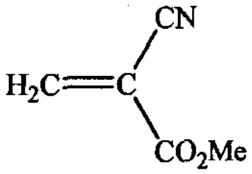

Figure 14 – ***Structure of cyanoacrylate.***

The fuming procedure is very sensitive to its environment. Often, fuming chambers are used that enable the atmosphere to be controlled and maintained, allowing optimisation and accurate repeatability. Typically, atmospheric pressure, normal room temperature and a relative humidity of 80% are considered appropriate for fuming processes. Lower humidity environments still give rise to polycyanoacrylate enhanced fingerprints, but they tend to be weakly developed. It has been suggested[120] that the high humidity is important as it allows any hygroscopic chlorides present in the print deposit, the opportunity to absorb water and initiate polymerisation of the monomeric cyanoacrylate vapour. It is often essential, however, to apply a fluorescent dye and utilise subsequent fluorescence examination to enhance the maximum number of fingerprints.

The versatility of cyanoacrylate fuming and its sensitivity to latent deposits makes it a fundamental tool in fingerprint analysis. Nevertheless, its sensitivity to aqueous traces means that it is a procedure that cannot be used if the sample has been, or is thought to have been, wetted; as uniform cover and saturation with polycyanoacrylate will result. The toxicity of the vapour itself (eye and respiratory irritant) means that user exposure must be limited, and expensive fuming chambers with extraction systems must be purchased for use in the laboratory. Portable fuming devices are currently available; typically a 'fuming wand' that involves the heating of a cyanoacrylate filled cartridge that delivers the vapour through a front facing aperture (similar in design to a butane torch).[147] However, such devices are often difficult to control and the results they provide are far inferior to conventional fuming chambers.[148]

In an effort to decrease fuming time and increase print definition, vacuum cyanoacrylate (VCA) fuming chambers have been developed.[149] It was found that although cyanoacrylate is easier to vaporise, and despite its claims at providing a more uniform coating across the sample surface, the visibility of the resulting prints is weak and further enhancement is always required (typically luminescent staining followed by scanning electron microscopy). Such requirements have spurred large debate concerning any added benefit VCA fuming actually holds over conventional cyanoacrylate fuming. Its main advantage is the fact samples do not need to be suspended above the cyanoacrylate source, as they will be under vacuum, but trials have found the technique, as a whole, to be significantly worse than the traditional method.[120]

More recently, a technique known as Vacuum Metal Deposition, or VMD, has become increasingly prevalent. VMD is arguably the most sensitive technique in current practice and is particularly useful at recovering prints from older non-porous artefacts. The process works on the assumption that fingermark contamination on a surface has the capacity to hinder homogenous deposition of metallic films, from the vapour state.[150, 151] Under high vacuum, elemental gold is evaporated and readily able to pass around the chamber containing the sample, where it deposits as a fine nano-layer, invisible to the naked eye. This gold film is uniformly spread across the whole sample and is able to penetrate the fingermark deposit, in a way that other metals cannot (zinc and cadmium, for example). A second metallic layer, this time in the form of zinc, is deposited in a similar manner, with a preference to condense on the exposed gold surface, and not under the fingerprint ridge residue. As a result, the fingerprint ridges are left essentially transparent whilst the background and fingerprint furrows become highlighted in grey coloured zinc; this phenomenon may be referred to as 'negative marking', where the ridge pattern itself is not being enhanced and viewed, but instead it is the background enhancement that gives rise to the observation of the print. It is thought that the primary mechanism for this technique centres around a variation in the size of the deposited gold nuclei, which, itself, depends on local variations and disturbances in the surface chemistry/topography of the sample. Processes involving the metallic nano-layer build up on the actual fingerprint ridge itself have been encountered,[152, 153] but their mechanism and reasoning is still unknown.

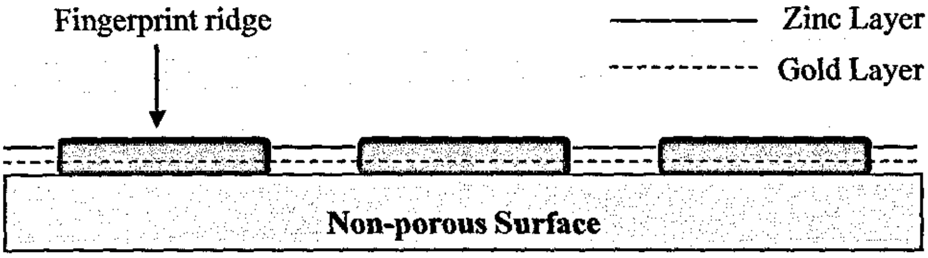

Figure 15 – ***Schematic representation showing the principle of fingerprint development by vacuum metal deposition.***

Although VMD is such a sensitive technique, each individual case results in differing levels of enhancement clarity. Although the conditions can be optimised and a constant environment established, pre-treatment of samples with a complementary process is occasionally required. The method of choice, in such circumstances, is that of cyanoacrylate fuming, particularly when polymer coated exhibits are to be analysed.[154, 155] Despite its benefits, there are drawbacks to VMD fingerprint detection processes: the extremely high initial cost of the apparatus and the necessity for experienced operators to perform analyses immediately restricts the remit. In reality, VMD enhancement is reserved for use on major cases, where all other viable techniques have not proved fruitful. The method of preference, in general, is cyanoacrylate fuming, coupled with luminescence staining; with VMD taking precedence for wetted and/or older samples.

Other non-porous latent print detection procedures are well known, but their use has become less common following the advancement and superiority of results, techniques such as VMD and cyanoacrylate fuming have given. Sudan Black and

Gentian Violet are both dyes that stain fatty constituents of the latent print.[120] Although not used on a regular basis, both of these techniques are excellent for recovering prints where the deposit contains a high percentage of sebaceous content. Gentian violet is especially useful for enhancing prints on the adhesive side of tapes.[120, 156]

In a similar manner to the treatment of porous surfaces, there are often small variations on the global scale relating to the proposed detection sequence for non-porous surfaces. A typical example, however, of a simplified guide is summarised in Figure 16.

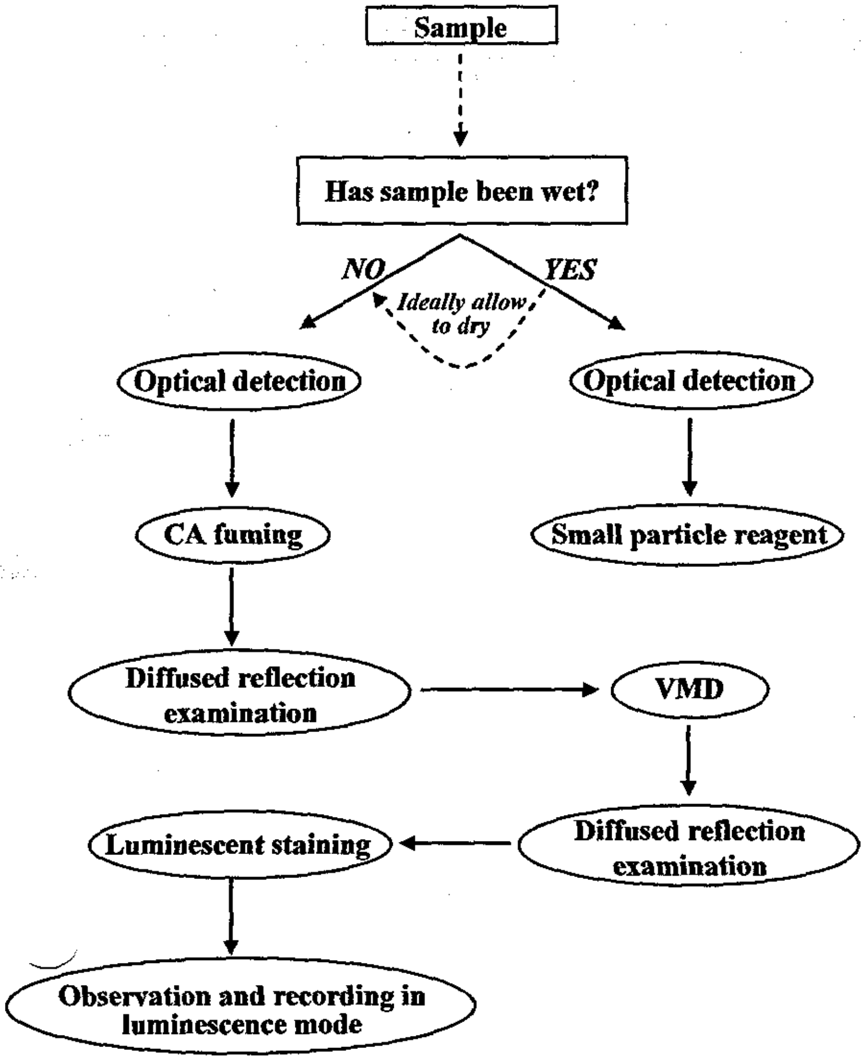

Figure 16 - ***Recommended detection sequence/process selection chart for fingerprint contaminated non-porous surfaces.***

Derived from Champod et al.[116] *and PSDB*[120]

1.3.5. Problematic Surface Types and Recent Advances in Fingerprint Detection

There is often a misconception that fingerprint detection techniques are so well developed that there may be a lack of requirement to develop further/alternative methods for enhancing fingerprints. In fact, on the contrary, fingerprint development advancements are constantly being developed with the aim to allow more facile analysis and increased sensitivity of the latent print. Some traditional methods (ninhydrin, cyanoacrylate fuming, DFO, *etc.*), although successful, can be time consuming and often lead to degradation of the sample, thereby inhibiting any further analysis. Less destructive techniques however, such as powdering or VMD, either suffer from decreased sensitivity or extremely high initial cost outlays, respectively.

Recent work across the forensic community has concentrated on the development of novel fingerprint detection methods to serve as stand alone variants, or supplementary techniques to those in current practice. Although extensive operational trials are required before new developments can be used in the laboratory, this new wave of detection techniques has the ability to strengthen the forensic arsenal.

The naphthoquinone, Lawsone (2-hydroxy-1,4-naphthoquinone), has recently been found to react with amino acid components of latent fingerprint residues on porous surfaces, such as paper, to afford a purple-brown stained ridge pattern that has photoluminescent properties.[157] Similarly, another novel dyeing agent, in the form of eosin-blue, was discovered to have comparable fingerprint developing capacity, on porous surfaces, to DFO and ninhydrin.[158] The advantage of eosin-blue over other commercially available fingerprint dyes is its extremely low cost and non-toxicity. Ninhydrin analogues themselves are becoming increasingly popular as sensitivity and print clarity can be 'fine tuned', and adaptation can be made for specific background and surface textures.[133]

Alternative fuming techniques are also being developed. Hirano and co-workers[159] have developed a process that involves the sublimation of two different dyes to enhance visualisation of latent fingermarks, up to several weeks old, on both white or clear non-porous surfaces. Separately, the two dyes, 1-amino-2-phenoxy-4-hydroxy-anthraquinone (red/purple in colour) and 1,4-bis(ethylamino)anthraquinone (blue in colour) are mixed with carbon, to ensure a constant burn, and kneaded into a type of incense stick before being lit. The sublimate is then readily able to interact with the sample suspended above it and preferential deposition of the dye molecules along the fingerprint ridges can be observed. Although the procedure is successful on its own, prior treatment *via* cyanoacrylate fuming yields significantly better enhanced prints; presumably the result of selective dye adhesion to the polycyanoacrylate.

Within the last ten years, research has also concentrated on characterisation of lipid components within latent fingermark deposits and their separation using thin layer chromatography (TLC).[160] This research has facilitated additional lipid-specific techniques to be developed, especially for use on currency, such as lanthanide-based developers[161] and iodine vapour,[120] where fixation of the print with α-naphthoflavone is required.

A new multi-metal-deposition (MMD) process has recently been proposed for use on a wide variety of substrates, although its current application is limited to glass samples only. The scanning electrochemical (SECM) imaging of MMD-enhanced latent fingermarks, described by Champod *et al.*,[162] develops fingermarks through the nano-layer deposition of gold, followed by silver. SECM is then used, with an $IrCl_6^{3-}$ redox mediator to detect the dissolution of silver, in the feedback mode. Consequently, high resolution images of the latent fingermark can be obtained.

Unfortunately, although the general composition of a latent print is known and chemical specific reagents/techniques can be used, it is quite common for fingerprint development techniques to be discovered through serendipity. The random mixture of latent residues and the constant introduction of novel materials and surface types means it is very difficult to predict what reagent, compound or process will have the desired results. There are still some everyday surfaces unable to render any successful fingerprint definition, despite the tens of different techniques currently known.

Perhaps the most important surfaces that, at present, elude detection techniques are that of fabrics, such as cotton, and low density polyethylene plastic wrap (or Clingfilm).[120] Fabrics are essential in the forensic sense as they can hold important fingerprint details from suspects. The only technique ever proven to yield successful fingerprint development of such surfaces was that of radioactive sulfur dioxide fuming. Radioactive sulfur dioxide dissolves in trace amounts of water present in the latent fingerprint. Subsequent autoradiography screening allows the visualisation of the print, however the definition is often very weak and screening itself can take several weeks. Radioactive SO_2 treatment has since been ceased due to its extremely high running costs, lengthy turn-around times, inapplicability on wetted samples, and inherent hazardous nature. There is yet to be a process to supersede it.

Plastic wraps can also hold vitally important evidence, especially in drug crimes where substances are often wrapped. In such circumstances, some techniques have the potential to give successful results, such as Sudan Black and Small Particle Reagent processing. However, these procedures rely on the chemical presence of fatty components. Often, drug wraps are washed with ether to remove traces of cocaine powder[115, 163] and, in doing so, the fatty components of the latent print are removed. There is no technique available, at present, that is able to develop fingerprints from plastic wrapping, following ether washings.

The final group of surface types that are problematic to the forensic scientist are those that have experienced intense heat exposure. The destruction of artefacts as a result of fire damage, from arson scenes, or intense heat evolved from the discharge of a firearm, for example, can lead to a myriad of problems for any required fingerprint detection. Until very recently,[164] there has been very little published concerning the recovery of fingerprint evidence from arson scenes and insufficient analysis of temperature induced destruction/decomposition of the latent print itself.

Although arson scenes have the additional problem of soot build up on the surface in question (that requires removal through other methods),[164] direct exposure of the latent print to a heat source is believed to cause degradation through volatile component loss and decomposition. Any volatile constituents in the latent deposit can be reasonably estimated to volatilise away from the deposit itself. Additionally, thermal decomposition of chemicals is common, thus rendering many chemical specific detection techniques inadequate for print enhancement. It has been suggested[164] that prints can be recovered from environments where temperatures have not exceeded 200°C, with a mixture of conventional methods. In situations where temperatures have exceeded this range, and presumably destroyed all organic content of the print, the only likely successful detection method remaining is VMD. In many examples, however, at best, only low resolution prints can be detected and many exhibits remain elusive for fingerprint development.

Perhaps a fundamental necessity in the field of fingerprint detection and development is a single, inexpensive technique that is able to visualise latent prints on both porous and non-porous, rough and smooth surfaces, without the need for extensive preparation or development time. Techniques that offer print detection on fabrics, plastic films and heat exposed surfaces are, of course, very much desired and until such advancements occur, there will always be a limitation to the variety of exhibits viable for print development. The applicability of new methods to analyse both dry and 'wetted' samples becomes pertinent, as most current techniques require the sample to have remained dry since deposition of the print. Such developments will allow the broad spectrum of current techniques to be consolidated into one main procedure, thereby reducing the requirement of complicated, multi-stepped and time-consuming processing sequences. In addition, there is, at present, no fundamental method of reversing any of the enhancement techniques in circulation. Once a fingerprint is developed on a surface through either physical, or chemical methods, there is no procedure/reaction available to remove the developed print from that sample. Accordingly, future work should also consider the potential of fingerprint development techniques to be 'reversible', or at least removable, following enhancement and appropriate data storage.

1.4. Characterisation Methods

During the course of this research, a broad range of characterisation techniques have been employed. Primarily, their role has served in both solvent and solid-state species characterisation, but three techniques in particular, that of Raman

Microscopy, Scanning Electron Microscopy (SEM), and powder X-ray diffraction (XRD), have facilitated more diverse and thorough observations to be ascertained.

Powder XRD has, for a long time, been used in the characterisation of solid state materials, where other methods, that typically require dissolution of the compound of interest, have failed. It is for this reason that most insoluble microporous materials (zeolites, sodalites, *etc.*) are identified through powder XRD analysis. The only significant prerequisite that is required in order to allow successful powder XRD patterns to be obtained, is a reasonable level of sample crystallinity. Sufficiently crystalline samples may range between anything from large individual crystals that will require gentle grinding so as to induce a 'powder' suitable for analysis, to polymicrocrystalline 'powders' that can be used in their native state. Sample preparation for powder XRD is often fairly straightforward and involves the packing of the powder, typically no less than 100 mg, into a flat plate sample holder, ensuring a flat surface is exposed to the incident X-ray beam.

The XRD process itself, as its name suggests, relies on the diffraction of X-ray beams, provided from a sealed source, by the crystallites of the sample. The natural shape and molecular lattice properties of the crystals afford a unique diffraction pattern (digitised following collection of scattering radiation by the instrument detector) that may be analysed in several ways. The most commonly used tool in powder XRD characterisation is sample (or phase) identification based on database matching. Such processes match experimental XRD patterns with those currently stored in a digital library (International Centre for Diffraction Data or Cambridge Structural Database), and allow successful synthesis of a target material to be confirmed (similar to fingerprint matching). Novel compounds are often more difficult to fully characterise, however. Their XRD pattern will not be stored within any database and often complementary characterisation methods (such as single crystal XRD, NMR and elemental analysis) are required for full characterisation, and cross-referencing of data, to be successful. Should other characterisation techniques not be favourable for certain compounds, or in order to check the suitability of structural assignments suggested by other analytical processes, Rietveld refinement may be used.

Rietveld refinement was developed by Hugo Rietveld in the late 1960s and allowed the properties associated with individual X-ray (or neutron) diffraction patterns (such as peak location, height, and width) to be used in order to ascertain essential aspects relating to the materials structure.[165-167] The refinement procedure utilises a least squares approach to refine a theoretical predicted line profile until it closely approaches, or matches, that of the experimental data set. Although the process requires a good insight to the plausible crystal structure to be known in advance, the Rietveld refinement method is widely used within solid state chemistry.

Another significant benefit of powder XRD, within this research, is its ability to monitor phase change within samples.[94, 99, 100, 168] Many materials undergo some sort of physical or chemical variation when exposed to altering environments; whether that be heat, pressure or gaseous atmosphere alteration. Sequential XRD data collection enables a varying profile to be plotted, highlighting initiation and termination of phase change, as well as the introduction and/or reduction of side-products within the bulk sample.

Raman spectroscopy, or microscopy, is a form of vibrational spectroscopy that complements traditional infrared spectroscopy and is often used on solid state samples, that either lack IR activity altogether, or exhibit complicated overlapping IR active bands. Its application relies on a different type of induced vibrational harmonics; incident light, that is of lower energy than that typically required to promote a molecule into an 'excited' electronic state, may be absorbed by a molecule and instead create a 'virtual excited state'. Although the existence of such a virtual state is short, and most of the light is scattered across a 360° plane (Rayleigh scattering), the energy of a small proportion of re-emitted light can differ from the incident ray itself and correlate to functional vibrational modes. Stokes and anti-Stokes lines are present within the Raman spectrum through excitation of ground state molecules by lower or higher frequency incident light, respectively. Despite many samples being suitable for Raman analysis, dark coloured materials that inevitably absorb a large proportion of light, and samples known to fluoresce, thereby masking the Raman effect, are sometimes problematic, without the addition of Fourier-transform enhancement.

On the contrary to IR spectroscopy, it is not a change in electronic dipole moment that is required for Raman activity, but a change in the polarisability of the molecular bond(s). In basic terms, the polarisability of the molecule, or the individual bond within the molecule, is the ease with which the associated electron cloud may be distorted.

Raman spectroscopy is commonly used for low frequency molecular vibrational studies (typically < 400 cm^{-1}), where heavier metallic coordination is of interest perhaps. Additionally, and conceivably more pertinent to this work, the use of Raman spectroscopy for analysis of microporous materials is of particular interest. Within the extended, regular framework structure of many microporous compounds, the broad (alumino)silicate stretches (typically *ca.* 330-500 cm^{-1}, 500-615 cm^{-1}, 700-850 cm^{-1} and 1000-1250 cm^{-1}) swamp any attempted IR characterisation, and make the observation of certain functional groups, especially in the fingerprint region, extremely difficult. Despite having an IR active dipole moment about the $(Al)SiO_4$ tetrahedra building units, the polarisability of the bonds is negligible. Thus, Raman spectroscopy on the aforementioned samples will yield a spectrum, free of framework bands, and show Raman lines relating solely to templating molecules or guest species within the microporous solid. That said, it becomes apparent that the study of host-guest interaction and molecular exchange can be monitored with less difficulty, and the feasibility of in depth and conclusive characterisation, through a combination of Raman, XRD, IR, elemental analysis and NMR, can be ascertained.

The use of SEM analysis has enabled visual differences between samples (morphology and crystal size, for example) to be monitored and compared. SEM allows the surface of a sample to be viewed, following its bombardment with high-energy electrons. The interaction pattern and variability across a sample surface enables an image to be developed that can give an insight not only to the topography of the material in question, but also into any electrical properties associated with it.

Commonly, scanning electron microscopes have the ability to obtain good resolution at magnification levels exceeding x 250,000. Such high magnification ranges facilitates not only bulk sample morphology analysis, but also the ability to directly observe any small changes in crystal habit and nature between individual crystallites across an entire sample. Degradation properties associated with heat and/or vacuum exposure of compounds are of particular importance, as excessive environmental strain may induce partial/total decomposition, or cause other defects that may be of interest.

Additionally, SEM analysis may also be coupled with Energy Dispersive X-ray Spectroscopy (EDX). EDX is an analytical technique that can be used across a bulk sample, or on a specific part of a crystal, to investigate and ascertain elemental composition. The process relies on the emitted X-ray response of the sample composites, following excitation from high energy particle bombardment, to afford a spectrum that can be referenced against known excitation wavelengths. Such a process allows both SEM and EDX analysis to be performed, *in situ,* within the sample chamber, and results in reliable elemental compositional analysis, as well as useful structural determination and morphology studies.

2. Reactions of Tetrasulfur Tetranitride and Disulfur Dinitride with Zeolite Matrices

The synthesis of disulfur dinitride, S_2N_2, traditionally requires prior preparation, and subsequent pyrolysis, of the parent dimer molecule, tetrasulfur tetranitride, S_4N_4. Though various routes to the latter are known (see, for example, Reference 11), bulk syntheses affording yields greater than *ca.* 15 g typically follow those proposed by both Becke-Goehring[6, 9] and Villena-Blanco.[5]

With large yields of S_4N_4 required for both subsequent reactions and conversion to S_2N_2, the reaction flask used in the synthesis of S_4N_4 was cooled appropriately ensuring the temperature of the reaction mixture was not allowed to fall below 20°C. The primary purpose served through placing the flask into a cold water/ice bath was to prevent the temperature from rising high enough that appreciable amounts of solvent were lost *via* evaporation. In essence however, the heat of reaction itself will prevent the temperature of the reaction mixture from falling below 20°C, despite the water-bath temperature falling close to 2°C. Omission of the water bath meant that the flow rate of ammonia had to be significantly reduced in order to maintain the temperature below 50°C. Although possible in practice, complications arose concerning persistent build-up of solid mass (largely ammonium chloride) within and around the gas-inlet tube aperture, thereby causing detrimental blockages. The absence of water bath cooling surrounding the reaction flask provided a yield decrease of approximately 55%, when compared to cooled runs.

Preliminary chlorination of sulfur(I) chloride, S_2Cl_2, to sulfur (II) chloride, SCl_2, was readily achieved following the passage of Cl_2 gas through the liquid for *ca.* 10 minutes. It was important at this point to remove all residual Cl_2 gas from the flask as the subsequent passage of ammonia into the reaction mixture had the capacity to induce the formation of the explosive compound, NCl_3. Rapid bubbling of N_2 gas directly into the solvent for 5 minutes, followed by passage around the flask headspace ensured no visible green Cl_2 atmosphere remained. It was found that the direct use of SCl_2, compared to SCl_2 obtained through S_2Cl_2 chlorination, did not provide S_4N_4 yields of any greater purity or quantity, although reaction times were reduced owing to omission of the initial S_2Cl_2 chlorination step.

Literature experimental commonly describes the reaction mixture in such syntheses to become very thick and often difficult to stir. Although the use of an overhead mechanical stirrer helps alleviate some of these difficulties, it is advised that dilution of the SCl_2 with CCl_4 helps facilitate stirring. That said however, the addition of CCl_4 causes an appreciable fraction of the generated S_4N_4 to enter the organic phase. Consequently, the CCl_4 phase must then be worked up, as well as the crude precipitate, in order to optimise the yield. However, owing to the satisfactory yield routinely obtained from the solid phase alone, work-up of the solution was usually omitted.

In recent times, with CCl_4 becoming increasingly restricted and now of both rare commodity and high expense, analogous syntheses of S_4N_4 were attempted using chloroform as the organic carrier solvent. Obviously, as a result of its decreased boiling point and increased volatility when compared to carbon tetrachloride, considerably more chloroform was needed to help maintain the total solvent volume in the reaction vessel to approximately 1400 cm^3, during the course of the reaction. Furthermore, and perhaps more importantly, significantly more S_4N_4 enters the chloroform organic phase compared to carbon tetrachloride. Additionally, the crude solid product yield is negligible and work-up of the deep red/orange solution is required for respectable S_4N_4 yields to be obtained. Not only, however, are the yields from such syntheses smaller in quantity, there is also increased impurity content present, when compared to the S_4N_4 product obtained from using carbon tetrachloride as the organic solvent.

Recrystallisation of the crude solid material was not conducted as documented within the literature methods.[5, 9] The suggested purification through soxhlet extraction with refluxing dioxane has inherent explosive risks associated with it, owing to the nature of repeated purity extraction and subjection of hot solvent to progressively purer S_4N_4 samples. Consequently, the preferred method of recrystallisation used, involved addition of hot toluene (*ca.* 90°C) to small batches of the crude solid material in a conical flask.

Figure 17 – ***The apparatus used to prepare crude S_4N_4.***

Following constant stirring for several minutes, the deep orange/red solution was carefully decanted into a hot, empty wide-necked conical flask and slowly allowed to cool to *ca.* 40°C, with glass wool lagging. Whilst still warm, the remaining solution was decanted back into the original conical flask (for recrystallisation of another batch of the crude material) and the freshly crystallised bright orange S_4N_4 needles allowed to dry in air on filter paper.

The purity of the dry, recrystallised product was initially ascertained *via* 'controlled' detonation. Although initially perhaps resembling a rather obscure method of purity analysis, it is important to consider potential impurities that may be present within the S_4N_4 sample, and relate these to other characterisation methods readily available. With the main contaminant of such a synthesis being elemental sulfur, a non IR active impurity, simple IR analysis of the crude material compared to the pure recrystallised product affords much the same spectrum; that of S_4N_4 itself. Other, more time-consuming techniques, such as powder XRD may be used, assuming crystallinity of the sulfur impurity is good, and confirmation of trace sulfur content in some older S_4N_4 samples have been found through such methods. Routinely however, when comparing several samples of S_4N_4, the method of choice involves placing a small amount of the sample (*ca.* 2-5 mg) onto the back of a mortar and applying a reasonable amount of friction to it, with the use of a pestle (either grinding or striking the sample). Such a process allows its spontaneous disassembly to be observed. In syntheses where high sulfur contamination is present, even following recrystallisation, the detonation is weak and produces only a quiet 'cracking' type sound. Conversely, however, when sample purity is high, only minimal friction is required to obtain sample detonation, producing very loud sound and, interestingly, as captured on camera, a purple halo effect at the point/time of detonation (see Figure 18).

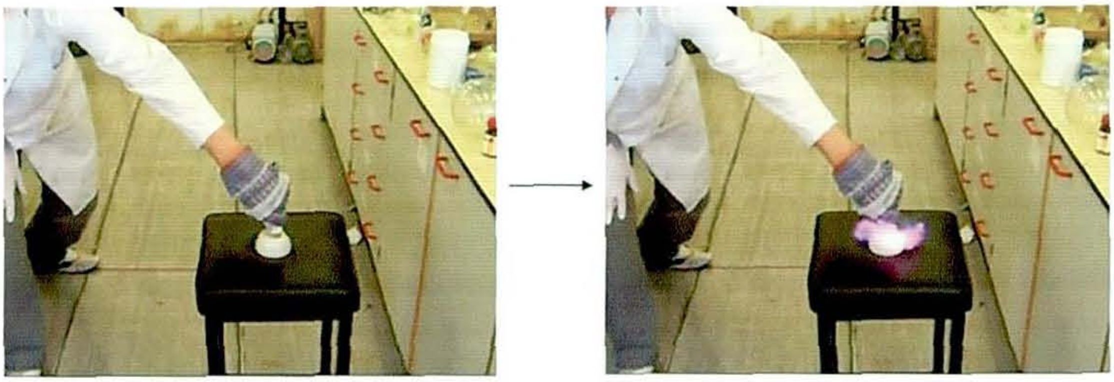

Figure 18 - ***Still frame images showing detonation of S_4N_4.***

The purple halo detonation effect is likely to be the result of the formation of various transient sulfur-nitrogen species, through disassembly of the S_4N_4 molecule itself. Likely intermediates may include the thiazyl monomer radical, SN·, as well as various other S_xN_y variants (namely S_2N_2), although the exact composition is unknown. Interestingly however, analysis of the detonation residue on the back of the mortar revealed a dark blue coloured circular area, initially thought to be $(SN)_x$, through colour alone. Subsequent IR analysis of this residue, along with detonation of S_4N_4 within the constraints of a sealed bag source and further IR analysis of obtained residues, were inconclusive in confirming such a hypothesis.

Further purity identification of recrystallised S_4N_4 samples can be achieved through Thin Layer Chromatography (TLC) analysis. Despite elemental sulfur being the major contaminant in S_4N_4 preparations, trace amounts of heptasulfur imide, S_7NH, are also known to form.[9] Following dissolution of S_4N_4 samples into CH_2Cl_2, TLC analysis using a 100% hexane eluent was found to provide good separation and resolution between S_4N_4 (yellow spot, $R_f = 0.19$) and any S_7NH that may have been present (colourless spot, UV active, $R_f = 0.87$).

As all S_4N_4 samples were required to be as pure as possible, elemental sulfur contaminated samples were progressively recrystallised, as before, until the impurity content was negligible. Minor contamination of S_4N_4 with S_7NH was best resolved by slurrying the sample in cold Et_2O for several minutes, to remove the imide impurity. TLC analysis of the resulting S_4N_4 sample allowed the purity to be monitored and repeated ether extractions were conducted as deemed necessary.

The use of S_4N_4 as both a direct reactant, as well as the precursor to S_2N_2, enables a myriad of chemistry to be investigated. Although solvent based S_4N_4 systems are commonplace, many solid-state applications inherently restrict the breadth of product characterisation. The desire to explore reactions and interactions of both S_4N_4 and S_2N_2 with various non-soluble, solid-state porous materials immediately highlighted the potential advantage of using an NMR active S_4N_4 species. Consideration that a ^{15}N labelled analogue of S_4N_4 could provide a useful insight into guest-host relationships was pertinent, although contemporary isotopic labelling methods may be considered inefficient.

Preparation of $S_4{}^{15}N_4$ using $^{15}NH_4Cl$ as the labelled starting material, and the formation of the $[S_3{}^{15}N_2Cl]Cl$ intermediate, has been shown to be feasible.[169] However, such a multi-stepped reaction, with extreme air sensitivity of the cyclic intermediate, coupled with problematic low-yielding syntheses, does not provide a facile, repeatable route to the target material.

Woollins *et al.*[19] have prepared the nitrogen labelled selenium analogue, $Se_4{}^{15}N_4$, *via* the introduction of a quantised volume of ^{15}N labelled ammonia gas, to a freeze-thawed diethylselenite solution, in a partially evacuated, sealed system. To date, however, the application of such a method for preparing $S_4{}^{15}N_4$, is unknown.

With the use of regular ammonia gas, as a test medium, modification of the aforementioned system was investigated (see Figure 19). Following extensive variation of the SCl_2 solubilising agent, it was found that optimal reaction conditions required a less volatile solvent: MeCN. Analogous reactions utilising solvents of increasing volatility, such as CH_2Cl_2 or EtOH, afforded the generation of NH_4Cl within the connecting tubing and headspace of the flask, prior to the ammonia gas actually entering/reacting with the SCl_2 solution. It is thought that the volatile nature of SCl_2 is more prevalent within a volatile solvent matrix, and as a result, despite the low temperature environment, vapour phase reaction of SCl_2 with the approaching ammonia gas arises in the headspace, instead of the solution.

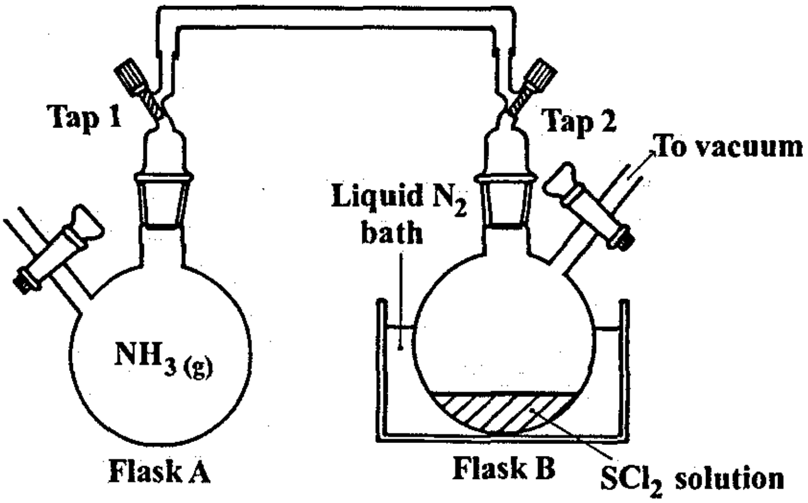

Figure 19 – ***Schematic representation of the quantised S_4N_4 synthesis setup.***

When MeCN is used, the SCl_2 solution must be frozen using liquid nitrogen and the vacuum within Flask B, and the connecting tubing, released by the opening of Tap 1. The ammonia gas is instantly pulled across into Flask B and becomes frozen above the SCl_2 solution. Removal of the liquid nitrogen bath allows the separated mixture to slowly warm to ambient temperature and the commencement of gentle stirring results in a vigorous exothermic reaction, producing a dark brown/orange mixture and NH_4Cl, which coats the glassware.

Conversely, when compared to the bulk synthesis of S_4N_4, such a small amount of product is likely to be dissolved in the solvent itself. Thus, work-up of the solvent, and the disregard of the precipitate, was required. Following repeated filtration through celite, TLC analysis on silica plates showed separation of two distinct species: S_4N_4 (yellow spot, $R_f = 0.18$) and SCl_2 (yellow-red spot, $R_f = 0.91$). Separation of the two materials was thought to be best achieved using a Bio-Beads Gel Permeation Column, which separates *via* molecular weight and size. Using CH_2Cl_2 as both the swelling agent and eluent the two products were readily separated and allowed to slowly evaporate to dryness, in air. The orange crystalline product was manually collected and pumped on to remove trace amounts of solvent. IR analysis confirmed the isolation of S_4N_4. Unfortunately, however, although showing good promise to be an appropriate small-scale and facile route to S_4N_4, and eventually $S_4{}^{15}N_4$, the procedure itself was found to have reproducibility flaws that render it inappropriate for use with expensive ^{15}N labelled ammonia sources.

2.1. Synthesis of TPA-ZSM-5, Na-ZSM-5 and H-ZSM-5

Once synthesised, the TPA-ZSM-5 zeolite contains the bulky tetrapropylammonium ion, trapped within the cavities. By transferring the product to a crucible and heating it in a box furnace at augmented temperatures, the tetrapropylammonium ion readily decomposes, affording propylamine and propene, to yield the sodium ZSM-5 derivative, Na-ZSM-5.

Often, catalytic or metal free investigation of ZSM-5 is required and it is thus necessary to obtain the acidic derivative that simply contains protons in the cavities of the zeolite, held close the framework structure through ionic attraction to anionic sites in the aluminosilicate structure.

$$\text{Na-ZSM-5} \xrightarrow{NH_4^+} NH_4\text{-ZSM-5} \xrightarrow{\Delta} \text{H-ZSM-5}$$

Equation 5 – ***The conversion of Na-ZSM-5 to H-ZSM-5.***

The reaction of Na-ZSM-5 with ammonium sulfate solution is an example of solution based molecular uptake, and in turn ion exchange, by a zeolite material, typical of that associated with molecular sieves. Ion exchange between the Na^+ and NH_4^+ cations results in the formation of the stable ammonium ZSM-5 intermediate. Prolonged heating of NH_4-ZSM-5 at 500°C induces decomposition of the ammonium ion, liberating ammonia gas, and provides the target material, H-ZSM-5 (see Equation 5). The inherent hygroscopic nature of ZSM-5 zeolites (and in fact many zeolite materials) means they must be stored in a thermostatically controlled oven at *ca.* 110°C, or dried at *ca.* 180°C for 24 hours prior to use.

As shown in Figure 20, comparison of the powder XRD patterns between TPA-ZSM-5, Na-ZSM-5 and H-ZSM-5 shows no decrease in sample crystallinity, despite extensive heating and cooling phases. In fact, sample crystallinity appears to initially improve following removal of tetrapropylammonium and again following conversion to H-ZSM-5 (as observed through the sharpening of all major reflections and an increase in reflection intensity). Additionally, progressive slight positive 2 Theta (2θ) shifts are evident when comparing the XRD pattern of each zeolite. Commonly, 2θ shifts occur when the unit cell volume/size changes within a compound, thereby affecting the reflected angle of the incident X-ray beam. Typically, positive 2θ shifts are the result of a decrease in unit cell volume/size and negative 2θ shifts are caused by increases in the unit cell volume/size. In the case of the homologous ZSM-5 series used here, the unit cell becomes smaller as the tetrapropylammonium ion is removed from the system, and again so following exchange of the larger Na^+ ions with smaller H^+ ions.

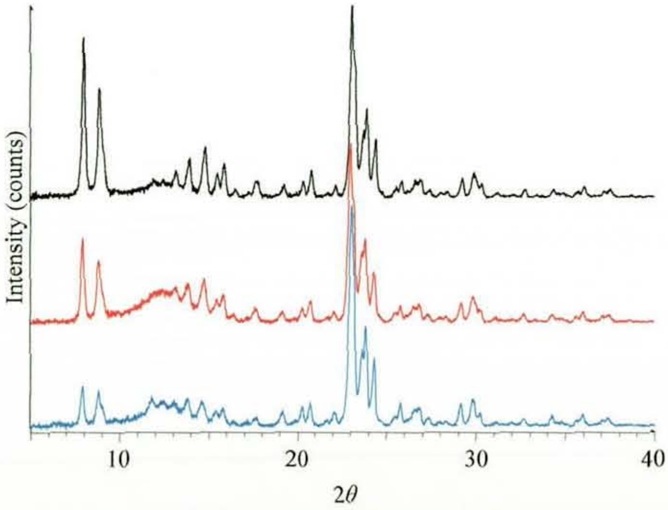

Figure 20 – ***Powder XRD comparison of TPA-ZSM-5 (blue), Na-ZSM-5 (red) and H-ZSM-5 (black).***

2.2. *Reactions of ZSM-5 zeolites with S_4N_4*

With a pore aperture of 5.1 x 5.5 Å, it is conceptually plausible to envisage molecular uptake and incorporation of a broad array of microscopic sized species into ZSM-5 matrices. Drawing reference to S_4N_4, the molecule itself has a diameter of approximately 3 Å, at its widest point, and is therefore theoretically able to fit into the channel voids of the ZSM-5 network. The ultimate intention to explore reaction and interaction chemistry of monomeric S_2N_2 with ZSM-5 matrices (see Section 2.3) made the S_4N_4/ZSM-5 system an obvious starting/reference point.

Initial work focused purely on solid-solid systems, where both reactants were used in their native solid state. Careful grinding of the two compounds predictably afforded an orange coloured homogenous powder and provided no definitive visible acknowledgement of a reaction, owing to the orange colour of S_4N_4 itself. The subliminal nature of S_4N_4 allowed the mixture to be heated, under vacuum, and any unreacted, excess S_4N_4 to condense and crystallise on the walls of the Schlenk, above the level of the oil bath. The zeolite product that remained was tan-orange in colour and closer inspection of the Schlenk itself interestingly revealed the formation of a collection of small white single crystals near the side-arm.

Unsure as to the origin or reason for the growth of these crystals, S_4N_4, H-ZSM-5 and Na-ZSM-5 were separately treated in an analogous manner (individually ground and heated under vacuum). This was done to eliminate the possibility of any unusual reaction impurity or side-product ($S_4N_4.nC_7H_8$, for example) being present in the starting material and presenting itself through sublimation. In each case, however, there was no evidence of any white crystal cluster growth.

IR analysis of the white crystals highlighted the presence of N-H stretches at approximately 3140 cm^{-1} and 1400 cm^{-1}. Although weakly diffracting, single crystal XRD proposed the unusual structure and presence of a disulfite group ($S_2O_5^{2-}$). Consultation with literature relating to such ionic moieties provided IR active stretches with good similarity to the data ascertained for these crystals.[170] The coinciding IR and XRD data,[171] suggest the structure and formation of ammonium disulfite, $[NH_4]_2[S_2O_5]$.

Such a product is surprising as it implies complete decomposition of the S_4N_4 molecule at some point of the grinding and heating stages, during its interaction with the ZSM-5 host material. Additionally, it is interesting to consider the origin of the oxygen and hydrogen atoms within the proposed structure. One consideration would be the dryness of the H-ZSM-5 and Na-ZSM-5 at the time of reaction. When the zeolite is synthesised, it forms as a water of crystallisation with approximately 27 water molecules per unit cell, as determined *via* single crystal X-ray diffraction characterisation. Regardless of its storage at 110°C prior to use, a partial hydration state may still exist. It is not immediately obvious, however, as to the exact nature of reactant decomposition and subsequent formation of the disulfite crystalline product.

Powder XRD of the tan-orange powder does suggest minor S_4N_4 residues within the sample, despite prolonged heating under vacuum. More importantly, however, a negative 2θ shift is evident, indicative of increased unit cell size, in this case owing to molecular incorporation, of presumably S_4N_4, within the zeolite channels. IR analysis of the final product showed only absorption bands associated with that of the MFI (**M**obil **Fi**ve) framework (H-ZSM-5 and Na-ZSM-5), and no evidence of S-N stretches was present. Understandably, the broad nature of the aluminosilicate stretches between *ca.* 1500 and 400 cm^{-1}, is certain to mask many, if not all, S-N stretches associated with S_4N_4. Henceforth, characterisation *via* IR is unlikely to offer any substantial insight concerning the host-guest system.

Modification of the aforementioned setup was considered essential in order to eliminate product contamination of S_4N_4, and allow definitive characterisation of the target material itself. The construction of a 'frit-diffusion' type apparatus, as shown in Figure 21, allowed both maximum exposure of the zeolite sample to S_4N_4, as well as elimination of S_4N_4 build-up within the product, owing to interaction of the nitride through its vapour state.

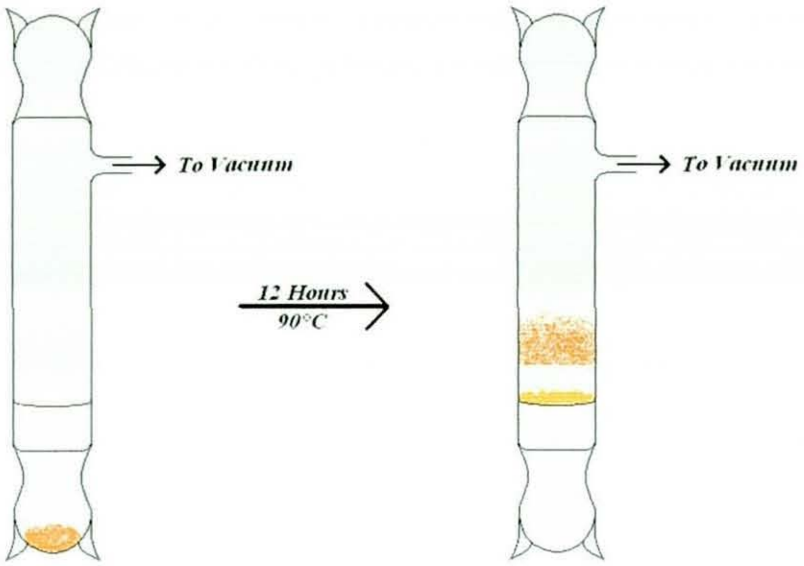

Figure 21 - ***Schematic representation of frit-diffusion setup.***

Ensuring the oil bath level surrounding the setup was kept at least one inch above the level of the frit meant that any unreacted S_4N_4 condensed suitably clear of the zeolite product, eliminating sample contamination. To facilitate isolation of the bulk zeolite-S_4N_4 product, it was possible to use a CH_2Cl_2 soaked swab to remove the crystallised S_4N_4 from the walls of the filter stick. The resulting product was dark yellow/tan in colour, free of residual S_4N_4, and showed a significant negative 2θ shift, as validated through powder XRD.

In light of the promise this preliminary work provided, the degree of sulfur-nitrogen loading within the framework was investigated. Using the frit-diffusion method, aliquots of the zeolite sample on the frit surface were taken, *in situ*, at pre-determined time intervals (1, 2, 4, 6, 7, and 12 hours), and elemental analysis used to monitor nitrogen content. The progression of the reaction provided sample aliquots that darkened in colour from pale yellow (1 hour), to a very dark tan (7 hours). Such an observation suggests increased incorporation of the S_4N_4 moiety, or equivalent species (i.e. any S_4N_4 fragment/decomposition product) into the zeolite. Essentially, it was considered important to load as much of the guest species into the zeolite in order to reduce the possibility, and severity, of disorder within the product, thereby facilitating characterisation attempts (disorder is likely to be caused by unequal/irregular distribution of guest molecules within the zeolite channels).

In the above reaction, nitrogen content increases linearly until 7 hours, when, surprisingly, a slight decrease is noticed, perhaps due to calcination of some of the occluded guest. Carbon content is negligible in the final product, but is evident at 1 and 4 hour intervals, in *ca.* 1% concentrations. As elemental analysis of both S_4N_4 and Na-ZSM-5 starting materials reveal no carbon content, it is believed that the carbon traces in the aliquots at these time intervals may be coming from organic volatiles within the vacuum grease used. It appears that the optimum loading conditions require sublimation of the nitride for 6-8 hours, as the nitrogen content of the zeolite product reaches 2.5% and 2.7%, respectively, before dropping to 2.3% following prolonged heating. The limitation of IR analysis to provide useful insight into S-N occupancy meant that Raman spectroscopy was favoured. With prior knowledge, through powder XRD, that no 'free' S_4N_4 remained within the sample, or coated to the sample surface, the observation of S-N bands in the Raman spectrum of the product meant that guest occlusion had occurred. The Raman bands showed good similarity to that of S_4N_4 itself (υ 722, 695, 531 and 231 cm^{-1}) with a slight offset in peak location due to spatial constraints within the zeolite channels.

Although exact structural characterisation of the zeolite product is not easily obtainable, especially following repeated unsuccessful attempts at preparing larger single crystals of ZSM-5 as proposed by Argauer and Landolt,[69] the combination of powder XRD, elemental analysis and Raman spectroscopy, all provide evidence supporting the inclusion of S_4N_4 within both Na-ZSM-5 and H-ZSM-5 systems. Moreover, analogous reactions conducted using the channel restricted TPA-ZSM-5 host, show no visible reaction occurs and subsequent elemental and powder XRD analysis confirms no change to the starting zeolite material. Such a comparison helps provide further evidence of incorporation of the S_4N_4 moiety within the zeolite network as opposed to simply coating its surface. With the framework of Na-ZSM-5, H-ZSM-5 and TPA-ZSM-5 being identical, and only the supporting cation varying between each, the bulky tetra-n-propylammonium group appears to hinder the uptake of S_4N_4.

Commonly, the majority of molecular sieve inclusion reactions tend to occur when the guest molecule is in solution. The solubility of S_4N_4 in both CH_2Cl_2, toluene and xylene therefore provided a basis to observe its interaction with the ZSM-5 zeolites through perhaps more conventional methods.

Woollins and co-workers have reported observations that increased reaction temperatures often favour solution based reactions involving S_4N_4, and have suggested plausible mechanisms involving its decomposition and reformation, possibly *via* more reactive species such as S_2N_2 or SN·, at these augmented temperatures.[17] Despite the inability to isolate and characterise the presence of the proposed monomer, S_2N_2, reactions between complexes such as $PtCl_2(PMe_2Ph)_2$ with S_4N_4 at high temperatures have provided an S_2N_2 containing product[17] and similar reaction conditions were considered to be a potential indirect source of the nitride for inclusion within the MFI framework. Not only would such a reaction pathway eliminate the risk of preparing pure S_2N_2, but the ease at which such a product could be generated will have been simplified multifold.

The reaction of a superheated toluene S_4N_4 solution (140°C) with H-ZSM-5 and/or Na-ZSM-5 afforded a dark yellow/tan coloured powder that appeared homogenous under microscopic examination. Visibly, the product closely resembled those obtained *via* solid-state sublimation reactions, but no evidence of S_2N_2 inclusion could be found through either powder XRD or Raman analysis. Additionally, it may be considered that generation of S_2N_2 during the course of the reaction, and subsequent occlusion of the monomer, may indeed be proceeded by polymerisation, to $(SN)_x$. Inevitably, such a process would afford a dark coloured product, analogous to the polymer itself, yet no such observation was noted.

Increasing the reaction temperature to 190°C, using xylene, gave much the same product, along with a dark red coloured impurity. The colour of the impurity was indicative of tetrasulfur dinitride, S_4N_2, and after allowing it to stand under nitrogen for *ca.* 3 days, followed by washing with Et_2O, pure S_4N_4 was obtained. Such observations for S_4N_2 have been previously reported.[17] The formation of S_4N_2 provides some evidence relating to the suggested decomposition of S_4N_4, in solution, at high temperatures, however it was not found possible to isolate the S_2N_2 monomer and there was no evidence to suggest its uptake, or subsequent polymerisation, within ZSM-5. This, of course, is not to say that S_2N_2 does not form during such a reaction; in essence the monomer may well be forming and entering the zeolite channels, but such elevated temperatures is likely to remove it from the framework through either decomposition or thermal-kinetic action.

The protonation of S_4N_4 is well documented within the literature.[172] Although reaction of the former with H-ZSM-5 does appear to provide a H-ZSM-5/S_4N_4 host/guest product, analogous to Na-ZSM-5, it was considered appropriate to cease using H-ZSM-5 as a host matrix and focus further work (based primarily around S_2N_2) on the sodium derivative, so as to avoid any complications that may arise through nitride protonation.

2.3. *Disulfur dinitride, S_2N_2*

The traditional synthesis of S_2N_2, and in turn $(SN)_x$, utilises a vertical type apparatus that consists of a heat source for the S_4N_4, typically an oil bath, a heat source for the silver wool, usually a tube furnace, and a cooled collection vessel. Another collection vessel can then be added to the setup and following extensive pumping of the 'as generated' S_2N_2, purification and isolation of larger single crystals of the nitride is observed (the storage of these crystals under static vacuum for more than 3 days affords single crystals of the polymer). This route to preparing S_2N_2 has been well documented and requires the fabrication of specialist glassware and the purchase of a customised tube furnace.[4, 27, 39, 48]

Following careful consideration and reference to traditional setups, the use of a purely vertical setup was discarded owing primarily to spatial considerations as well as restricted versatility such an arrangement provided. Instead, a tailored, more compact variation of the traditional apparatus, as shown in Figure 22, was constructed.

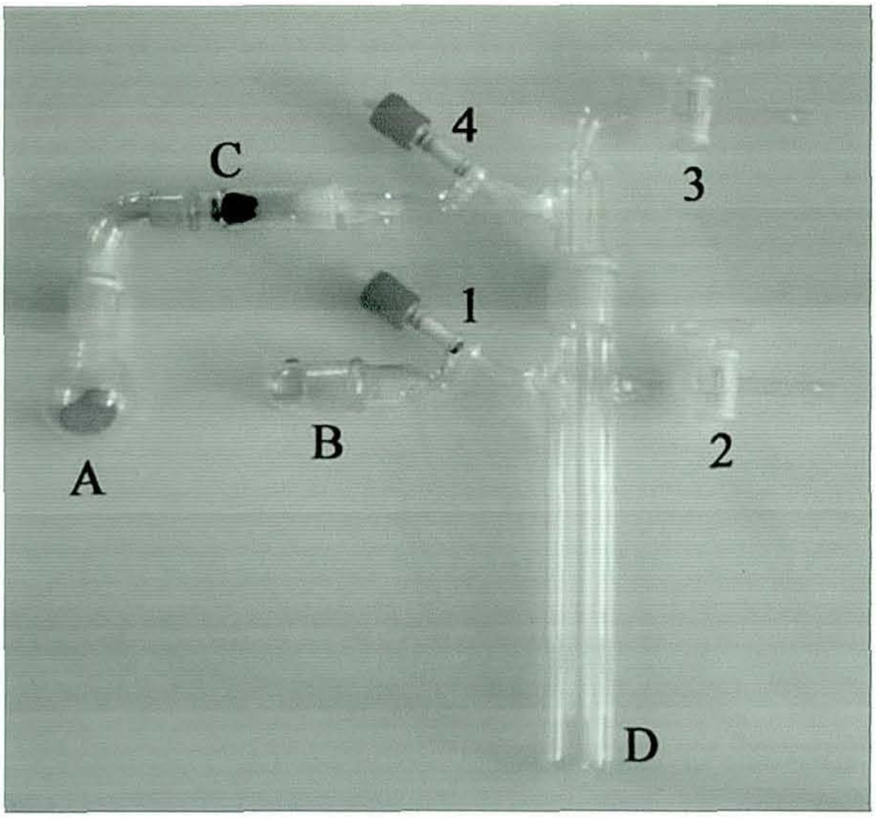

Figure 22 - ***Apparatus used to prepare S_2N_2/$(SN)_x$ and allow interaction of the former with various materials.***

In a typical synthesis, the entire system is placed under high dynamic vacuum through Tap 3. Although a Schlenk line hose may be used, direct attachment of vacuum tubing from the vacuum pump itself offers a greater vacuum (*ca.* 0.01 mbar). Heating of freshly re-crystallised S_4N_4, in Flask A, was achieved using a thermostatically regulated oil bath that was found to operate most efficiently at 90-100°C. Owing to the distance of Flask A from the base of the setup, the oil bath required support from a standard lab-jack. Once in vapour form, the S_4N_4 is then able to pass through high purity grade, heated silver wool in connecting Tube C. The silver wool is heated directly by a temperature controlled Isopad S45 heating tape that is wrapped around Tube C, along its length, ensuring a maximum gap of 0.5 cm from the top of the oil bath to the base of the heating tape. The tape provides a constant operating temperature of *ca.* 300°C. The provision of as small a gap as possible between oil bath heating and tape heating ensures that vapour deposition, and re-crystallisation, of S_4N_4 within the connecting tube was eliminated, as the temperature gradient, coupled with high vacuum, is sufficient enough to allow the nitride vapour to pass through the silver wool. It should be noted that the density of packing within the silver wool plug can dramatically affect both the rate of conversion to S_2N_2 and the level of impurity contamination. Densely packed plugs were found to significantly reduce the rate at which S_4N_4 was used up during the course of the reaction, often resulting in >12 hour runs. When plugs were not packed enough, reaction times would decrease to *ca.* 2 hours, and S_4N_4 contamination increased as a result. A moderately well packed plug was found to provide the optimal product, with total reaction times between 5-6 hours. Furthermore, care was taken when handling and preparing the silver wool as findings have suggested an increase in hydrogen concentration within the resulting $S_2N_2/(SN)_x$ product of up to 5%, due to transfer contamination. Following conversion of the S_4N_4 to, primarily S_2N_2, the volatile monomer can then be pulled through into the collection vessel D. The use of a liquid nitrogen cold trap means that isolation of S_2N_2 is possible, and its growth as colourless/white crystals is evident along the central stem within D.

Although S_2N_2 is the principal product of such reaction, other minor impurities are inevitably obtained. The formation, for example, of a red/brown band towards the top of the collection vessel is indicative of S_4N_2.[4] Contamination with S_4N_4, both in the earlier stages of the reaction when catalytic activity of the silver wool is perhaps reduced and through dimerisation of S_2N_2, is also common. To help reduce the effects of contamination from the latter, it was found that by allowing the heating tape to warm to temperature and heat the silver wool for *ca.* 30 minutes before heating the S_4N_4, contamination of the dimer was reduced. Additionally, glass wool cladding/lagging from the edge of the heating tape to the top of the liquid nitrogen trap ensured most of the product was isolated in the collection vessel itself, as opposed to some coating the walls of the glassware around Tap 4. Following repeated reaction runs and slight setup variations to help improve/optimise the conversion process, the ability to favourably reduce reaction time to *ca.* 2-3 hours, whilst still maintaining product purity was highlighted. The fabrication of a shorter connecting tube helped reduce the distance that the generated S_2N_2 vapour had to travel before condensing in the collection vessel. Using analogous density packed silver wool plugs and the same vacuum levels as before, conversion of the S_4N_4 was found to be as clean as prior routes, despite reduced conversion times. Evidently, the practical application of such optimisation facilitates a more 'routine' operation that hitherto required extended heating phases and hence augmented risks of S_4N_4 sample degradation.

Following the generation of the S_2N_2 product, closure of Taps 3 and 4 create a static vacuum within the system. Alternatively, prior to sealing the system, both Flask A and connecting tube C can be removed if desired and this was found to be best achieved by quickly passing dry nitrogen gas through the setup, *via* Tap 2, removing the RBF and connecting tube, and closing Tap 4 before placing the remaining setup back under vacuum. By keeping the liquid nitrogen trap in place at this point, the amount of S_2N_2 lost when passing nitrogen gas through the setup is significantly reduced. Under the static vacuum, removal of the cold trap allows the vessel to warm to ambient temperature and facilitates volatilisation of the reactive S_2N_2 product. If kept under static vacuum for prolonged periods of time (> 3 days) solid-state conversion to $(SN)_x$ readily occurs (discussed in more detail in Section 5.1).

The promise of S_4N_4/ZSM-5 occlusion compounds based on preliminary work strengthened the plausibility of inclusion of the smaller S_2N_2 moiety within similar frameworks. Despite having a reduced molecular diameter (*ca.* 1.7 Å) when compared to the S_4N_4 dimer, its increased reactivity and preferential spontaneous polymerisation process to $(SN)_x$ allowed its isolation and stabilisation within an ordered channel network to be questioned.

Although some success at incorporating $(SN)_x$ into functional systems has been achieved,[63] examples of chemical derivatisation of the polymer or growth of the polymer within new environments has been extremely limited. On the latter front, shortly following the discovery of properties associated with $(SN)_x$, efforts were made to incorporate it into clathrate, intercalate and zeolitic systems.[113] A clathrate is a solid mixture in which small molecules of one compound or element are trapped in holes within the crystal lattice. Clathrates themselves are often referred to as enclosure or cage compounds as they literally enclose the guest molecules (an example of hydrosodalite is shown in Figure 23). Intercalation compounds, however, trap ions or molecules between layers in a crystal lattice and as such, there is no formal chemical bonding between the host crystal and the trapped molecules (an example of muscovite, a layered clay similar to kaolinite, is shown in Figure 23).

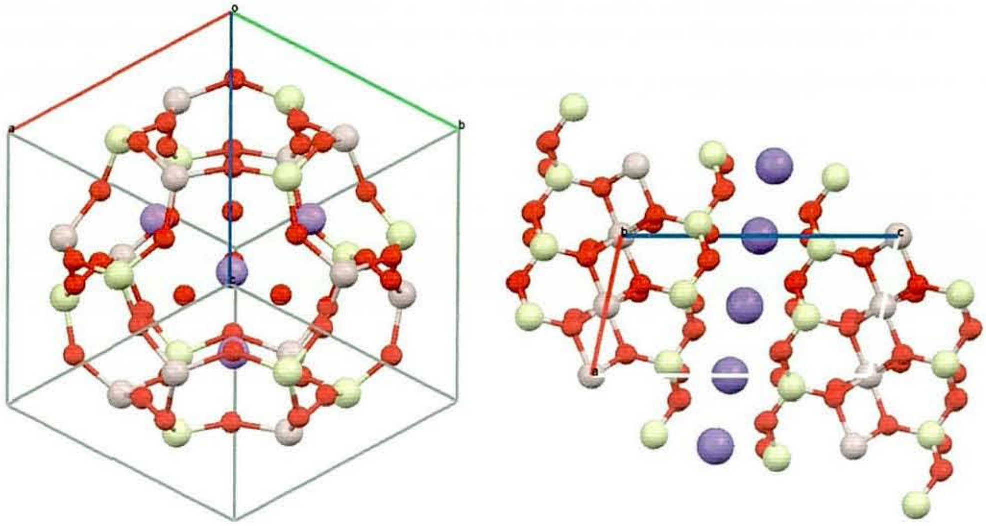

Figure 23 - ***Crystal structure of the hydrosodalite clathrate system (left) and muscovite intercalation compound (right).***

Structures taken from Dann et al.[103] *and Sidorenko et al.*[173]

The initial suggestion of $(SN)_x$ incorporation within such ordered frameworks by Love and co-workers[4] concentrated on solvent based interaction of S_2N_2 with the latter, with the hope to invoke S_2N_2 uptake followed by its polymerisation to $(SN)_x$. Although their initial findings, that concentrated on PHTP and thiourea matrices, appeared somewhat promising in that black filamental type growth, of presumably $(SN)_x$, was observed along the crystal axis, fundamental characterisation and actual incorporation of any moiety within a framework (as opposed to along the crystal facet itself) was absent. Additionally, when investigating the pure zeolite, mordenite, no visible changes were observed. More recent findings through the Hulliger research group, concluded that such analogous reactions did not provide any indication of $(SN)_x$ formation within any of the chosen host systems and suggested that any dark filamental growth may have been indicative of *in situ* $(SN)_x$ formation within the mixture.

Given the ever-expanding advances within zeolite chemistry and their increasing ease of synthesis, and in light of the intense current interest in so-called 'molecular wires', or 'insulated molecular wires', reconsideration of the ability of S_2N_2 to polymerise within porous systems becomes germane. The introduction of the intrinsically conducting $(SN)_x$ wire into such a host is a conceptually obvious modification that thus far has proven to be synthetically impractical, but one that could, potentially, be extremely beneficial to the nanoscale development of electronic devices, for example.

Insulated molecular wires (IMW's) adopt the premise that an 'insulating' outer sheath or coating has the ability to prevent cross talk or short circuit within an electronic system. Commonly IMW's have a composition similar to that illustrated in Figure 24 below, and can be pictured as being analogous to a zeolite system containing $(SN)_x$ wires within independent channels.

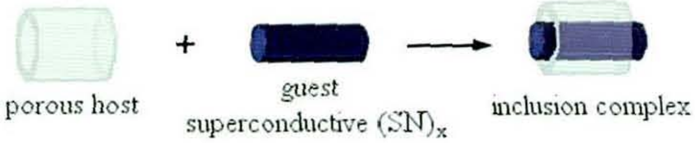

Figure 24 - ***Schematic representation of IMW composition using $(SN)_x$ as the proposed guest species.***

The ability, therefore, to use a zeolite framework, such as ZSM-5, as both an S_2N_2 host system and subsequent structure directing material to form $(SN)_x$ wires became directly pertinent, but alternative methodologies relating to host/guest interaction was required, based on prior unsuccessful attempts by both Hulliger and Love *et al.*[75, 113]

Owing to the inherent high volatility of S_2N_2 at room temperature, under a vacuum atmosphere, it was thought that the placement of various target zeolite samples in close proximity of the nitride source would allow suitable interaction between the two to occur. The provision of the side-arm (B) and in turn an appropriate air-tight vessel (such as a Schlenk tube, flask, *etc.*), allowed a zeolite sample to be loaded within a small or large sample vial and placed directly into the setup. Typically, addition of the target zeolite was conducted whilst passing nitrogen gas through the system when removing Flask A and connecting tube C. It was possible to place the sample vial containing the zeolite both directly into the side-arm, sealing the system using a Viking adapter, or into a Schlenk and sealing the system using the Schlenk itself. Either way, after placing the system under static vacuum, and allowing the setup to warm to room temperature, the S_2N_2 that was isolated in the collection vessel (D) was readily able to diffuse around the setup and enter the side-arm, where it could interact as appropriate with the target material. The necessity for a strictly vacuum based system at this point was essential as it permitted an increased vapour pressure, and hence volatility, of the S_2N_2 species, thereby allowing its diffusion into the side-arm.

Many traditional syntheses of $S_2N_2/(SN)_x$ ensure that isolation of the former follows a repeated condensation re-crystallisation procedure, whereby the 'as generated' S_2N_2 is purified following extensive pumping and subsequent condensation into another collection vessel. Although allowing the monomer to be isolated in its purest form, at liquid nitrogen temperatures, once thawed to room temperature the solid-state polymerisation process is frequently unclean. Despite removing any S_4N_2 residues from the bulk sample, the most common impurity at this stage, although minor, arises from the dimerisation of S_2N_2 to S_4N_4. Moreover, the isolation of purer S_2N_2 samples significantly increases its explosive tendencies and where frequent use is concerned, such a risk is preferentially avoided. As a result, and owing to the fact that any S_4N_2 and S_4N_4 contaminants are inherently involatile at room temperature, it was considered appropriate not to further purify the S_2N_2, but instead allow it to interact with the zeolite samples *in situ*.

Many of the compounds that were initially allowed to interact/react with S_2N_2 were chosen, primarily, based on their potential for guest encapsulation. Typically, zeolite type molecular sieves, lamellar solids and sodalite materials were investigated, but initial reactions of S_2N_2 in its vapour phase concentrated on using Na-ZSM-5 as the target receptor. The addition of a small sample vial containing dried Na-ZSM-5 to side-arm B, and its evacuation, allowed Tap 1 to remain open. Following removal of the liquid nitrogen trap from around the collection vessel, the system warmed to room temperature and the volatile S_2N_2 product could be seen to diffuse around the setup (visible indications included orange colouration of the vacuum grease around the ground glass joints and faint blue colouration of various parts of the glassware). Within approximately sixty seconds, discolouration of a portion of the white zeolite, nearest to the aperture of Tap 1, to a dark blue-black colour had occurred. Following further interaction (*ca.* 7 minutes) the entire Na-ZSM-5 had homogenously adopted the same blue-black colour. So as to ensure thorough and maximum interaction of S_2N_2 with the zeolite sample, the setup was left untouched overnight. Although no obvious visible colour change had occurred after this time, microscopic examination of the product revealed contamination with small, interspersed orange crystals. Owing to the likely occurrence of *in situ* S_2N_2 dimerisation, the formation of such orange crystals strongly suggested S_4N_4 formation and it was thus important to wash the dark blue-black product with dried, de-gassed CH_2Cl_2 until the filtrate ran clear (i.e. all S_4N_4 had been removed). Dried solvents were used to minimise the risk of molecular water uptake into the zeolite channel system. Reduction of the orange filtrate, to dryness, and subsequent IR analysis showed good similarity for S_4N_4. Thorough drying of the zeolite sample was readily achieved under reduced pressure and repeated microscopic examination suggested sufficient purification of the sample.

With such an intense colour being adopted by the final zeolite product (very similar in colour to bulk samples of $(SN)_x$, but lacking the bronze lustre that can sometimes be seen from certain viewing angles) and in light of the fact that within S-N chemistry as a whole, there are few other examples of such dark blue-black chromophores, with the exception of S_4N^-,[12] it was considered likely that the S_2N_2 had interacted in some way with the Na-ZSM-5 and induced polymerisation. With $(SN)_x$ sample storage being much debated amongst the literature,[36, 51, 52, 174] it was interesting to note that storage of the dark blue product in atmospheric conditions appeared feasible in the short term (< 3 days), yet prolonged exposure affords the onset of decomposition; similar to that of $(SN)_x$ itself. When stored under an atmosphere of nitrogen however, product stability was maintained in the longer term, with no visible signs of degradation after several months.

Initial colouration of the Na-ZSM-5 to its darkened state, although suggestive of $(SN)_x$ inclusion, still required conclusive verification to ensure that a simple coating of the zeolite surface was not occurring and indeed the colour change was the direct result of occurrences within the zeolite channels. Henceforth, analogous exposure of both nepheline and TPA-ZSM-5 target reagents to S_2N_2 vapour was investigated. In the case of the former, atomically, its surface construction and topography is an almost identical match to that of ZSM-5, yet it lacks a channel network system (*i.e.* non porous) and is therefore unable to act as a host matrix. TPA-ZSM-5 understandably provides an identical surface to that of Na-ZSM-5, but the large tetra-*n*-propylammonium cation within the channels has been found, especially in the case of S_4N_4, to restrict and exclude entry of potential guest molecules into the zeolite framework. As a direct result of such non porosity, exposure of both nepheline and TPA-ZSM-5 to S_2N_2 vapour should, if anything, only afford a surface type effect that can be used to allow direct comparison between the Na-ZSM-5/S_2N_2 product.

Following reaction, both nepheline and TPA-ZSM-5 showed no significant change in colour. Only slight discolouration of the immediately exposed surface, to a very pale grey/blue (as shown in Figure 25), was evident (microscopic analysis found no homogeneity of colour when larger agglomerated areas of the sample were crushed). It appears that, in the case of TPA-ZSM-5, although the framework of the two zeolites is identical and the surfaces are the same, the difference in reactivity is the result of the cation within the pore. The larger tetrapropylammonium cation appears to obstruct the ability of the S_2N_2 to enter the pore, whereas the smaller Na^+ ion has no hindering effect.

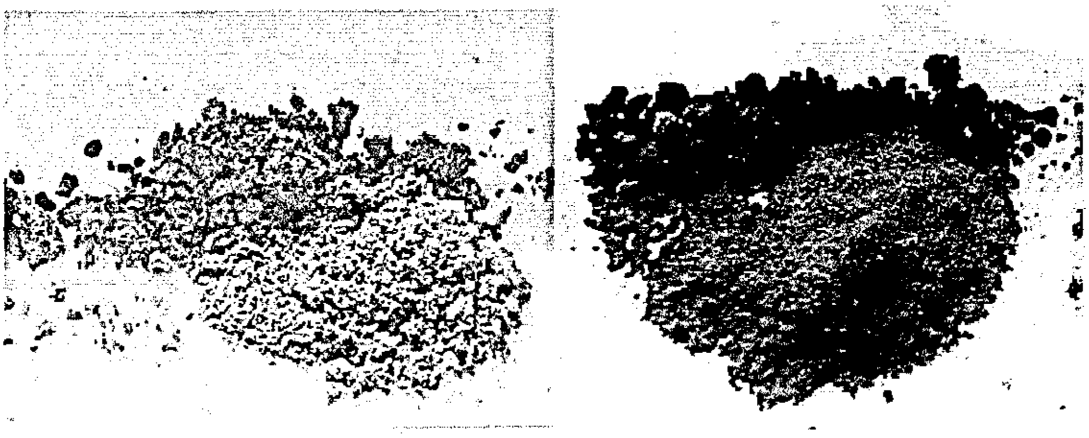

Figure 25 - ***The products obtained when TPA-ZSM-5 (left) and Na-ZSM-5 (right) are exposed to S_2N_2 vapour for 16 hours.***

Masking of many significant S-N bands by the numerous broad aluminosilicate stretches of ZSM-5 rendered infrared spectroscopy weak with regards to product characterisation. IR analysis of the product, however, did highlight one sharp peak, at 694 cm^{-1}, that falls between the framework tetrahedra windows and is indicative of a slightly blue-shifted S-N vibration within $(SN)_x$, as proposed by Passmore[175] and as indicated through IR analysis of $(SN)_x$ itself. More importantly, perhaps, powder

XRD studies of the Na-ZSM-5/S_2N_2 product (see Figure 26) revealed an intense decrease in reflection intensity and a significant negative 2θ shift that is coherent with many systems that encapsulate guest molecules, including that shown by S_4N_4/ZSM-5 as discussed previously. The reduced 2θ shift typically arises due to the increased occupancy of the partially vacant channels within the MFI framework of ZSM-5, and also warrants reduced reflection intensity. The noticeable broadening of the zeolite reflections is indicative of a loss of periodicity in the structure that is associated with disordered occlusion of a host species. Additionally, the absence of 'free' $(SN)_x$ reflections in the XRD pattern helps provide further evidence of a non-surface effect.

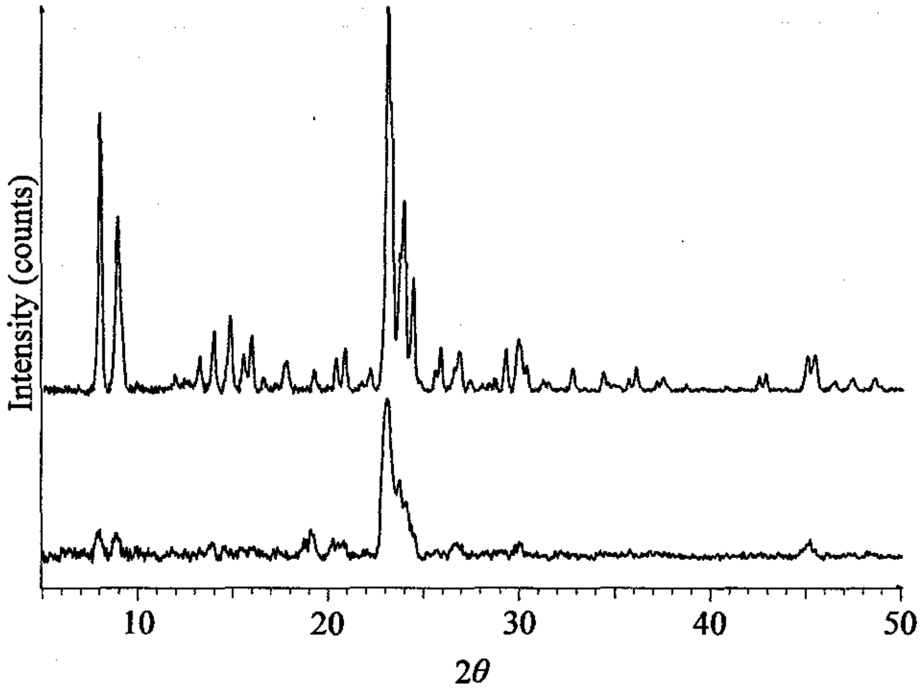

Figure 26 - ***Powder XRD comparison of Na-ZSM-5 before (upper) and after (lower) exposure to S_2N_2 vapour for 16 hours.***

The use of Raman spectroscopy was considered imperative in helping to provide greater insight into the exact nature of the product species. Direct Raman analysis of the blue-black sample highlighted the distinct presence of several strong S-N bands that are analogous in nature to that of $(SN)_x$ itself, but crucially exhibit a slight, but significant, shift in their exact frequency as a result of restrictive vibrational freedoms within the channel voids (as shown in Figure 27).

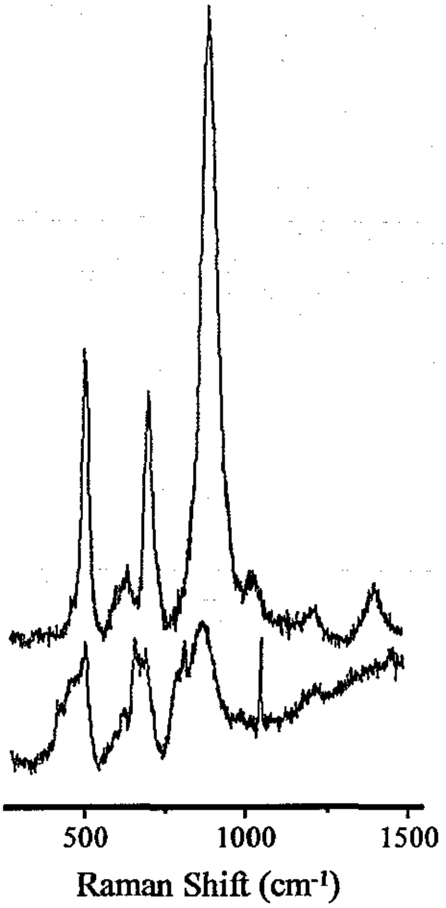

Figure 27 - ***Comparison of the Raman spectra between $(SN)_x$ (lower) and the blue-black Na-ZSM-5/S_2N_2 product (upper).***

Raman spectroscopy is commonly used when analysing zeolite systems, as the aluminosilicate framework is not Raman active. The Raman effect occurs when light impinges on a molecule and interacts with the electron cloud of the corresponding bonds. The incident photon initially excites one of the electrons to a virtual state, followed by relaxation to a vibrational excited state, thereby generating a Stokes Raman scattering effect. Should the molecule already adopt an elevated vibrational state, the scattering is referred to as anti-Stokes Raman scattering. In essence, a molecular polarisability change, or deformation of the electron cloud, is required for the molecule to exhibit Raman effect. The intensity of such an effect is determined by this polarisability change and Raman shift is equivalent to the vibrational mode involved. With reference to the occluded ZSM-5 system therefore, the polarisable nature of the thiazyl backbone of $(SN)_x$ allows its Raman spectrum to be observed with no interference from the aluminosilicate zeolite framework, which remains unchanged.

While the synthetic procedure described above (see also Section 6.28 for precise experimental) depicts somewhat optimised reaction conditions, faster reaction times between the zeolite and the S_2N_2 can be achieved by adding a small vial containing the former to the main flask (D), containing the nitride source, and sealing the system under static vacuum, as before. In this case, complete colouration of the Na-ZSM-5 occurs within seconds (< 1 minute). Unfortunately however, it was discovered that though this method brings about a faster conversion, it proves harder to avoid contamination with other impurities that form *in situ* and often fall into the sample vial. Although perforated stoppers can help alleviate some contamination, the increased risks associated with directly adding glass vials to freshly generated S_2N_2 means the method of choice remains with the side-arm approach.

Further confirmation of the inclusion of $(SN)_x$ within the ZSM-5 channels stems from the chemical (un)reactivity of the system. In contrast to many other S-N species, such as S_4N_4, the use of $(SN)_x$ as a synthon in, for example, transition metal reactions, has been little studied. As part of this investigation, it was found that a stirred suspension of the polymer, in CH_2Cl_2 or THF, slowly dissolves as it reacts with the Pt(0) species, $Pt(PPh_3)_3$, to generate $Pt(S_2N_2)(PPh_3)_2$ (see Section 5.1.2). Crucially for this study however, the Na-ZSM-5-$(SN)_x$ product (as it shall be known) does not react in the same manner - even stirring for many days does not result in any loss of the dark blue-black colour. Furthermore, decomposition of $(SN)_x$ readily occurs following its exposure to basic solutions; however in the case of the occluded system, its exposure to concentrated ammonia solution results in decomposition over a much longer timeframe (typically several hours). Had this material simply been zeolite coated with $(SN)_x$ on its surface, then it would be expected to react in effectively the same manner as 'free' polymer. That it does not, provides confirmation that the $(SN)_x$ is present within the zeolite structure, protected from reaction with the platinum species.

It becomes important to consider the amount of $(SN)_x$ introduced to the Na-ZSM-5 in a typical reaction. With the application of mass change experimental and elemental analysis, deeper insight into the host-guest system can be achieved. Dried Na-ZSM-5 was weighed out into a small sample vial and the walls of the vial were then covered with Parafilm to help eliminate the occurrence of surface deposition of $(SN)_x$ on the vial itself. Following standard synthesis of S_2N_2, the sample vial containing the zeolite was placed into the side-arm of the setup and allowed to interact with the S_2N_2 vapour, overnight. Removal of the parafilm and re-weighing of the sample vial revealed a mass increase of 32.4 mg. In order to remove any S_4N_4 impurities that tend to form *in situ*, the product was centrifuged with CH_2Cl_2 as the supernatant, until washings ran clear. The combined washings were allowed to evaporate to dryness in pre-weighed sample vials and the mass of the resulting S_4N_4 impurity residue was calculated to be 20.7 mg. Re-weighing of the blue-black zeolite product also confirmed a mass loss of 20.7 mg, from S_4N_4 extraction. The mass of $(SN)_x$ added to 102.3 mg of Na-ZSM-5 therefore amounts to 11.7 mg, which equates to approximately 2.54×10^{-4} moles of polymer added to the system. Additionally, it was also possible to remove $(SN)_x$ from the ZSM-5 channels, through calcination, and monitor mass loss. Sample exposure to temperatures greater than 250°C for several hours results in polymer decomposition, essentially to SO_2 and NO_2, and a total mass loss of 11.5 mg.

The question of the degree of $(SN)_x$ loading into the cavities of the zeolite can be at least partially addressed through elemental analysis investigations. Results show, as anticipated, negligible carbon and hydrogen content with significantly increased nitrogen composition (4.4%), following purification. Assuming an elemental analysis error limit of 0.3% and by using the mass change experimental findings it is possible to calculate the number of SN units, per Na-ZSM-5 unit cell.

By altering the value of **x** in Na-ZSM-5-$(SN)_x$:

If **x** = **19**

r.m.m. $(SN)_x$ = 875
r.m.m. N in $(SN)_x$ = 266

266 / (5792 + 875) x 100 = 3.99% (~ 4% = lower error limit)

If x = 22

r.m.m. $(SN)_x$ = 1013
r.m.m. N in $(SN)_x$ = 308

308 / (5792 + 1013) x 100 = 4.53% (~ 4.6% = upper error limit)

Consequently, it appears that per molecule of Na-ZSM-5, there are 19-22 S-N repeat units per unit cell. To confirm the plausibility of such calculations, it is important to consider the unit cell parameters of Na-ZSM-5[69, 77, 176] and relate these to the corresponding data:

Cell Parameter	Distance (Å)
a	20.07
b	19.92
c	13.42

Table 3 - ***Cell parameters of Na-ZSM-5.***

Where *b* is the axis dimension of the two large 10T pores (see Figure 28 below), likely to hold the incorporated polymer.

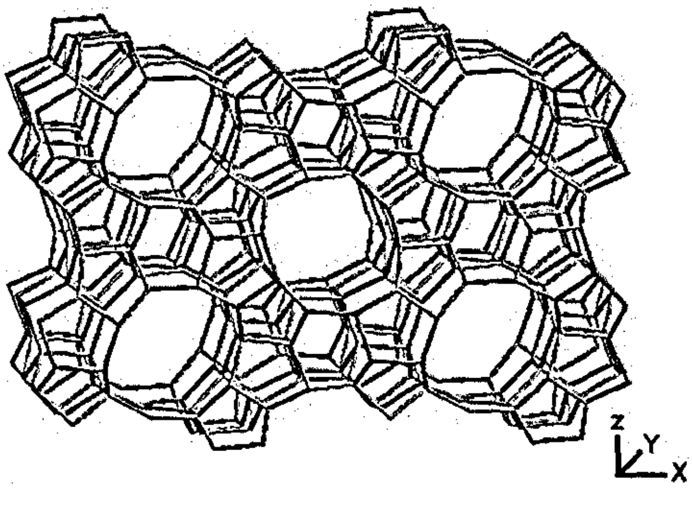

Figure 28 - ***Wireframe structure of the MFI framework viewed along the b-axis showing the large 10T channel network.***

As there is a total of two entire pores present per Na-ZSM-5 unit cell:

$$2 \times 19.92 = 39.84 \text{ Å}$$

Based on single crystal data for $(SN)_x$,[47] the linear distance between S_1 and N_2 is 2.886 Å.

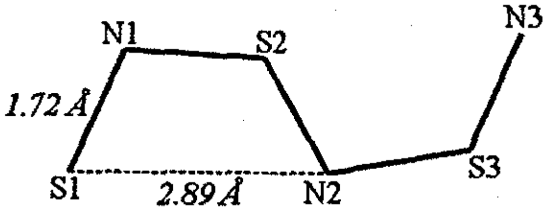

Figure 29 - ***Schematic representation of a single $(SN)_x$ chain, illustrating the S_1-N_2 distance.***

Thus, if **x = 19**:

$19 / 2 = 9.5$ S_2N_2 units

Total chain length = 9.5 x 2.886 Å
= **27.42 Å**

If **x = 22**:

$22 / 2 = 11$ S_2N_2 units

Total chain length = 11 x 2.886 Å
= **31.75 Å**

Therefore, allowing for the 0.3% error through elemental analysis, the total S-N chain length per Na-ZSM-5 unit cell equates to between 27.4 and 31.8 Å. As the total Na-ZSM-5 *b*-axis pore length, per unit cell, is 39.8 Å, the polymer loading calculation can be deemed at least feasible. Taken at face value, this calculation would suggest 77% of available pore length has been taken up by polymer; in reality, however, this is a very approximate figure as it of course takes no account of the exact spatial arrangement of the polymer within the zeolite channels. If desired, precise calculation of polymer loading within the channels is perhaps only achievable through the monitoring of pre- and post- reaction gaseous absorption differences, which may provide indication of the total void volume left within the channel network following polymer occlusion.

Thus far, attempts to generate crystalline material of sufficient size and quality to facilitate full characterisation by single crystal XRD have been unsuccessful. The three-day synthesis of TPA-ZSM-5, used routinely to obtain the ZSM-5 zeolites, affords a polymicrocrystalline product composed of flat-sided plates, typically less than 5 Å in diameter (see Figure 30a), that are too small for single crystal X-ray analysis. Literature resources acknowledge the possibility to prepare larger, macroscopic sized, single crystals of TPA-ZSM-5, using sodium aluminate and silica as the framework source and tetrapropylammonium bromide as the templating agent.[69] Although larger crystals of TPA-ZSM-5, and in turn Na-ZSM-5, were obtained following the described experimental (see Figure 30b), both synthetic reliability and product sample quality (*e.g.* increased crystal fracture) was found to be undesirable.

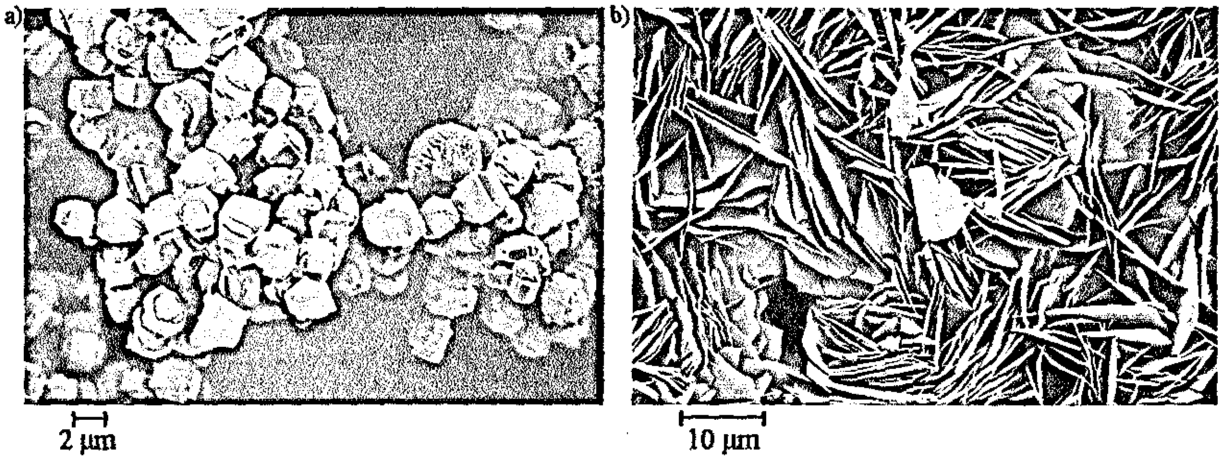

Figure 30 - ***SEM images of (a) polymicrocrystalline ZSM-5 and (b) larger ZSM-5 crystallites, obtained through different synthetic approaches.***

Several attempts at preparing the larger ZSM-5 crystals have provided reaction products with varying phase composition. Rarely, ZSM-5 has been isolable, with no evident impurity content, but most syntheses result in mixed phase products. In a typical reaction, two distinct solid products separate during cooling, within the stainless steel autoclaves: a 'loose' white solid suspended within the solvent, and an extremely hard white solid that remains at the bottom of the Teflon cup. Independent isolation of each solid and subsequent powder XRD analysis (see Figure 31) reveals the former is composed mainly of TPA-ZSM-5, but is contaminated with analcime ($Na[AlSi_2O_6]H_2O$). Analysis of the harder solid shows no TPA-ZSM-5 content, but instead the presence of largely analcime, with some sodium aluminate silicate hydrate ($Na_{1.4}Al_2Si_{3.9}O_{11.5}H_2O$) as a minor component.

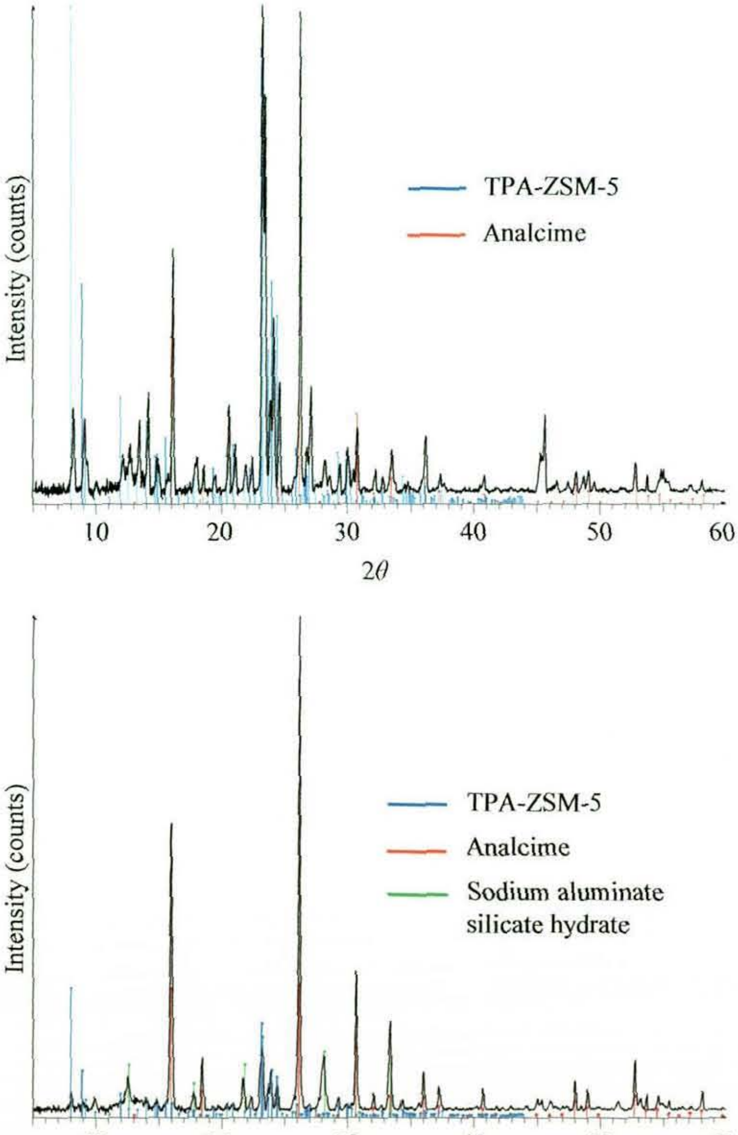

Figure 31 - ***Powder XRD pattern of both solid products obtained during the attempted preparation of larger ZSM-5 single crystals: loose solid (upper), hard solid (lower).***

The formation of analcime impurities within both products is perhaps surprising in so much as the material has never been seen during analysis of the regularly employed polymicrocrystalline ZSM-5 synthesis. Kamiya *et al.* suggest however, that there is indeed increased probability of analcime contamination during ZSM-5 preparation, when using NaOH as the mineralising agent.[177] That said however, the substitution of alkaline hydroxides to either lithium or potassium variants did not provide a cleaner target material. Consequently, the large analcime content in the solid product at the bottom of the Teflon cup is perhaps less surprising owing to its increased density when compared to ZSM-5. Extended heating times from 8 days (as suggested in the literature) to 16-20 days did not provide any greater purity samples. The insoluble nature of all mixed phase components (ZSM-5, analcime and sodium aluminium silicate hydrate) means that isolation of the minor ZSM-5 component is unobtainable using conventional, freely accessible methods.

As previously discussed, despite its low reproducibility rate, larger crystals of ZSM-5 were obtained from such a route. Interaction of these zeolite crystals, following careful removal of the tetrapropylammonium template, with freshly generated S_2N_2 vapour resulted in dark blue-black colouration, similar to that observed when using the 'powdered' ZSM-5 material. Unfortunately, however, both attempted single crystal XRD studies of the occluded $(SN)_x$ product, and high flux synchrotron radiation analysis, did not provide sufficient diffraction intensity to enable structure refinement to be obtained. It is thought that the morphology of ZSM-5 as it crystallises is partly responsible for such poor diffraction. The initial formation of very thin crystalline plates and the slight degradation of the crystals likely to be caused during template removal *via* calcination is believed to be the determining factor responsible for insufficient diffraction during investigation.

The inherent conductive properties associated with $(SN)_x$ and its subsequent inclusion within the inert, insulating ZSM-5 matrix allows conductivity effects to be questioned. Unfortunately, attempts made to analyse conductivity changes within the occluded Na-ZSM-5-$(SN)_x$ system have, to date, been unsuccessful. Pellet formation of the sample was achieved with the use of a KBr press and die, and differing pressures exerted (2 - 10 tons) to try and induce varying degrees of point-point contact within the resulting pellets. Conductivity was monitored using a Jandel

Universal Four-Point Conductivity Probe, but all attempts provided a conductivity value below the minimum threshold of the HM20 test unit, meaning the sample was more insulating in nature than a typical semi-conductor. Principally, a lack of bulk conductivity in this system may be attributable to the likely disorder and increased number of defects along the S-N backbone in the polymer chain, once encapsulated within the small crystallites of the zeolite. The anisotropic conductive nature of $(SN)_x$ is well known[4, 33, 37, 39, 178] and it may be postulated that increased conductivity may only be observed along the ZSM-5 *b*-axis itself, that contains the polymer wires. Should this in fact be the case, the only feasible method of conductivity analysis will involve monitoring conductivity directly across single crystal facets using miniaturised electrode contacts, attached to the crystal surface. Owing to the time-scale involved and specialist nature of such an application, conductivity analysis within such a system was not investigated further.

It is clear, however, that the reaction of S_2N_2 vapour with Na-ZSM-5 constitutes the first example of a conceptually obvious means of modifying conducting $(SN)_x$, and as such, the results should stimulate considerable interest in the (re)investigation of similar systems.

Tetra-*n*-propylammonium fluoride silicalite-1, $Si_{96}O_{192}[(C_3H_7)N]_4F_4$, is a zeolite material that also adopts the MFI framework type, but differs from ZSM-5 with respect to its neutral framework construction. The absence of aluminium atoms from the framework tetrahedra results in a purely silicate based arrangement, that lacks anionic character. Consequently, the necessity to balance the framework charge with Group 1 metal ions becomes redundant. Unlike ZSM-5, following removal of the template molecules from the channel pores *via* calcination, silicalite-1 exists as a pure silica zeolite framework, with no supporting cation present. Its pore aperture is essentially identical to ZSM-5, with the only significant compositional alteration being the absence of the Na^+ ion.

Exposure of template-free silicalite-1 to S_2N_2 vapour was investigated in order to ascertain any fundamental differences between the two MFI zeolites in terms of their reactivity. Following approximately 15 minutes of exposure to the vacuum/S_2N_2 atmosphere, the silicalite-1 material began to show signs of pale blue-grey colouration. The colour intensity deepened significantly over the next hour, and after a further 15 hours, resulted in an identical dark blue-black colour to that exhibited by Na-ZSM-5-$(SN)_x$. Removal of the S_4N_4 impurity, with CH_2Cl_2, and drying under reduced pressure, permitted both powder XRD and Raman spectroscopy analysis to be obtained. Powder X-ray findings (Figure 32) were indicative of those previously observed for the ZSM-5 system, with cogent decreased reflection intensities for the major reflections at 8-9°, 18°, 23-25° and 45-46° 2θ, and a negative 2θ shift. Raman analysis similarly suggested the incorporation of $(SN)_x$ within the zeolite channels as a result of slightly shifted Raman bands, analogous in nature to that of the free polymer itself. The use of elemental analysis helped allow comparative conclusions to be drawn regarding the degree of loading between the two zeolite systems and indicated no significant difference in nitrogen content (*i.e.* polymer occlusion).

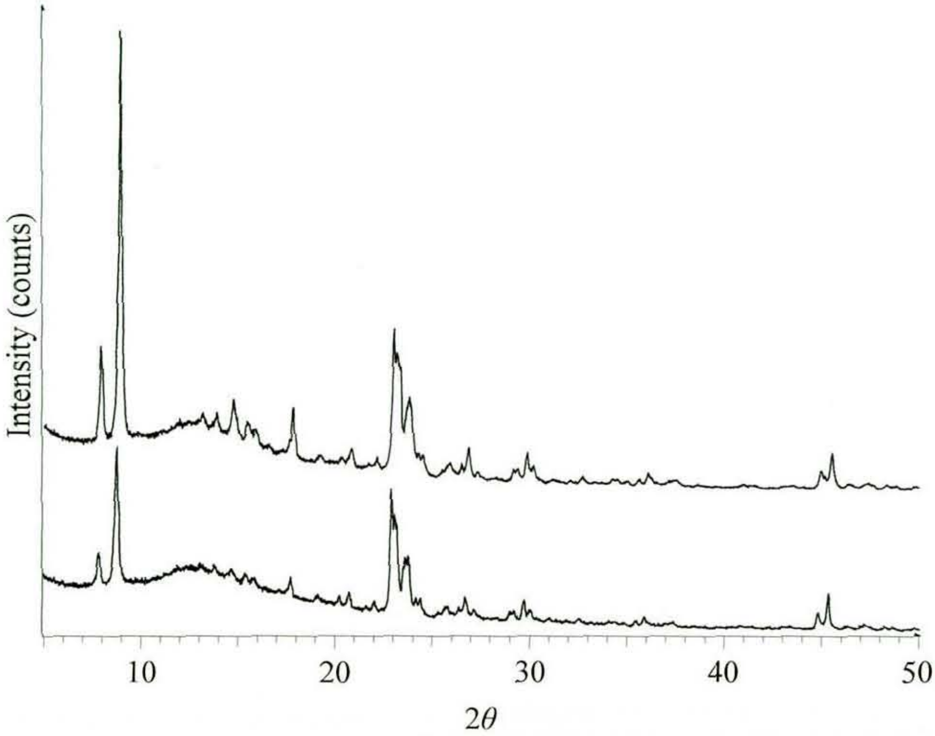

Figure 32 - ***Powder XRD patterns of template-free silicalite-1 before (upper) and after (lower) exposure to S_2N_2 vapour.***

The presence/absence of charge-balancing metal ions does not appear to affect the reaction of the MFI zeolites with S_2N_2 vapour. The aluminosilicate framework of Na-ZSM-5 and the silicate framework of silicalite-1 react similarly and afford products both analogous in colour, and through characterisation trends. The major difference, however, stems from the time required for full uptake of S_2N_2 and its conversion to $(SN)_x$. In the case of Na-ZSM-5, complete blue-black colouration is achieved over several minutes, with extended exposure times ensuring complete uptake. Silicalite-1, however, requires significantly longer exposure, regardless of its proximity to the nitride source, and is perhaps due to the absence of cations within the channel network. In Na-ZSM-5, Na^+ ions are held closely to the aluminosilicate framework; owing to the electronegative nature of $S_2N_2/(SN)_x$, through π-bonding/delocalisation, potential 'catalysis', resulting in increased $(SN)_x$ formation, can be attributed to the ionic interaction between the sodium cation of the framework with the thiazyl chain. Conversely, silicalite-1 contains no cation and polymerisation is solely dictated by correct alignment of S_2N_2 oligomers, due to conformational restrictions, and subsequent self-assembly of $(SN)_x$. Accordingly, the increased polymerisation time required for the silicalite-1/$(SN)_x$ system can be explained.

2.4. Interaction of S_2N_2 with other microporous materials

In light of the successful occlusion of S_2N_2 within the Na-ZSM-5 framework and its subsequent polymerisation to $(SN)_x$, various other microporous host systems were investigated for their potential to incorporate and stabilise the polymer. Suitable host systems were again selected based on their pore aperture width in relation to S_2N_2 and knowing that a *ca.* 5 Å diameter works well, in the case of ZSM-5.

Initial focus was concentrated on the layered intercalation compound, kaolinite (or kaolin). Kaolin is a naturally occurring phyllosilicate clay mineral that belongs to the feldspar family, with a typical composition $Al_2Si_2O_5(OH)_4$. Typically, phyllosilicate materials are sheet silicates that form parallel sheets of silicate tetrahedra with an Si_2O_5 ratio that are linked through oxygen atoms to octahedral sheets of alumina octahedra. Importantly, the intra sheet separation distance within the kaolin lattice is in the range of 4-5 Å, which closely resembles the pore aperture width of the MFI framework. Essentially, therefore, it is feasible to envisage intercalation of S_2N_2 within the restrictive layered arrangement of kaolin and as a result induce polymerisation (see Figure 33).

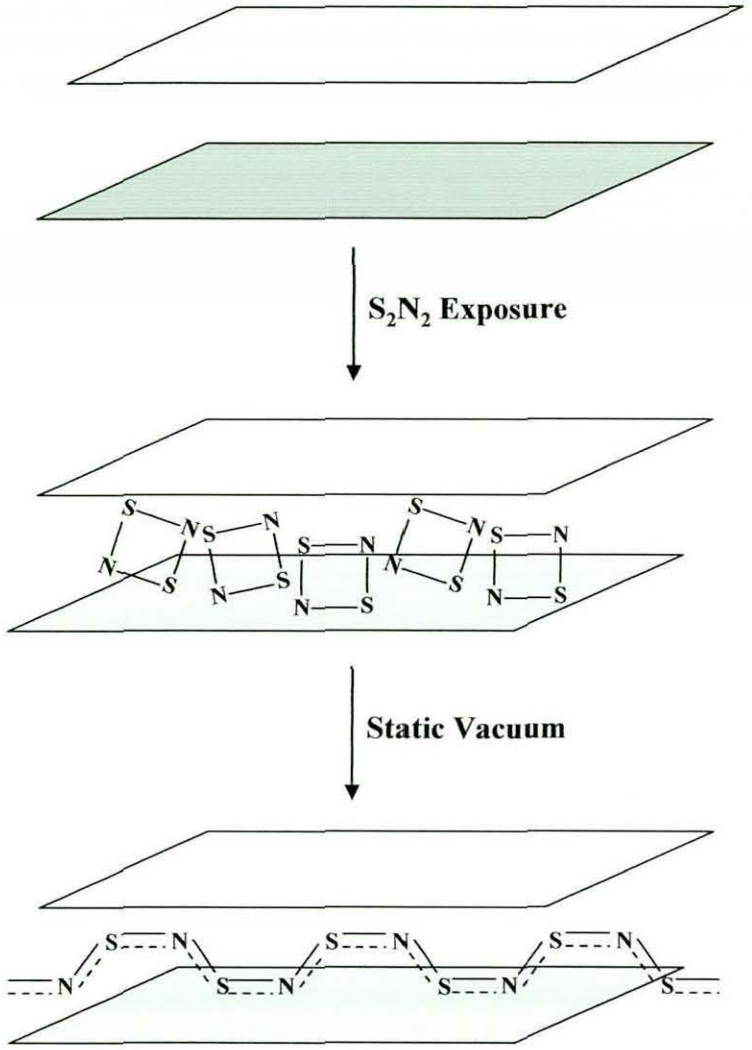

Figure 33 - ***Schematic mechanism describing the proposed method of $(SN)_x$ intercalation within kaolin.***

Introduction of the dried white kaolin material to the S_2N_2 source was achieved in much the same manner as Na-ZSM-5 and a blue colouration was immediately visible following 10-15 minutes of exposure. Complete colouration of the kaolin material was achieved over the next hour but its appearance differed slightly from the analogous ZSM-5 reaction product. Following washing with CH_2Cl_2, microscopic examination of the resulting product showed a homogenous sample with strong dark blue colouration, as shown in Figure 34.

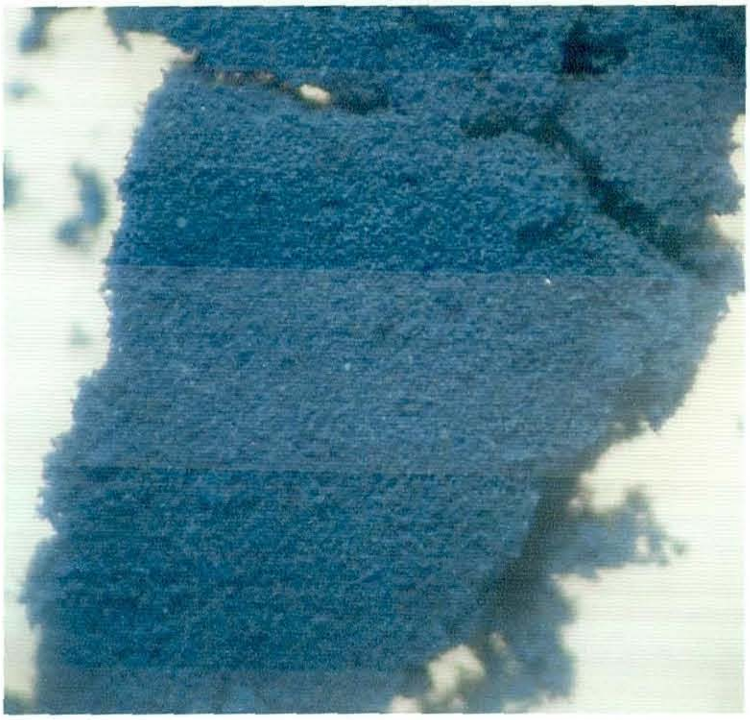

Figure 34 - ***The product obtained when kaolin is exposed to S_2N_2 vapour.***

IR analysis of the reaction product did not provide any greater insight into the exact nature of the material as the broad silicate bands that dominate the fingerprint region masked all potential S-N vibrational stretches. Raman spectroscopy, however, did indicate the formation of $(SN)_x$, with slightly shifted Raman bands as would be expected for an intercalated variant. Powder XRD of the product, as shown in Figure 35, did not reveal any additional reflections that may have indicated the surface coating of $(SN)_x$ over the white kaolin powder. Instead, the two main kaolin reflections at 12.5° and 25° 2θ were found to decrease significantly in intensity and therefore indicate the introduction of a guest species within the kaolin layers. A slight negative 2θ reflection shift further strengthens support for the introduction of $(SN)_x$. It should be noted that the kaolinite sample was found to contain trace amounts of illite impurity (a layered clay species that contains bulky cations within the intercalation sheets) that did not react in any way with the S_2N_2 due to the restrictive nature of its structure.

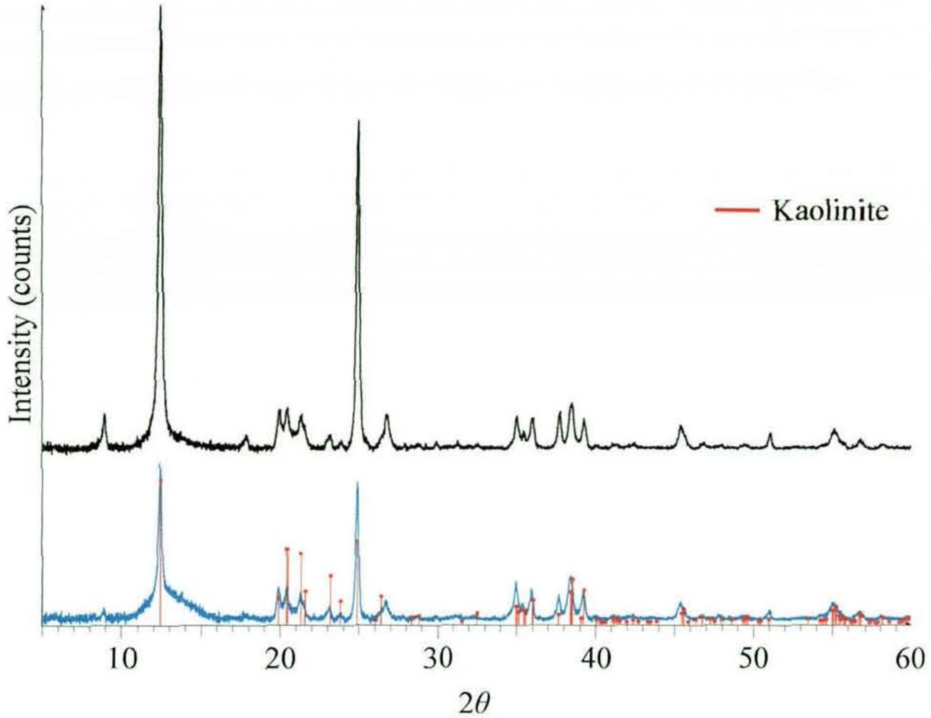

Figure 35 - Powder XRD comparison of kaolin (upper) with kaolin-$(SN)_x$ (lower).

To help further verify that there was no surface effect occurring during the course of the reaction, a calcined kaolin sample was exposed to S_2N_2 vapour, and compared. Calcined kaolin is a standard kaolin sample that has been heated to extremely high temperatures so that its internal layered type structure is broken down, whilst its exterior surface remains essentially unchanged; nepheline, mullite and cristobilite phases are known to be contained in the final calcined sample.[179, 180] Exposure of calcined kaolin to S_2N_2 vapour did not result in any discolouration of the former, even following 24 hours. In a similar manner to TPA-ZSM-5, the absence of a free channel, or layer arrangement, to accommodate the nitride, results in there being no possibility of S_2N_2 or $(SN)_x$ inclusion, and further confirms that the colouration of the kaolin sample stems from guest intercalation.

Figure 34 above, of the kaolin-$(SN)_x$ product, depicts a more blue coloured material than that of Na-ZSM-5-$(SN)_x$ (more blue than blue-black). Although not differing greatly in colour, with perhaps only a slight difference in shade, the naturally occurring impurity content, often associated with kaolinite samples, was considered responsible. Commonly, samples of kaolin can vary in purity from an almost clean material to one containing illite, iron oxide and various other minerals. The presence of iron (oxide), that often gives a red/pink tint to the kaolin sample, can be made attributable for the slightly bluer hue of the final $(SN)_x$ intercalated product. In fact, purer kaolin samples that were subsequently exposed to S_2N_2 vapour for the same length of time resulted in analogous dark blue-black colouration to that of Na-ZSM-5-$(SN)_x$. Alternatively, the orientation of the $(SN)_x$ guest within the kaolin layered arrangement may be considered to have the ability to slightly alter the colour of the resulting product. In Na-ZSM-5, inclusion within the host matrix is forced to occur within and along the mono-directional channels, resulting in the formation of a dark blue-black occlusion complex. In the case of kaolinite, formation of an intercalation compound may occur within the two-dimensional void between the aluminosilicate layers. Hence, it is plausible that a different guest orientation can give rise to a small, yet visible, colour variation.

The importance of advances within biological modification is an area of research that will remain active almost indefinitely. Research by Lerman concerning intercalation of ethidium molecules within deoxyribonucleic acid (DNA) has provided the basis for DNA modification and adaptation. As shown in Figure 36, DNA is essentially a long polymer that is composed of repeating units, called nucleotides. The chain itself is typically 22-24 Å wide, with a single nucleotide unit occupying a length of 3.3 Å.

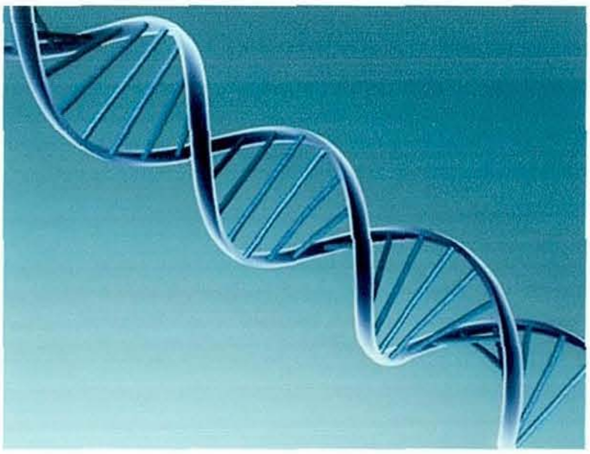

Figure 36 - ***A simplified structure of the DNA double helix.***

A large class of molecules have been found to intercalate into the space between two adjacent base pairs within the DNA double helix structure. These molecules are mostly polycyclic, aromatic and planar, and therefore function as ideal nucleic acid stains. Often, DNA intercalators are used in chemotherapeutic treatment of cancerous cells, to inhibit DNA replication. In order for an intercalator to fit between base pairs, the latter must separate by over *ca.* 3 Å, inducing local structural changes to the DNA strand, such as partial unwinding of the double helix and lengthening of the strand itself. In turn, such structural modifications can lead to functional changes, often involving inhibition of transcription and replication processes, which makes intercalators potent mutagens and, as a result, DNA intercalators are often carcinogenic.

In theory therefore, intercalation of a S-N moiety, within the DNA structure, is plausible. Although polymer strand formation along and within the entire double helix is hindered, the vacant sites between base pairings were thought to provide a suitable host location for S-N oligomers and in turn, $(SN)_x$. Although perhaps not immediately evident as to the specific use of such an intercalation product, it would be suffice to assume that at the very least, the likely blue-black colour of the product could facilitate DNA detection through sample staining.

Following prolonged exposure to S_2N_2 vapour, DNA (Na^+ salt) appears to develop the characteristic dark blue-black colour, associated with $(SN)_x$. In contrast to Na-ZSM-5, kaolinite and other zeolite systems where a pore-hindered analogue exists, it was not possible to attempt analogous reactions with a DNA material that contained restricted or destroyed intercalation sites. Therefore, it proved difficult to confirm whether colouration of the DNA was due to internal encapsulation of $S_2N_2/(SN)_x$, or whether a simple surface effect was the cause. Additionally, due to the amorphous nature of the DNA source, powder XRD analysis was unrewarding. Elemental analysis did provide an indication of increased nitrogen content following DNA exposure to S_2N_2 and Raman spectroscopy again confirmed the presence of $(SN)_x$, although there was no significant shift in the location of the Raman bands. It becomes clear, therefore, that S_2N_2 has been found to target DNA samples, and as a result, polymerisation can be seen to occur either within the intercalation sites of the double helix structure, or on the surface of the DNA itself. Although fundamental characterisation is thin, essentially owing to the limitation of most sample identification techniques with such a complicated amorphous material, confirmation of $(SN)_x$ formation cannot be disputed. The potential use of $(SN)_x$ as a staining medium on DNA residues, either *via* intercalation methods or surface sorption, was found to be at least plausible, but a wider array of DNA materials and clearer characterisation methods are pertinent to helping fully understand the system.

In all of the successful reactions discussed above, for Na-ZSM-5, silicalite-1, kaolinite and DNA, formation of the polymer-based product is relatively quick. In fact, for Na-ZSM-5, complete coloration of the zeolite occurs within several minutes of exposure to the nitride source. Hitherto, such a rapid conversion of S_2N_2 to $(SN)_x$, in the solid state, is unknown, with typical polymerisation occurring over 3-4 days.[4, 27, 29, 39, 48, 181] The specific pore diameter, or bottleneck diameter at the narrowest point, was considered to be responsible for the selective uptake of S_2N_2 in each case, whereby each host system had occlusion sites no narrower or wider than 4.5 or 5.5 Å, respectively. The specific dimensions of the available channel/pore/layer appeared to be the 'driving force' for inclusion of S_2N_2 within the host matrix, as the site was deemed large enough to allow S_2N_2 to enter, but small enough to occlude the monomer so that polymerisation could occur, whereby it then remained trapped within the framework.

The synthesis of numerous zeolite systems that are built around either larger, or narrower, pore diameter networks was considered important in order to monitor altering effects of their reaction with S_2N_2. Both AFI (SAPO-5 and $AlPO_4$-5), LTL (Linde Type L) and FAU (Faujasite) zeolite samples were prepared (see Figure 37) and independently exposed to S_2N_2 vapour. In each case, there were no visible signs of reaction, and the combination of powder XRD and Raman analysis of the zeolite sample, post-S_2N_2 exposure, suggested no overall change in zeolite composition and, therefore, no incorporation of either S_2N_2 or $(SN)_x$.

The AEI framework, as adopted by $AlPO_4$-18, is composed of narrow pore apertures, that can feasibly only accommodate very small molecular species. Upon exposure to S_2N_2, in a similar manner to the larger pored zeolites, no visible reaction occurs and is again suggestive of resistance to polymer inclusion.

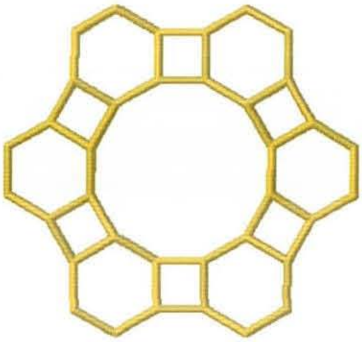

AFI

7.3 x 7.3 Å

LTL

7.1 x 7.1 x 7.1 Å

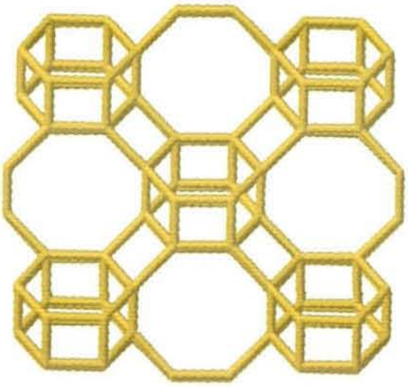

AEI

3.8 x 3.8 x 3.8 Å

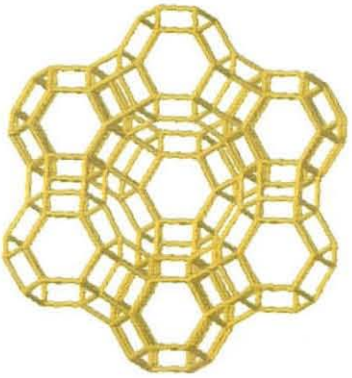

FAU

7.4 x 7.4 x 7.4 Å

Figure 37 - ***Structures of AFI, LTL, FAU and AEI zeolite frameworks, with maximum pore diameters labelled.***

There does, therefore, appear to be a determining factor concerning plausible and successful incorporation of monomeric S_2N_2 within these porous zeolite systems. The specific width of the pore aperture seems to play its part in facilitating S_2N_2 uptake: too large, in the case of $AlPO_4$-5, SAPO-5 and Faujisite, and the S_2N_2 is readily able to diffuse in and out of the zeolite cavities without fixation; too small, as displayed by $AlPO_4$-18, and the S_2N_2 is physically unable to enter the channel voids. It appears the optimum pore diameter of *ca.* 5 Å allows numerous S_2N_2 monomer units to enter the framework and once incorporated, the intimacy of the molecules caused by the spatial constraints of an occluded species, initiates the polymerisation process, thereby explaining the rapid polymerisation rate.

Crowns, or crown ethers, are heterocyclic compounds, which, in the simplest form, are oligomers of ethylene oxide. The repeating unit in such structures is that of ethyleneoxy, -CH_2CH_2O-. Typically, crown ethers are known for their ability to solvate cations due to the position of the oxygen atoms within the molecule, and their ability to coordinate to cations within the ring structure. The physical size of the interior void within the crown ethers help determine the cation that can be bound. In a similar manner to molecular sieves, size exclusion/inclusion principles apply. Although many crowns, such as 18-crown-6, consist of just carbon, oxygen and hydrogen, *thio* derivatives are also known. In the case of the latter, oxygen atoms are replaced with sulfur, and a mixed sulfur-oxygen crown is obtained.

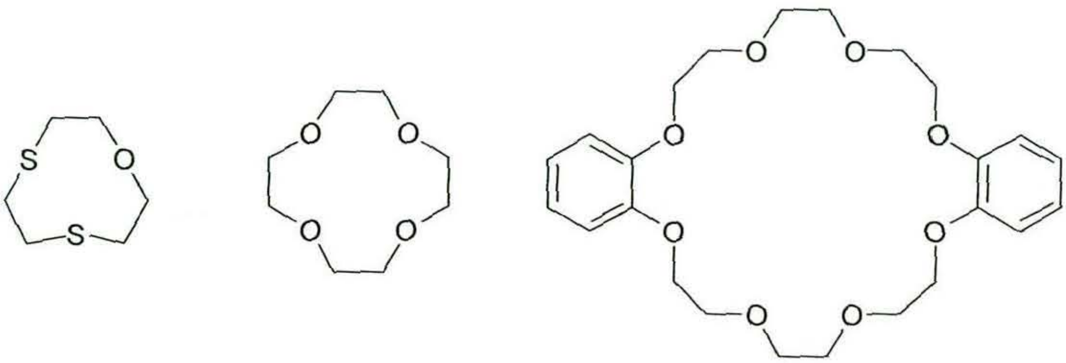

Figure 38 - ***The structures of various crown ethers.***

It is known of several crown systems that stacking of numerous monomer units along a particular axis orientation can create a channel pore, as displayed by rotaxanes for example.[107] It may therefore be considered that ordered stacking within the crown lattice can afford a channel, through which the insertion of $(SN)_x$ strands may be achieved. Alternatively, the presence of a self-assembling polymer precursor, in the form of S_2N_2, may indeed invoke ordered stacking of the crown ether repeat units, so that a pore network around an $(SN)_x$ wire, is created. Crown systems that are inherently liquids (oils) at room temperature were hoped to offer a degree of solubility to the polymer, should incorporation of the latter have proved successful.

The exposure of several crown species to S_2N_2 vapour, in wide capillary tubes, was not found to yield any product that was characteristically dark blue-black in colour. Instead the oily [18]aneO_5S, [12]aneO_3S and [9]aneO_2S crowns reddened in colour almost immediately, and small orange-red needles grew within the oil after approximately one hour. Prolonged overnight exposure to the nitride vapour resulted in an increased concentration of crystal growth, but no colour change to the oil. Careful removal of a single crystal from each of the capillary sample tubes and subsequent XRD analyses confirmed the formation of S_4N_4, as presented in Figure 39. It is believed that increased moisture content of the crown systems, as a liquid, may be attributable to the instantaneous dimerisation of S_2N_2, giving rise to the growth of the S_4N_4 crystals.

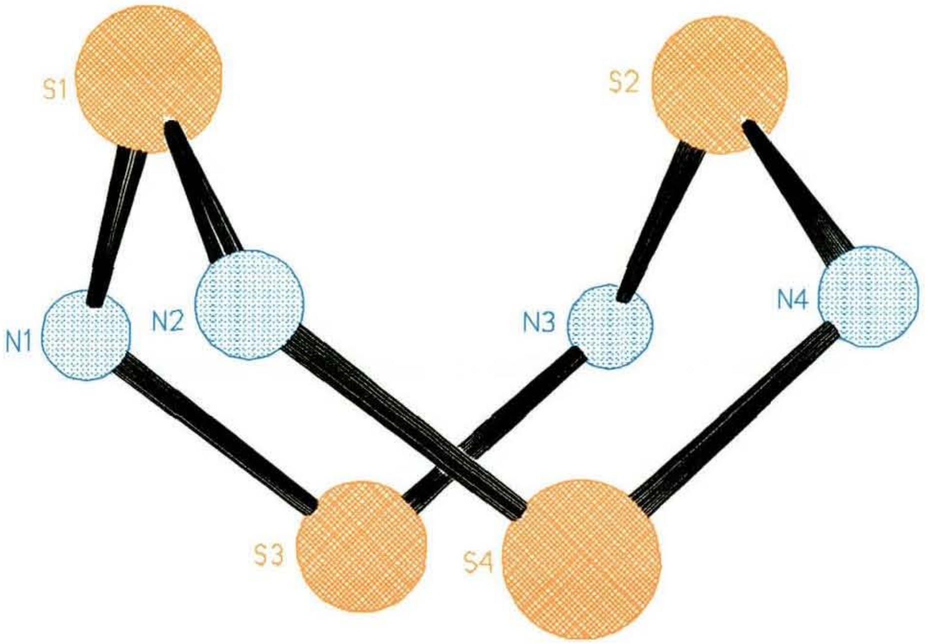

Figure 39 – ***A ball-and-stick representation of the X-ray structure of S_4N_4 as obtained through interaction of S_2N_2 vapour with [18]aneO_5S, [12]aneO_3S and [9]aneO_2S crowns.***

Reaction of the white solid [14]aneS_4 and [18]aneO_4S_2 crown systems with S_2N_2 vapour affords bronze coloured crystalline products in each case. Microscopic examination of the samples suggested the observed colour change was the result of surface bound aggregation of, presumably, $(SN)_x$ single crystals to the individual particles of the crown. The white colour of the crown starting material was still clearly visible, under high magnification, with interspersed groupings of polymer crystal clusters. The anisotropic nature of $(SN)_x$ in terms of colour, often results in it adopting a bronze lustrous appearance. In this case, therefore, it may be likely to assume that the surface of the crowns provide a suitable environment for $(SN)_x$ growth, without facilitating any intermolecular reaction.

Conversely, the interaction of dibenzo-24-crown-8 with S_2N_2 vapour affords a glimmering black coloured crystalline product. In this instance, it is important to note that the dibenzo-24-crown-8 material is, natively, of crystalline appearance. Analysis under microscope does not indicate any sort of $(SN)_x$ crystal adhesion to its surface, but instead, a universally distributed blackening is observed. The reaction product is again subject to S_4N_4 impurity contamination and subsequent washing with CH_2Cl_2 dissolves both the S_4N_4 and the crown itself, leaving only a black coloured residue. Both Raman and IR spectroscopy of the remaining residue shows good similarity to that of $(SN)_x$, but it is not clear whether incorporation of the latter occurs during the course of such a reaction. Regardless, any interaction between the $S_2N_2/(SN)_x$ and the crown system does not to appear increase the solubility of the polymer. Attempted single crystal XRD analysis of the black crystals did not provide any further insight relating to the structure of the product, perhaps itself suggestive of a polymer surface coating, as diffraction of dibenzo-24-crown-8 single crystals is readily achievable using analogous methods.

3. Reactions and Interaction of S_2N_2 with Latent Fingerprints and Inkjet Ink Residues

Nearly half a century ago, the discovery of the fascinating conductivity properties associated with $(SN)_x$ stimulated considerable interest in both the polymer itself and in its precursor, S_2N_2. Interest in both species continues to this day, and recent work has, for example, probed the structure of both the monomer[25] and the polymer,[30] and re-addressed the polymerisation process.[31, 46] For all this interest, however, and despite the intensity of the initial work that was prompted by the first observations of superconductivity,[4] practical applications of the polymerisation process, and utilisation of the polymer, have largely remained elusive. Although some success at incorporating the polymer into functional systems has been recorded (see examples quoted in reference 39), the efficiency and stability of such arrangements appears to have mitigated against realistic applications.

During the course of this work, the synthesis of both S_2N_2 and $(SN)_x$ were initially undertaken in order to allow their reaction chemistry and molecular occlusion capacity to be studied. Throughout these investigations, an unexpected observation was noted regarding the interaction of S_2N_2 with forensically pertinent materials, and showed that polymerisation may be induced, and visualisation of the material effected through the resulting dark blue/black polymer. Subsequent technique development has since afforded two cutting edge techniques that have attracted tremendous interest across the world-wide forensic community.

3.1. Initial observations - Fingerprints

S_2N_2 can be readily generated *via* the thermal cracking of S_4N_4 through silver wool, and in the course of previous work that concentrated on loading this material into microporous cavities (see Chapters 2 and 4), a modified apparatus assembly was fittingly developed, enabling efficient and safe production of the former, in reasonable quantity. These occlusion type reactions were brought about by introducing the zeolite materials into static vacuum systems containing S_2N_2; the volatile nature of the latter then meaning that simply warming the system to ambient temperature, under reduced pressure, allowed the nitride to diffuse into the target samples. During the course of such work, however, it became apparent that the S_2N_2 vapour interacted with latent fingerprints that were randomly present on the sample vials used to contain the microporous materials.

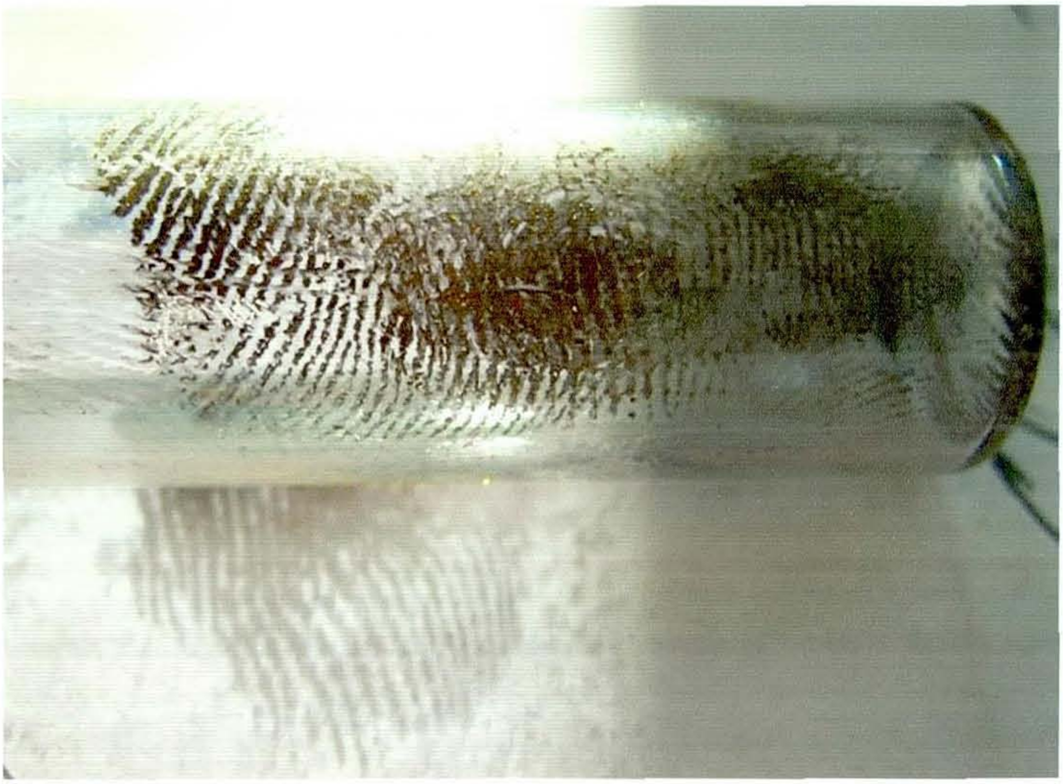

Figure 40 – ***An example of the $(SN)_x$ enhanced fingerprints on a glass sample vial as observed during initial zeolite occlusion studies.***

Subsequent experiments revealed that these initial observations were not purely coincidental and perhaps the result of an obscure contaminant on the surface of the fingers used to hold the sample vial. Instead, latent fingerprint deposits appeared to be reproducibly enhanced by nitride vapour, and presented themselves as dark blue/black enhanced ridge patterns. This initially serendipitous observation lead to a more systematic evaluation of the interaction process and enabled its limitations to be widely investigated.

3.2. Latent fingerprint detection using S_2N_2

Samples containing latent fingerprints (those invisible to the human eye) on a broad range of media were introduced to freshly generated S_2N_2 atmospheres, using the same reaction vessel and procedure to that previously employed in the zeolite work (see, for example, Section 2.4). Figure 41 illustrates examples of prints obtained from six different substrates, chosen primarily to represent as wide a variety of porosity, chemical composition and morphology as possible. In all cases, it became apparent that the interaction of S_2N_2 with the fingerprint deposits readily induced polymerisation, which has then progressed with time, eventually imaging the print in a way that it becomes visible to the human eye, without the need of complementary lighting *etc.*

Typically, sample exposure times spanned over 2-3 hours in duration, with prints often being enhanced on the more non-porous materials (foil, glass, plastics) over several tens of minutes, compared to slightly longer time-frames for the more porous samples; presumably the result of increased adsorption of the nitride vapour by the substrate itself. It is imperative to note a number of points regarding this effect: firstly, the materials in question were not primed or cleaned in any way and were simply used "as received". Additionally, and of greatest importance, fingerprints placed on the materials were not deliberately charged with excess secretions by intentional loading, they were merely applied as straightforward thumb or finger prints, from a number of individuals, in a manner consistent with the everyday deposition of prints pertinent to forensic application. Finally, owing to the dark blue/black colour of the $(SN)_x$ polymer, all of the enhanced prints shown in Figure 41, have simply been photographed and digitally stored. There was no need for digital picture enhancement following image capture, or indeed any form of complementary imaging technique to aid the contrast of the nitride coated ridge pattern, from the background to which it was adhered.

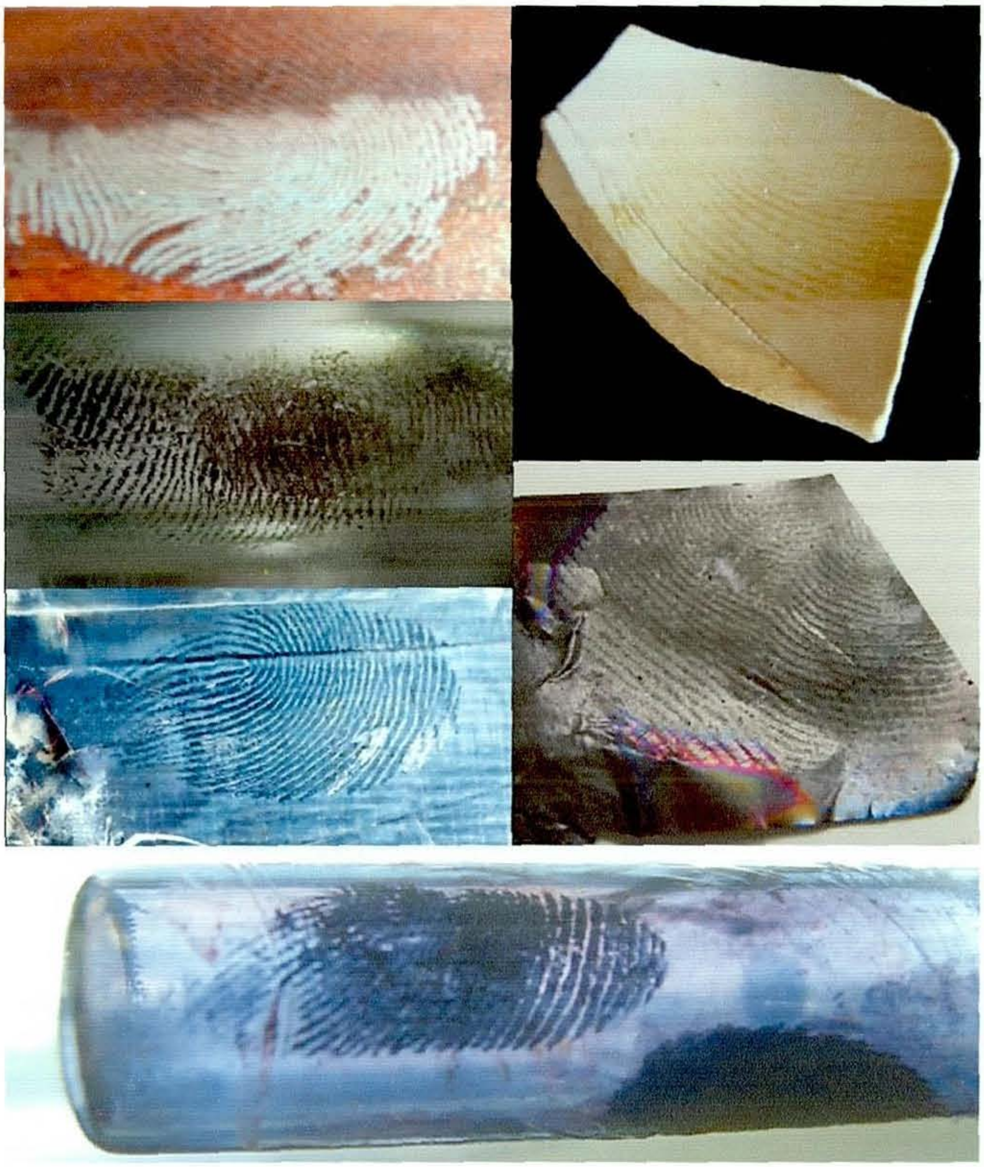

Figure 41 – ***The induced growth of $(SN)_x$ over latent fingermark residues on various sample surfaces (Clockwise from top left: wood, ceramic pottery, aluminium foil, clingfilm, adhesive tape, glass).***

In order to obtain an indication pertaining to the level of resolution achieved from the enhanced prints shown above, 20x magnification of, in this instance, a paper sample, clearly shows the high print clarity that is attainable (see Figure 42). This example helps illustrate the preferential blue/black deposition over the fingerprint ridge pattern itself, compared to the 'background' paper. The fingerprint remains so clear that microscopic physiological features, such as ridge deltas (the area of the fingerprint where there is a triangulation or dividing of the ridges), are readily identifiable.

Figure 42 – ***$(SN)_x$* enhanced latent fingerprint on paper, viewed under 20x magnification.**

The presence of the polymer, $(SN)_x$, in the 'developed' fingerprints is strongly hinted at by the unique colour of the material (dark blue/black, though golden in strong reflected light), as there are few chromophores of this nature within sulfur-nitrogen chemistry. Its formation, however, may be confirmed through the use of Raman microscopy, as illustrated in Figure 43. The *in situ* Raman spectra of several enhanced fingerprints, from a variety of substrates, clearly show good comparison to that of $(SN)_x$ itself and indeed helps confirm growth of the latter across the fingerprint ridge pattern.

Prolonged exposure (overnight) to S_2N_2 vapour was occasionally found to 'overload' the fingerprint contaminated samples and typically resulted in a dark coating across the entire surface. Despite the fingerprints still being preferentially targeted by the polymer (the prints had a much denser distribution of $(SN)_x$ across them), their contrast to the remainder of the sample was reduced, but suitable images were still readily obtained. Accordingly, general practice was modified so that once prints were suitably developed, the samples were removed from the setup, photographed, and stored.

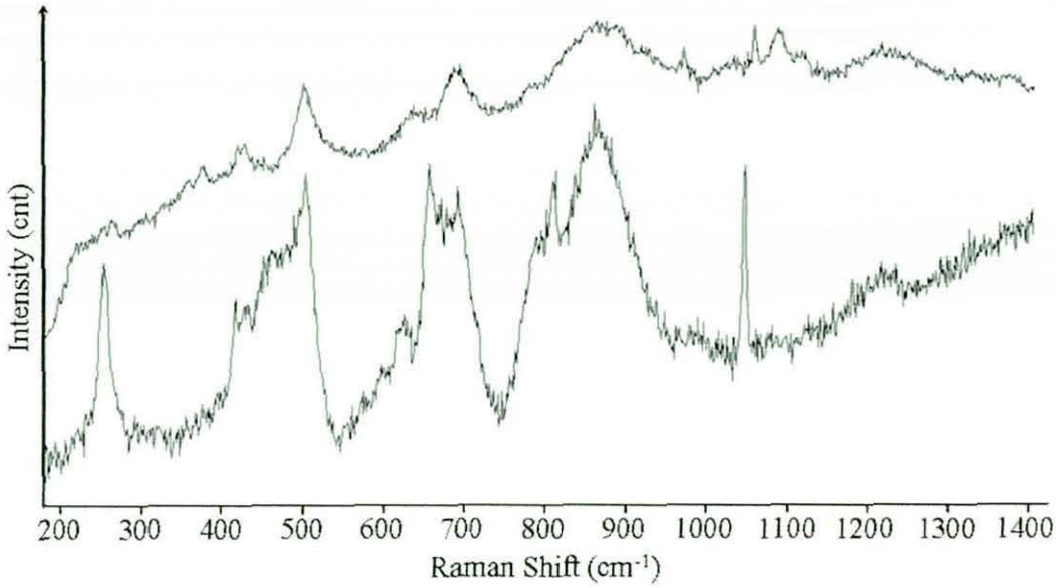

Figure 43 – ***Comparison of the Raman spectrum of $(SN)_x$ (lower) with that grown across the latent fingermarks (upper), obtained through in situ Raman microscopy.***

Once enhanced with $(SN)_x$, the developed prints appear to be air stable for many days (at least) and, if anything, are even more stable to aerial hydrolysis than bulk samples of the pure polymer. All samples remain indefinitely stable under an inert atmosphere, however, and was the storage method of choice for longevity purposes.

Although the typical colour of the $(SN)_x$ developed fingerprints appears largely dark blue/black under standard room lighting conditions, the anisotropic golden lustre can be induced when the samples are viewed under strong reflected light. This fascinating property of $(SN)_x$ allows enhanced prints on both light, dark and multi-coloured surfaces, to be readily observed. A suitable example of this application is the development of fingerprint residues on darker and/or multi-coloured surfaces (such as household refuse bags or paper money, as shown in Figure 44) and the subsequent use of high intensity polarised light (from a fibre optic light source) to allow visible observation of the ridge pattern.

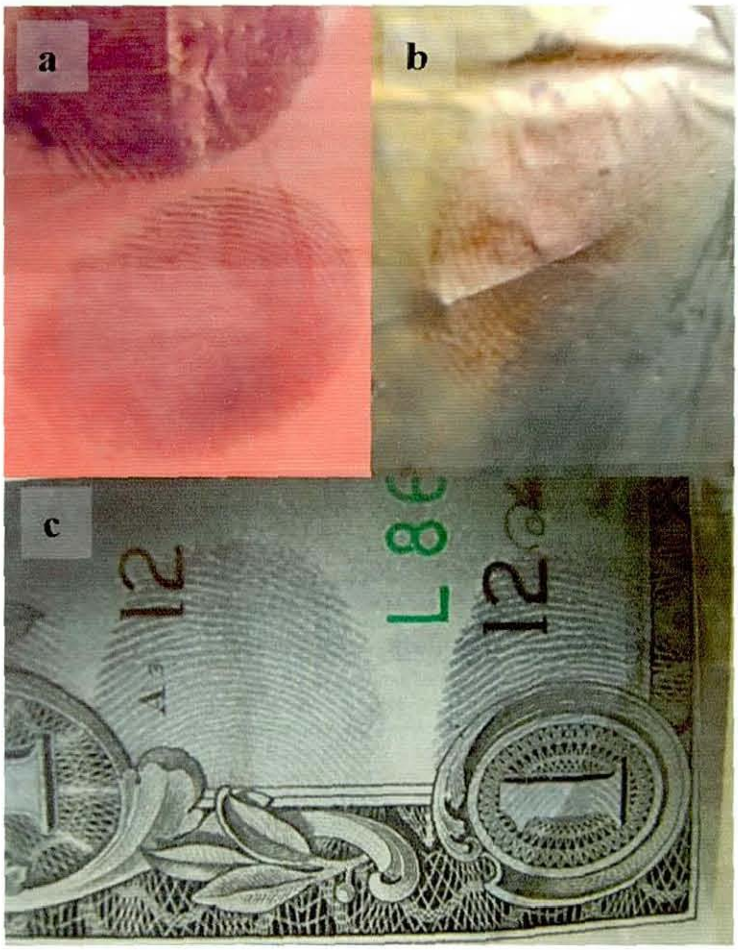

Figure 44 – $(SN)_x$ *enhanced fingerprints on (a) a red recycling refuse bag, (b) a black household refuse bag and (c) a US one dollar note.*

While latent fingermarks may be visualised on most of the above mentioned surface types, using one, or several, techniques in current circulation, there are two predominant substrates that have eluded forensic science fingerprint detection: fabrics and spent cartridge casings.

3.2.1. Cartridge casings

Until very recently, the detection of latent fingerprint residues on spent cartridge casings (fingermark residues placed on a cartridge by an individual when loading a gun and retrieved after firing) have troubled forensic scientists across the world. Principally, the problems arise through a combination of environmental stressors experienced by the metal casing surrounding the bullet, during firing. Despite many variables being present across the range of ammunition and cartridge type used, all cartridge casings typically experience severe flash temperatures, coupled with varying degrees of friction, as the shell exits the chamber of the gun. Consequently, retrieval of any fingerprint evidence immediately becomes challenging as not only is most, if not all, organic print content destroyed during the high temperature transient phase, but any friction has the capacity to remove the fragile latent residues.

Corrosion science has proved to play a pivotal role in recent developments that have concentrated on the detection of latent fingermarks on metal surfaces. A technique has been developed by John Bond that utilises redox reactions taking place between the surface of a metal and a fingerprint residue.[182] It is believed that 'aggressive' ions present in the latent deposit, such as chloride, have the capacity to microscopically corrode the metal surface, allowing subsequent electrostatic imaging procedures to visualise the ridge pattern, even following wiping or washing of the sample.[183] This said however, when applied to discharged cartridge casings, although feasible, the success rate of the technique falls to levels below 10%,[183] presumably the result of both thermal and frictional stressors during loading and ejection. Moreover, the cascade powder (conductive toner powder) used to image the fingerprints during electrostatic charging becomes extremely vulnerable to disturbance once the charge is removed. Accordingly, it was found that by subjecting the metal to temperatures approaching 600°C, the powder would bind to the surface and have a reasonable degree of fixation. Unfortunately, in terms of a practical forensic application, the extreme heating conditions required to set the visualised print means that the cartridge casings often become warped and distorted, preventing any subsequent exhibit analysis (for example, comparison microscopy looking at hammer markings and unique gun barrel grooving).

The desire for a non-destructive, highly reproducible technique, suitable for use on spent cartridge casings, therefore becomes of tremendous interest. The interaction of S_2N_2 with a small 5 mm cartridge was thought to be an appropriate starting point. Such a cartridge was readily available, in 'blank' form, and although likely to experience lesser thermal degradation through firing (when compared to more mainstream 9 mm rounds, for example) it provided a suitable platform to assess the plausibility of this technique. In this instance, a 'normal' fingerprint was placed around the centre of the cartridge and then loaded into the chamber of the pistol, using tweezers. Following discharge, the casing was retrieved, again using tweezers, and placed into the side-arm of the S_2N_2 setup. Following approximately 20 minutes of nitride vapour interaction, a faint ridge pattern became visible. Over the course of several hours, the polymer enhanced print intensified in colour (see Figure 45) but overnight S_2N_2 saturation appeared to 'overload' the sample and resolution between the print and the brass casing background was slightly reduced.

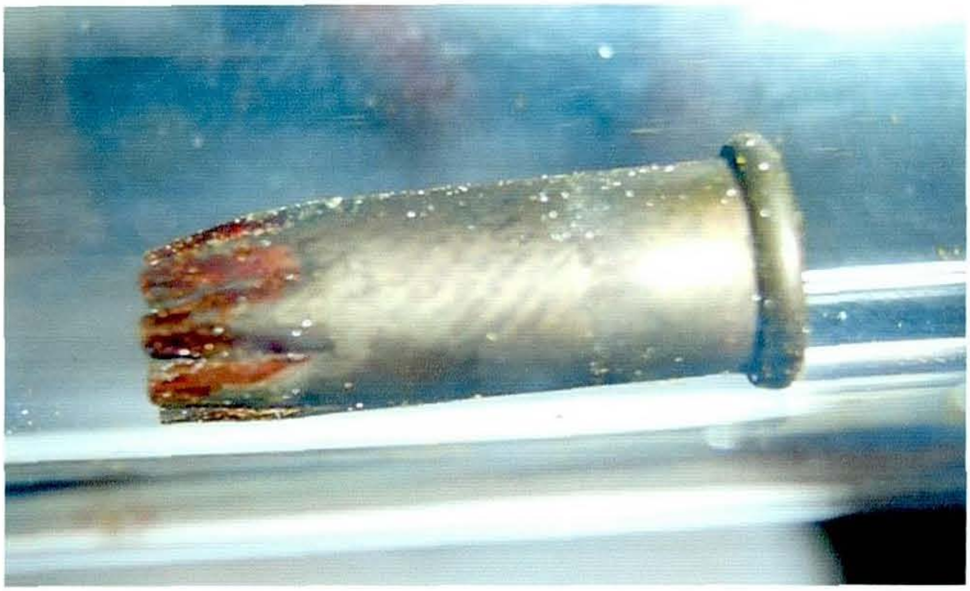

Figure 45 – ***$(SN)_x$ enhanced fingerprint on a spent cartridge shell; photograph taken in situ through the glass side-arm.***

In light of such findings, and following discussions with various forensic organisations, an assortment of spent cartridge casings became available for enhancement attempts. The casings themselves ranged from 9 mm handgun rounds, to large rifle rounds, but all samples were typically handled prior to firing and the casings then stored in a large 'bin' for approximately six months (therefore simulating an ageing effect). Upon exposure to S_2N_2, fingerprint residues from the largest of the samples, a rifle cartridge casing, became noticeably enhanced over the course of *ca.* 30 minutes. Similarly, the $(SN)_x$ enhanced print intensified in colour (and contrast) over the next hour, and was removed from the setup at this point to reduce the risk of polymer overloading.

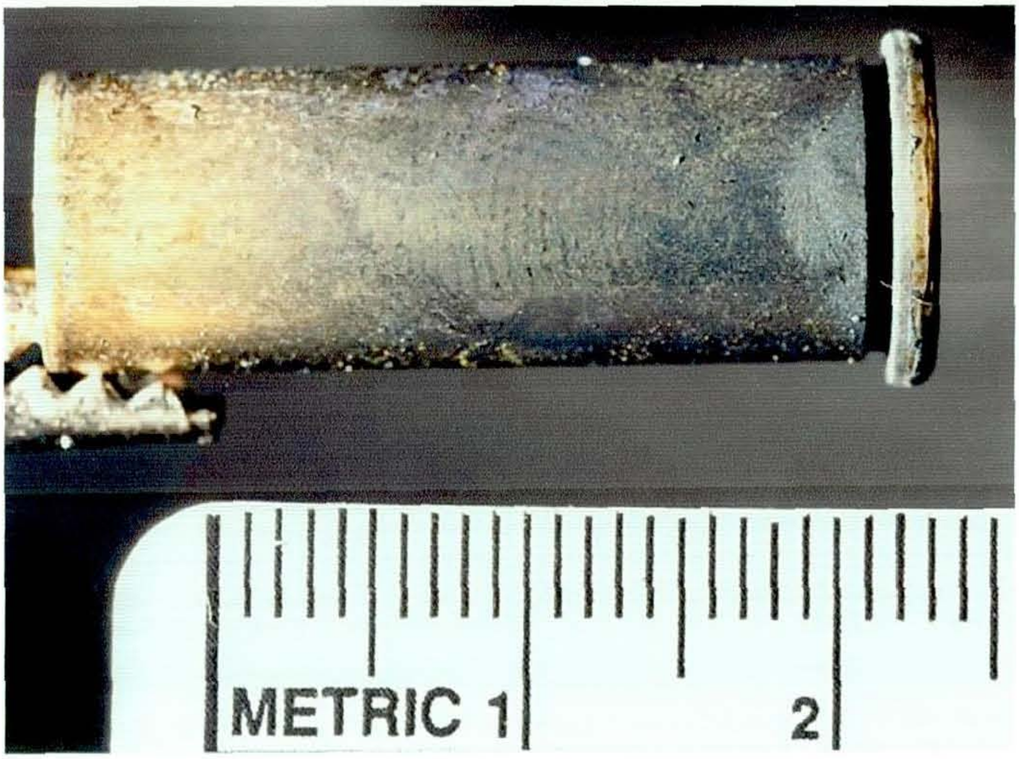

Figure 46 - *$(SN)_x$ enhanced fingerprint on a spent rifle cartridge casing.*

3.2.2. Fabrics

Currently, there is no proven process for the development of latent fingerprints on fabrics (cotton, nylon, synthetics, *etc.*). Only in rare circumstances where there are signs of blood stained fingerprints, are prints plausibly detected, but even then, the success rate is very low. The radioactive sulfur dioxide process was thought to offer the possibility of fingerprint development in some cases, but it has since proved unsuccessful in the limited number of suitable cases that have been treated.[120, 184] The protocol behind the proposed radioactive SO_2 technique was that SO_2 gas was hoped to dissolve in the water present in latent fingermarks. Consequently, following exposure to the radioactive gas, the presence of fingerprints were hoped to be detected and recorded using autoradiography. Unfortunately, the process itself proved highly inefficient, required specialist facilities and trained staff, development times could take several weeks, and the running costs and inherent radioactive risks, were high.

Accordingly, the use of S_2N_2 as a fingerprint development tool was again tested, with particular focus on latent fingerprint contaminated fabric samples. Initial work looked at the plausibility of latent print enhancement on a new, unused cotton sample. In this case, the fabric was removed from the packaging, cut accordingly to size (*ca.* 5 x 5 cm) and several fingerprints were deposited at various locations across the sample. The use of a graduated optical microscope allowed the 'threads per millimetre' value (tpmm) of 6 to be determined from this specific sample. The tpmm value provides an indication into the spacing of individual fabric fibres that constitute the overall exhibit in question; evidently, it is believed that fabrics possessing fewer tpmm will prove significantly more problematic at retrieving print definition and characteristics, as significant ridge detail will be lost in the 'voids' between each thread. Home Office Scientific Development Branch (HOSDB) research has postulated a minimum of 3 tpmm should be the minimum requirement for useable fingerprint determination.[184]

Following exposure to the vacuum S_2N_2 atmosphere for *ca.* 20 minutes, the cotton sample itself remained largely unaffected, but the latent fingerprints became selectively enhanced. Over the course of several hours (the sample was left in the setup overnight) the fingerprints were markedly enhanced and clearly stood out from the white cotton background. Following removal from the setup, the ridge pattern appeared highly detailed, with noticeable physiological print characteristics.

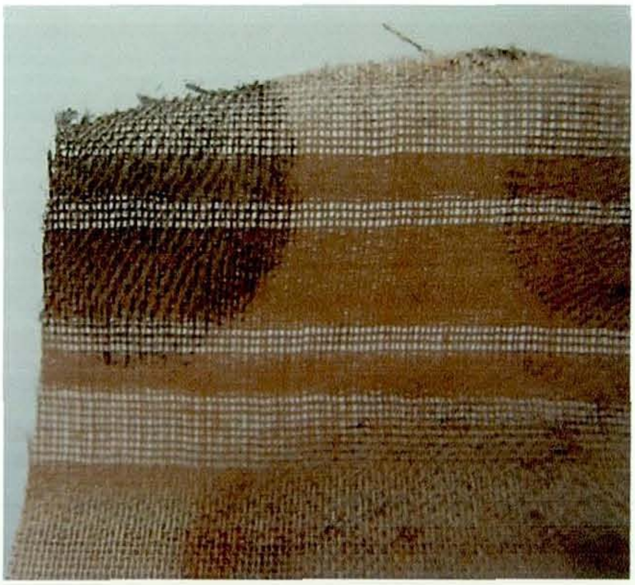

Figure 47 – *$(SN)_x$* *enhanced fingerprints on cotton.*

Attempted fingerprint detection on other fabric samples was also attempted: namely nylon, and synthetic mixtures. In both cases, suitable print definition was obtained following overnight S_2N_2 vapour exposure (see Figure 48). It appears, therefore, that the fabric material does not seem to restrict the applicability of this technique in terms of latent fingerprint detection.

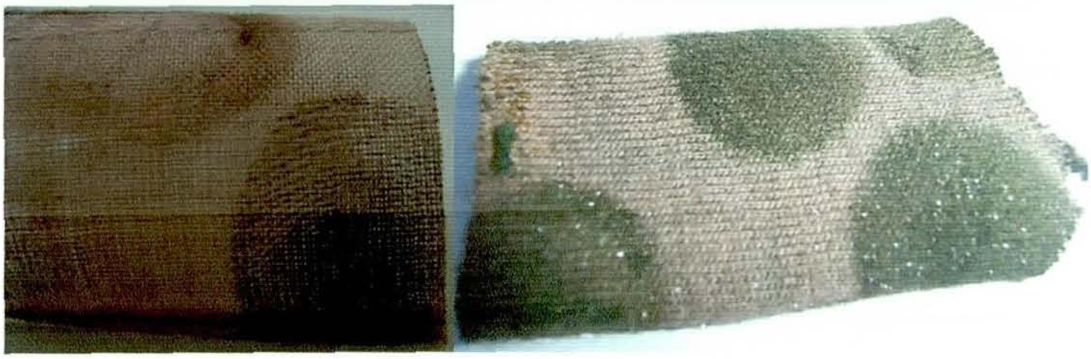

Figure 48 - ***(SN)$_x$ enhanced fingerprints on nylon (left) and a mixed synthetic fabric (right).***

A caveat must perhaps be acknowledged, however, as over the time frame of this study, it was not experimentally plausible to investigate every fabric sample type in production. It was found, though, that the effects of creasing and/or folding of the materials did not detrimentally effect the $(SN)_x$ development process.

3.2.3. The interaction process

It became important at this point to try and address the nature of the initial interaction between S_2N_2 and the materials present within the latent prints. With a myriad of potential print components present in each individual latent residue, and an array of plausible contaminants arising from typical daily activities (sebum, lipids, wax esters, *etc.*), pin-pointing one, or even several, species responsible for the induction of $(SN)_x$ growth, was a task far greater than experimental constraints permitted. Accordingly, in order to help identify which class of components (WSD or NWSD) may be responsible for the interaction, comparative tests were conducted. Interestingly, however, it was found that prints could be developed from both paper and plastic samples which (after placement of the fingerprint) have been soaked under water or under ether, and then dried. It was expected that different components of the print would be removed in each case (the WSD removed during immersion in water and the NWSD removed following immersion in ether), but either residue appeared to still be amenable to this technique, thereby suggesting that more than one class of component can interact with the nitride. With respect to forensic application, samples that have been previously wetted possess reduced chance of fingerprint development using conventional methods (largely the result of many techniques targeting aqueous components within the sweat secretion). Moreover, ether immersion is often used within illegal drug organisations to help remove traces of illicit drugs, such as cocaine,[163] from plastic wraps and packaging, and has, hitherto, provided numerous problems during attempted fingerprint detection (simply the plastic wraps themselves are notoriously difficult to obtain prints on).

Thermal treatment of samples was considered to be another pertinent method of removing volatile organic components from the latent deposit. In this case, fingerprint contaminated metal samples (aluminium) were heated (up to 500°C) in a furnace for extended periods of time (24 hours) before being exposed to either S_2N_2 vapour, or $(SN)_x$ sublimate (see Section 3.6). In both instances, successful print development resulted.

Attention duly focussed on the interaction of S_2N_2 vapour with various 'dominant' individual fingerprint components. Several amino acids, fatty acids, lipids, and solvents were spotted onto paper, in a grid like fashion (see Figure 49) and, after extensive air drying, exposed to S_2N_2 vapour.

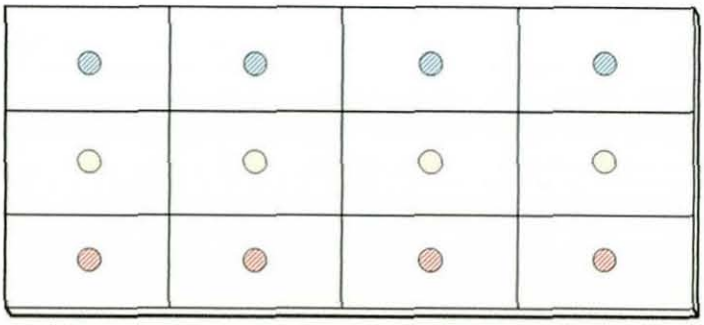

Figure 49 – ***Schematic representation of the spot-test grid used during S_2N_2 interaction studies.***

Initial results appeared to suggest preferential nitride affinity for both fatty acid and oil based materials; in this instance, oleic acid (an unsaturated fatty acid), capric acid (a saturated fatty acid) and mineral oil. Most intense $(SN)_x$ colouration was evident across both fatty acid spots, with intensified nucleation over the oleic acid residue. It is thought that the unsaturated nature of the latter has the capacity to interact more strongly with the reactive S_2N_2 moiety, therefore increasing the colour of the overlaying $(SN)_x$. Subsequent testing also suggested reasonable S_2N_2 affinity for some amino acid components (alanine and aspartic acid).

The effect of liquid traces were readily observed by spotting various solvents onto paper, in a similar manner to that described above, and exposing it to S_2N_2. It became clear that nearly all solvent spots were 'enhanced' in conductive $(SN)_x$, following less than an hour of S_2N_2 interaction. In this case, it is strongly believed that the spotting of various solvents onto a fibrous substrate, such as paper, induces a conformational change to the fibre orientation that is detected and enhanced by the nitride vapour, presumably the result of preferred nucleation, *vide infra*. Accordingly, when analogous tests were repeated using rigid plastic substrates, there appeared to be no significant enhancement, following thorough drying, of either aqueous or organic solvent marks.

Despite the associated trends observed above, it remains unclear as to the exact nature of the interaction process/mechanism involved during these studies. The formation of $(SN)_x$ across target components (fingermarks, fatty acids, *etc.*) is readily confirmed *via* Raman spectroscopy, and it can be argued, therefore, that no dominant reaction occurs between the S_2N_2 moiety and the responsible target constituent. However, there must be some sort of initial interaction that induces rapid polymerisation of surplus S_2N_2, selectively across the fingermark, presumably through heterogeneous nucleation. Heterogeneous nucleation is a localised building of one particular chemical component, *via* physical processes, that often forms at preferential sites, such as phase boundaries, or impurities.[185] Essentially, in this instance, the latent fingerprint residue is believed to act as a diverse impurity contaminant and attract S_2N_2 to its surface, whereby it becomes adhered (itself catalysed by any oily/fatty secretions present on the fingertips at the time of deposition) and is therefore readily able to react, and polymerise, with additional

S_2N_2 molecules. Additionally, and as briefly discussed earlier, surfaces comprised of a fibrous arrangement, such as papers, or a fine metallic oxide layer, as seen in some metals, have the capacity to undergo physical topographical changes following the deposition of a ridge skin impression.

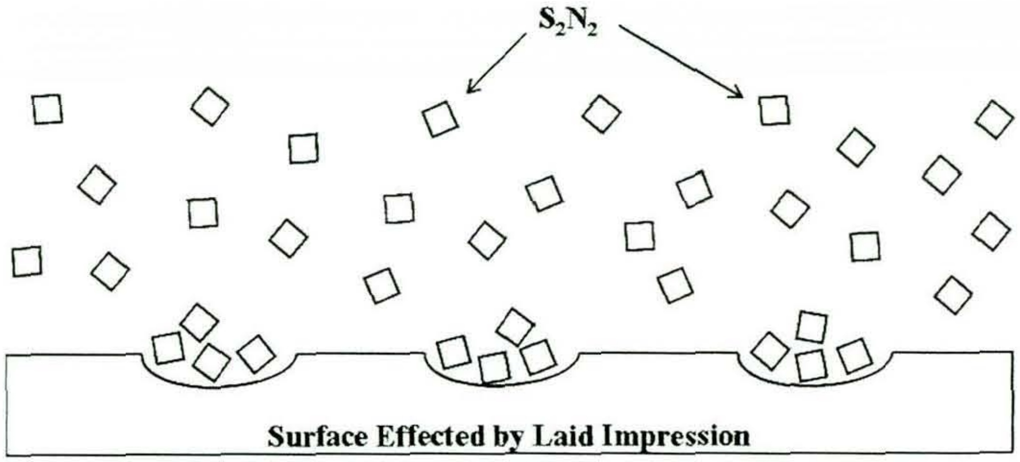

Figure 50 – ***Schematic representation of topographical surface alterations thought to induce $(SN)_x$ formation.***

Accordingly, their exposure to S_2N_2 vapour is thought to offer preferred nucleation sites owing to discrete surface areas that may serve as S_2N_2 'traps' which slow down or hold the nitride molecules for extended periods of time, compared to the free-flowing ambient vapour phase (see Figure 50). As a result of this, aggregations of S_2N_2 molecules are conceivably formed, and their polymerisation to $(SN)_x$ is thereby facilitated.

3.2.4. Ageing of prints

Latent fingerprints deposited on both aluminium foil and rigid plastic were aged for up to 2 weeks to determine the sensitivity of the S_2N_2 interaction over time. Following their exposure to the nitride vapour (two day old, week old and two week old samples were analysed), $(SN)_x$ enhanced fingerprints were developed over the course of several hours. It was found that, despite the time required for visualisation of the prints being slightly longer than that needed for 'fresher' deposits, the ridge detail, in all instances, was clearly made visible. Moreover, some of the (six month aged) fingerprint contaminated spent cartridge casings, discussed in Section 3.2.1, developed sufficient ridge detail following S_2N_2 exposure.

After searching various old storage containers for sealed artefacts that were sure to have been handled at some point (a long time ago), but remained untouched since, a 21 year old train ticket was found, stored in a plastic wallet ever since its use. Following careful removal from the protective wallet, using tweezers, a large portion of the ticket was cut (top two thirds), placed into the side-arm of the setup, and exposed to S_2N_2 vapour overnight. Upon removal from the system, the ticket appeared to be overloaded with lustrous blue/bronze polymer, but no obvious signs of fingerprint detail. With the knowledge that some the polymer may be slightly decomposed over time, it was hoped that by leaving the sample in atmospheric conditions for several days/weeks, enough polymer would be removed allowing any underlying detail to be observed. Indeed this proved to be the case, and following approximately one week of aerial hydrolysis, very faint fingerprint detail was visible under acute lighting conditions, as shown in Figure 51.

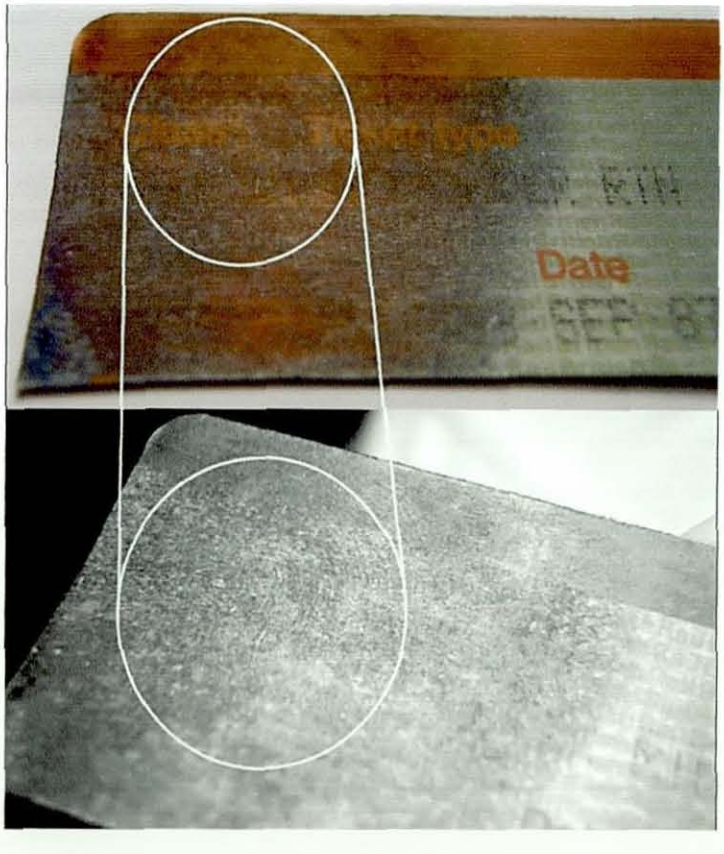

Figure 51 – ***Photograph showing an $(SN)_x$ enhanced fingermark obtained from a 21 year old train ticket.***

It became clear that this example constituted perhaps one of the oldest latent fingermarks to be successfully detected and enhanced within forensic science practice, and inevitably provides some indication as to the sensitivity and applicability of the S_2N_2 technique. Although the ageing process does seem to reduce the concentration of latent residue components on the immediate sample surface, their exposure to S_2N_2 has the capacity to induce localised polymerisation across the ridge pattern, irrespective of age (within experimental reason).

3.2.5. Conclusion

Despite the long history of fingerprint analysis, there is still a keen and highly active interest in the development of new techniques for latent fingermark enhancement/imaging.[133, 142, 157-159, 162, 164] Of all types of fingermark evidence, the latent print is not only the most commonplace, but also the most difficult to detect since they are largely invisible and typically require either chemical (ninhydrin, DFO, *etc.*), optical (luminescence, UV, *etc.*) or physical (powdering, VMD, MMD, *etc.*) treatment to differentiate them from the substrate material to which they are bound. Unfortunately, due to the ever increasing array of surface types and materials (porous, non-porous, semi-porous, textured, re-cycled, *etc.*) most contemporary detection techniques are effective on some substrates, but not others. Often, therefore, multi-step sequencing of detection techniques becomes essential for optimised clarity of results.[116, 184] Intriguingly, it appears that $(SN)_x$ growth across fingermark residues is not affected by surface type; it has been shown that good detection is possible on both porous, semi-porous and non-porous substrates. Moreover, common problematic samples, such as aluminium, fabrics and spent cartridge shells, have all provided reproducible positive results.

The use of S_2N_2 to selectively target, develop and enhance latent fingerprints on both discharged cartridge casings and various fabrics, in a non destructive manner, is currently the only method of its type within the worldwide forensic community. Such a ground-breaking technique has the capacity to significantly bolster the forensic arsenal and not only allow new exhibits to be examined more thoroughly, but also those involved in 'cold case' investigations to be re-addressed.

The use of an inexpensive, non destructive, solvent-free, self-imaging material may be considered the ideal technique for latent fingerprint detection; especially if its use could be extended to various different surface types. In many ways S_2N_2 fits the bill very effectively, thanks to the versatility of the media upon which prints may be developed, the fact that exposure times are relatively low (prints start to develop within minutes of exposure), both wetted and dry substrates may be examined, and that it is non destructive and non solvent based. Moreover, the conductive nature of the deposited $(SN)_x$ could, in theory, be utilised to digitally acquire images of the fingerprint ridge pattern (using conductive feedback that 'maps' areas of high/low resistivity). The unique anisotropic colour of $(SN)_x$ has also been shown to offer print identification on a variety of coloured backgrounds; a factor that often proves problematic with many conventional visualisation methods.[184] Clearly, however, there are some limitations to the technique, thanks to the fact that the apparatus required for the generation of S_2N_2 would, in its current guise, preclude portability (thereby being more suited to stand-alone laboratory testing); in addition, care is required in the handling of the S_4N_4 starting material. That said, the continued requirement for new fingerprint imaging methods means that the versatility of the technique could make it viable, following protocol optimisation, to complement or supersede other vacuum deposition techniques currently in practice.

3.3. Inkjet Ink

In light of the successful application in using S_2N_2 to detect and enhance latent fingermark residues, its interaction with other substrates/components was duly investigated. The focal point centred around inkjet ink; most inkjet printers function through the use of a print cartridge, consisting of tiny electrically heated chambers, that are constructed *via* photolithography. In order to produce an image, or indeed blocks of text, a current pulse must be passed through the heating elements, thereby creating a steam explosion within a chamber, affording a bubble that propels a droplet of ink onto the desired surface (typically paper). Hence, all inkjet printed images are comprised not of block ink patches, but tiny spots that, when viewed as an entirety, appear to be constant. It was proposed that the inkjet ink may have the capacity to act as a nucleation site for polymer growth, in an analogous manner to that suggested for the fingerprint deposits; as, in essence, the ink serves as an 'impurity' on a relatively constant medium (in this instance, paper).

In order to ascertain any sort of S_2N_2 affinity towards the inkjet ink components, faint wash-out type images (very pale, almost 'watermarked', variants of a standard image) were prepared using appropriate image editing software (typically Adobe Photoshop Elements) and printed onto standard 80 g/m^2 plain paper (Figure 52 (a)). After allowing the image to dry for several hours, it was introduced to the side-arm of the S_2N_2 setup and exposed to the nitride vapour. Within several tens of minutes, the image became noticeably darker in colour, with no significant colouration to the non-ink-printed areas of the sample. Following overnight enhancement, the image appeared much more vivid and of significantly greater resolution and contrast when compared to the initial wash-out image (Figure 52 (c)). Photographic editing using similar software allowed both the starting wash-out image (Figure 52 (b)) and the same image following S_2N_2 exposure (Figure 52 (d)) to be contrast enhanced to the same degree, thereby markedly enhancing the effect already visible to the naked eye.

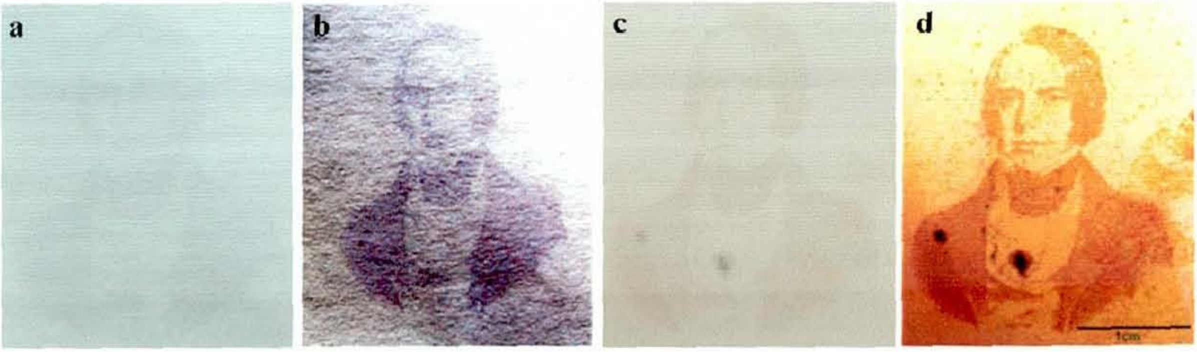

Figure 52 – *William Gregory, (a) printed in washout, (b) contrast enhanced, then (c) exposed to S_2N_2 vapour and (d) contrast enhanced.*

These findings suggested that there was indeed a preferred affinity of S_2N_2 to interact with inkjet ink residues and induce, presumably, polymerisation to $(SN)_x$, as seen for latent fingerprint deposits. Raman spectroscopy of the enhanced inkjet images further confirmed this hypothesis and showed good coincidence with Raman bands attributable to $(SN)_x$ itself. In essence, the resulting $(SN)_x$ enhanced images possess conductive properties that may help form the basis of conductive printed media, such as PCB's (printed circuit boards).

Interestingly, closer examination of the sample shown in Figure 52, above, revealed that polymer formation had also occurred on the reverse side of the paper (*i.e.* the 'blank' side of the paper that was not directly printed onto). This observation suggested that a significant quantity of one (or more) ink components had passed through the paper and remained on the reverse side as a colourless, mirror-image replica of the original image (whereby it only became visualised upon exposure to S_2N_2). It appeared, therefore, that not only could it be confirmed that a colourless component of the original inkjet ink was volatile enough to diffuse through to the back of the paper, and remain there unchanged, but S_2N_2 is sensitive enough to detect and enhance this material, in the form of dark blue/black $(SN)_x$.

3.4. Inkjet-trace imaging using S_2N_2

The diffusion of various inkjet ink components through a sheet of paper, onto its reverse, begged the question as to the level of contact transfer (the transfer of one or more components of the inkjet ink from the original printed surface, to another surface that has come into contact with the former) that may be both plausible, and subsequently detectable through exposure to S_2N_2.

The most pertinent and practical scenario relating to such transfer was considered to be the interaction of an inkjet printed document with the inside surface of an envelope (*i.e.* mimicking the act of sending a document through the postal system). Such an approach revealed that S_2N_2 is exceptionally sensitive to these inkjet ink components, so much so that invisible traces left by direct contact with an envelope surface can in fact be enhanced. This phenomenon is illustrated in Figure 53; here, text has been printed onto a sheet of paper and allowed to dry (*ca.* 1 hour) before being placed into an envelope. This was left overnight (with a small book placed on the envelope to ensure constant contact between the envelope itself and the printed surface inside) and then the envelope opened, the contents removed, and the patch of the envelope that had been in contact with the printed text was cut out. At this stage, the area in question appeared completely blank; upon exposure to S_2N_2, however, the text transferred from printed paper to envelope, *via* the small amount of ink diffusion, became 'developed'. Upon removal from the vacuum apparatus, and photographed, the presence of text is clearly visible (in, of course, a mirror image).

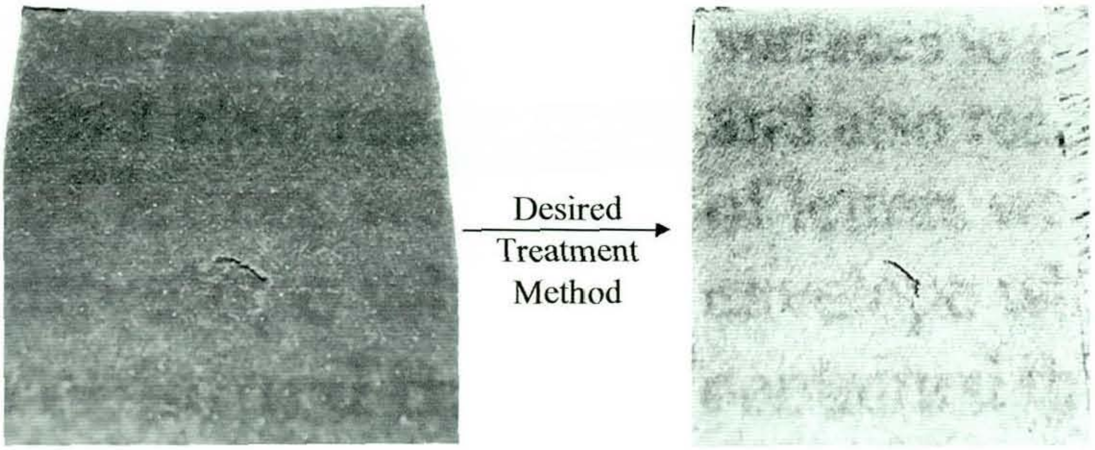

Figure 53 – ***Close-up of the image obtained when a sample area (ca. 1" width) from the inside of an envelope, which had been in contact with 12-point inkjet text, was exposed to S_2N_2.***

Note that before exposure, the area appeared completely blank and that the above is the raw image, with no processing to the original digital photograph, besides colour removal from the paper and a mirror image reflevtion. Subsequent digital processing can further resolve the text via simple contrast enhancement.

Further work highlighted the fact that the interaction of S_2N_2 with traces of inkjet components is so sensitive that the minute amounts of the latter diffusing through an entire sheet of paper can be detected. Thus, as shown in Figure 54, an image was printed, allowed to dry as before and placed into an envelope; a sheet of paper was placed onto the envelope and the combination again weighted to keep the components in place. After several days the external sheet was removed and the area adjacent to the image within the envelope cut out and exposed to S_2N_2 in the usual manner. Although rather poorly resolved, the image from inside the envelope is nevertheless clearly visible (in this case the image has been contrast enhanced).

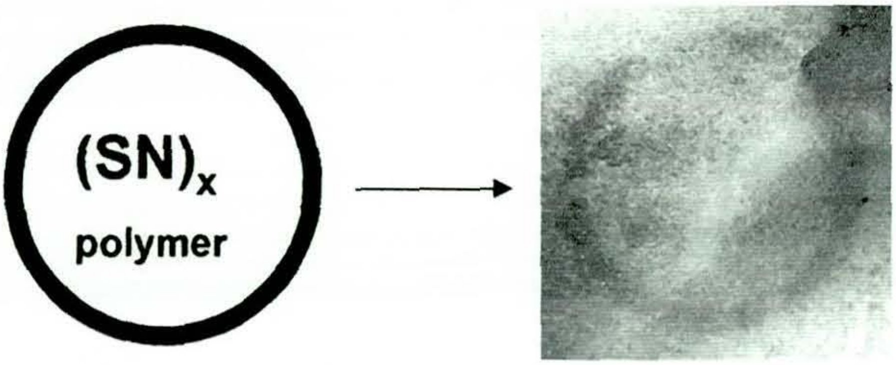

Figure 54 – ***(left) Original image printed out in inkjet and then placed in an envelope; (right) contrast enhanced image obtained without opening the envelope (using an additional contact sheet), via enhancement using S_2N_2.***

This result clearly indicates that initial interaction of S_2N_2 with a component of the inkjet ink may be initiated at extremely small quantities of the latter; presumably then further crystallisation of the polymer occurs over this initial product, and thus the image is 'built up'. This diffusion experiment also shows that it must be a liquid component of the ink that is responsible for the effect. Direct contact of printed paper to blank sheets could transfer small amounts of solid material which may, conceivably, act as nucleation sites for polymer growth. However, this could not produce results such as those illustrated in Figure 54.

3.4.1. DART Mass Spectrometry

It was important at this point to try and ascertain the nature of the inkjet ink components that were readily diffusing through the paper and remaining intact, inducing polymerisation of S_2N_2, upon contact. Conventional characterisation methods proved inconclusive as the trace quantities of ink components travelling through sheets were not isolable in sufficient quantity to permit any form of crystallisation or spectroscopic measurements.

Attention duly turned to the use of mass spectrometry; with a particular focus on the highly sensitive 'AccuTOF DART' technique. This form of mass spectrometry utilises **Accu**rate **T**ime-**o**f-**F**light measurements on **d**irect sample **a**nalysis in **r**eal time, to provide the user with exact mass measurements (to 4 d.p.). The technique itself is ideally suited in obtaining exact masses of trace compounds as a constant high mass resolution is present and there is no requirement to compensate resolution and sensitivity. The DART walk-up instrument was considered an ideal characterisational tool for these particular samples as it utilises a novel non-contact sampling method for mass spectrometry at atmospheric pressure, under ambient conditions. Moreover, DART can be used to analyse both gases, liquids and solids on various surfaces (the technique is often on silica gel plates, following TLC).[186]

Accordingly, the transfer of ink components upon contact with other paper sheets was investigated using the above mentioned mass spectrometric technique. Initial data was obtained from a neat ink sample, in both liquid form (directly from the ink cartridge, see Figure 55, upper) and following printing (*ca.* 3 x 3 cm black square printed onto 80 g/m^2 paper, see Figure 55, lower). The presence of 3 dominant components can be clearly identified and characterised using the AccuTOF mass analyser, and in turn provided a molecular composition of C_4H_7NO (2-pyrollidone), $C_9H_{21}NO_3$ (triisopropanolamine) and $C_{11}H_{18}N_4$ (tri(propylene glycol) methyl ether). Each of these liquids was subsequently confirmed as serving a particular role within inkjet ink formulations, thereby supporting the initial suggestions of the DART analysis. Interestingly, the triisopropanolamine (TIPA) component does not appear present in the ink following printing (and drying), therefore suggesting its presence is relatively short lived due to evaporative loss.

Blank mass spectra were also obtained on un-printed areas of paper in order to eliminate the possibility of any of the aforementioned peaks being attributable to some product of the paper fabrication process, and indeed no pertinent mass peaks were found.

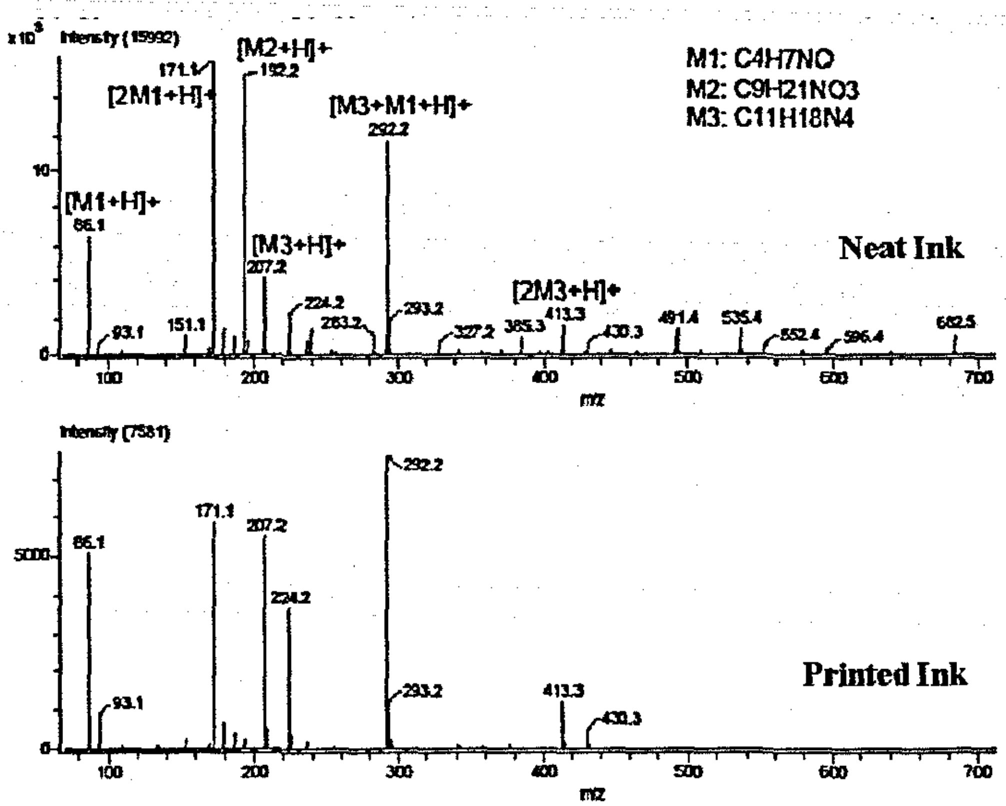

Figure 55 – ***AccuTOF DART mass spectrum of neat inkjet ink (upper) and inkjet ink following printing onto paper (lower).***

Through replication of the contact transfer process (two pieces of paper stacked onto the original paper sheet containing a printed black square and weighted for *ca.* 4 days), it was possible to analyse the contact areas of both contact sheets, adjacent to where the ink printed image was located. As illustrated in Figure 56, the first contact sheet (the one placed directly onto the printed image) was found to contain substantial traces of both 2-pyrollidone (M1) and tri(propylene glycol) methyl ether (M3). Similarly, the second contact sheet (the sheet placed directly onto the first contact sheet) contained both M1 and M3 components, in slightly lower concentrations (*ca.* 50% less), as would be expected *via* a diffusive type process.

The components present on both contact sheets are colourless, viscous organic liquids that possess low volatility and slow evaporation rates. The materials are typically used within ink formulations as solvents and homogenising agents and can be considered perhaps the most likely component to diffuse through the printed surface onto subsequent contact sheets; whereby it will largely remain untraceable by sight, for prolonged periods of time. Intriguingly, the images obtained from contact

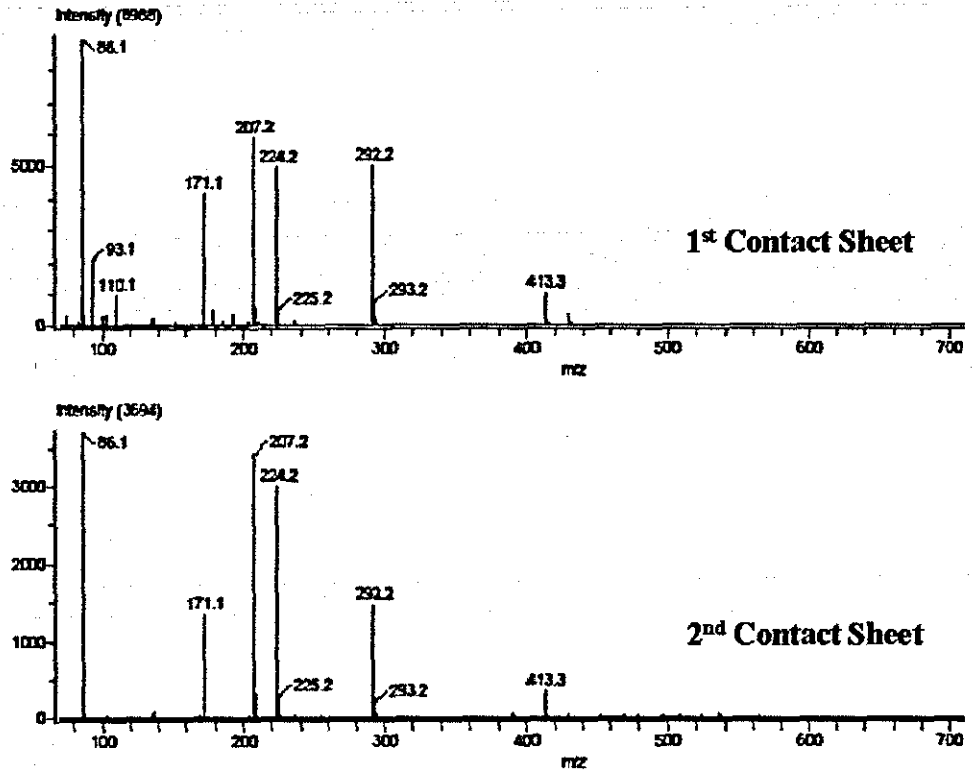

Figure 56 - ***AccuTOF DART mass spectrum of the contact area adjacent to a printed image on the first (upper) and second (lower) contact sheets.***

transfer experiments show a good degree of resolution and almost identical likeness to the original ink printed motif; an indication that ink component running/bleeding during diffusion must be absent from a macroscopic perspective. Perhaps the only feasible explanation of such an effect is either the high surface tension of the liquid phases or the combined effect of evaporation from the contact sheet surface coupled with progressive absorption of the ink components, therefore negating the possibility of bleeding.

Spot-testing investigations, in an analogous manner to that employed in Section 3.2.3, highlighted the affinity of S_2N_2 for both 2-pyrollidone and tri(propylene glycol) methyl ether, with dark blue-black $(SN)_x$ colouration prevailing after several hours of exposure. Interestingly, however, the nitride vapour also appeared to distinguish areas of the spot test strip that had been exposed to deliberate loading of some organic solvents (namely acetone and CH_2Cl_2, applied using a TLC spotter), in order to provide a suitable blank standard (*i.e.* a related substance thought not to interact in any way with S_2N_2). This observation suggested that in fact the effect that was being seen was the result of a change in the topographical paper surface as a result of changes in paper fibre orientation following wetting; as there was no feasible way that traces of the organic solvents themselves (6 small drops) actually still remained (as samples were typically dried for at least 16 hours in a fume hood).

These conclusions were further explored through analogous spot test studies on rigid non-porous substrates, namely polypropylene. In this instance, the three components (M1, M2 and M3) as well as acetone, toluene, hexane, CH_2Cl_2 and water, were spotted across the sample surface, in a grid like fashion, and allowed to dry overnight before being exposed to S_2N_2. The results from this investigation suggested that there was predominant nitride affinity, and induced polymerisation, across the tri(propylene glycol) methyl ether spotted areas, with some epitaxial $(SN)_x$ growth noted over 2-pyrollidone residues. None of the other test solvents were detected and/or enhanced by the S_2N_2 vapour.

Accordingly, it appears that the contact of solvent systems with porous media, with particular reference to paper, can be detected by S_2N_2 vapour, presenting itself in the form of $(SN)_x$; presumably the result of changes in the surface fibre orientation induced *via* wetting. The preferential affinity of S_2N_2 towards significant colourless inkjet ink components (2-pyrollidone and tri(propylene glycol) methyl ether) is observed regardless of surface type/morphology however, as no other solvent systems were detected following wetting of plastic substrates; and it is perhaps the latter of these two components that is responsible for the contact transfer observations discussed in Sections 3.3 and 3.4.

3.5. Written Indentations

The implication that surface topography changes could be sensitively detected and enhanced using the $S_2N_2/(SN)_x$ system offered the possibility to explore the effects of written indentation impressions on paper. Indented writing, or second page writing, is the impression from a particular writing instrument (usually a pen) that is captured and visualised on the subsequent sheets of paper found below the one that contains the original text/image (usually 1-4 sheets below is the limit). Currently, Electrostatic Detection Apparatus (ESDA) provides the only feasible method of detecting such impressions, and is commonly used in questioned document examination. This process relies on the passage of a high voltage static charge across the document in question, thereby inducing a variably charged surface, with denser static charge remaining within any impressions that may be present. Visualisation of the impressions is readily afforded following surface covering with cascade (toner) powder.

Figure 57 – ***A written impression, three sheets below the original text, detected and enhanced by $(SN)_x$.***

In a similar manner to the ESDA technique, sheets of paper were retrieved from a stack (up to 5 down), several sheets below where the original text was fashioned and individually exposed to S_2N_2. Within several minutes of nitride interaction, the original text could clearly be seen on most of the samples (1-3 sheets below the original text, see Figure 57) and overnight exposure resulted in faint impression enhancement of the 4th sheet down from the original stack. No impressions were retrieved from the 5th sheet.

3.6. $(SN)_x$ sublimation

The subliminal nature of $(SN)_x$ was elucidated during the mid 20th century, and despite inconclusive evidence pertaining to the nature of the vapour phase species (see Section 5.1.6), it is clear that the polymer reforms, upon condensation, predominantly as thin (epitaxial) films. The sole use of $(SN)_x$, and its sublimation directly onto samples discussed above (latent fingerprints, inkjet ink and written impressions) was considered favourable in both minimising (and simplifying) the glassware setup as well as facilitating portability; an issue that the S_2N_2 technique precludes.

Using the apparatus shown in Figure 58, target samples were readily exposed to $(SN)_x$ 'vapour' by carefully wrapping them around the cold finger (A) and fixing them in place with adhesive tape. Initial cooling of the samples was induced using a slurry of ice placed into the cold finger, but subsequent work revealed a more facile and effective result could be achieved by placement of the sample, attached to the cold finger, in a refrigerator for *ca.* 10-60 minutes, dependent on the insulating properties of the material in question.

Figure 58 – *$(SN)_x$ sublimation setup.*

The polymer itself (typically *ca.* 20 mg, although suitable detection and enhancement was found feasible using only 3 mg of $(SN)_x$) is loaded into the base of the setup (B) and, once the cold finger is attached, heated to between 130-140°C, under dynamic vacuum, whereupon it readily sublimes and condenses across the target sample. It was found that the use of a static vacuum did not facilitate sublimation onto the cold finger, and simply resulted in polymer decomposition as a result of prolonged heating.

In most instances, the deposition of $(SN)_x$ appeared to target the contaminant of interest, whether it be latent fingerprint deposits, inkjet ink, or written indentations, with significant resolution prevailing from background deposition. The speed of development was on the order of several tens of seconds for nearly all the samples tested, however fingerprint residues on fabrics were found to take significantly longer to be enhanced (*ca.* 2-3 minutes), presumably owing to the porous nature of the weave pattern.

Wash-out printed inkjet images became markedly enhanced after only several seconds of $(SN)_x$ vapour exposure, yet samples from contact transfer procedures failed to provide any indication of detection/enhancement. This observation is largely indicative of the variation between the dominant volatile species present between the two techniques; whereas S_2N_2 is the predominant (only) volatile species in the original large setup, the sublimation of $(SN)_x$ is thought not to provide substantial quantities of the latter, but instead yield other S-N moieties, that evidently do not interact with inkjet ink residues in the same way.

One drawback of the sublimation technique as it currently stands, is the inability to evenly condense $(SN)_x$ films across the sample surface. The vertical approach adopted through the use of a cold finger, bearing the sample, inevitably means that the lower portion of the sample becomes more heavily coated with the polymer, compared to the upper sections (due to the vapour condensing at coolest location closest to the bulk source). Unfortunately, mounting the sample in a horizontal orientation was not physically plausible due to the necessity to fabricate custom apparatus that would take account of sample dimensions, methods of cooling, *etc*. In essence, therefore, fingerprints and written impressions were more readily enhanced towards the bottom of the sample, but overloading proved to be an issue if the sample was not removed shortly after sublimation commenced; in contrast, prints and impressions towards the top of the sample became well resolved and enhanced with minimal overloading. It was found, therefore, that by altering the location of the sample on the cold finger (fixing it slightly higher up in most cases), greater clarity of the target contaminant could be achieved.

As briefly eluded to earlier, the most problematic surface type to develop fingerprints from, using this method, was that of fabrics (primarily cotton). It was believed that the weave pattern of the material gave rise to polymeric growth on the cold finger behind the sample, as opposed to directly onto the fabric itself (due to the cold finger being cooler than the sample). Evidently, there were no physical means to alleviate this issue, but faster sublimation rates were hoped to directly induce $(SN)_x$ growth across the fabric samples as the speed of condensation would be so fast that it would almost overload the cold finger and therefore also deposit on the sample surface. In order to achieve this, the bulk $(SN)_x$ sample was heated, with caution, to 140-145°C under dynamic vacuum and allowed to condense on the thoroughly cooled (*ca.* 1 hour) fabric/cold finger assembly. Following several minutes exposure to the vapour, the fabric samples became coated with $(SN)_x$ and the latent fingerprint outlines became visible. Unfortunately, in many cases, no ridge detail (or very little) was evident, resulting in a collection of 'empty' prints, and it is believed that this is the result of the augmented deposition rates, as seen in analogous VMD attempts.[187] When the sublimation temperature was lowered by several degrees Celsius, a mixed selection of fingerprints were detected; some showed partial ridge detail, and others remained 'empty'.

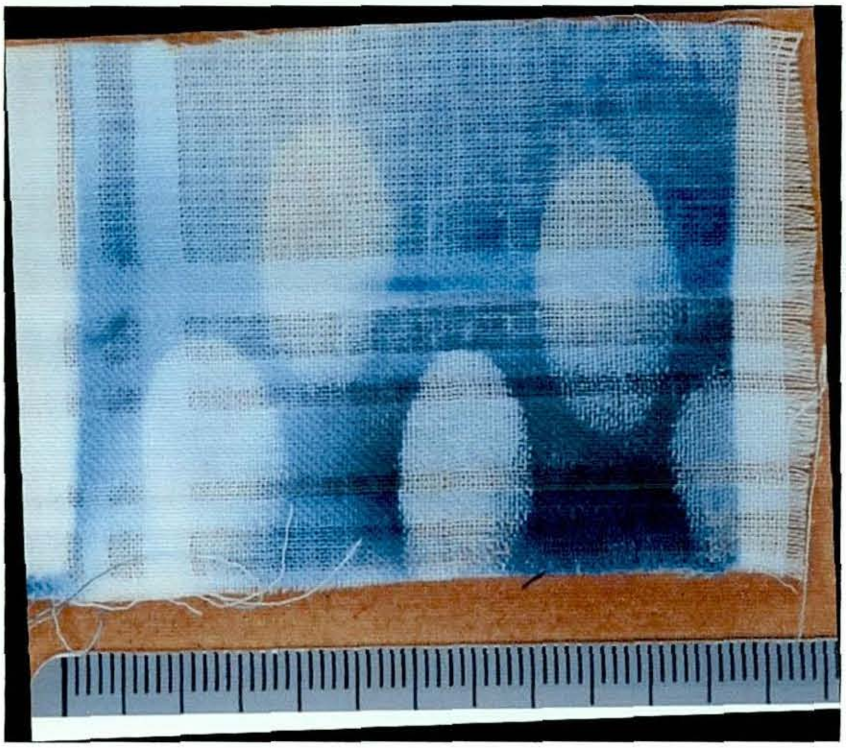

Figure 59 – ***'Empty' fingerprints obtained from the rapid sublimation of $(SN)_x$ onto fabric samples.***

In order to analyse discharged cartridge casings using the sublimation technique, a modification to the apparatus was required in order to accommodate the cartridge shells. Accordingly, the cold finger was discarded and instead replaced with a suitably sized glass stopper, fixed with a length of copper wire that contained a suitable clasp/clamp at the end (crocodile clip, or similar). The spent shell was then clamped in place and the combination allowed to cool in the refrigerator, as before.

Following cooling, the stopper was securely fixed to the sublimation tube, allowing the cartridge casing to be suspended several inches above the polymer. Heating of the latter, under vacuum, readily afforded $(SN)_x$ film growth across the metal casing and fingerprints were indeed developed in this fashion. Both 5 mm, 9 mm and various shotgun casings were duly investigated, and positive results were obtained in all instances (see Figure 60 (b) below).

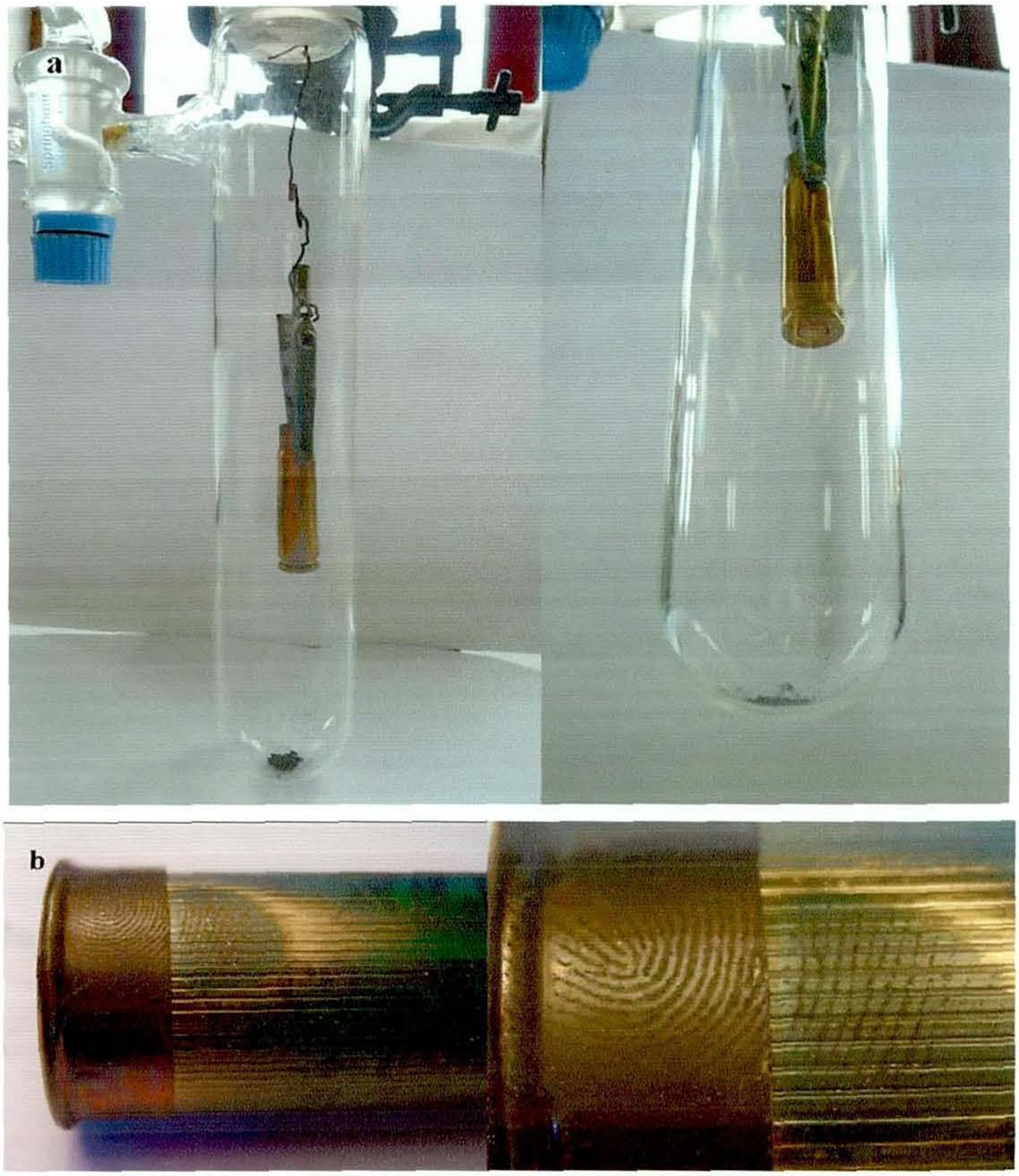

Figure 60 – *a) The clasp assembly used to hold cartridge casings during $(SN)_x$ sublimation experiments, and b) a fingerprint developed using this process on a spent shotgun cartridge.*

3.7. Covert Operation: Removal of $(SN)_x$ using ammonia

Aerial hydrolysis of thin $(SN)_x$ films has been shown, especially in the case of the inkjet work, to partially remove/decompose the polymer in a manner that facilitates the image of interest (fingerprint, inkjet ink or written impressions) to be visualised more favourably, following initial overloading. The rapid decomposition of $(SN)_x$ upon exposure to basic solutions is a property that allows the glassware to be thoroughly cleaned and traces of $(SN)_x$ to be removed. Accordingly, the exposure of bulk samples of $(SN)_x$ to ammonia gas was found to provide some interesting observations (see Section 5.1.5), but its exposure to epitaxial films grown across various substrates induced another effect that could conceivably serve as a complementary forensic tool.

The passage of ammonia gas into Schlenk flasks containing $(SN)_x$ enhanced fingerprints, written impressions or contact ink-transfer images on a myriad of substrates, induced a noticeable de-colourisation within several seconds, that was complete following prolonged exposure to the gas (usually *ca.* 10 minutes, but several hours was needed in the case of some fabric samples). In most examples, there were no visible or physical signs of any prior $(SN)_x$ staining, or indeed any treatment method, following NH_3 decomposition. Moreover, once rid of the $(SN)_x$ film, the samples were found to be suitable for enhancement once again, using either the S_2N_2 or $(SN)_x$ sublimation treatment methods, meaning that a certain degree of reversibility was present. This interesting reaction sequence has the fundamentals required for use in 'covert' situations, where discretion is paramount and samples must not appear to have been tampered or interfered with at any point. Typically, most mainstream fingerprint detection techniques result in an enhanced print that is relatively stable and unable to be removed following treatment.

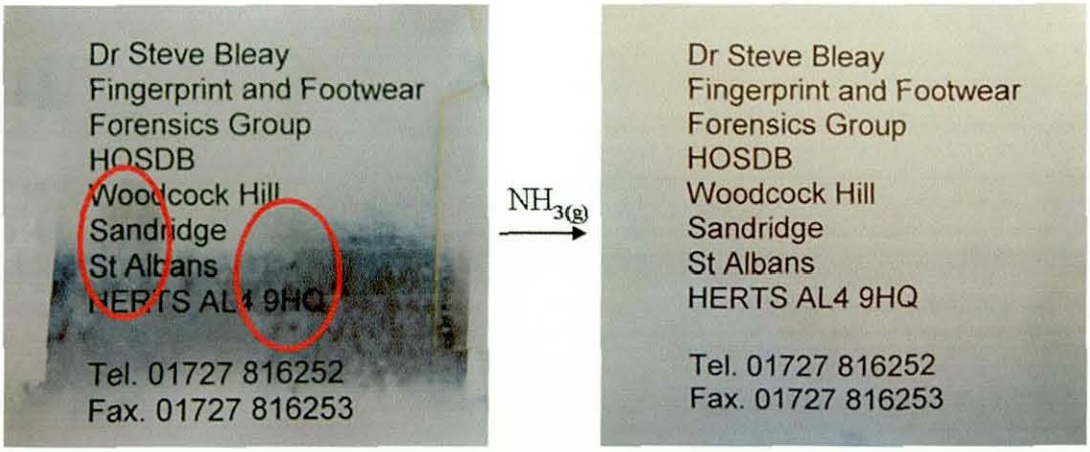

Figure 61 – ***Latent fingerprints enhanced with $(SN)_x$ (left) and removed following exposure to ammonia gas (right).***

The promise that the $S_2N_2/(SN)_x$ system may offer forensic scientists is vast, and it is clear that, despite extensive research following its discovery, there is still much to be learnt about this fascinating inorganic polymer. Importantly, it has been demonstrated that this initially serendipitous observation can actually afford a viable new method to add to the forensic arsenal. In a general sense, however, the lesson to be learnt here is that there are surprises to be had from the unlikeliest of sources and research must be open to lateral thinking and be ready to build upon chance observations.

4. Synthesis, Reactions and Potential Uses of Novel Silica Sodalite Materials

The sodalite family of compounds adopt the general formula $M_8[TT'O_4]_6[X]_y$ whereby uniform linking of TO_4 tetrahedral units creates a highly ordered three-dimensional microporous framework structure. Tilting of the tetrahedra away from their normal orientation planes, and deviation of the perfect tetrahedral geometry around T(T'), facilitates incorporation of guest molecules (X) within the framework voids. The diverse aluminosilicate sodalite materials possess a charged framework meaning the occluded guest cations and anions, in such systems, are required to perform a charge-balancing role. The nature of the guest ions in these examples, and the fundamental ionic interactions that exist between framework and guest, means that the sodalite cage (or β-cage) becomes largely filled, and it proves experimentally impractical to remove these ion clusters without complete collapse (decomposition) of the framework itself.

The synthesis of sodium bromide sodalite, NaBr-SOD ($Na_8(Al_6Si_6O_{24})Br_2$), sodium chloride sodalite, NaCl-SOD ($Na_8(Al_6Si_6O_{24})Cl_2$), lithium chloride sodalite, LiCl-SOD ($Li_8(Al_6Si_6O_{24})Cl_2$), and nosean, $Na_8[Al_6Si_6O_{24}][SO_4]$, according to known literature methods, allowed the interaction of ionic guest occluded sodalite materials, with S_2N_2, to be readily investigated. Exposure of the aforementioned sodalite materials to freshly generated S_2N_2 vapour, in an identical manner to that described previously (see Section 2.4 or 6.23), provided no clear indication of nitride interaction/occlusion. In each instance, the colour of the sodalite sample remained unchanged, even following 24 hours of S_2N_2 exposure, and subsequent powder XRD analysis, as shown for NaBr-SOD in Figure 62, showed no deviation of the characteristic sodalite reflections.

Unsurprisingly, the presence of the bulky guest ions in each sodalite compound hinders the uptake of the S_2N_2 monomer into the framework and thereby inhibits the formation and occlusion of $(SN)_x$ within the channel system. Ideally, therefore, perhaps only a template-free sodalite structure was considered plausible in facilitating $S_2N_2/(SN)_x$ incorporation within the constraints of the channel system.

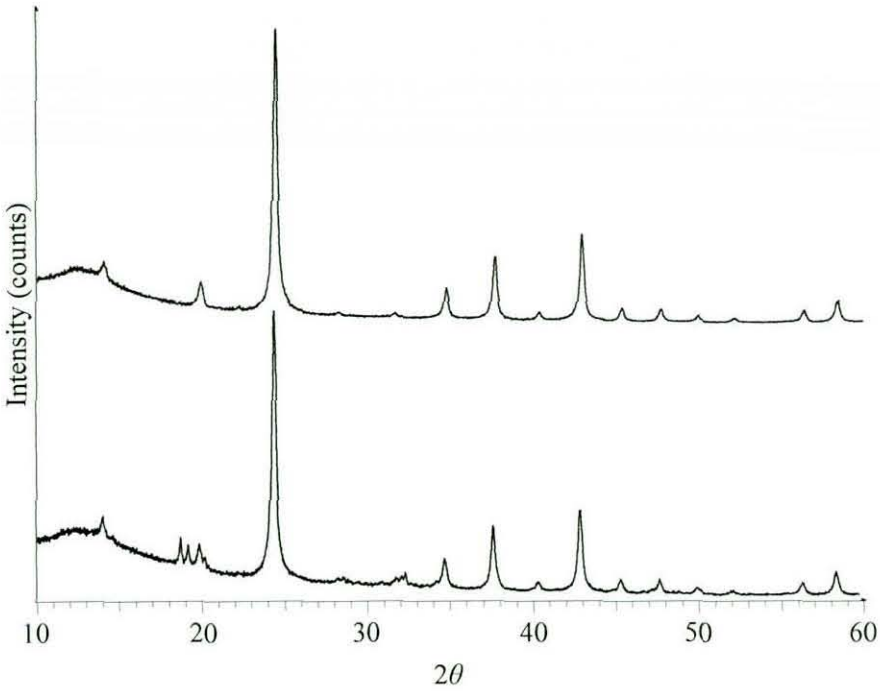

Figure 62 – ***Powder XRD pattern of NaBr-SOD (upper) and NaBr-SOD following exposure to S_2N_2 vapour.***

4.1. Ethylene glycol silica sodalite, EGS-SOD

The synthesis and isolation of a template-free sodalite material has, hitherto, eluded experimental capabilities. The use of sodalite precursors that are built around charged aluminosilicate frameworks is understandably ill-suited with regards the preparation of template-free materials, as counter ions are not only fundamentally required to serve as a templating species, but to also help balance the charge of the framework itself. For these reasons, the filled silica sodalites of general formula $Si_{12}O_{24}{\cdot}X$ (where the guest molecule, X, is typically ethylene glycol, ethylene diamine, ethylamine, or 1,3-dioxalane)[89-91, 99] have attracted considerable interest, as both framework and template are neutral, thereby allowing the interaction energies of both moieties to be modelled.[94-98] The primary use of these modelling studies, supported in part by extended computational calculations, has enabled both high temperature and template-free silica sodalite modifications to be predicted, with the added suggestion of a putative rhombohedral form of sodalite.[99] Despite many past attempts at synthetically preparing a template-free sodalite system, none have thus far been successful. In essence, the provision of an 'empty' silica sodalite material has the capacity to offer a wide variety of chemistry to be performed on the product, and in light of continued interest in the use of porosil frameworks to act as a host for conducting $(SN)_x$ wires, the synthesis of template-free silica sodalite immediately became a pertinent challenge.

The starting point for this work stemmed from the preparation of ethylene glycol occluded silica sodalite (from hereupon abbreviated to EGS-SOD) that was first prepared by Bibby and co-workers, from non-aqueous systems.[89] Initial attempts to prepare EGS-SOD using a hydrothermal approach, whereby all reactants (sodium hydroxide, fumed silica and ethylene glycol, in a 3:2:40 ratio, respectively) were placed into stainless steel autoclaves and heated at the desired temperature for 25 days, afforded a white material that was largely amorphous in nature, as suggested by powder XRD, and provided no similarity to that known for EGS-SOD.[89, 94] As shown in Figure 63, repeated hydrothermal synthetic attempts showed no greater progression towards formation of the desired product, despite reduced and/or extended reaction times.

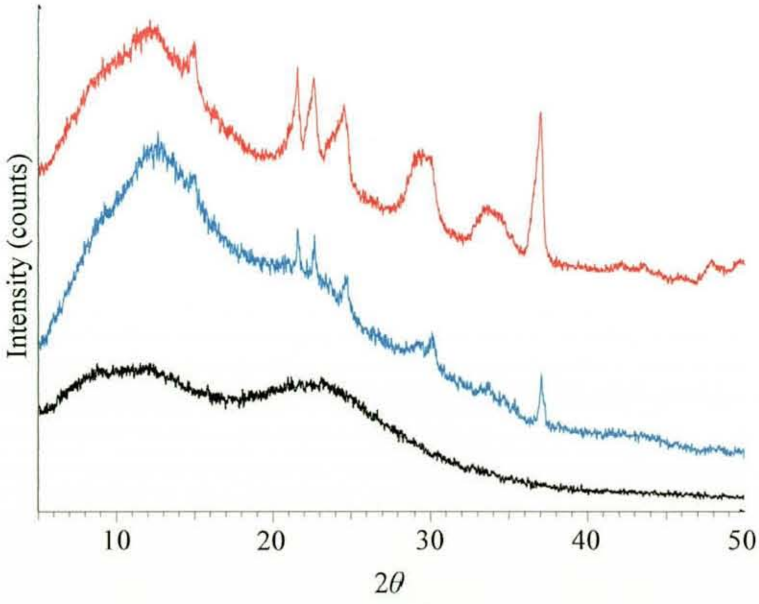

Figure 63 – ***Powder XRD patterns of the products obtained after 12 days (lower), 20 days (middle) and 25 days (upper), during the attempted hydrothermal synthesis of EGS-SOD as described by Bibby.***

Separately, synthesis of EGS-SOD was also attempted through standard 'reflux' procedures. With all starting materials in a suitable RBF and a reflux condenser in place, the mixture was heated to, and maintained at, 150°C, and stirred for 25 days. During the course of the reaction, the initially colourless solvent darkened in colour to yellow and finally progressed to a deep orange-red, possibly indicative of the formation of a sodium derivative. Over the next few days, increasing amounts of white precipitate began to deposit and it was ensured that any solid residues adhered to the walls of the flask were periodically scraped back into the reaction mixture. Following complete reaction time, it was important to filter the suspension whilst it was still hot, so as to reduce any impurity contamination, through precipitation. After drying in an oven, the white solid product was characterised *via* powder XRD analysis, and subsequent database matching showed good similarity to that of EGS-SOD (as shown in Figure 64).

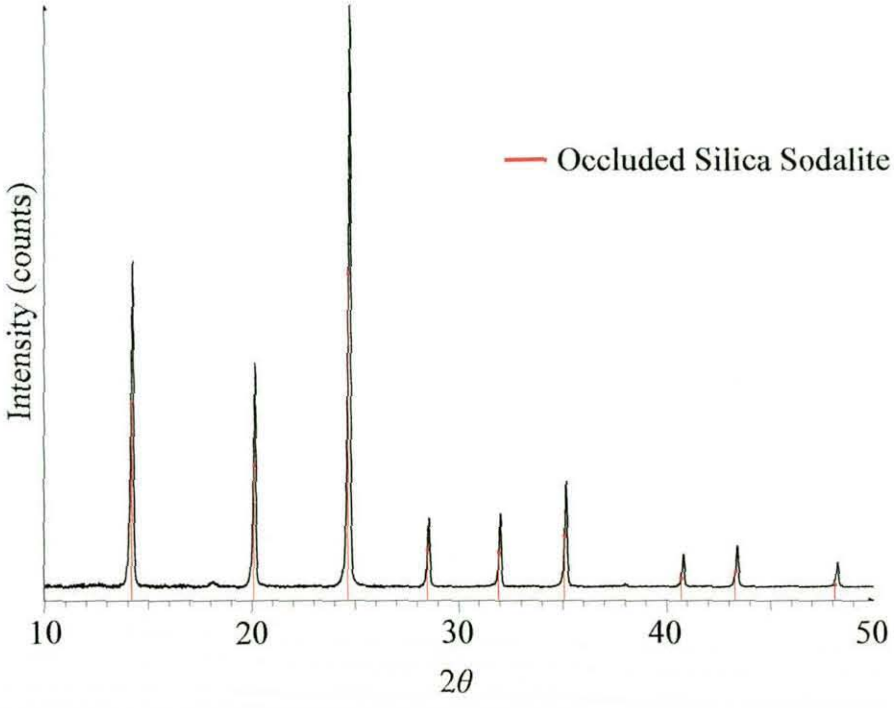

Figure 64 – ***Powder XRD pattern of EGS-SOD obtained following the Bibby synthesis, under reflux conditions.***

The excessive reaction times required for synthesis of the EGS-SOD parent material, following the Bibby method, limited its potential throughput, and meant that turnaround times for EGS-SOD synthesis, and its subsequent use as a reagent, were verging five weeks in duration. Although scaling up the initial reaction mixture seemed theoretically plausible, experimental practice highlighted the introduction of a slight amorphous phase, coupled with minor analcime impurity, to the resulting sodalite samples.

An alternative route to EGS-SOD was suggested by Qisheng *et al.*,[188] using similar reagents but with different stoichiometry, and appeared to be more favourable with regards to reaction times. The hydrothermal treatment of sodium hydroxide, fumed silica and ethylene glycol, in a 1:2:40 ratio, respectively, at 180°C for 3 days, was found to afford high purity EGS-SOD in good yield (*ca.* 87%). Powder XRD analysis of this sodalite product did suggest greater sample crystallinity when compared to the product obtained from the successful Bibby route (sharper, more intense reflections), and is likely to be attributable to the absence of stirring during hydrothermal synthesis. Moreover, owing primarily to the fact that reaction time was reduced almost tenfold, the Qisheng route became the method of choice for all subsequent EGS-SOD syntheses.

The sodalite framework itself is typically, at room temperature and pressure, a perfectly ordered cubic lattice system that crystallises, in the case of EGS-SOD, in the $Im\bar{3}m$ space group. Owing to the high symmetry element associated with such a system, the resulting powder XRD pattern, as shown above in Figure 64, depicts well resolved reflections that lack any 'splitting', commonly attributed to a system of lower symmetry (monoclinic, orthorhombic, *etc.*). Importantly, the morphology of the sodalite crystallites usually means that 'preferred orientation effects' are not seen in their XRD patterns. 'Preferred orientation' is the name given to the phenomenon that arises when crystallites of the bulk sample have increased, or preferential tendency to be favourably oriented in one direction compared to another. The ideal X-ray sample should consist of crystals, or crystal fragments, that are completely oriented at random. It is widely acknowledged that such an absolute random orientation of particles, within the polycrystalline sample, may only exist should the shape of the crystallites be perfectly spherical. In many 'real' samples, however, preferred orientation of particles is always present and thus the measured reflection intensities have a slight erroneous factor associated with them. In the case of sodalite, the individual particles approach spherical morphology during crystallisation;

crystallising, in fact, as truncated octahedra (a polyhedron). Scanning Electron Microscopy (SEM) images of the EGS-SOD samples obtained from the Qisheng method (see Figure 65), clearly illustrate the unique morphology of these sodalite crystallites. As a result of this particle shape, preferred orientation effects during sodalite X-ray analysis becomes significantly reduced, and there were no recorded instances of the latter during investigation.

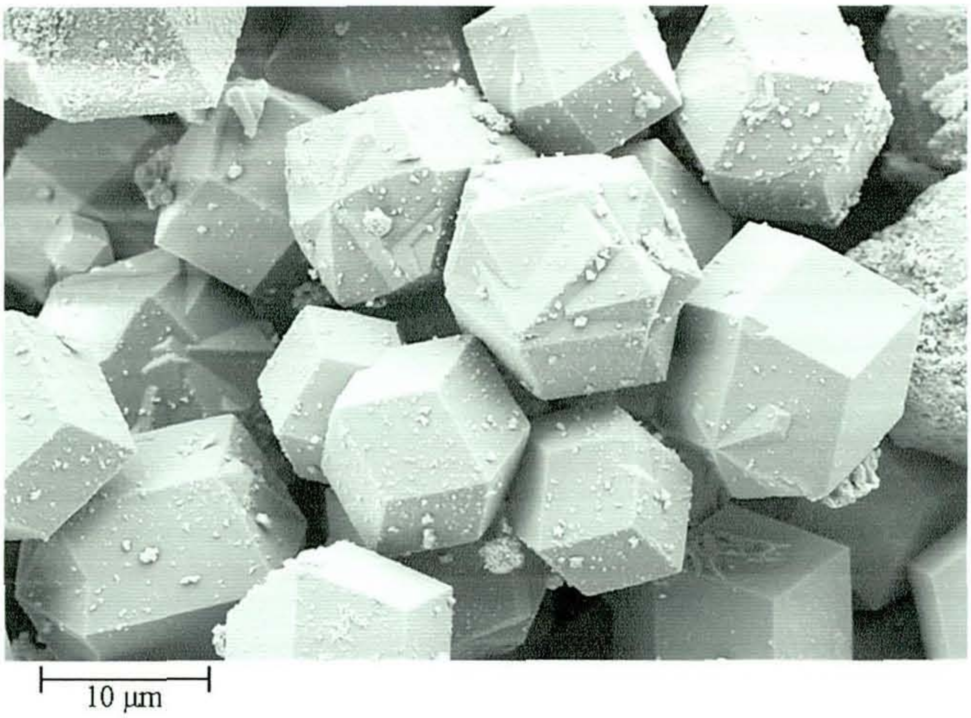

Figure 65 – ***SEM image of EGS-SOD as prepared according to Qisheng.***

As part of the characterisation of the EGS-SOD material, temperature resolved single crystal X-ray diffraction studies were undertaken at both 150K and ambient temperatures, using high flux synchrotron radiation. Observations from these studies seem to, in part, bolster the suggestions from previous theoretical work relating to temperature induced phase transformations of the sodalite crystal system.[100] To date, single crystal structure determinations of silica sodalite materials has been very limited, presumably the result of often temperamental syntheses and/or poor quality crystal samples.

At low temperature (150K), X-ray analysis of a suitable EGS-SOD crystallite showed the material to exhibit a monoclinic ($P2_1/m$, a = 7.387(3), b = 12.492(5), c = 7.546(3) Å, β = 110.174(6)°) structure with the formula $Si_3O_6 \cdot C_2H_6O_2$ (see

Figure 66). While the crystal system is as predicted from just 12 reflections in a neutron diffraction study performed by Smith *et al.*,[94] this unit cell is different. In this case, the ethylene glycol ligand exhibits two fold disorder, but is otherwise well defined and makes weak OH···OSi hydrogen bonds to the silica sodalite cage (H···O *av.* 2.64 Å).

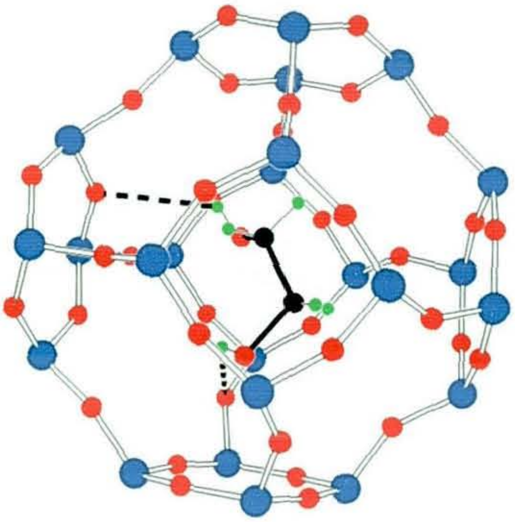

Figure 66 – *Single crystal X-ray structure of EGS-SOD at 150K.*

Upon warming to ambient temperature and collection of another X-ray data set, the increased librations of the encapsulated ethylene glycol moiety lead to a fully expanded sodalite cage, with zero tilt angle ($a = 8.903(12)$ Å, space group $Im\bar{3}m$), as shown in Figure 67. At this temperature, the disorder/librations prevented the development of a point atom model for the ethylene glycol, and meant the guest was included in the model as a region of diffuse electron density, utilising the Platon "Squeeze" procedure.[189]

The results of these X-ray studies raised the question as to the effect of continued temperature increase on the sodalite structure. In the first documented synthesis of silica sodalite from non aqueous systems, Bibby and Dale[89] suggested the partial loss of ethylene glycol could be observed through thermogravimetric analysis (TGA) and mass spectrometric techniques, yet, more importantly, the bulk isolation and thorough characterisation of a complete guest-free system was considered impossible.[89, 90, 190]

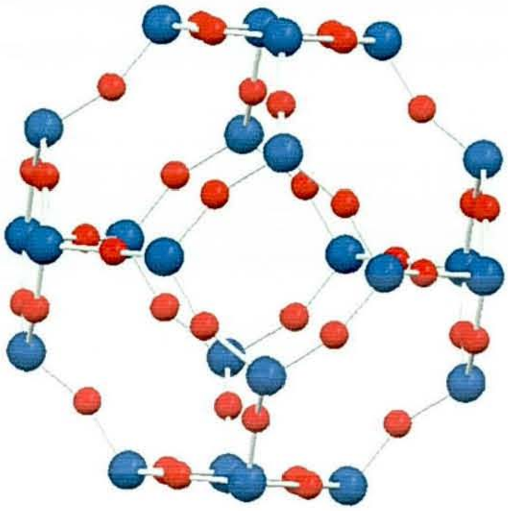

Figure 67 – ***Single crystal X-ray structure of EGS-SOD at room temperature.***

However, following further investigations on our part, it transpires that through careful thermal treatment the ethylene glycol template can be completely removed to afford either a cubic or rhombohedral phase, dependent on the treatment method used.

Controlled thermal treatment of EGS-SOD, using an Anton-Parr HTK 1200 heating stage fitted to a powder diffractometer, from room temperature (*ca.* 20°C) to 830°C, at 50°C intervals with 200 second dwell times between each run to allow equilibration, indicated a progressive phase transformation. As illustrated in Figure 68, there is a significant reflection intensity change between the two dominant sodalite reflections at 14° and 24° 2θ, as well as a slight, but important, positive 2θ shift. The phase change appears complete at *ca.* 680°C and the resulting powder XRD pattern is indicative of a simple cubic phase, with cell parameter $a = 8.79298(12)$ Å.

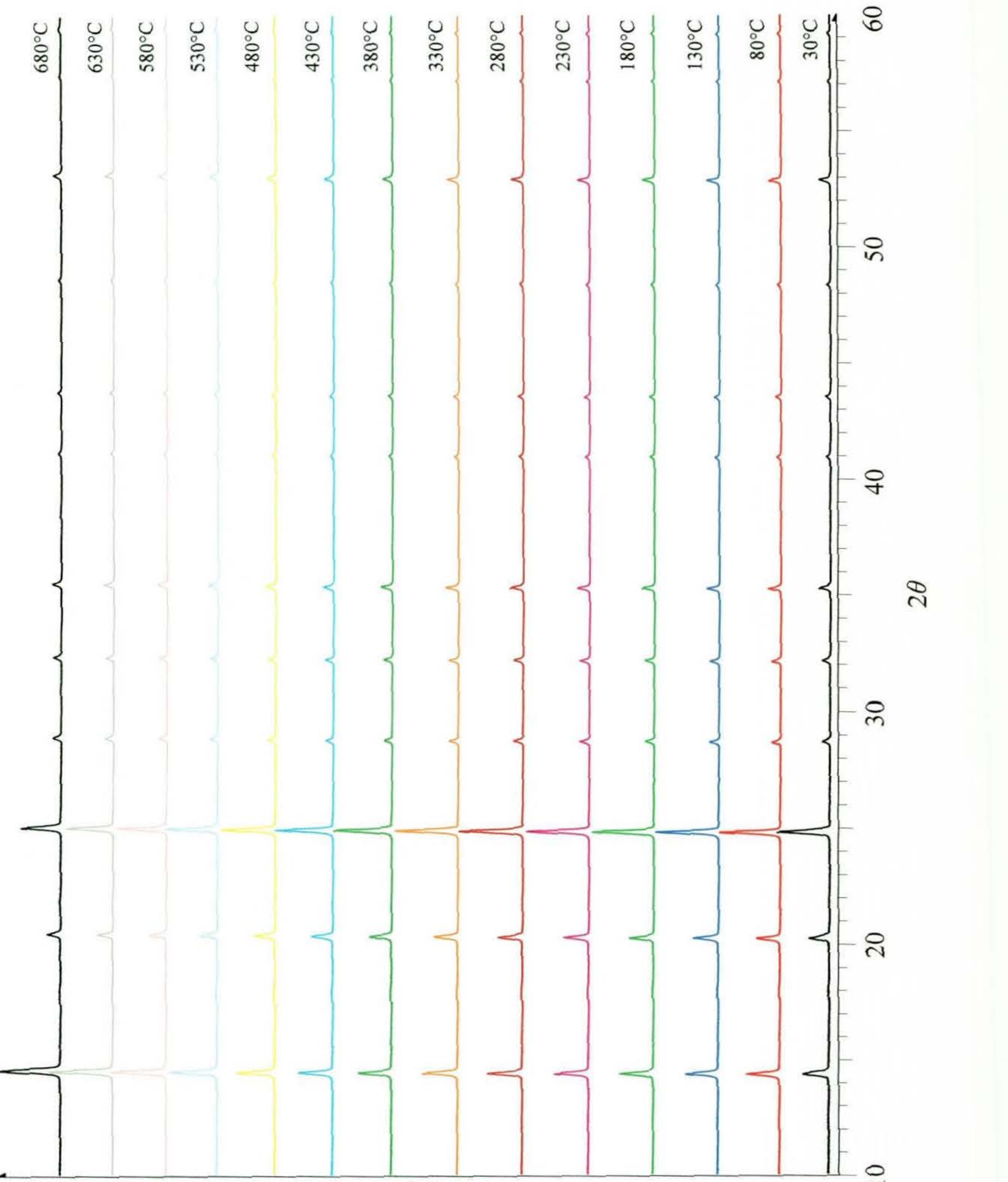

Figure 68 – *Powder XRD patterns showing the phase transformation of EGS-SOD during controlled thermal treatment from room temperature to 680°C.*

Subsequent Rietveld analysis of these data revealed a partially collapsed framework, crystallising in the cubic space group I $\bar{4}3m$, with a tilt angle of 16.4°, as illustrated in Figure 69. Further augmented temperature exposure of this sodalite, up to almost 1000°C, resulted in no visible signs of decomposition, a trait of silica sodalite that was initially suggested by Behrens *et al.*,[99, 100] or indeed any further structure re-arrangement.

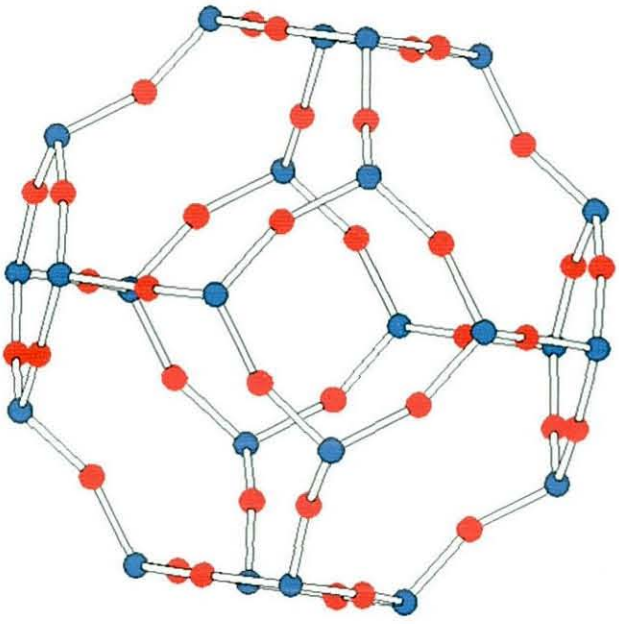

Figure 69 – *Crystal structure of cubic silica sodalite as modelled via Rietveld refinement, showing one cage unit.*

Following removal of the sample from the heating stage, the bulk product, at this point, appears dark grey in colour; differing substantially from the pure white appearance of the EGS-SOD starting material (see Figure 70 (a) and (b)). However, optical microscopy of the product, under reflected light, shows individual particles to in fact be much brighter in appearance, suggestive of the presence of a very tenuous layer of, presumably, elemental carbon as surface contamination (due to volatilisation of the organic moiety from the framework). Elemental analysis of this product helps confirm the absence of the ethylene glycol guest molecules from sodalite system, with effectively no carbon or hydrogen present. This observation is further supported through Energy Dispersive X-ray analysis (EDX), which indicates the presence of silicon and oxygen only, in an approximate 1:2 ratio.

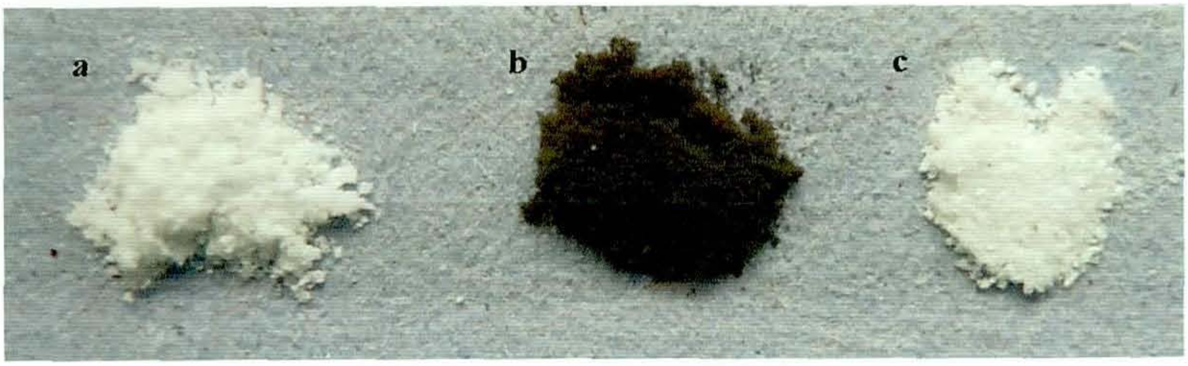

Figure 70 – ***Photographs of (a) EGS-SOD, (b) cubic S-SOD and (c) rhombohedral S-SOD.***

IR and Raman data were found to support the structural analyses given. Data collected from the EGS-SOD parent material clearly confirms the high symmetry $Im\bar{3}m$ structure, with only four well resolved IR active framework bands,[191] while the presence of the ethylene glycol moiety is further evidenced by the 870 cm^{-1} band in the Raman spectrum (slightly shifted from that observed for free ethylene glycol at 863 cm^{-1}). IR analysis of the carbon coated, cubic $I\bar{4}3m$, sodalite material, is indicative of a preserved sodalite framework, with lower symmetry as the triply degenerate SiO symmetric stretch splits into two bands (790 and 601 cm^{-1} *vs.* 773 cm^{-1}). Moreover, Raman analysis gives support to the carbon coating theorem as the spectrum becomes dominated by fluorescence. Thus, all the evidence leads to the conclusion this initial heating stage successfully removes the template molecule, leaving an empty silica sodalite molecule, crystallised in a cubic form, and coated with a (very) minor carbon impurity.

It was considered plausible that the carbon coating around the guest-free sodalite material may be serving as a 'scaffold' to offer the cages increased rigidity from total collapse and decomposition to simpler SiO_2 arrangements (quartz, cristobalite, tridymite *etc.*).[100] The question of its removal therefore becomes germane. Initial attempts concentrated on extended and prolonged heating of the carbon coated material to temperatures exceeding 1000°C, but no visible differences became apparent. Furthermore, prolonged heating at *ca.* 400°C, under high dynamic vacuum, similarly appeared to make little difference to the state of the sodalite sample.

It was eventually found that removal of the carbon coating was indeed readily achieved through exposure of the material to an oxygen atmosphere, at 680°C, for several days. The resulting product was a pure white coloured material, whose powder XRD pattern was no longer indicative of a purely cubic system (see Figure 71). The apparent movement away from a perfect cubic geometry presented several problems pertaining to full characterisation of the product. The preservation of a sodalite diffraction pattern (similar reflection spacing and intensities) was suggestive of the maintenance of the sodalite structure, but the introduction of additional reflections meant that either a shift away from cubic geometry, or the presence of a new impurity phase, had occurred. Sporadically, non-spherical groups/molecules have been known to enter regular cubic lattice systems and induce a distortion of the unit cell along one or more axes, which in turn results in an appropriate phase transformation (the introduction of dicarbide to some regular cubic lattice arrangements can induce a cubic to tetragonal phase transformation, for example).[192] Subsequent database searches, however, of common silica impurity components, coupled with theoretical calculations of predicted 2θ diffraction angle locations for tetragonally distorted silica sodalite, did not reveal any suitable comparisons for the additional reflections, and it was concluded that an alternative geometry phase (*i.e.* other than cubic) was solely responsible for the diffraction pattern change.

Unfortunately, attempts made at obtaining single crystal XRD data on the carbon-free final product, were initially unsuccessful. Subsequent SEM analysis of this material highlighted the occurrence of detrimental fractures across most sample particles and implied that the extensive heating and non-regulated cooling rates (samples were typically removed from the tube furnace and allowed to cool) during the multiple step synthesis, were perhaps responsible for such crystallite defects. In addition, loss of the ethylene glycol template molecules during the initial heating stage (to afford the intermediate, empty cubic silica sodalite product) was thought likely to induce physical strain on sample particles, and thereby result in physical deformations to some extent.

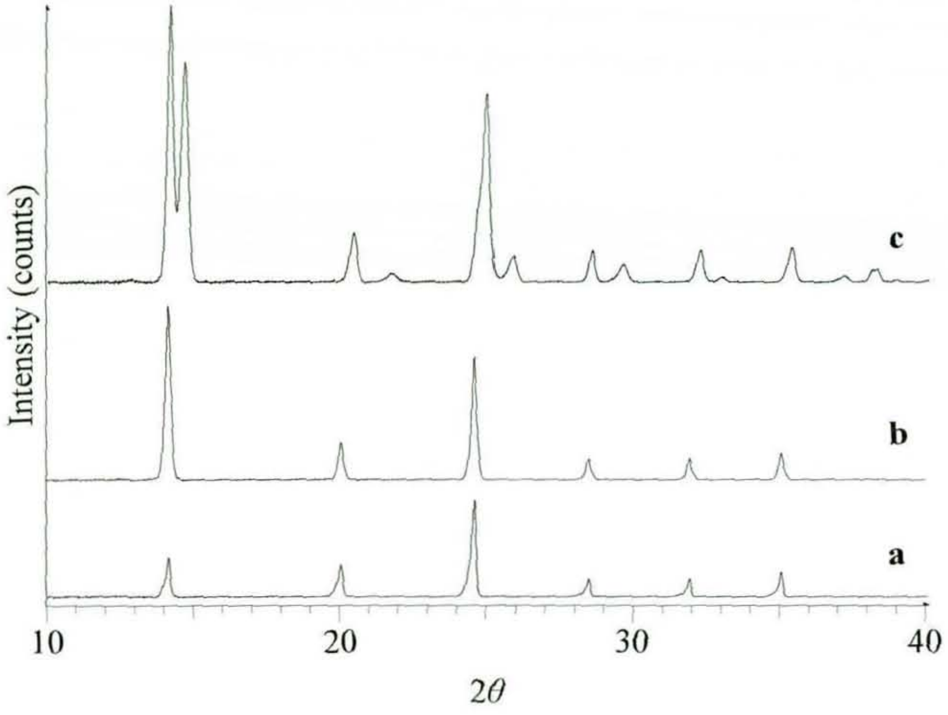

Figure 71 – ***Powder XRD patterns obtained for EGS-SOD at (a) room temperature, (b) after heating at 680°C under nitrogen to convert to cubic silica sodalite and (c) subsequently after heating under an oxygen atmosphere to afford rhombohedral silica sodalite.***

A new approach was considered that took into account the excessive strains put on the sample through heating/cooling cycles. With the use of a thermostatic controller, integrated into the tube furnace, it was possible to gradually heat (1°C min^{-1}) and cool (0.1°C min^{-1}) each of the sodalite materials to the target temperature. This method, coupled alongside slow programmed ramped cooling of the initial EGS-SOD material during hydrothermal synthesis, had the capacity to produce individual single crystals of both increased size and quality. Resultantly, following steady, controlled heating and cooling of the EGS-SOD starting material, its carbon coated intermediate, and the final product, SEM analysis (see Figure 72) revealed that the smaller of the resulting final crystallites (those typically < 15 μm in diameter) were fracture free and suitable for single crystal structure determination using high flux synchrotron radiation, at Daresbury Laboratory SRS Station 9.8.

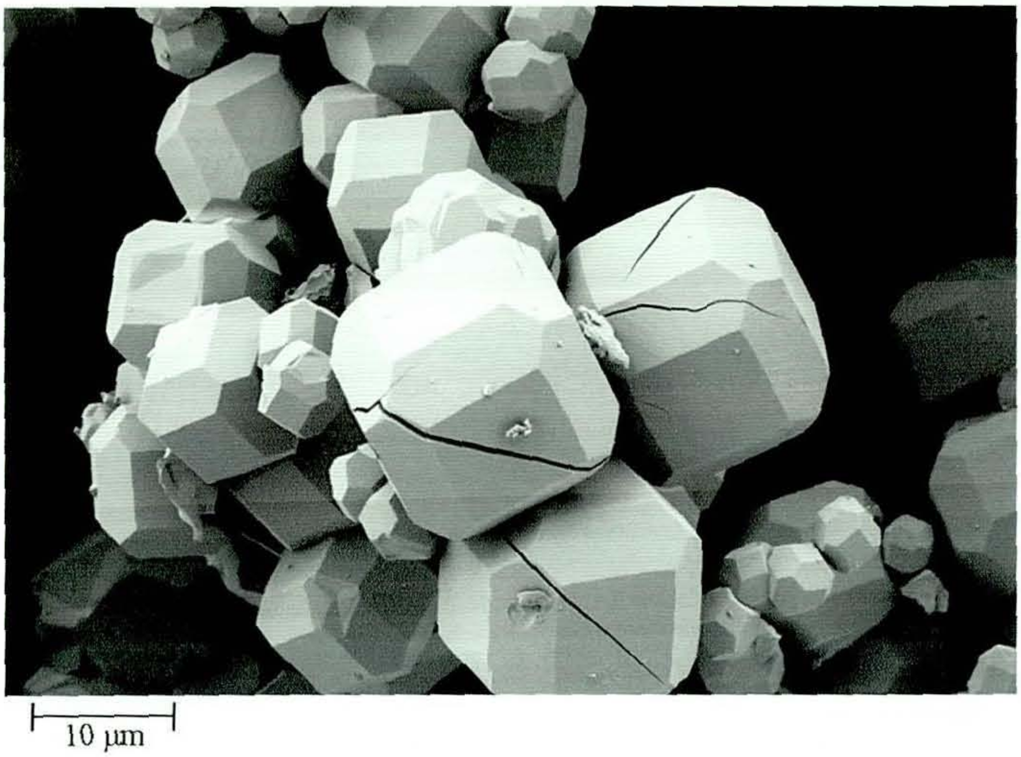

Figure 72 – ***SEM image of rhombohedral silica sodalite following controlled heating and cooling cycles. The smaller crystals were selected for single crystal structure determination.***

It is important to note the presence of both partially fractured and unaffected components within the bulk sample, shown above in Figure 72. Although SEM analysis can clearly distinguish between the two crystal 'types' present, single crystal selection, on this scale, by the operator, required several attempts to obtain a fracture free example, suitable for data collection. Data from this study, however, (see CSD depository, 419757) resulted in a well refined structure (R = 4.56 % [for 579 observed reflections with $F^2>2\sigma(F^2)$]) of a template-free, pure silica sodalite, crystallised in the rhombohedral space group, $R\,\bar{3}$ ($a = b = 12.441(2)$, $c = 7.0911(12)$ Å, $\alpha = \beta = 90$, $\gamma = 120°$) (see Figure 73). The structure itself is merohedrally twinned *via* the twin law [0 1 0 1 0 0 0 0 -1] with a 20.3(3)% occupancy of the minor twin component. The channel system can clearly be seen to be free of ethylene glycol, a fact further confirmed by measurement of the electron count in the voids of the structure using the 'calc solv' routine within the Platon suite of programs.[189]

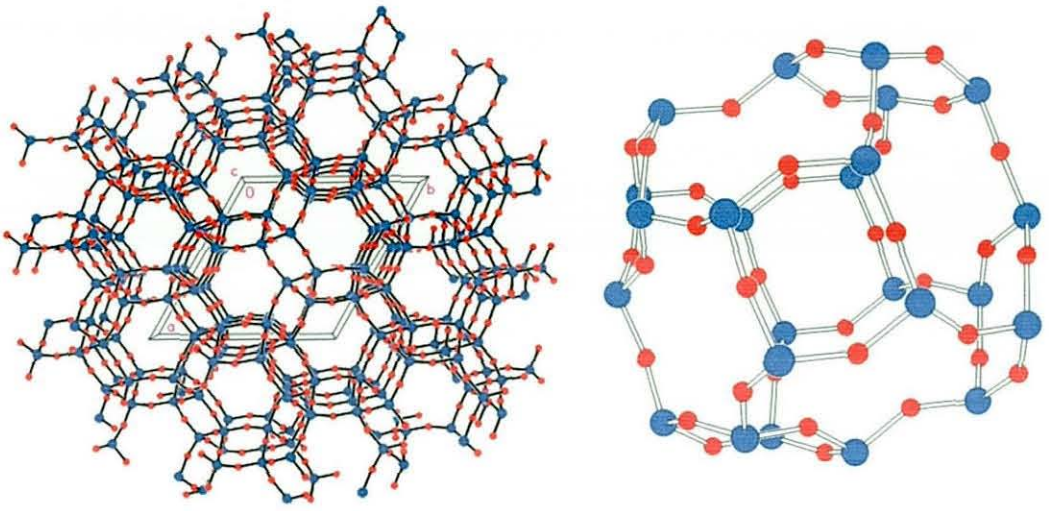

Figure 73 – ***Single crystal structure packing diagram (left) and one cage unit (right) of pure rhombohedral silica sodalite.***

Three voids were found to be present per cell, each with a volume of 84 Å^3, but containing only two electrons per void. This residual electron density is clearly far too low to constitute the presence of any molecular species, such as CO_2. It has been previously suggested that the latter can be formed within the sodalite cages, upon heating of EGS-SOD,[193] but not only is this precluded, in this example, by the above X-ray data, IR and Raman spectroscopy also confirms the absence of any CO stretches associated with such a product. In this case, a single Raman active band at 466 cm^{-1} is observed, while the drop in symmetry from cubic to rhombohedral is evidenced in the IR spectrum by further splitting of the symmetric SiO stretch into three bands (790, 612 and 601 cm^{-1}). The separation between oxygen atoms on opposite sides of each 6-ring cage window is *ca.* 5.0 Å, so when the covalent radius of oxygen is taken into account this leaves an open pore aperture diameter of *ca.* 3.4 Å, which is sufficient for the ingress of a variety of small molecular species (*vide infra*).

Solid state ^{29}Si MASNMR (as shown in Figure 74) further reinforces the occurrence of a distinct new silicon environment, as would be expected following movement away from a perfectly symmetrical cubic arrangement, with the occurrence of a ^{29}Si shift at -117.42 ppm (compared to -122.47 ppm for EGS-SOD).

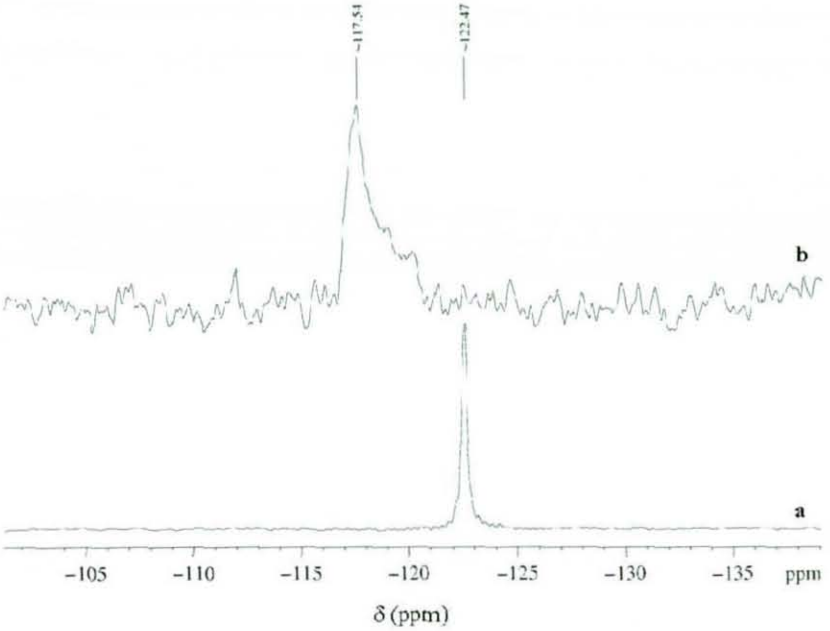

Figure 74 – ***Solid state ^{29}Si MASNMR of (a) EGS-SOD and (b) rhombohedral S-SOD.***

Predictably, generation of the simulated powder XRD pattern, based on the CIF data ascertained during single crystal diffraction studies of rhombohedral silica sodalite, shows high similarity with the experimental data (shown in Figure 68) obtained prior to single crystal analysis.

In light of the above studies, and their findings, it is clear that these results constitute the first reported preparation of a template-free silica sodalite, and, in fact, the first example of a rhombohedral sodalite isolated at both ambient temperature and pressure. The synthesis of a pure silica sodalite, with the absence of template/guest moieties, therefore has the capacity to facilitate clathration studies of the former with a myriad of smaller molecular species, including that of the $S_2N_2/(SN)_x$ system.

Accordingly, exposure of rhombohedral silica sodalite samples to S_2N_2 vapour, through analogous methods to that described for Na-ZSM-5 (see Section 2.4) afforded an intense dark blue/black coloured product within approximately thirty minutes of exposure (as shown in Figure 75).

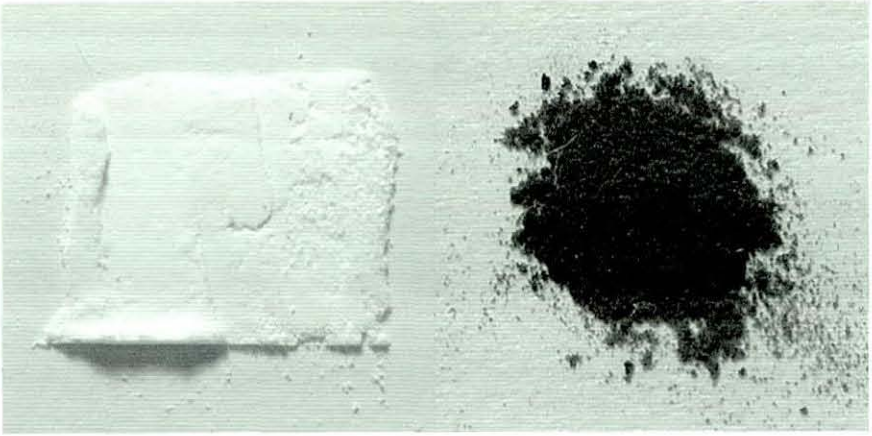

Figure 75 – *Comparison of the colour of a sample of rhombohedral silica sodalite before (left) and after (right) exposure to S_2N_2 vapour.*

Following prolonged interaction time (typically 16 hours) and subsequent washing with CH_2Cl_2 to remove S_4N_4 impurities, powder XRD data of the product (see Figure 76) showed a significant shift in the X-ray pattern to a higher d-spacing, and a notable change in the reflection intensities. Moreover, no residual $(SN)_x$ reflections were seen in the XRD pattern of the product, as would be expected for a guest-occluded variant. This behaviour is analogous in nature to that observed for Na-ZSM-5, and is indeed indicative of the polymerisation of S_2N_2 within the sodalite framework.

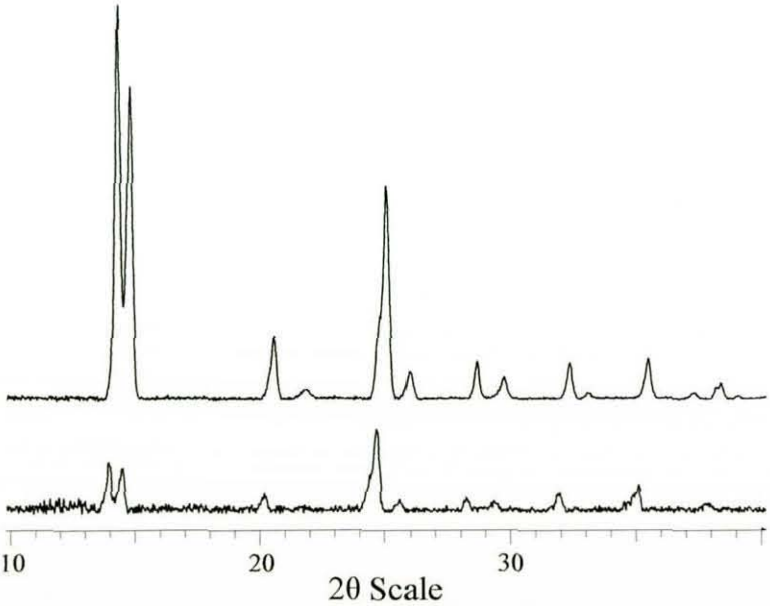

Figure 76 – *Powder XRD pattern comparison between rhombohedral silica sodalite (upper), and rhombohedral silica sodalite following exposure to S_2N_2 vapour and subsequent occlusion of $(SN)_x$ (lower).*

In addition, this hypothesis is further supported by the fact that reaction of the resulting material with $Pt(PPh_3)_3$ does not cause any visible decolourisation (as observed for the free polymer), therefore indicating that the polymer cannot simply be on the surface of the sodalite and must be inaccessible to the large platinum complex (i.e. occluded within the cage structure). Again, this mirrors results obtained during the Na-ZSM-5/S_2N_2 investigations, as do results of Raman spectroscopy (see Figure 77) on this product (hereinafter referred to as $(SN)_x$-SOD), which highlighted the occurrence of slightly shifted $(SN)_x$ bands within the spectrum, further supportive of polymer inclusion.

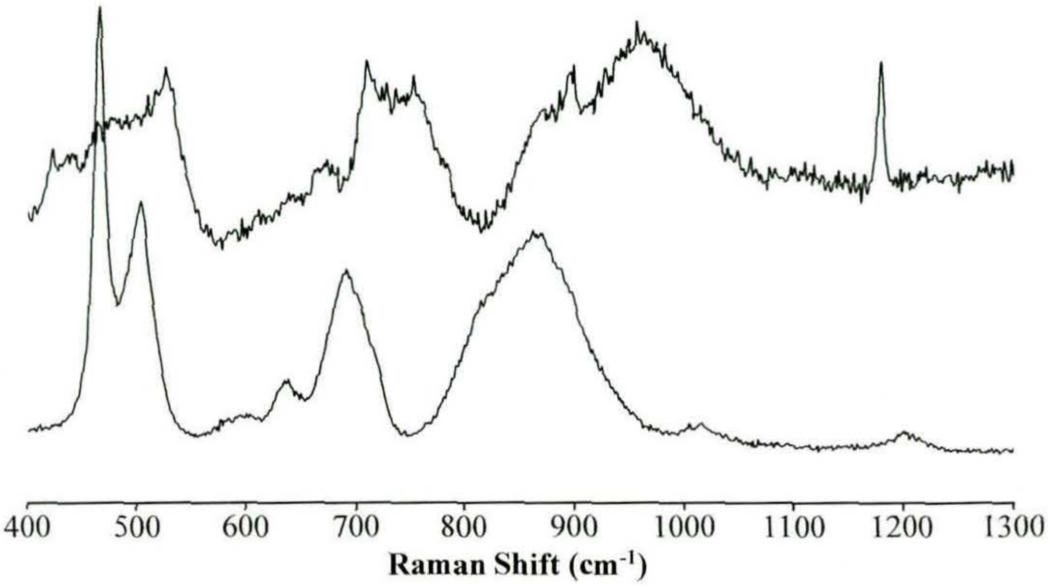

Figure 77 – *Raman spectrum comparison between $(SN)_x$ (upper), and rhombohedral silica sodalite following exposure to S_2N_2 vapour and subsequent occlusion of $(SN)_x$ (lower).*

In summary, therefore, the thermal treatment of ethylene glycol silica sodalite at 680°C, under a nitrogen atmosphere, successfully removes the templating agent, and results in the formation of cubic silica sodalite, with a minor carbon coating impurity. Upon heating to 680°C, under an oxygen atmosphere, this material readily transforms, in the solid state, to a rhombohedral form of the empty silica sodalite, which in essence, serves as a novel polymorph of silica. Importantly, the pore aperture of the 6-ring windows of the sodalite cages remain essentially un-altered, thereby maintaining the characteristic 3.5 Å diameter essential for many 'sieve' type applications. Moreover, its relatively facile synthesis offers the capacity for a wide variety of chemistry to be performed upon the product, particularly based on the neutral sodalite cages acting as nanoscale reaction chambers (in a similar manner to that initially proposed for the buckminsterfullerene, C_{60}, framework) for use in both catalysis based and intra-porous reactions. Such promise is immediately confirmed by the observation of $(SN)_x$ incorporation within the aforementioned sodalite.

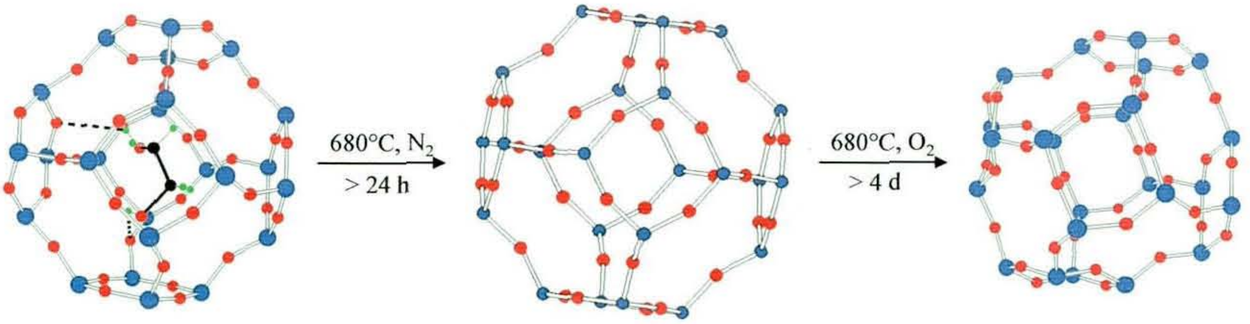

Figure 78 – ***The overall synthesis of rhombohedral silica sodalite (right) from EGS-SOD (left), through the intermediate cubic silica sodalite (centre).***

4.2. Other silica sodalites

Although template removal from other silica sodalite systems would essentially result in the same product, a pure silica sodalite, its investigation was considered important in order to provide a broader understanding of the system itself with regards to ease of template removal, and similarities/differences between sodalite structure re-arrangement.

In the original literature, Bibby[89] suggests the synthesis of a propan-2-ol silica sodalite is readily achieved through stoichiometric substitution of ethylene glycol, with the former. The structure and spatial occupancy similarities between the two template molecules theoretically permits successful generation of both forms of sodalite. Unfortunately, however, experimental attempts, using both hydrothermal and reflux conditions, coupled with substitution of ethylene glycol with propan-2-ol following the Qisheng method,[188] did not provide any sodalite type product. The synthesis of other silica sodalite variants (those containing either 1,3-trioxane, ethanolamine, or ethylene diamine as template molecules) were not attempted, owing primarily to more complicated experimental procedures, and increasing time constraints, owing to extended heating phases. It cannot be said, therefore, that all silica sodalites behave in an analogous manner to that displayed by EGS-SOD. However, the fundamental construction of the silica sodalite cage, and the similarity in constituent assembly of each template molecule, offers a reasonable assumption that behaviour, based on thermal treatment, should be analogous across the range.

4.3. Potential applications of rhombohedral silica sodalite

Owing to its lack of a template molecule, thereby creating a structure resembling that of a 'nano-reactor', the use of rhombohedral S-SOD as a potential catalyst for utilisation within mainstream organic processes, was duly investigated. Two major reactions, Friedel-Crafts alkylation/acylation and Diels-Alder, typically require the presence of either a silicon, aluminium, or sodium source, which are used as a catalyst, or in providing a critical intermediate species.

The structure of rhombohedral S-SOD has the capacity to provide a host environment for the reaction between two molecules (guests), providing their diameter is smaller than that of the pore aperture itself. In addition, failing inclusion of the potential guest species into the sodalite cages, interaction with the framework atoms from the external perimeter may invoke appropriate intermediates to catalyse the reaction of interest.

The Diels-Alder, 2 + 4 cycloaddition reaction, involves the addition of a conjugated diene, to a substituted alkene, affording a substituted cyclohexene product (as illustrated in Figure 79 (a)). The Friedel-Crafts acylation reaction involves acylation of an aromatic ring, by an alkyl chloride or acid anhydride, in the presence of a Lewis acid, to produce a phenyl ketone (see Figure 79 (b)). In each case, the presence of electron withdrawing constituents, namely in the form of carbonyl functional groups, offers both increased product stability and reaction initiation through nucleophilic attack of the δ^+ dipole moment, within the carbonyl moiety.

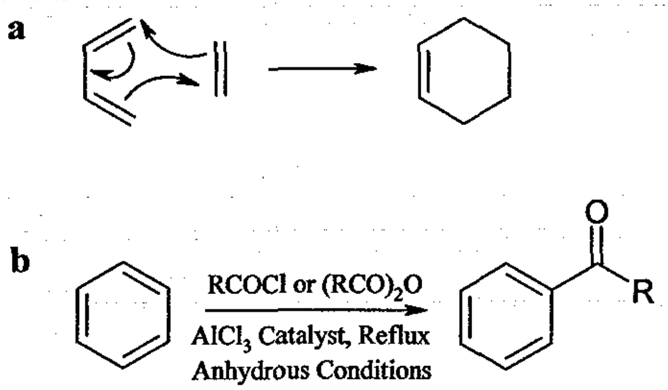

Figure 79 – ***(a) The Diels-Alder reaction; (b) The Friedel-Crafts reaction.***

In each case, the introduction of specific electron withdrawing species into the sodalite cages was envisaged to induce partial intermolecular bond formation between the δ^- oxygen atoms, and the δ^+ framework silicon atoms, thereby promoting the tendency for nucleophilic attack from the conjugated alkene species.

Attempted Diels-Alder reactions within the vacant rhombohedral S-SOD cages, using hexa-2,4-diene and methyl vinyl ketone, were found not to provide any signs of successful reaction, as judged by both powder XRD, IR and elemental analyses of the insoluble sodalite product (which remained unchanged), and ^{1}H NMR of the resulting mother liquor (which showed only starting material peaks). Friedel-Crafts reactions were similarly attempted, whereby rhombohedral S-SOD was stirred for 16 hours with acetyl chloride, followed by the addition of toluene to the mixture, for a further 16 hours. The subsequent addition of ether to the suspension was hoped to help remove the target product, methyl acetyl phenone, from the sodalite cages, and leave it in solution, facilitating ease of isolation.

The inability to predict whether the desired product could readily be removed from the sodalite structure, following its formation, meant that work-up of both the solid and mother liquor were required. Consequently, following filtration and washing of the sodalite product with ether, the solid was dried before analysis *via* powder XRD. Diffraction data suggested possible inclusion of a guest species within the structure, as indicated through slight negative 2θ reflection shift and a small degree of reflection intensity reduction.

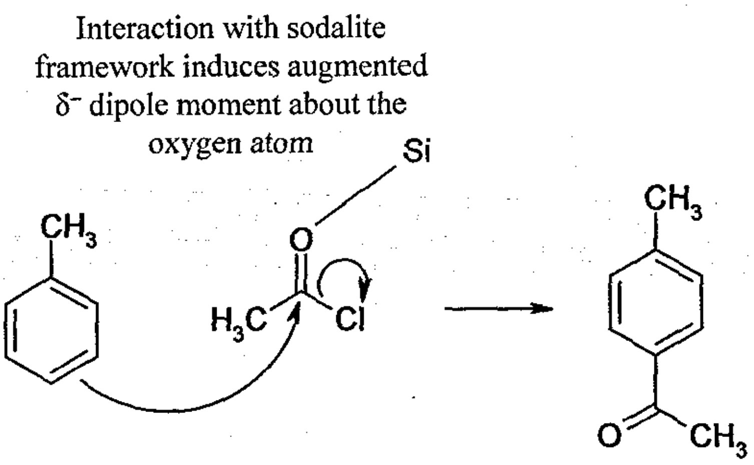

Figure 80 – ***Proposed reaction scheme for the Friedel-Crafts acylation reaction using rhombohedral S-SOD as a nano-reactor matrix.***

Elemental analysis confirmed the introduction of carbon and hydrogen, with a ratio of approximately 8:1, respectively, which approaches that expected for methyl acetyl phenone. Infrared spectroscopy was, as expected, largely dominated by broad silicate stretches across the fingerprint region. The occurrence of weak, but noteworthy, peaks at 1720 and 1637 cm^{-1} indicates the presence of RCOR and/or RCOH groups, as would be predicted for the target molecule.

After reducing the combined filtrate (mother liquor and ether washings) to dryness, a translucent pale yellow oil was obtained. ^1H NMR analysis of this material afforded a complex spectrum, of which, full peak identification became problematic. Nonetheless, analysis of the 7–8 ppm chemical shift region highlighted the occurrence of an AA'BB' pattern at 7.45 and 7.65 ppm. When considering the nature of the reaction species, and the structure of the target material itself, such a pattern is typical for a di-substituted phenyl ring, as exhibited by methyl acetyl phenone. COSY NMR analysis further revealed that these quartet groups were found to couple to each other, as predicted for a para-substituted product. Additionally, the methyl group, belonging to the toluene fragment of the product, was observed at 2.36 ppm, closely matching its expected shift of *ca.* 2.6 ppm. The acetyl ketone fragment, with an expected chemical shift between 1 and 2.5 ppm, was not easily observed amongst the various other peaks in that region, and is an indication as to the low yield of the target material.

Whilst the use of rhombohedral S-SOD does appear to promote the Friedel-Crafts acylation reaction detailed above, the resulting product is in such low yield that full, clear characterisation is not permitted. Moreover, these findings suggest that there is currently limited benefit in using template-free silica sodalite as a potential 'catalyst' for such reactions. It is believed that, in this case, the 6-ring pore aperture, in relation to reactant size, becomes the determining factor in reaction success. Both starting materials are of similar size, thus meaning competition for inclusion within the sodalite matrix increases accordingly. With the actual spatial occupancy and likely molecular arrangement within the β-cage being hard to predict, it is perhaps expected that efficiency of reactant uptake will be low, thereby restricting the progression of any subsequent reaction.

4.3.1. Hydrogen storage

The potential to store hydrogen for subsequent use as a fuel, in the form of H_2 gas, is becoming increasingly pertinent. The current methodologies in practice span a broad array of approaches, but conventional applications have concentrated around chemical compounds that release H_2 gas, upon heating. A universally acknowledged pre-requisite for the storage of hydrogen, is a system that is both compact and safe to store and transport. The use of cryogenic vessels and high-pressure storage tanks is therefore inadequate. An alternative, perhaps, would be the storage of hydrogen through encapsulation within microporous media, such as zeolites, sodalites, *etc.* The use of such systems for the storage and release of various gases is a well documented property,[194-196] yet its real applied potential for hydrogen storage has only recently become acknowledged.[108-111, 194, 197, 198]

In most circumstances, current procedures rely on the principle that the hydrogen guest molecules are forced into the cavities of the host system, under both elevated temperatures and pressures. Accordingly, following cooling to room temperature, the hydrogen molecules become clathrated (trapped) within the framework and can only be released following heating. Many literature investigations have concluded that the most suitable microporous hydrogen storage materials are those that contain an increased proportion of β-cage units, as framework 'building blocks'. Zeolites such as NaA, KA, LiA, NaX, NaY and sodalite itself, have all been found to offer amenable storage conditions for elemental hydrogen, however percentage by weight measurements have rarely exceeded *ca.* 2% (the Department of Energy has suggested a minimum standard of 9% by weight for all hydrogen storage materials by 2015). Storage of the small hydrogen molecules themselves is believed to occur within the sodalite cages of the aforementioned molecular sieves, and not the larger 8-ring α-cages as initially suggested by Fraenkel and co-workers.[110]

The bulk isolation of template-free pure silica sodalite, presents, possibly, the first example of an ideal, theoretically viable, hydrogen storage material, as the framework is based entirely upon adjoining sodalite β-cage units. Such a compound should conceivably offer the perfect environment for the reversible occlusion of hydrogen gas, with increased storage capacity (w/w%) compared to other microporous materials. Aside from storage/release of hydrogen through physical reaction, two other principles apply; absorption and adsorption. In absorptive hydrogen storage, hydrogen is absorbed directly into the bulk of the material. In simple crystalline metal hydrides for example, this absorption occurs by the incorporation of atomic hydrogen into interstitial sites in the crystallographic lattice structure. Adsorption based hydrogen storage may be subdivided into both physisorption and chemisorption, based on the energetics of the adsorption mechanism. Physisorbed hydrogen is more weakly energetically bound to the material than is chemisorbed hydrogen. Sorptive processes typically require highly porous materials to maximise the surface area available for hydrogen sorption to occur, and to allow for easy uptake and release of hydrogen from the material. With reference to rhombohedral S-SOD, it may be envisaged that either sorption process may readily occur. The provision of vacant β-cages and an un-hindered channel system should allow hydrogen molecules to pass into the voids and fill them accordingly. Additionally, the dominant oxygen content within the sodalite framework has the capacity to induce hydrogen bonded arrangements, following uptake of elemental hydrogen itself.

Typical experimental procedures concerning hydrogen storage in molecular sieve systems use specialist reaction chambers that allow both temperature and pressure to be independently varied, whilst also facilitating the introduction of dry hydrogen gas across the sample. The absence of such equipment posed a fundamental challenge that was not easily overcome. Instead, a simplified arrangement was constructed (as shown in Figure 81) that used a thermostatically regulated heating chamber and relied solely on atmospheric pressure conditions.

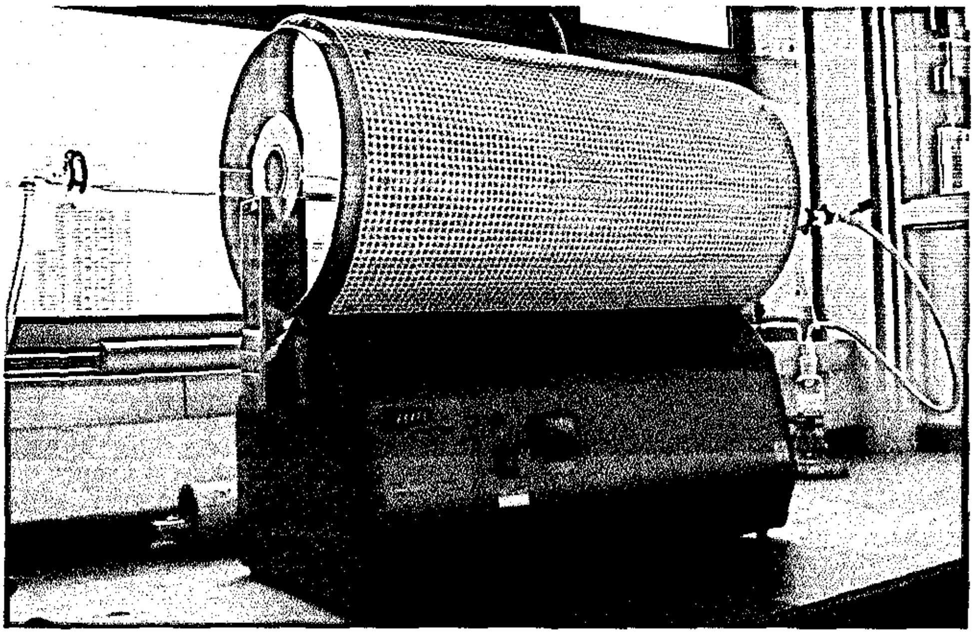

Figure 81 – ***Photograph showing the setup used for hydrogen storage attempts within rhombohedral S-SOD.***

Thorough drying of the sodalite material was essential so as to remove any occluded water molecules from the cages and provide maximum room for hydrogen inclusion. Hydrogen content analysis of the resulting sodalite material, following saturation, was deemed most feasible using a high accuracy microbalance to provide a direct indication of percentage change, by weight. The subsequent use of elemental analysis was then considered to be useful in confirming mass change calculations.

In a typical reaction, pre-weighed sodalite samples (*ca.* 100-120 mg, in an aluminium foil crucible) were introduced to the hydrogen purged tube furnace and allowed to equilibrate to the desired temperature for several hours. The introduction of hydrogen gas ensued for *ca.* 6 hours, after which time the samples were allowed to cool, and re-weighed. Analysis of the mass changes did not appear favourable for hydrogen sorption properties, using this method. The mass of the final samples did not significantly alter, with some findings actually indicating a mass deficit; thought to be the result of prolonged heating at augmented temperatures removing trace amounts of water, previously strongly occluded within the sodalite and not removed during initial drying.

Unfortunately, it is difficult to deduce whether the use of rhombohedral S-SOD as a hydrogen store, or the hydrogen storage technique itself, is the determining factor in reaction success/failure. The silica sodalite in question has many favourable characteristics that are believed to make it a suitable recipient for elemental hydrogen storage, but perhaps practical limitations have thus far eluded its potential applications to be determined. Nevertheless, its unique structure and inherent molecular sieve type properties, provide rhombohedral S-SOD the potential to be utilised in a wide variety of chemical reactions and techniques; those including simple host-guest interactions, as displayed with the $S_2N_2/(SN)_x$ system, or in potentially more fundamental storage applications for use with smaller molecular species, such as H_2, CO_2, NH_3, *etc.* Equipment limitations have largely prevented such investigations, on our part, during the course of this research.

4.4. Hydrosodalite

The application of storing hydrogen within rhombohedral S-SOD stimulated interest into the potential use of other host systems that were considered compositionally 'fit-for-purpose'. Following extensive investigation, Fraenkel[110] and Langmi[108] concluded that the presence of charge-balancing cations, held close to the β-cage pore apertures, were important in determining the percentage uptake of elemental hydrogen. Their findings suggested that hydrogen storage increased accordingly as cation size reduced. Larger cationic substituents were found to prevent hydrogen uptake through pore-blocking, whereas smaller cations were shown to increase the number of stored hydrogen molecules, owing primarily to the provision of active binding sites (in the form of the cation itself) for the hydrogen molecules. It follows, therefore, that LiA, for example, acts as a better hydrogen storage material than NaA and KA, respectively.

Fittingly, another sodalite material was considered suitable, whose structure closely resembled the compositional preferences outlined above. Hydrosodalite, $X_6[AlSiO_4]_6$, is an aluminosilicate sodalite compound that is typically formed using sodium as the charge-balancing cation (X). The sodalite itself exists with eight occluded water molecules per repeat cage unit, which have been found to be readily removed through controlled heating methods.[103] Ion-exchange procedures in which the sodium cation is replaced by lithium, are known,[103] although 100% conversion is considered unlikely.

The synthesis of the desired lithium hydrosodalite, and following dehydration, lithium sodalite (Li-SOD), requires the preparation of the hydroxysodalite precursor. Following literature methods,[103] sodium hydroxysodalite was readily obtained, in good yield, and its conversion to sodium hydrosodalite achieved through gentle reflux in water for two days. The resulting material underwent ion-exchange in a refluxing lithium nitrate solution for a similar length of time, before being dehydrated, under observation, on a powder diffractometer heating stage, which allowed determination of a suitable dehydration temperature range (as shown in Figure 82 (a)). The powder diffraction data suggests the water molecules begin to be removed from the sodalite at 190°C, and complete dehydration is achieved at 270°C, affording Li-SOD, $Li[AlSiO_4]_6$. These findings differ slightly from those previously reported, where TGA analysis suggested a temperature range of 200-250°C for dehydration.[103]

Calculation of the percentage lithium conversion of the hydrosodalite was obtained using atomic absorption spectroscopy, following the preparation of standardised solutions. Findings suggested a lithium conversion of approximately 72%, which relates well to other documented syntheses. Prolonged ion-exchange reactions were not found to increase the lithium content of the product, but in fact a decrease in its overall crystallinity was noted, as a result of thermal degradation and mechanical action on the sodalite particles, during stirring under reflux.

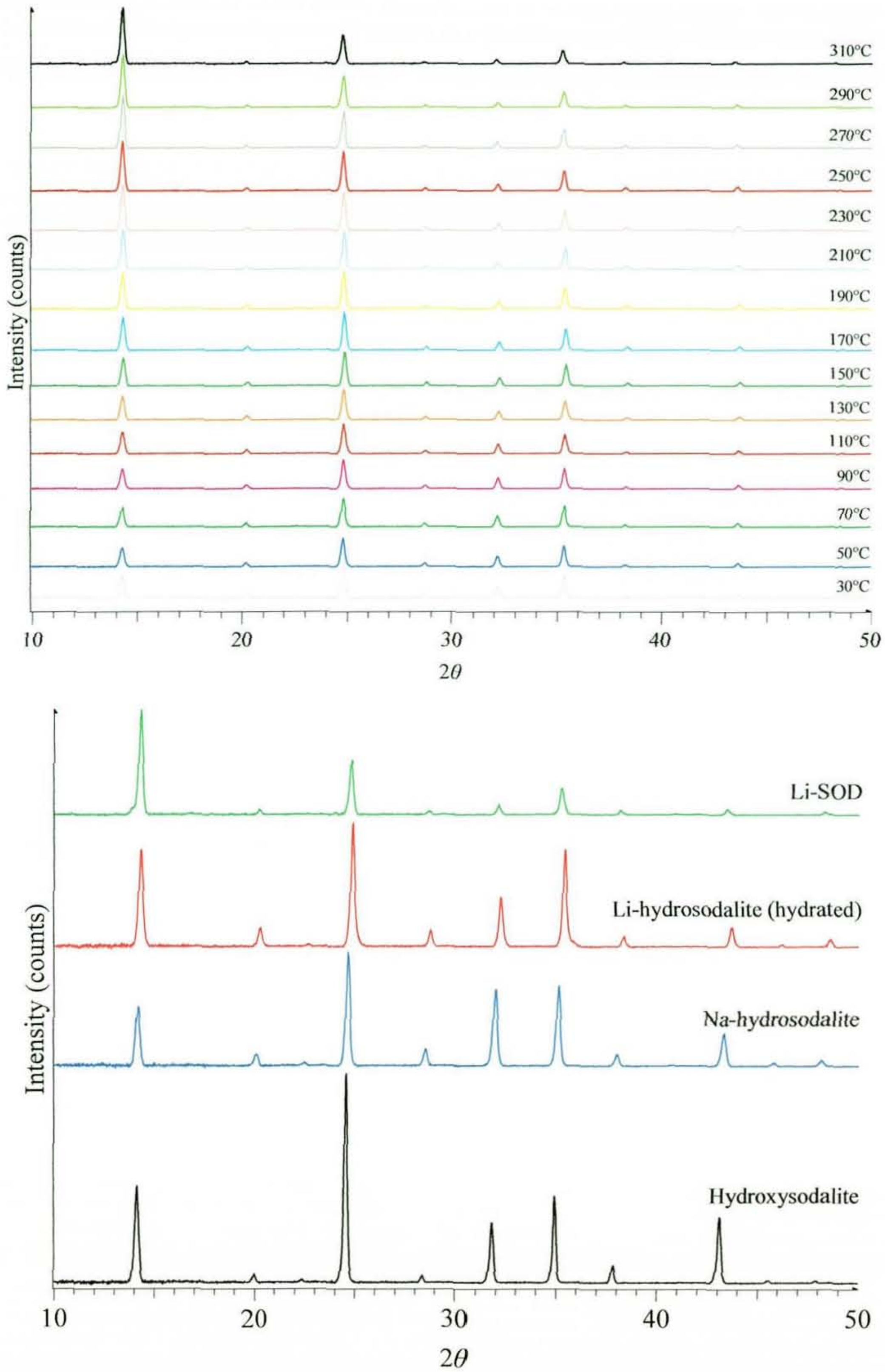

Figure 82 – ***Temperature controlled powder XRD patterns showing the removal of water from lithium hydrosodalite (upper) and powder XRD patterns showing the conversion of sodium hydroxysodalite to Li-SOD (lower).***

Exposure of the dehydrated lithium sodalite material to dry hydrogen gas was attempted, in an identical manner to that previously described for rhombohedral S-SOD (see Section 4.3.1). Initial findings suggested that prolonged sample exposure to the hydrogen atmosphere afforded a slight, but significant, increase in mass (1 - 3 mg), equating to 1-3 w/w%, if assumed to be the result of elemental H_2 storage. Despite some repeated exposure experiments providing similar results, the reproducibility was poor and often no significant deviation in mass was observed. Moreover, a post-exposure mass increase derived purely from H_2 storage, and not the absorption of water from atmospheric exposure, would be expected to provide elemental hydrogen content of significantly greater than the *ca.* 15%, obtained experimentally.

The increasing desire to utilise alternative fuel types mean that storage media play a critical role in the overall process. Despite hydrogen storage capabilities of the two aforementioned sodalite materials not appearing feasible using the setup described in Figure 81, there is strong belief that both these materials have the fundamental pre-requisites to host elemental hydrogen and provide suitable storage conditions. The unique 'spherical' shape, and lack of a template, within rhombohedral S-SOD means that maximum loading of the H_2 guest may be achieved, under appropriate conditions, as there is essentially no steric hindrance or channel restrictive moieties to interfere with occluded molecules. Separately, the presence of the small Li^+ cation within the Li-SOD framework may prove critical in its success at incorporating hydrogen within its structure, as deemed feasible from previous literature findings. Thorough testing is therefore required, using 'fit-for-purpose' equipment, such as an Intelligent Gravimetric Analyser (IGA) system,[108] that is able to both alter the temperature and pressure within the sample chamber, as well as facilitate the introduction of the hydrogen gas and monitor mass changes across the sample. Subsequent TGA analysis, or *in situ* reverse phase IGA analysis, should allow occluded hydrogen gas release to be monitored, with varying temperature effects.

5. Novel Utilisation of $(SN)_x$, and Constituents Thereof

5.1. *Poly(sulfur nitride), $(SN)_x$*

The preparation of $(SN)_x$ is traditionally achieved through the thermal pyrolysis of S_4N_4, through silver wool, affording S_2N_2, which then undergoes spontaneous solid-state polymerisation to poly(sulfur nitride). Despite other chemical and electrochemical synthetic methods being known for $(SN)_x$ preparation (see reference 39 for examples), their low yields often render them inappropriate during investigative studies.

Using the custom glassware described in Section 2.3, generation of S_2N_2 is readily achieved within several hours. Whereas work described previously directly utilised the S_2N_2 monomer through immediate sample introduction to the setup, and subsequent *in situ* sample interaction, further studies concentrated solely on the reaction and interaction of the fully polymerised material. Accordingly, suitable conversion methods were required in order to ensure that all S_2N_2 had been converted to $(SN)_x$, prior to its collection and storage.

In a typical synthesis, and following the removal of Flask A and connecting tube C from the setup as described earlier, the closure of Tap 3 creates a static vacuum within the system. The removal of the liquid nitrogen cold trap allows the vessel to gradually warm to ambient temperature and in turn facilitates volatilisation of the reactive S_2N_2 product as temperatures approach 20°C. When kept under this static vacuum environment for prolonged periods of time (> 3 days) solid-state conversion to $(SN)_x$ readily occurs, presumably through similar mechanistic pathways to those suggested by Mikulski and co-workers in Figure 4.[28, 29]

The volatile nature of S_2N_2 means that, upon warming to ambient temperature and allowing to stand for an hour, the majority of the glassware becomes coated in a dark blue coloured $(SN)_x$ film, that appears golden in colour at certain viewing angles. Single crystals of $(SN)_x$ are also formed, but with size constraints of *ca.* 1mm in length. Should concentrated single crystal growth of the latter be desired, it was found that lowering the ambient temperature to *ca.* 10°C, provided the best results; where only a minor surface coating resulted, and the growth of larger single crystals of $(SN)_x$ became favoured. Storage at these reduced temperatures, however, inevitably induced slower conversion to the polymeric product (> 6-10 days). The resulting cuboidal shaped crystals were found to be between two and three millimetres in diameter.

The provision of Tap 2, in the setup, allowed the freshly prepared $(SN)_x$ to be readily stored under a nitrogen atmosphere, in a Schlenk type manner, and completely eliminated any potential for atmospheric exposure – a unique conception in this setup. During traditional $S_2N_2/(SN)_x$ preparations, pumping on the generated S_2N_2 for 24 hours at reduced temperatures, allows the monomer to be isolated in its purest form (essentially a double sublimation process). Even though this method removes minor S_4N_2 impurities, the solid state polymerisation of the re-condensed S_2N_2 is not always 'clean', and often dimerisation of the latter, to S_4N_4, is observed, meaning it must subsequently be removed. Additionally, isolation of 'pure' S_2N_2 has been shown to significantly increase its explosive tendencies.[199] Accordingly, the *in situ* polymerisation method was considered most appropriate, with the knowledge that any remaining impurities could be easily removed by careful washing with an appropriate dried, de-gassed solvent: dichloromethane. Both S_4N_4 and S_4N_2 are highly soluble in CH_2Cl_2, and the removal of this filtrate *via* canulation affords only pure $(SN)_x$ polymer.

IR analysis of the resulting dark blue-black polymer, showed good correlation to that reported by Banister and Hauptman:[175] υ 1015, 695, 638, 501, 287 cm^{-1}. Raman analysis of the bulk product also provided a suitable, impurity free, spectrum (see, for example, Figure 77). Elemental analysis of freshly prepared $(SN)_x$ samples were found to have some degree of hydrogen content (< 3%), presumably the result of minor hydrolytic action during atmospheric sample exposure in preparation for analysis itself.

SEM analysis of the polymer highlighted its characteristic striated nature. Interestingly, images of the $(SN)_x$ 'plates' grown on the walls of the collection vessel, show both a smoother surface topography (from the surface in direct contact with the glassware, see Figure 83 (a)) and a more typical surface (the 'growth' surface, see Figure 83 (b)).

Figure 83 – ***SEM image of two $(SN)_x$ plates showing both (a) 'smooth' and (b) 'growth' surface types.***

SEM analysis of the $(SN)_x$ single crystals depict a purely striated appearance (as shown in Figure 84), a characteristic associated with poly(sulfur nitride).

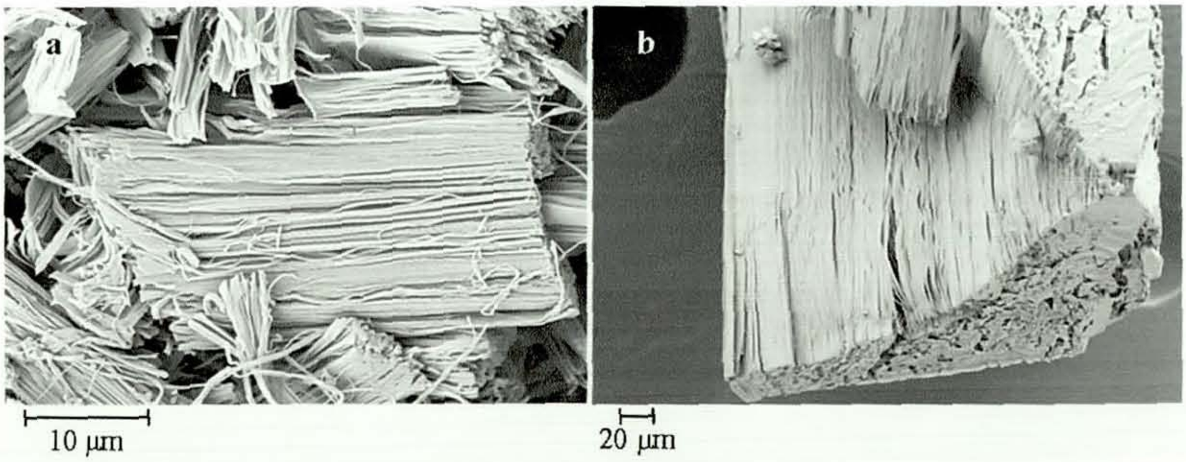

Figure 84 – ***SEM image of (a) an $(SN)_x$ 'bundle' and (b) an $(SN)_x$ single crystal.***

The SEM images, shown above, concur with the fibrous structure initially suggested by Boudeulle in 1975.[47] Street and Greene[33] proposed that such a striated arrangement is likely to be the result of the polymerisation process originating from S_2N_2 defects. The polymerisation can then occur rapidly in the chain direction, but perpendicular to the chain, polymerisation is inhibited due to significant differences in lattice constants between the monomer and the polymer itself. Resultantly, crystals such as those shown in Figure 84 are readily obtained directly from S_2N_2.

5.1.1. The polymerisation process

Traditional theories support the argument for S_2N_2 polymerisation to occur as the result of severe 90° bond strain within the four-membered cyclic molecule, that induces a structural rearrangement to a more kinetically favoured molecule, $(SN)_x$. Accordingly, breaking of an S-N bond in adjacent molecules creates a pair of di-radical S_2N_2 intermediates that are then able to join. As the process repeats itself, the polymer chain length increases and $(SN)_x$ is formed.

A more recent computational theorem discounts the aforementioned mechanism owing primarily to its likely procession through a region where the electronic nature of the surface becomes very complex, and hence, unlikely. Instead, it has been proposed that $(SN)_x$ is in fact formed following an intersystem crossing, that is preceded by a vertical excitation of the S_2N_2 species. This 'triplet' species is then able to relax and polymerisation occurs in a direction approximately perpendicular to the mean plane of the ring.[31]

Although computational predictions are useful in assimilating a myriad of theoretical data, experimental evidence is pivotal to fully elucidating a particular structure, mechanism, *etc*. To date, only two major studies have directly looked into the polymerisation process of S_2N_2 to $(SN)_x$. Müller and co-workers used an *in situ*, time-resolved powder XRD technique to help explain the polymerisation process involved and found some evidence to support the initially suggested mechanism.[46] Additionally, Heeger *et al*. employed a mixture of time-resolved single crystal XRD and ESR techniques to support the proposed polymerisation mechanism.[28]

Importantly, however, despite their attempts at analysing a 'partially polymerised' S_2N_2 crystal, evidence pertaining to a structural re-arrangement within the S_2N_2 lattice system, to generate $(SN)_x$, has largely eluded explicit clarification.

During the course of the $S_2N_2/(SN)_x$ synthetic work, the growth and isolation of an S_2N_2 single crystal was desired in order to allow XRD data to be ascertained. Isolation of such a crystal was readily achieved by creating a temperature gradient across the collection vessel, using a constant stream of liquid nitrogen poured over one point in the side-arm (see Figure 85), that allowed the freshly synthesised S_2N_2 to re-crystallise at the desired location, thereby enabling ease of removal from the setup.

Figure 85 – ***Photograph showing the method used to isolate single crystals of S_2N_2 used for XRD.***

Under a flow of nitrogen, an appropriately sized single crystal was chosen by its high quality visual appearance, and removed from the side-arm before being mounted onto the glass fibre. The colourless-gold/blue crystal was immediately cooled to -123°C, under a cryostream, and a full sphere data set was obtained. The crystal was found to exhibit an un-twinned monoclinic ($P2_1/c$, a = 4.4834(5), b = 3.7748(4), c = 8.4435(9) Å, β = 106.4117(12)°) structure with the formula S_2N_2 (see Figure 86) that was symmetry generated from the SN asymmetric unit. The perfectly planar molecule closely resembles the crystal system proposed by Müller, from Rietveld refinement of the S_2N_2 powder diffraction pattern,[46] and that initially described by Heeger *et al.*[28]

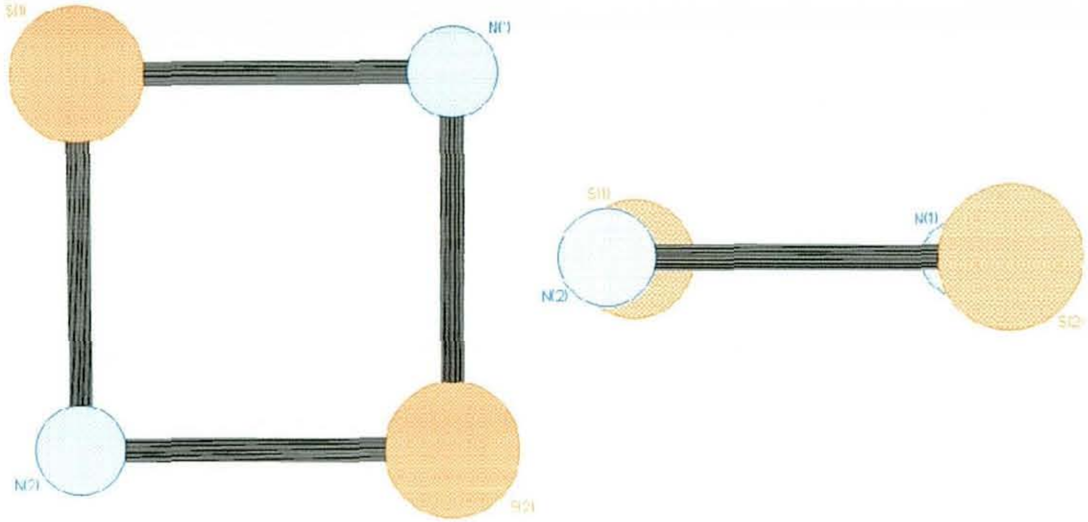

Figure 86 – ***Single crystal structure of freshly prepared S_2N_2.***

Accordingly, the S-N-S (90.31(5)°) and N-S-N (89.69(5)°) angles correspond to those expected for a perfectly square planar molecule and do not significantly differ from those previously reported.[28] The stacking arrangement depicts a herringbone pattern (see Figure 87) which is characteristic for close-packing molecular crystals of flat planar molecules, and also coincides with previously reported data.[28, 29, 46]

After leaving the S_2N_2 crystal at ambient temperature, under nitrogen, for a further five hours, a hemisphere data set was obtained, again at -123°C. Despite the quality of the crystal diffraction data being slightly diminished, the structure of the S_2N_2 molecule was found to move away from a perfectly planar arrangement. The unit cell was again solved as monoclinic, with a space group assignment of $P2_1/c$ ($a = 4.473(6)$, $b = 3.818(5)$, $c = 8.546(12)$ Å, $\beta = 105.105(16)$°), which shows slight unit cell alterations compared to those previously observed for the 'fresh' S_2N_2 crystal.

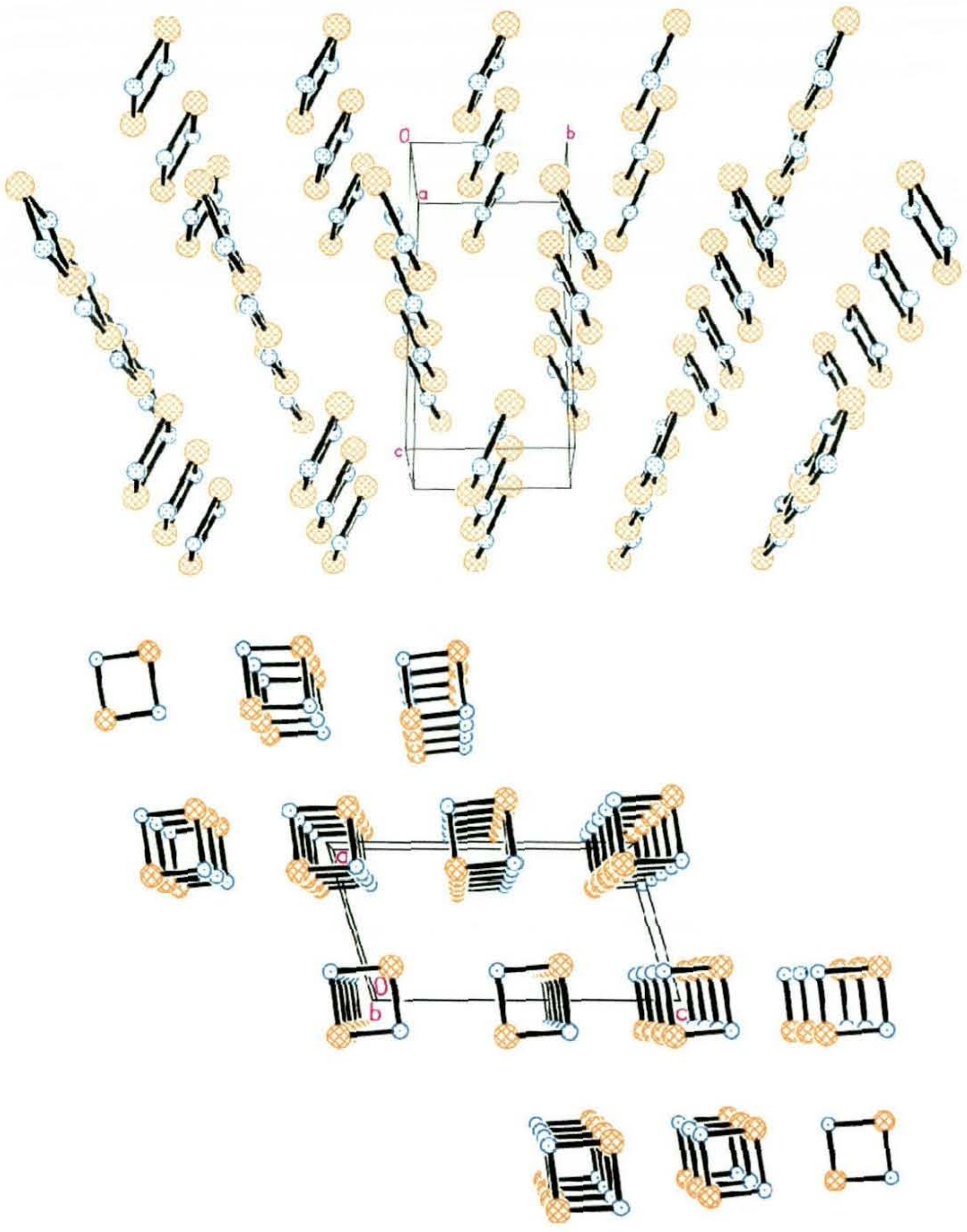

Figure 87 – ***Single crystal packing diagram of freshly prepared S_2N_2 showing its herringbone arrangement.***

Importantly, Figure 88(right), shown below, illustrates the molecules deviation from the horizontal mean plane, with a slightly 'puckered' structure evident. Analysis of the molecule viewed along the *c*-axis (Figure 88 (left)) also shows a slight, but significant, broadening of the S(2)-N(2) bond, thereby creating a more trapezoidal cylic arrangement, compared to the perfectly square planar structure as seen above in Figure 86. There appears to be some degree of disorder within this crystal system, with cyclic S_2N_2 molecules potentially occupying two adjacent unit cell positions; a factor attributable to the initiation of phase change caused by irregular re-arrangement of the initially planar thiazyl rings.

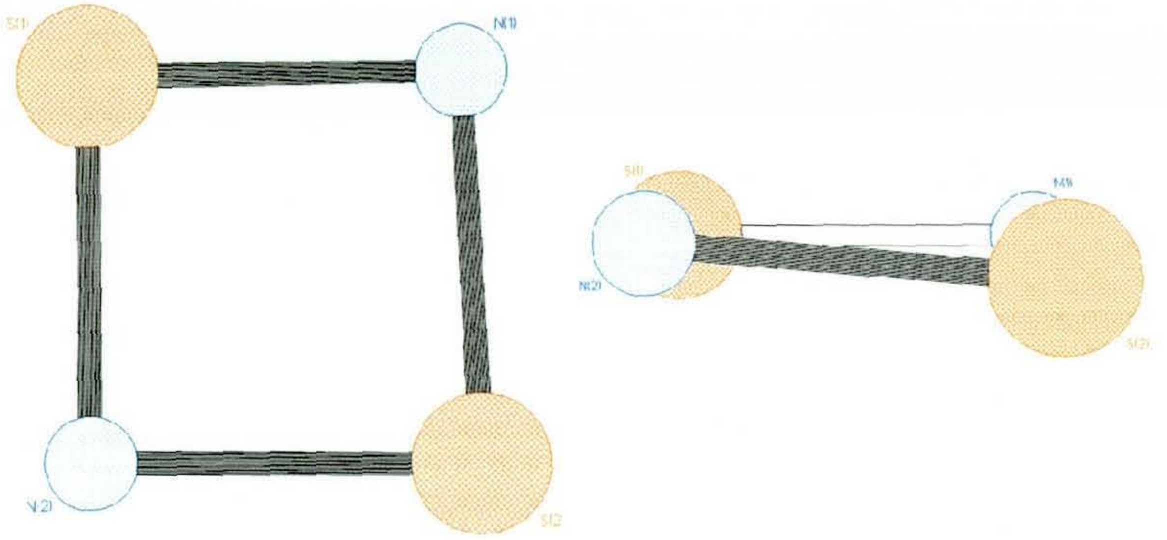

Figure 88 – ***Single crystal structure of S_2N_2 five hours into the polymerisation process: (left) shows the slight transition towards a trapezium shaped molecule and (right) shows the planar deviation as viewed along the a-axis***

In this instance, the apparent movement away from a perfectly planar structure helps provide the first documented structural evidence to support the S-N bond extension/cleavage reaction initiation sequence. Elongation of the S(2)-N(2) bond to 1.673 Å provides a net increase of 0.018 Å when compared to the freshly prepared S_2N_2 sample. Additionally, broadening of the S(1)-N(1)-S(2) and narrowing of the N(1)-S(2)-N(2) bond angles, to 91.2° and 87.0° respectively, is indicative of such a phenomenon and clearly indicates the onset of a transition towards the *cis*, *trans* $(SN)_x$ polymeric structure. The stacking arrangement within this transient S_2N_2 crystal system does still appear to exhibit the typical herringbone pattern usually associated with this molecular lattice. It is notable, however, that the spatial arrangement of independent S_2N_2 units within this unit cell differs from the 'fresh' starting material packing plot shown in Figure 87. In the case of the former, two complete S_2N_2 molecules can be seen to stack within the constraints of the unit cell; compared to six contributing molecules for the starting material. The spatial re-arrangement of adjacent S_2N_2 molecules is indicative of phase change initiation within the crystal system and the decreased R^2 value further suggests a loss of crystallinity symptomatic of such transitions.

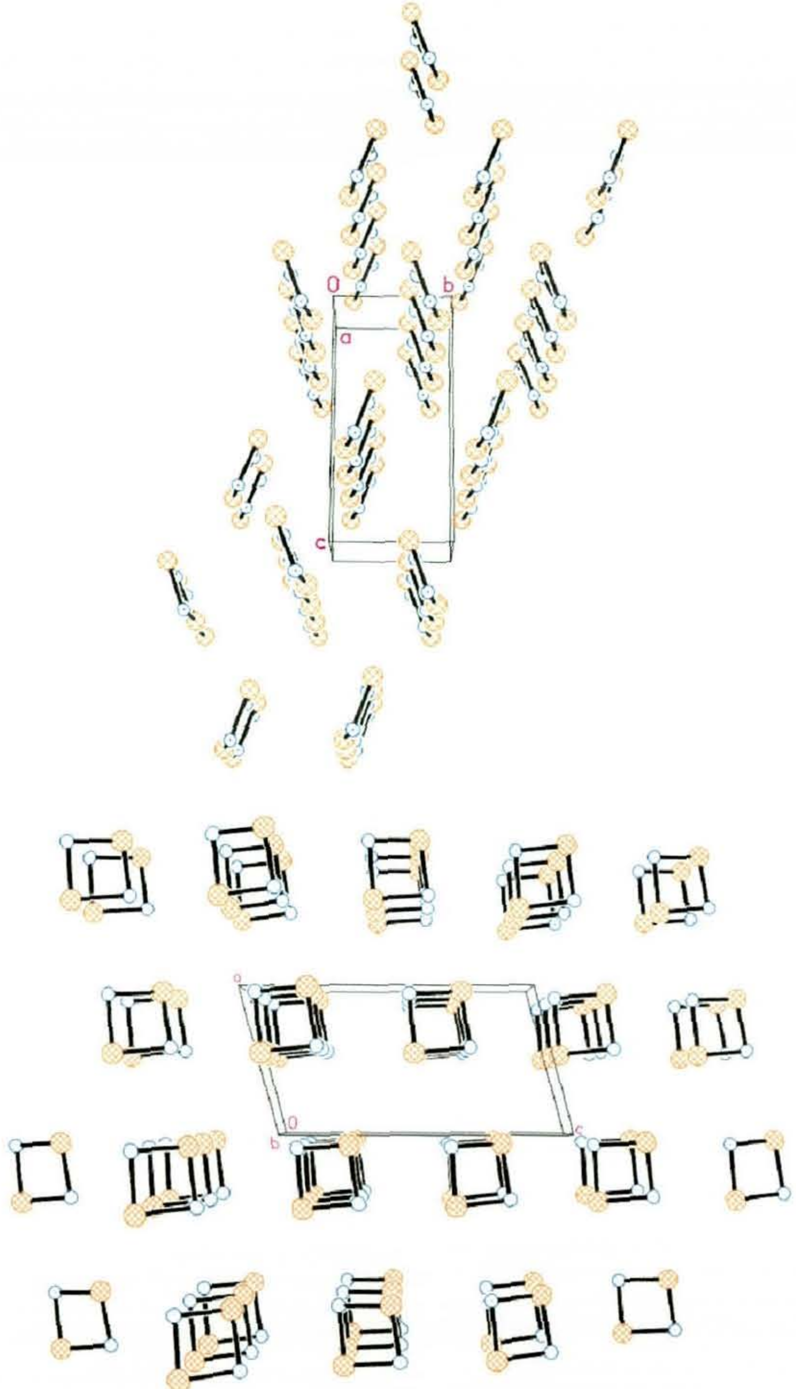

Figure 89 - ***Single crystal packing diagram of S_2N_2 five hours into the polymerisation process.***

As perhaps expected with phase/species transitions during time-resolved studies, the crystallinity of the sample can vary significantly based on its particular composition at a said time. Accordingly, diffraction quality is directly affected and the progression from the first data set to the second showed some non-detrimental signs of minor crystal degradation. Further polymerisation time (five hours), under nitrogen, and collection of another hemisphere data set indeed resulted in a weakly diffracting sample. Nonetheless, extensive characterisation attempts and consultation with Cell_now (computer software focussing on unit cell determination) concluded that the structure was again monoclinic, with a space group assignment of $P2_1/c$ ($a = 4.442$, $b = 4.450$, $c = 7.671$ Å, $\beta = 109.94°$). Based on the matrix data set, it appeared that at this point in the study, the crystal had undergone complete conversion to $(SN)_x$, providing evidence of unit cell parameters co-inciding with the latter.[28, 47, 200]

A further data set was recorded six hours later and the quality of the diffraction data was indicative of a higher degree of sample crystallinity, which itself is suggestive of a more stable, regular, single phase product. This unit cell was similarly monoclinic with a space group assignment of $P2_1/c$ ($a = 4.110$, $b = 4.436$, $c = 7.442$ Å, $\beta = 109.59°$), indicating that no further structure transformation had occurred.

Saliently, it appears that time-resolved single crystal XRD studies into the S_2N_2 polymerisation process have helped to provide some structural clarification relating to molecular re-arrangements within the crystal lattice in order to facilitate polymerisation. The initial deviation of the square planar molecule from the mean plane appears to be caused by S-N bond elongation and a narrowing/broadening of the S-N-S/N-S-N bond angles, respectively. Closer intimacy of adjacent S_2N_2 molecules as a result of this structural transformation enables suitable intermolecular interaction, presumably in the form of radicals (as suggested by ESR), to promote bond formation and polymer chain growth. Surprisingly, in this instance, polymerisation of the starting S_2N_2 crystal appears complete after *ca.* 12 hours, which is somewhat quicker than expected for $(SN)_x$. Consequently, diffraction data sets would need to be collected on a more frequent basis, with minimal dwell times between runs, in order to possibly allow a more progressive structural phase change transformation to be monitored.

5.1.2. Reactions of $(SN)_x$

To date, reaction chemistry of $(SN)_x$ is unknown, with no reported experimental findings amongst the literature. In contrast to other S-N species, such as S_4N_4, the use of $(SN)_x$ as a synthon in, for example, transition metal reactions, has been little studied. In part, such limitations have stemmed from the lack of solubility and thermal instability exhibited by the polymer, coupled with the arduous conditions and hazardous reagents required to synthesise it in bulk. However, these factors aside, the characteristic electronegativity of $(SN)_x$, created by delocalised charge along the polymer backbone, should stimulate interaction with various metal ion centres and allow a range of reactions to be studied. The potential attachment or fragmentation of the polymeric chain to a metal centre was hoped to allow the characteristics of $(SN)_x$ to be modified through suitable alteration of the electronic properties of the chain substituents. Additionally, once complexed, the solubility of the product may be predicted to increase, thereby enabling further investigations into reactivity of the $(SN)_x$ system, through single phase solution reactions.

Consequently, the reaction of $(SN)_x$ with an array of metal complexes was investigated. Although many reactions appeared not to elicit any visible signs of reaction, several were found to provide characterisable reaction products.

As briefly discussed in Section 2.3, the reaction of the Pt^0 species, $Pt(PPh_3)_3$, with $(SN)_x$, under a nitrogen atmosphere, appeared to provide a successful reaction, affording a dark orange coloured solution (preceded by a green intermediate colour). Following precipitation with dry Et_2O, the pale orange/yellow solid was analysed *via* $^{31}P\{^1H\}$ NMR in freeze thawed $CDCl_3$. Analysis of the resultant NMR spectrum and cross-reference to known literature findings,[18, 201] allowed full characterisation of the product. The singlet peak at 43.32 ppm was believed to be attributable to a side-product, triphenylphosphine sulfide, $Ph_3P=S$, and the two sets of doublets from the oxidised Pt^{II} species, $Pt(PPh_3)_2S_2N_2$ (shown in Figure 90).[18]

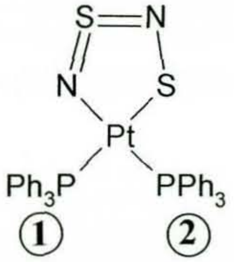

Figure 90 – ***The structure of $Pt(PPh_3)_2S_2N_2$.***

As shown in Figure 90 above, environment 1 is accredited for giving rise to the doublet peak at 23.56 ppm, with two corresponding sets of doublet Pt satellites at 32.29 and 14.83 ppm (^{1}J(Pt-P) 2827 Hz, ^{2}J(P-P) 23.1 Hz). Environment 2 is responsible for the doublet peak found at 11.34 ppm, flanked by another two sets of doublet Pt satellites at 20.55 and 2.10 ppm (^{1}J(Pt-P) 2995 Hz, ^{2}J(P-P) 23.1 Hz). The phosphorus atom, belonging to the phosphine group in environment 2, displays a larger Pt-P coupling constant as a result of the net shorter Pt-P bond arising from slight withdrawal of electron density from the nitrogen, *trans* to the phosphorus. Interestingly, the analogous reaction of S_4N_4 with $Pt(PPh_3)_3$, instead of $(SN)_x$, affords exactly the same principal product, $Pt(PPh_3)_2S_2N_2$, but over a slightly shorter timescale.

Reaction of the phosphine, PPh_3, with $(SN)_x$, in CH_2Cl_2, immediately gave an orange coloured solution. *In situ* $^{31}P\{^1H\}$ NMR showed two dominant singlet peaks at -5.49 ppm, corresponding to residual PPh_3, and 43.07 ppm, which was assigned to $Ph_3P=S$. Subsequent evaporation of the filtrate yielded a dark orange/brown oil which darkened with time to a red colour. These findings are coherent with those reported for the reaction of S_4N_4 with PPh_3 by Chivers and co-workers, who also noted the formation of the cyclic 1,5bis(triphenylphosphinimino)cyclotetrathiazene, $(Ph_3P=N)_2S_4N_4$, product.[201] Observation of the latter, from the $(SN)_x$ reaction, was not noted despite a change of solvent system.

When reacted in excess with the dimer $[Pt(\mu\text{-}Cl)Cl(PPhMe_2)]_2$, $(SN)_x$ again appears to afford similar products to those associated with analogous reactions of S_4N_4. An *in situ* $^{31}P\{^1H\}$ NMR of the resultant deep cherry red solution produced a multitude of peaks across the spectrum. The singlet observed at -21.13 ppm (^{1}J(Pt-P) 3403 Hz) showed good similarity to [Pt(S_2N_2H)Cl(PMe_2Ph)] and -9.24 ppm (^{1}J(Pt-P) 2117 Hz) to $PtCl_2(S_4N_4)(PMe_2Ph)$.[17, 202] Additionally, the presence of $PtClS_4N_4$ was also suggested *via* mass spectroscopy (m/z 379; $[PtS_4N_4]^+$).

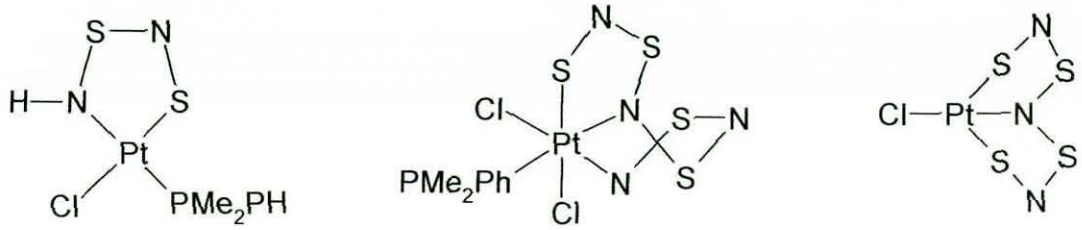

Figure 91 – *The structures of Pt(S_2N_2H)Cl(PMe_2Ph) (left), $PtCl_2(S_4N_4)(PMe_2Ph)$ (middle) and $PtClS_4N_3$ (right).*

Concentration of the filtrate and its passage through a Bio-Beads Gel Permeation column allowed isolation of the yellow [Pt(S_2N_2H)Cl(PMe_2Ph)] fraction, but no further products were isolable. TLC analysis of the collected red fraction still showed mixed phase composition, but a suitable separable solvent system was not found.

Reaction of $[Pd_2Cl_6][PPh_4]_2$ with $(SN)_x$, in CH_2Cl_2, at room temperature did not provide any visible signs of reaction. When a similar reaction was attempted using superheated CH_2Cl_2, at ca. 90°C, using a Young's tube setup as shown in Figure 92, a darkening of the solvent from pale orange/brown to deep red/brown became evident over several minutes. Following reduction of the solvent volume and a layering of hexane onto the mother liquor, slow diffusion resulted in two distinct crystal types: dark red-brown and pale beige/orange needle like single crystals. Prior investigations by Woollins *et al.*, where S_4N_4 was used as the ligand source, described analogous observations to those shown through reaction of the polymer with the binuclear palladium complex, resulting in the formation and single crystal characterisation of brown $[PPh_4]_2[Pd_2(\mu\text{-}S_2N_2)Cl]$ and orange $[PPh_4]_2[Pd_2(\mu\text{-}S_3N_2)Cl_4]$.[203] It appears, in this example, the only significant difference between the two reactions is the required initiation temperature. At room temperature, S_4N_4 reacts readily with the $[Pd_2Cl_6][PPh_4]_2$ species, but the $(SN)_x$ reaction was only driven by augmented temperatures.

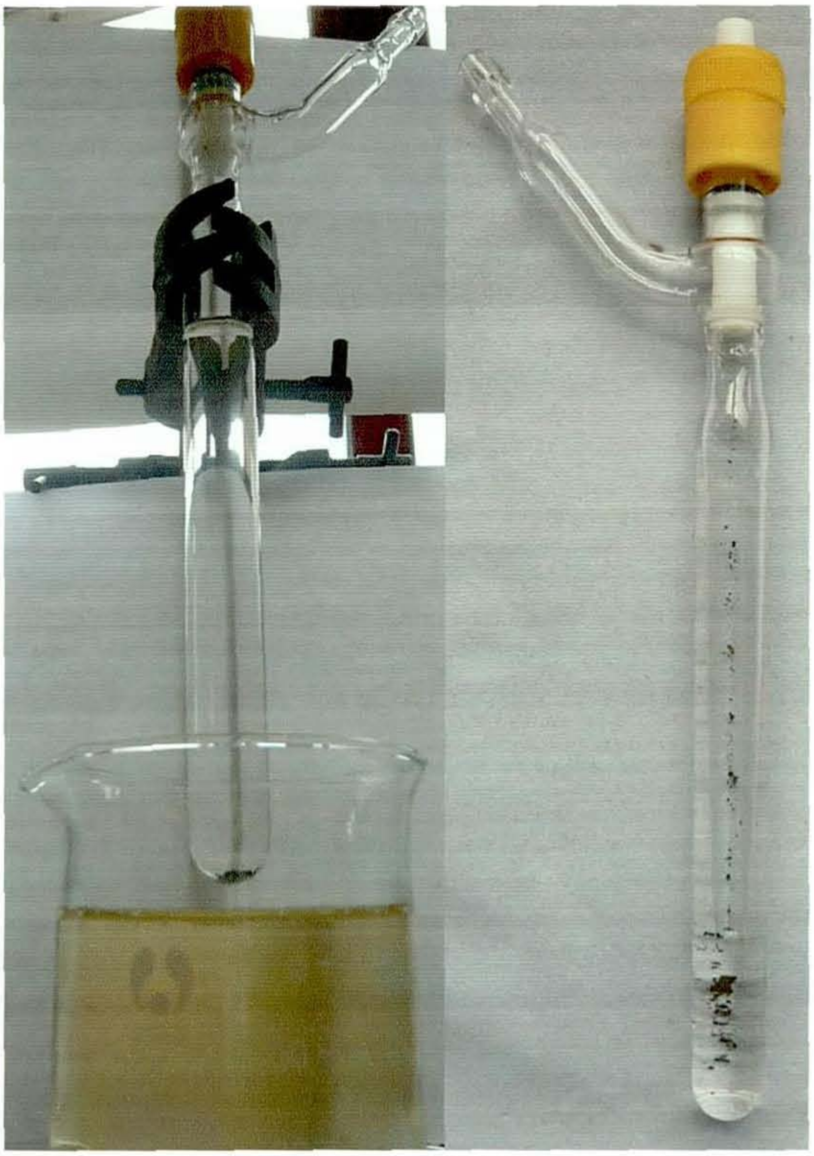

Figure 92 – ***The Young's setup used during superheated solvent reactions.***

During the reaction of S_4N_4 with $MCl_2(MeCN)_2$ or $MCl_2(PhCN)_2$ (where M = Pd or Pt), at room temperature, a dark red-brown precipitate is formed. The isolated solid appears insoluble in most common solvents and displays only partial solubility in warm CH_2Cl_2. Attempted characterisation of this material has not provided any conclusive results and crystallisation attempts have been unsuccessful. It is thought, however, that the inherent insolubility of the product, coupled with its dark appearance, may be indicative of the formation of a Pd/Pt-S_4N_4 type polymeric species. When the reaction is conducted using $(SN)_x$ instead of S_4N_4, similar observations are noticed over a slightly longer timeframe. The precipitate in this reaction appears deeper brown in colour and is again partially soluble in warm

CH_2Cl_2. Attempted crystallisation of this product *via* both hexane layering, ether vapour diffusion and freeze-thaw hexane layering did not provide any suitable crystals for XRD analysis. Repeated reactions were attempted where the mixture was not stirred or agitated in any way. After *ca.* 24 hours of standing, slight glimmering facets could be seen at the bottom of the solution and after four further days, small dark red-brown cubic crystals were visible. Unfortunately, subsequent single crystal XRD studies on these crystals revealed only the formation of the Pd_6Cl_{12} cluster. Recent findings on this front have shown that when allowed to stand, solutions of $PdCl_2(PhCN)_2$ afford X-ray quality dark red prisms.[204] It appears that this supramolecular aggregation product has been encountered during the course of crystallisation, and no further insight into the main reaction product was obtainable.

The un-stirred, static reaction of the anhydrous Cu (II) salt, $CuCl_2$, with $(SN)_x$ appeared to show signs of reaction, primarily through strong solution colour change from yellow/green to deep orange. Prolonged standing for *ca.* 3 days afforded small crystallites at the bottom of the solution that did not appear to increase in size over a further 7 days. Following removal of the orange solvent, which did not prove to be S_4N_4 as determined *via* TLC analysis, the colourless hexagonal crystals were allowed to dry in air. Attempted single crystal XRD resulted in a weakly diffracting sample that showed signs of powder rings, thereby inhibiting positive structural identification. It was considered that the hexagonal crystals formed during the reaction were some form of Cu (I) salt, owing to their colourless nature. Concentration of the filtrate and subsequent crystallisation attempts did not afford any crystals suitable for analysis. In contrast to $(SN)_x$, the static reaction of S_4N_4 with anhydrous $CuCl_2$ leads to the formation of anthracite black, shiny crystals of the adduct, $S_4N_4{\cdot}CuCl$.[11, 205] These particular crystals belong to the monoclinic space group and contain Cu-Cl zigzag chains that are bridged by the bidentate binding of two S_4N_4 rings, thereby resulting in the tetrahedral coordination of the Cu atoms. No such reaction appears evident when $(SN)_x$ is used as the nitride source, however.

Other attempted reactions with $(SN)_x$, where $PtCl_2(COD)$, $[RuCl_2(p\text{-cymene})]_2$ and $FeCl_3$ were used as target metal centres, did not provide any visible signs of reaction, despite the reaction of S_4N_4 with the latter, for example, affording the adduct $S_4N_4{\cdot}FeCl_3$.[206, 207]

The reaction of $(SN)_x$ with various transition metal centres has provided conclusive evidence to support its promise as a thiazyl ligand source, but in a manner different to that initially desired. It appears that conservation of the polymer backbone, or other substantial oligomeric assemblies, and their binding to the metal centre does not prove experimentally feasible. Instead, successful reaction pathways seem to occur in a similar fashion to those seen for S_4N_4, often involving the formation of the S_2N_2 ligand. However, it is perhaps not strictly correct to assume polymer decomposition to S_4N_4 and its subsequent reaction as if this were the case, all attempted reactions should have, in theory, produced products identical in nature to those already known for analogous S_4N_4 reactions. The reactions of $Pt(PPh_3)_3$, PPh_3, $[Pt(\mu\text{-}Cl)Cl(PPhMe_2)]_2$ and $[Pd_2Cl_6][PPh_4]_2$ with $(SN)_x$ were all found to afford the expected products of the corresponding S_4N_4 reaction. In the case of $CuCl_2$, $FeCl_3$, $PtCl_2(COD)$ and $[RuCl_2(p\text{-cymene})]_2$, either no visible reaction was observed, or the reaction products appeared to differ from those expected from S_4N_4.

It is plausible that the successful reactions discussed above were initiated through some cumulative degree of polymer decomposition/degradation, resulting from the action of the corresponding reagents. In turn, the formation of inherently more reactive S-N species, such as S_4N_4, S_2N_2 or $SN\cdot$, facilitated the formation of the reaction products already discussed. Alternatively, it was initially thought that prolonged stirring of the polymer in solvents such as CH_2Cl_2 may itself induce decomposition. A simple test reaction where $(SN)_x$ was stirred in dried, de-gassed CH_2Cl_2 for 48 hours, showed no significant visible changes to the material and the mother liquor remained colourless, indicating that the liberation of S_4N_4 had not occurred. In summary, therefore, it is difficult to attribute a precise reaction pathway for reactions of $(SN)_x$ with the various transition metal complexes discussed above. It appears that polymer decomposition through prolonged solvent effects does not occur, suggesting therefore that the polymer reacts spontaneously with the chosen reagents. Unfortunately, reaction products not offered *via* analogous S_4N_4 reactions have, hitherto, eluded isolation.

5.1.3. The decomposition of $(SN)_x$

In light of findings from the reactions of $(SN)_x$ with various transition metal complexes, and owing to the extensive use of the former during the course of these investigations, a more complete understanding of atmospheric decomposition pathways was required in order to acknowledge potential impurity phases within air exposed polymer samples. Moreover, fingerprint detection from sublimed $(SN)_x$, as discussed in Section 3.6, was found to not be significantly affected by sample purity: a small amount of impurity content still resulted in favourable polymer interaction with the latent prints and suggested therefore that any contaminants did not effect the function/properties of $(SN)_x$ itself.

Analysis of the atmospheric polymer decomposition was conducted using time-resolved *in situ* powder XRD. This method enabled the polymer sample to be loaded into the flat plate sample holder and its initial XRD pattern obtained. Subsequent patterns were then readily collected at set time intervals (over a fifteen day period), without the need to re-load the sample into the holder, thereby reducing both particle orientation effects, and *x*-offset shifts caused by deviations in sample position on the holder itself. Individual data sets were collected over 100 minutes across the 2θ angles of 5-60°.

Analysis of the first X-ray pattern showed a fairly high degree of crystallinity from *ca.* 17-45° 2θ, that was preceded by slight amorphicity as indicated by the broad hump between 5° and 15° 2θ. As expected, the data set itself exhibited good ICSD similarity to that expected for $(SN)_x$ (see Figure 93) based predominantly around the dominant reflections at 23-24°, 27-28°, 31° and 41° 2θ.

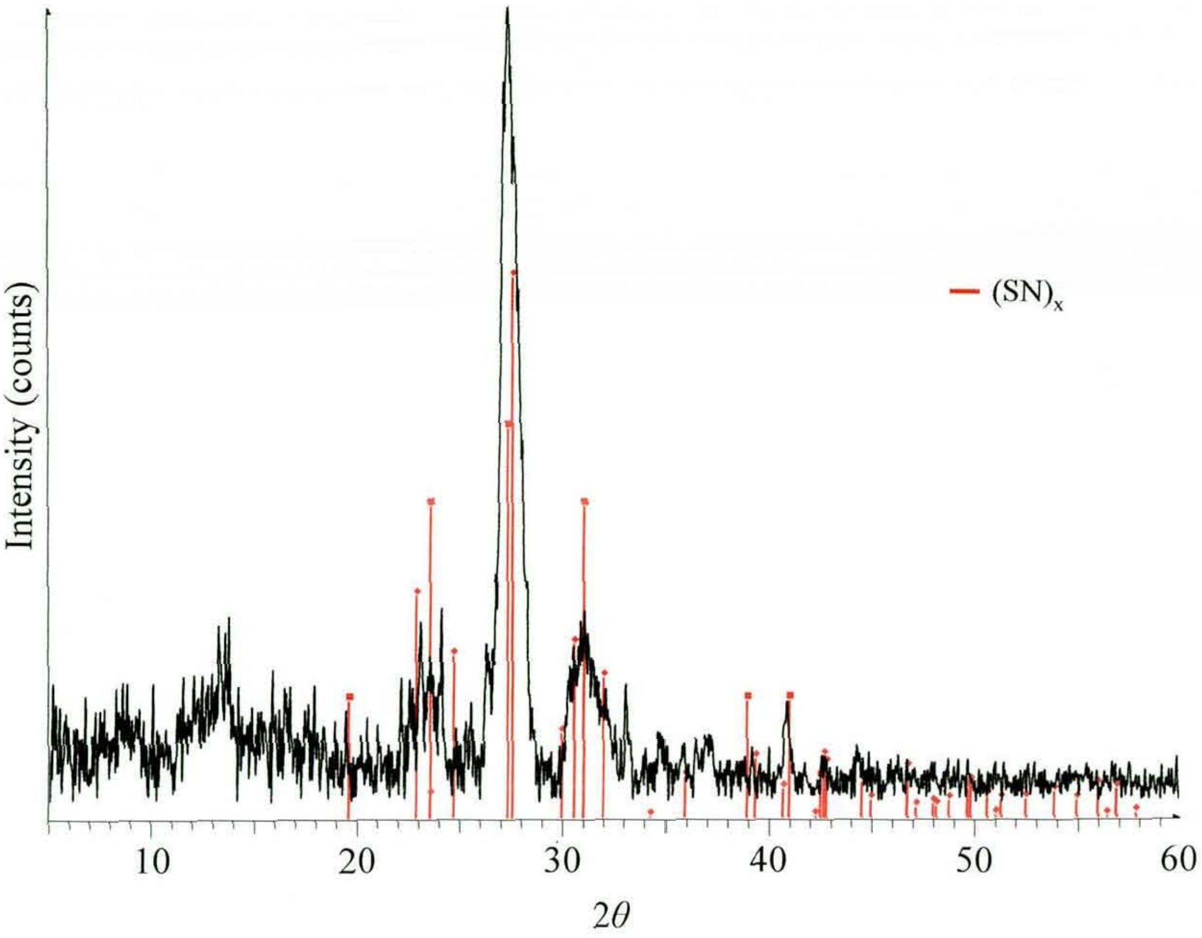

Figure 93 – ***Powder XRD pattern of $(SN)_x$.***

The next diffraction pattern was ascertained after 48 hours of the sample standing in atmospheric conditions and subsequent progressive data sets collected at regular time intervals thereafter, up to fifteen days. As can be seen in Figure 94 below, over the course of the study impurity components begin to appear in the diffraction pattern, suggesting a mixed phase composition of, predominantly, $(SN)_x$ and two other major decomposition products.

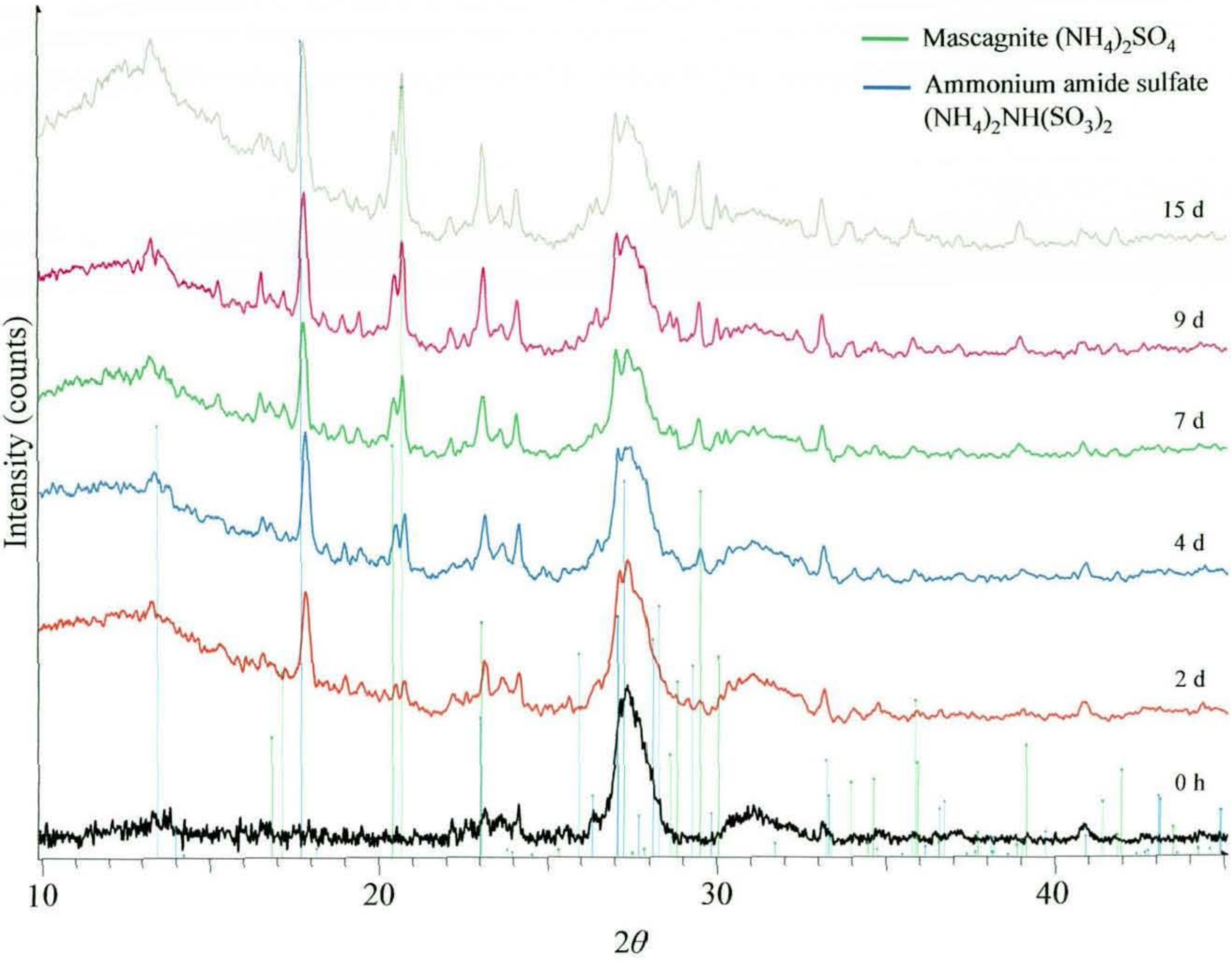

Figure 94 – ***Powder XRD patterns showing the decomposition of $(SN)_x$ over fifteen days.***

The gradual introduction of mascagnite, $(NH_4)_2SO_4$, and ammonium amide sulphate, $(NH_4)_2NH(SO_3)_2$, appears to increase cumulatively in relation to the duration of atmospheric sample exposure. The latter diffraction patterns (an example of which is shown in Figure 95) suggest a proportional reduction in $(SN)_x$ content, with dominance exhibited by the ammonium salt species.

Interestingly, over the course of polymer decomposition, the formation of S_4N_4 appears absent. It was suggested that during some of the transition metal reactions of $(SN)_x$, decomposition of the polymer, to S_4N_4, may have been induced, thereby promoting reaction through the cyclic moiety instead of the polymer itself. This decomposition study has perhaps enabled such a hypothesis to be dismissed and has also allowed the decomposition pathway to be further understood.

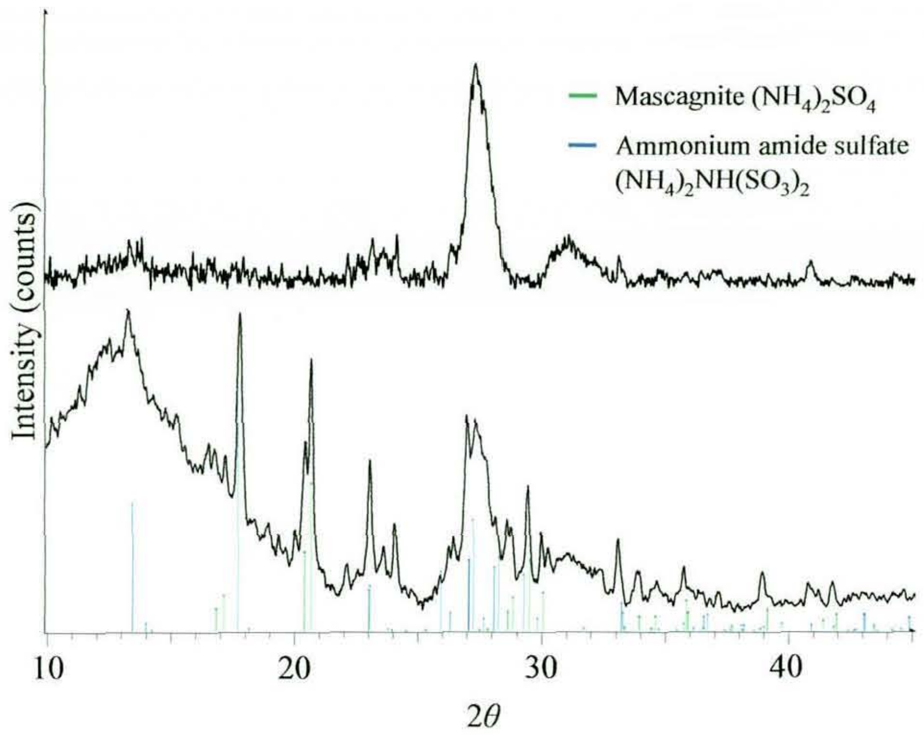

Figure 95 – ***Powder XRD comparison of $(SN)_x$ (upper) and $(SN)_x$ following atmospheric exposure for 15 days (lower).***

Additionally, with reference to the sublimation reactions discussed in Section 3.6, the purity of the polymer appears not to be detrimental in terms of reaction success, due to the non-subliminal nature of its decomposition contaminants (which remain at the bottom of the setup and do not interact with any of the samples).

5.1.4. Novel synthetic route to $(SN)_x$

Despite synthetic routes to both crystalline and powdered $(SN)_x$, ppsn, being known, the precursors used in each case may be considered by some as either potentially hazardous, or problematic to obtain and store over prolonged periods of time. An alternative route to $(SN)_x$ that is both simple, safe and high-yielding, was considered favourable as it would readily allow a number of studies to be conducted on the material and hopefully help stimulate (re)interest into the polymeric system across the broader scientific community.

Following on from research by Woollins *et al.* that focused upon the reactions of various S-N species with liquid ammonia,[208, 209] specific attention was directed towards the cyclic [S_3N_2Cl]Cl system. Conventional preparation of the former is usually achieved following protocol suggested by Woollins[210] or Jolly *et al.*[211] Both methods utilise the same core reagents: ammonium chloride, sulfur monochloride and elemental sulfur (see Equation 6), but their stoichometric ratios differ. Attempted synthesis of [S_3N_2Cl]Cl using the 1:2:1 ratio, as suggested by Woollins, was found to be temperamental, and did not regularly afford the desired deep red coloured crystalline product. Instead, it was found more efficient to use the 3:2:1 ratio described by Jolly to obtain the target material, in plentiful yield. A notable consideration observed during synthetic attempts was the increase in crystallisation rate when a constant flow of cool air was directed across the air condenser, immediately above the reflux point. Product crystallisation was typically complete following six hours and it was imperative to first pump on the sample to remove any S_2Cl_2, SCl_2 and HCl impurities that may be present, before storing the dark red crystalline product under a nitrogen atmosphere, as immediate darkening of the crystals was evident upon exposure to the atmosphere.

$$4\,S_2Cl_2 + 2\,NH_4Cl + S \longrightarrow [S_3N_2Cl]Cl + 8\,HCl + 6\,S$$

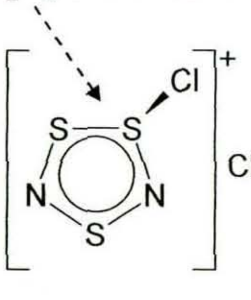

Equation 6 – *The synthesis of [S_3N_2Cl]Cl.*

The initial study, where [S_3N_2Cl]Cl was directly added to liquid ammonia and the reaction monitored through ^{14}N NMR, found that the principal reaction product was that of the $S_3N_3^-$ ion, as summarised in Equation 7. Subsequent treatment of the product was not reported.

$$S_3N_2Cl^+ + NH_3 \longleftrightarrow S_3N_3^- + 3\,H^+ + Cl^-$$

Equation 7 – *The reaction of [S_3N_2Cl]Cl with liquid ammonia.*

After preparing [S_3N_2Cl]Cl, it was important to use the material as quickly as possible owing to its inherent air and moisture sensitivity (sample degradation was even observed during prolonged storage under a nitrogen atmosphere). The addition of the material to liquid ammonia, under a steady flow of nitrogen, resulted in a vigorous exothermic reaction that was stirred as rapidly as possible, ensuring the walls of the RBF became coated with the orange coloured product so as to maximise exposed surface area. The ammonia was allowed to evaporate, using gentle heating where appropriate, and it became important to break up large solid masses with a glass rod; the exact nature of the product species at this point is unknown. To ensure complete removal of the ammonia, the product was pumped on for several minutes, which resulted in substantial darkening of the immediately exposed sample surface. Prolonged pumping for *ca.* 2 hours resulted in complete darkening of the material to a black colour, with an apparent golden shimmer at certain viewing angles.

The initial colour of the product had particular similarity to films/plates of $(SN)_x$, grown, for example, *via* sublimation of bulk polymer samples, or during volatilisation of S_2N_2, as described previously. IR analysis of the material, as a nujol mull to allow direct comparison to ppsn data reported by Passmore,[175] confirmed the presence of the characteristic S-N bands, *vide infra,* along with various other absorption bands, initially assigned as impurity components.

It was considered inevitable that such a reaction pathway, with the potential formation of radical and/or highly reactive ionic moieties, could easily result in the formation of numerous S-N compounds. Thus, washing of the bulk product with an array of solvents was conducted to help remove any impurities, thought likely to be present. Initial extraction with CH_2Cl_2 afforded a dark orange/red filtrate that, following evaporation in air and IR analysis, was found to be S_4N_4. Continued extraction with THF, MeCN, EtOH and acetone all resulted in the collection of progressively paler orange filtrates that were similarly determined to be S_4N_4.

At this point, microscopic examination of the product suggested a white contaminant was interspersed amongst the sample. Subsequent washing of the sample with de-ionised water, and evaporation of the filtrate to dryness, afforded a white solid whose IR spectrum and powder XRD pattern showed strong similarity for NH_4Cl.

Following solvent extraction, the remaining product was a finely divided black powder that appeared to be very static in nature – similar to $(SN)_x$ prepared in Section 5.1. IR analysis of this material showed good coincidence for $(SN)_x$, but was still suggestive of S_4N_4 contamination. Progressive refinement of the purification methods afforded high purity ppsn samples following soxhlet extraction for 24 hours, using CH_2Cl_2 as the solvent, preceded by sample washing with de-ionised water. Both elemental, IR and Raman analyses provided data attributable with $(SN)_x$. Sample crystallinity was judged to be largely amorphous owing primarily to an absence of reflections in the powder XRD pattern.

Prolonged storage (> 14 days) of ppsn samples prepared through this novel route, showed signs of decomposition to S_4N_4. For this reason, all subsequent reactions were conducted as soon as physically possible to ensure the reaction of interest occurred *via* the polymer itself and not a decomposition product.

Reactions of ppsn with various transition metal complexes show good similarity to those described for $(SN)_x$ as prepared through conventional methods (see Section 5.1.2). The formation of analogous reaction products through similarly visible reaction pathways helps provide further proof into the formation of $(SN)_x$ from $[S_3N_2Cl]Cl$. Sublimation of the ppsn sample, at 135°C, however, does not result in the formation of a single phase sublimate species. Condensation of the resulting vapour generates three visible coloured films: red/orange, purple and blue-black.

5.1.5. Interaction of $(SN)_x$ with ammonia gas

During synthesis of ppsn from the liquid ammonia route described above, the introduction of ammonia gas to purified polymer samples resulted in a visible surface tarnishing (light green in colour). Pumping on this tarnished material for several minutes appeared to revert the colour of the sample back to its natural golden black. Repeated cycles using an ammonia Schlenk line, where ammonia was introduced to the ppsn and then subsequently pumped on, resulted in a reversible type reaction that eventually ceased after *ca.* 6 runs, affording an orange coloured product. IR analysis of this final material provided a spectrum indicative to S_4N_4, with no evident polymer stretches.

This reaction appeared highly repeatable, and all ppsn samples exhibited similar behaviour. IR studies during the course of the NH_3/vacuum cycles were conducted and findings suggested that, prior to pumping, large N-H stretches were evident between 3300 and 3500 cm^{-1}, with the polymer absorption bands remaining largely unaltered. IR analysis following extended pumping resulted in typical S-N stretches expected for $(SN)_x$. It was found however, that as the cycle repetitions continued, the introduction of S_4N_4 impurities escalated, culminating in almost complete decomposition to the latter.

The exposure of ammonia gas to $(SN)_x$ samples prepared *via* the traditional thermal pyrolysis of S_4N_4 were also investigated. In this instance, the bulk polymer sample was gently powdered, under nitrogen, using a pestle and mortar, so as to ensure maximum surface area exposure to the NH_3 vapour. Using similar methods to the ppsn work, exposure of the $(SN)_x$ material to NH_3 resulted in identical surface tarnishing (light green in colour), but over a longer timeframe (typically *ca.* 1 hour). The reversibility of the system was again monitored through prolonged sample exposure to high dynamic vacuum, but complete conversion back to the original dark blue-black colour only resulted following several hours of pumping (compared to several minutes for ppsn samples). Subsequent NH_3/vacuum exposure only resulted in polymer decomposition, with no reversible phase apparent after the first complete cycle. IR analysis displayed similar trends to those seen for ppsn, but the final decomposition product appeared to contain a mixture of products, including S_4N_4.

Based on the findings above, it is proposed that the introduction of ammonia gas to $(SN)_x$ samples results in either of two interaction effects. The fibrous nature of $(SN)_x$, as shown earlier in Figure 84, may be suitable to host small molecular species, in this case NH_3, within interstitial locations that separate individual strands/fibres within the particle as a whole. Accordingly, the lack of a fully clathrated environment means that complete guest occlusion does not result and exposure to high vacuum allows the NH_3 to be readily removed from the system. Perhaps more likely, however, is the formation of an NH_3 adduct species, whereby weak interaction of both S-N and N-H moieties results in a weakly bound NH_3 to the main thiazyl backbone, that is readily broken under high dynamic vacuum. Such a phenomenon could help explain the decomposition effects following prolonged NH_3/vacuum cycles, resulting in the formation of S_4N_4. The interaction of the basic NH_3 source with $(SN)_x$ may invoke detrimental structural re-arrangement over the course its addition/removal, that enables the formation of simpler S_4N_4 units.

5.1.6. Sublimation

The sublimation of $(SN)_x$ and its subsequent condensation across latent fingermark residues proved both feasible and highly successful (see Section 3.6). The exact composition of the vapour phase species, during sublimation, attracted significant interest several decades ago, but conclusive evidence largely eluded experimental investigation. The nature of the gaseous $(SN)_x$ component is still undecided, with strongest evidence suggesting the dominant presence of an $(SN)_4$ tetramer which, upon condensation, reforms the polymeric $(SN)_x$ chain.[212, 213] This proposal is perhaps logically the most viable reaction sequence, yet other vapour phase species have also been suggested: S_2N_2, $S_3N_3^+$, $SN\cdot$ and S_4N_4, for example.[4, 212] Previous work illustrated the capacity of various microporous materials to occlude S_2N_2, from its vapour state, and in turn induce rapid polymerisation within the highly ordered channel network system, forming $(SN)_x$. The direct sublimation of $(SN)_x$ into identical host matrices therefore became of immediate interest.

Using an identical frit-diffusion type setup (as employed during the S_4N_4/zeolite investigations, see Figure 21), exposure of dry Na-ZSM-5 to the volatile components of $(SN)_x$ was readily investigated. Upon exposure to the sublimate, the zeolite sample showed immediate signs of yellow colouration, which darkened in colour to a dark yellow/mustard over the next thirty minutes. Extended exposure to the $(SN)_x$ vapour did not result in any further colour change. Powder XRD analysis of the reaction product was indicative of guest occlusion trends encountered thus far; with decreased reflection intensity and slight negative 2θ shift (see Figure 96). Raman spectroscopy of the product suggested some bands that were similar in nature to $(SN)_x$ (489 cm^{-1}), but on the whole, the spectrum appeared to be unique in terms of S-N moieties studied to date.

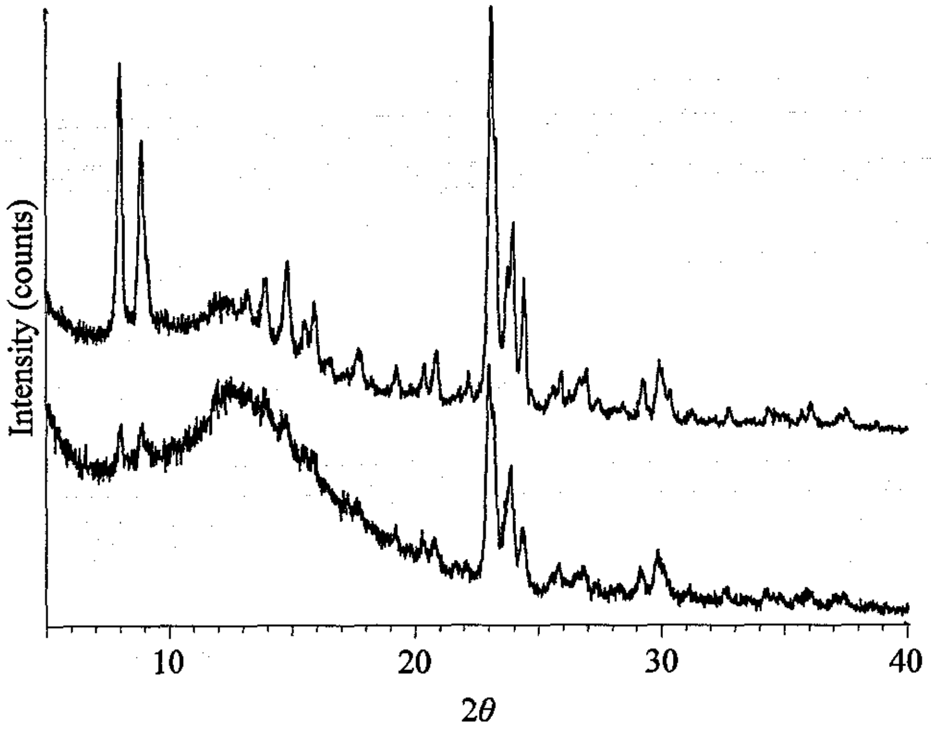

Figure 96 – ***Powder XRD pattern of Na-ZSM-5 (upper) and Na-ZSM-5 following exposure to $(SN)_x$ sublimate (lower).***

Interestingly, upon standing in a well lit room, samples appeared to undergo a distinct colour change from dark yellow/mustard to a deep red. When subsequently left in the dark, the colour of the samples seemingly reverted back to the original dark yellow; suggesting a visibly reversible photochromic effect. Direct exposure of this zeolite material to intense light, generated from a fibre optic source, indeed resulted in the rapid conversion (*ca.* 5 seconds) to the reddened colour.

To help understand this effect further, the component of light responsible for the sample colour change was investigated by means of UV/Vis reflection spectroscopy. Initially, a 'base' spectrum was established for the dark yellow material and this was compared to another spectrum that was obtained following intense light stimulation. Although sample reflectance decreased significantly following light exposure, over the next hour of the study the material appeared to return to its original 'base' state, as judged through progressive time resolved UV/Vis scans. It appears, therefore, that the photochromic effect is not only visibly reversible, in that the colour readily switches between yellow and red, but it is reversible in a chemical sense (i.e. following excitation, the system returns to its original non-excited state and has identical properties).

The use of interference filters allowed the wavelength of light associated with the sample colour change to be isolated. Interference filters are optical filters that typically reflect one or more spectral bands, but transmit others, while maintaining a negligible coefficient of absorption for all wavelengths of interest. The use of an array of interference filters that selectively allowed the passage of only one major light component from the visible spectrum enabled data to be ascertained relating to the likely wavelength of light responsible for the photochromic transition within the Na-ZSM-5 samples. Both UV and IR light sources were not found to initiate the chromic effects and it was eventually deduced that both blue and green light, with operational frequencies of *ca.* 475 and 510 nm, respectively, stimulated colour change within the samples. It was found that prolonged sample exposure (*ca.* 1 hour) to such wavelengths of light resulted in a further colour change from deep red, to blue/purple. Extended exposure appeared to 'fix' the colour of the sample and it remained blue/purple indefinitely, when stored under nitrogen.

Although the exact nature of the host species obtained from sublimation of $(SN)_x$ over Na-ZSM-5 is still unknown, it is likely that the zeolite channels serve as a molecular trap for one, or several, volatile matrix components of the polymer sublimate. In turn, the yellow species appear to undergo a reversible photochromic effect in the presence of strong light sources, emitting radiation of *ca.* 470-520 nm, and prolonged exposure affords an irreversible colour change to a blue/purple material. The colour of the resulting sample is somewhat indicative of $(SN)_x$, albeit not as dark blue/black in appearance, and Raman spectroscopy indeed suggested greater similarity to $(SN)_x$ than seen previously. The potential for occlusion of a highly reactive S-N moiety within the ZSM-5 channels, during sublimation of $(SN)_x$, could then lend itself to photo-induced re-arrangement (to a red coloured species), that in turn readily forms the thiazyl backbone of $(SN)_x$ and remains trapped within the Na-ZSM-5 channels.

The reversibility of the initial yellow-to-red transition appears highly reproducible and is perhaps indicative of tenebrescent behaviour, as observed within some sodalite type materials. Interestingly, however, this particular system becomes unique as there is no intergral β-cage framework to serve as an electron trap, as is the case for sodalites. Instead, vacant anion sites across the crystal lattice of the MFI framework must be acting as an F-centre and be responsible for the photochromic effect observed.

The use of stable photochromic materials is constantly expanding, and their potential use in the pigment industry (particularly zeolite materials) is of increasing interest. Despite an exact mode of action being unknown for this system, its unique properties and intriguing conversion pathway has the potential to attract further interest, from both an application perspective and a mechanistic approach.

5.2. Poly(thiazyl bromide), $(SNBr_{0.4})_x$

Although the synthesis of highly conductive $(SNBr_{0.4})_x$ is well documented,[61-63] little is known about its chemical reactivity; largely the result of preferential investigations into conductivity traits and potential applications, rather than chemical derivatisation. Subsequently, solid-state reactions involving $(SNBr_{0.4})_x$ were duly investigated and were primarily focused around plausible ion-exchange capabilities of the bromide moieties, located within interstitial voids across the polymer lattice.

The direct bromination of $(SN)_x$ to yield $(SNBr_{0.4})_x$ was not chosen as the preparative method of choice to obtain bulk samples of the latter (owing primarily to extended synthesis times). Instead, sample preparation followed anaerobic protocol described by Dehnicke and Demant[63] where $(NSCl)_3$ was reacted with Me_3SiBr in CH_2Cl_2 at *ca.* -60°C, and showed good similarity for $(SNBr_{0.4})_x$ *via* both IR and elemental analyses. Sample degradation was readily noticed upon exposure to the atmosphere for several minutes, whereby the dark blue/black powder (slightly darker in colour than $(SN)_x$) began to turn green.

Owing to the insolubility and thermal instability of $(SNBr_{0.4})_x$, neither single-phase solution reactions, nor solid-state heating investigations, were plausible. Attention was therefore directed towards both mixed phase solvent/solid (suspension) and solid-solid grinding reactions. All work was conducted under a nitrogen atmosphere, using either Schlenk line methods for the suspension reactions, or a glove box for grinding experiments.

5.2.1. Grinding Reactions

A variety of ionic compounds were selected to be ground with samples of $(SNBr_{0.4})_x$, ensuring a stoichiometric ratio of 0.4:1, respectively, was preserved. The samples were ground using an agate pestle and mortar, in a nitrogen purged glove box, for a minimum of two minutes, ensuring a homogenous sample resulted. The proposed reaction product in each case, suggested below in Equation 8, was monitored *via* powder XRD.

$$(SNBr_{0.4})_x + 0.4\ Li[TCNQ] \longrightarrow (SN[TCNQ]_{0.4})_x + LiBr$$

$$(SNBr_{0.4})_x + 0.4\ Na[BF_4] \longrightarrow (SN[BF_4]_{0.4})_x + NaBr$$

$$(SNBr_{0.4})_x + 0.4\ Na[BPh_4] \longrightarrow (SN[BPh_4]_{0.4})_x + NaBr$$

$$(SNBr_{0.4})_x + 0.4\ NaI \longrightarrow (SNI_{0.4})_x + NaBr$$

Equation 8 – ***Proposed ion-exchange reactions of Li[TCNQ], $NaBF_4$, $NaBPh_4$ and NaI with $(SNBr_{0.4})_x$.***

The use of powder XRD was not intended to directly analyse the target compound, $(SNX_{0.4})_x$ (where X = the relevant anion), but instead allow the predicted side-products, LiBr or NaBr, to be observed, both of which are suitably crystalline for XRD.

With the exclusion of the $Ba(BF_4)_2$ reaction product, the diffraction patterns obtained clearly illustrate successful identification of both NaBr and LiBr in the respective samples. Such observations immediately suggest plausible ion-exchange and the formation of novel substituted thiazyl polymers, obtained through simple solid-state grinding reactions.

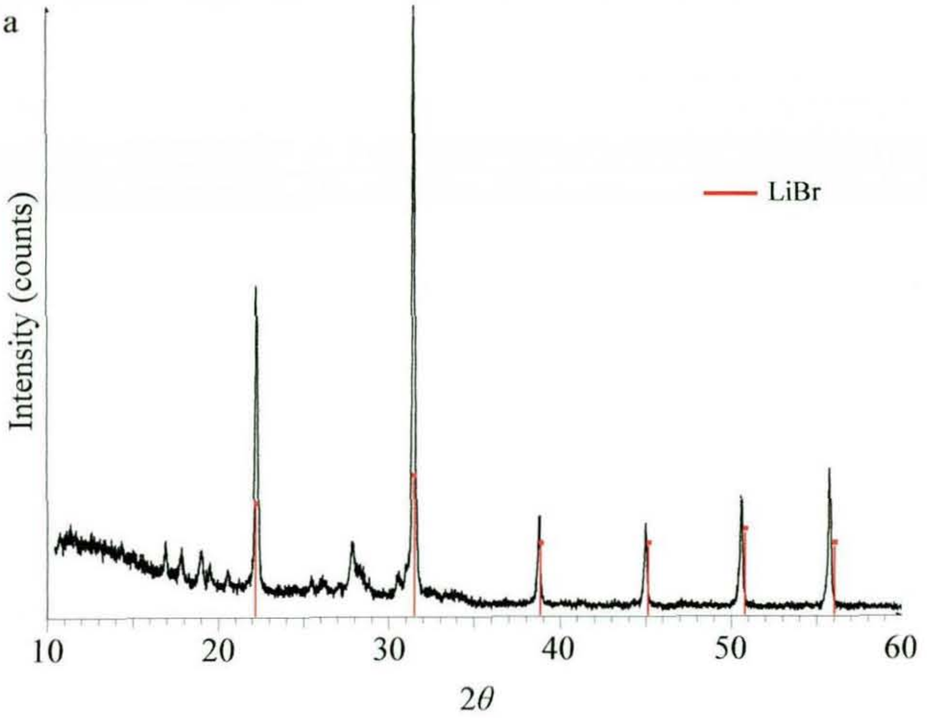
a
LiBr
Intensity (counts)
10
20
30
40
50
60
2θ

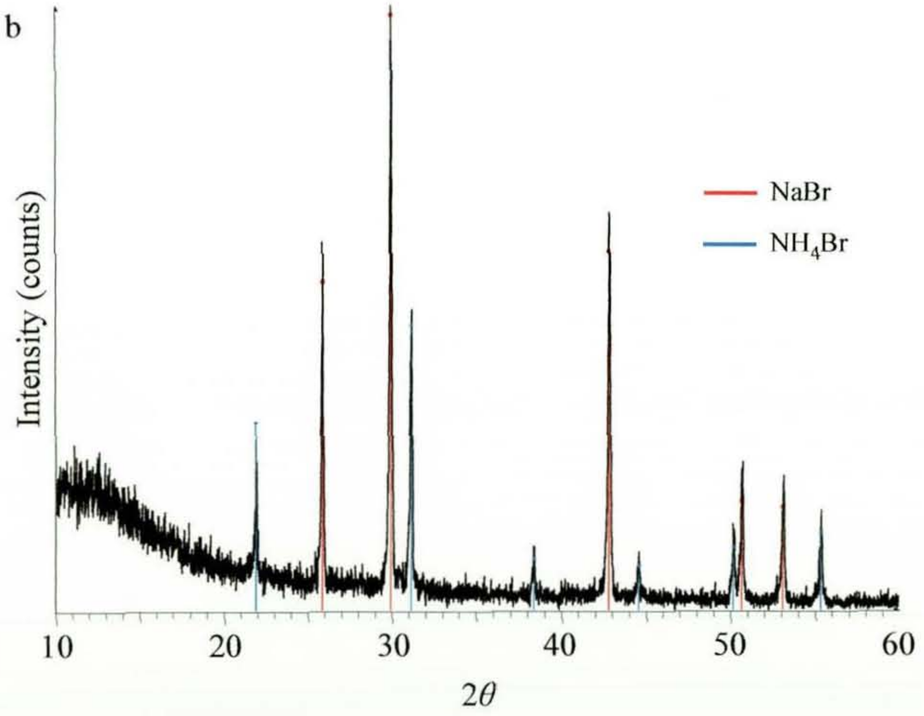
b
NaBr
NH4Br
Intensity (counts)
10
20
30
40
50
60
2θ

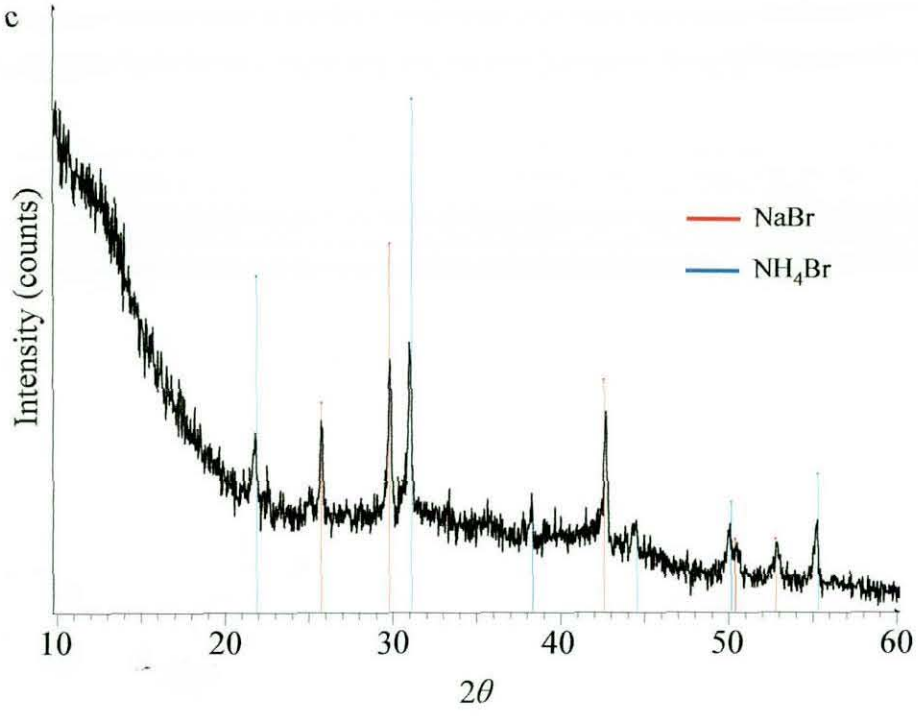

Figure 97 – ***Powder XRD patterns of the products obtained from $(SNBr_{0.4})_x$ ion-exchange reactions with (a) LiTCNQ, (b) $NaBPh_4$ and (c) NaI.***

5.2.2. Suspension Reactions

In a similar manner to the grinding investigations described above, mixed phase, solution/solid reactions were attempted using identical ion donors to those previously mentioned. Accordingly, following dissolution of the ionic compounds in CH_2Cl_2, $(SNBr_{0.4})_x$ was added to each and allowed to stir for 24 hours, after which time the suspension was collected *via* filtration and again analysed using powder XRD. The filtrate in each instance was orange in colour and IR analysis of the resulting solid, following evaporation, suggested S_4N_4 as the dominant species.

Interestingly, powder XRD analysis of the final dark blue-black solids identified almost identical diffraction patterns to those obtained from the solid-state grinding experiments (see Figure 97). The significant presence of both LiBr and NaBr in the respective samples is again indicative of successful ion-exchange between the bromide moiety within the thiazyl bromide system and the appropriate anion constituent of the counter-reagent.

Washing of the blue/black product with de-ionised water was found to successfully remove the NaBr or LiBr salt from the mixture, however more definitive characterisation techniques for the remaining $(SNX_{0.4})_x$ product were not immediately obvious. The lack of solubility of the substituted polymeric system and its poor crystallinity meant that desirable single crystal XRD was not feasible. Additionally, solid-state NMR was considered unlikely to offer insight into the exact nature of the anion constituent, but perhaps only provide an indication of changes to the ^{81}Br chemical shift, owing to electronic effects of the interstitial anion component.

In spite of not being able to obtain suitable characterisation of the substituted polymer species, initial evidence relating to the formation of the predicted side-products suggests that some degree of ion-exchange has occurred during both suspension and grinding reactions. The facile synthesis of substituted $(SN)_x$ materials allows a variety of compositions to be selectively prepared, chosen primarily around intrinsic properties. The addition, for example, of the conductive TCNQ moiety to the inherently conductive polymer lattice, has the theoretical capacity to create substituted polymer samples with superior conductivity capabilities.

5.3. Trithiazyl trichloride, (NSCl)$_3$

A known synthesis of $S_3N_3Cl_3$, or $(NSCl)_3$, involves the chlorination of S_4N_4 in a suitable solvent system.[214] Perhaps a safer, more amenable method of preparation, however, is the direct chlorination of $[S_3N_2Cl]Cl$, and was the method of choice during these investigations. It was found that the preferential passage of pure Cl_2 gas from a source cylinder could be avoided if Cl_2 was formed *in situ* during the reaction of $KMnO_4$ with concentrated HCl, and subsequently allowed to diffuse across crystalline $[S_3N_2Cl]Cl$ to form the bright yellow, crystalline $(NSCl)_3$ product.

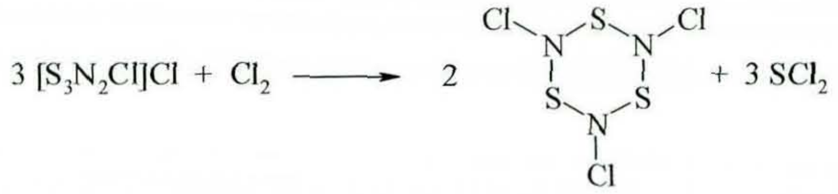

Figure 98 – ***The synthesis of (NSCl)₃.***

An intriguing property associated with $(NSCl)_3$ is its ability to depolymerise during vacuum thermolysis. Sublimation of the trimer, under either dynamic or static vacuum conditions, is readily achieved at temperatures ranging from 80-110°C and a green gaseous phase may be seen. Upon rapid cooling, the gas condenses to a green liquid which almost instantly solidifies as the yellow $(NSCl)_3$, as identified *via* IR spectroscopy. When cooled more slowly, the green liquid phase is not observed, but is instead replaced by gradual disappearance of the green vapour and the formation of yellow $(NSCl)_3$ crystals around the glassware. There exists, therefore, a vapour phase equilibrium between $(NSCl)_3$ and its monomeric equivalent, NSCl.

$$(NSCl)_{3(s)} \xrightleftharpoons{\Delta} 3\,NSCl_{(g)} \qquad \Delta H^\circ = 46.2 \pm 1.5\ kcal/mol$$

Equation 9 – ***The equilibrium obtained during thermolysis of (NSCl)₃.***

The isolation of the green NSCl species has largely remained elusive, despite extensive attempts to isolate the material. *In situ* vapour phase IR analysis has been shown to allow transient NSCl to be observed and its spectrum acquired, prior to its trimerisation back to $(NSCl)_3$.[215-218] The gas state structure of monomeric NSCl has also been identified using microwave spectroscopy and suggests a bent molecular structure ($<NSCl = 118°$) with sulfur-nitrogen bond lengths of *ca.* 1.450 Å, consistent with substantial triple bond character.[219] The preferred formation of the thiazyl monomer, NSCl, over the hypothetical thionitroso isomer, SNCl, can be largely explained by means of molecular orbital calculations which indicate the former to be substantially more stable than the latter.[220, 221] Robertson and McNaughton have used IR spectroscopy, for example, to deduce the plausible decomposition of NSCl upon exposure to atmospheric conditions and/or moisture.[215] Their findings suggest a two-step decomposition that initially affords the reactive vapour phase sulfinylimine, thionyl imide (HNSO), which in turn is hydrolysed to

NH_3 and SO_2. The formation of HNSO occurs as the result of nucleophilic replacement of the chloride substituent in NSCl, thereby losing the thiazyl triple bond. In essence, hydrolysis of NSCl results in the replacement of Cl^- by OH^- and subsequent isomerisation of thiazyl hydroxide to HNSO prevails.

$$NSCl + H_2O \longrightarrow [N{\equiv}SOH] \longleftrightarrow HNSO + HCl$$

$$HNSO + H_2O \longrightarrow NH_3 + SO_2$$

Equation 10 – *The suggested decomposition of NSCl.*

To date, monomeric thiazyl chloride has only been stabilised through its coordination to transition metal centres.[222-224] Accordingly, the isolation of NSCl within the constraints of a microporous framework was considered an alternative method of stabilising the reactive monomer. The selection of zeolite compounds with appropriate pore diameters was paramount and was largely dictated by the molecular diameter of the NSCl unit (*ca.* 3.1 Å).[225] It was hoped that following uptake of the monomer, it would be successfully occluded within the channel voids and remain largely unchanged (as the spatial constraints would be such that trimerisation back to the starting material would be restricted), thereby facilitating both direct species characterisation, property analysis and the potential for subsequent reaction chemistry. Despite a predicted pore diameter of approximately 3-5 Å being required, a range of host materials with varying pore apertures were used in order to allow optimum constraints to be ascertained.

Custom apparatus was fabricated that allowed vapour phase NSCl to be freely generated from its trimer, $(NSCl)_3$, and passed directly over target zeolite samples, *in situ* (see Figure 99). The technique relied on the ability of $(NSCl)_3$ to readily depolymerise and sublime, as the monomer, under heated static vacuum conditions (unlike $(SN)_x$ sublimation which requires a constant dynamic vacuum). Consequently, the production of NSCl within the constraints of the RBF facilitates plentiful interaction of the vapour with the zeolite that is spread across the 'well-plate'.

Figure 99 – ***The custom apparatus used during in situ NSCl reactions with various zeolite media.***

5.3.1. ZSM-5

The initial zeolite chosen for these investigations was Na-ZSM-5. The *ca.* 5 Å channel void diameter of the MFI framework was considered suitable to allow unhindered NSCl diffusion into the pores, but small enough to limit its subsequent expulsion.

During exposure to excess NSCl vapour, thoroughly dried Na-ZSM-5 was observed to take on a pale yellow colour after several minutes. The colour change to the zeolite sample continued to proceed through a dark green intermediate (*ca.* 20 mins) before culminating in a dark blue/black coloured product after 1 hour. Interestingly, the colour of the resulting material matched reasonably well with $(SN)_x$ occluded variants discussed previously, albeit slightly lighter in colour. The lack of other known blue/black S-N chromophores could perhaps be indicative of some sort of poly thiazyl product, trapped within the zeolite framework. Conversion of both $(NSCl)_3$ or NSCl to $(SN)_x$, or polymeric constituents thereof, are not known amongst the literature, and such an observation would present itself as surprising. However, when considering the nature of the supporting cation within the framework channels,

Na^+, it may be hypothesised that the formation of an ionic side-product, NaCl, may result in the liberation of a reactive NS moiety, that is free to polymerise to $(SN)_x$.

Following removal from the system, however, and exposure to air, the blue/black colour of the zeolite sample faded rapidly to a pale straw yellow; suggesting a high degree of air sensitivity. Occlusion of a polymeric species within the zeolite channels would typically be considered to offer a relatively high degree of stability to the guest molecule(s). In this case however, there appears to be no net stabilisation and decomposition occurs readily under atmospheric conditions. The potential for surface coating effects therefore become valid, but analogous NSCl interaction with channel restricted TPA-ZSM-5 provided no visible signs of reaction. It appears, therefore, that the colour change observed during the reaction of NSCl with Na-ZSM-5 occurs within the zeolite pores themselves, and this analogy is supported by powder XRD (see Figure 100), which clearly shows decreased reflection intensity and a slight negative 2θ shift.

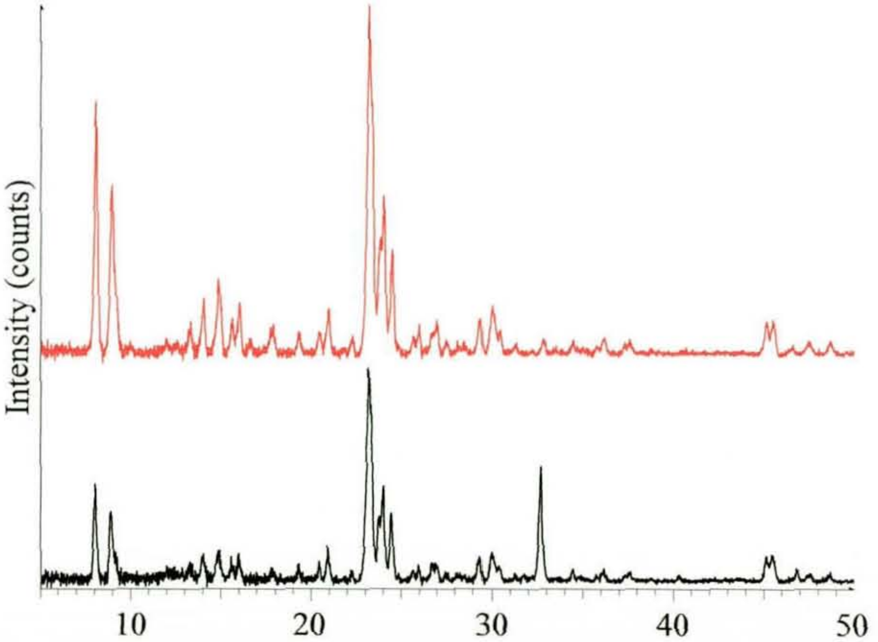

Figure 100 – ***Powder XRD comparison of the product obtained during the reaction of Na-ZSM-5 with NSCl vapour (lower) and Na-ZSM-5 (upper).***

Additionally, there appeared to be some impurity phase present within the sample mixture and subsequent database searches identified this to be ammonium chloride.

It was believed that XRD data collection, run quickly under atmospheric conditions, may have induced hydrolysis of a minor surface coated deposit from the reaction itself; a small degree of zeolite surface coating is likely from condensation of NSCl over the substrate. Accordingly, time-resolved powder XRD studies were conducted that monitored the compositional changes of $(NSCl)_3$ during prolonged atmospheric exposure. Figure 101 clearly suggests that the dominant solid decomposition product is that of ammonium chloride, and assignment of the impurity component, shown in Figure 100, can be verified as being the result of condensation and subsequent hydrolysis of $(NSCl)_3$ on the surface of the zeolite sample.

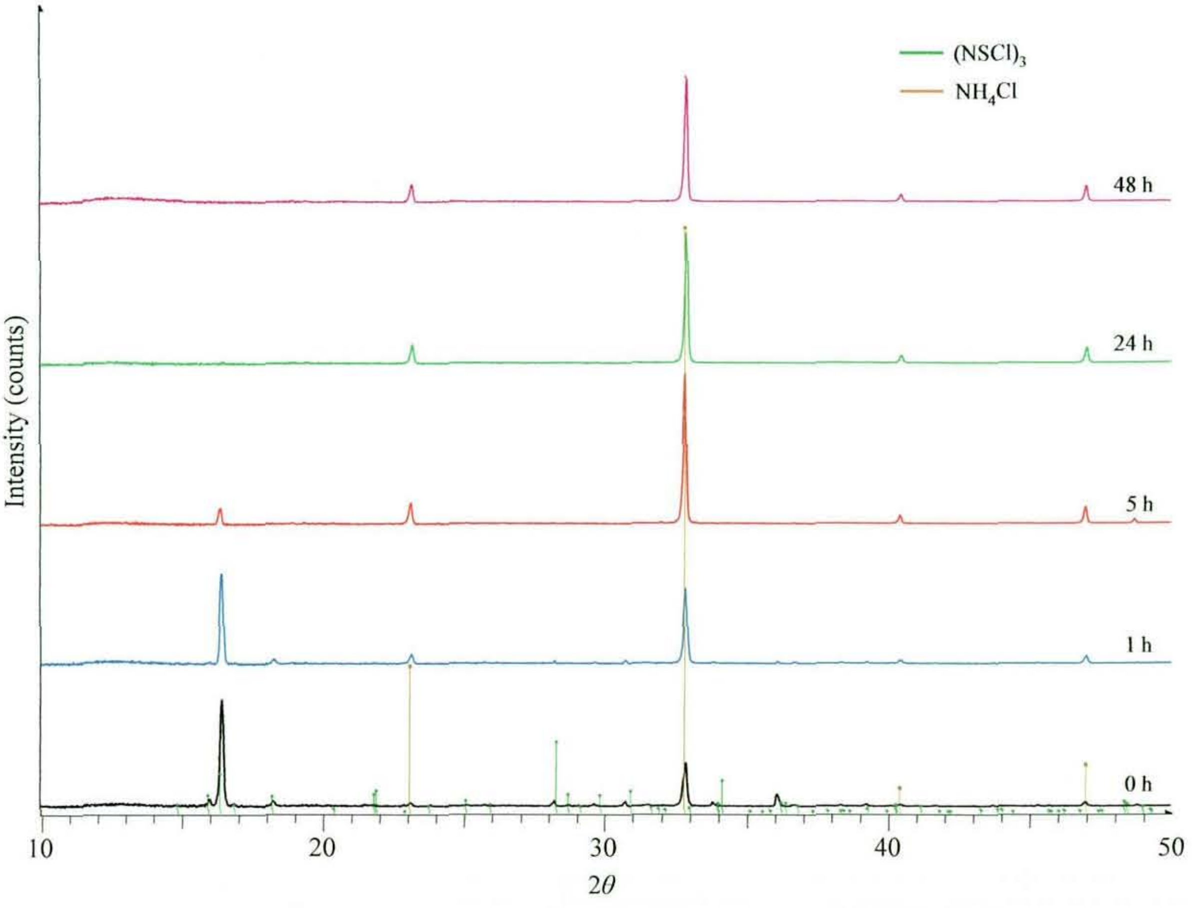

Figure 101 – *Time-resolved Powder XRD patterns showing the atmospheric decomposition of $(NSCl)_3$.*

IR analysis of the dark blue/black reaction product required KBr disc preparation in an inert glove box/bag atmosphere. The acquired spectrum, although dominated by the broad aluminosilicate bands of ZSM-5, highlighted the presence of N-H stretches (owing to minor hydrolysis obtained whilst running the spectrum) and a peak at

702 cm^{-1}, indicative of a polymeric S-N functional mode as seen in Na-ZSM-5-$(SN)_x$ and slightly shifted from that observed in free $(SN)_x$ itself. Additionally, Raman microscopy allowed some similarity to be observed between $(SN)_x$ and the blue/black zeolite product from this reaction.

The instability of the reaction product, however, does imply that the formation of occluded $(SN)_x$ is not actually occurring, despite some similarities being seen during characterisation attempts, *vide supra*. Further studies did not allow greater insight into the nature and/or composition of the product in question, and subsequent work focused on attempts to stabilise the reaction product using alternative zeolite hosts.

5.3.2. Silicalite-1

Despite having an identical framework composition and pore aperture width to ZSM-5, the interaction of silicalite-1 with NSCl was investigated to see if the absence of a supporting cation significantly altered the course of the reaction. Earlier work, that focussed on the polymerisation of S_2N_2 within both Na-ZSM-5 and silicalite-1, showed no significant difference between the two reaction products and it was concluded, therefore, that the Na^+ ion held close to the perimeters of the ZSM-5 channels, did not have an active role in the occlusion of S_2N_2 and the subsequent formation of $(SN)_x$. When introducing NSCl monomer to Na-ZSM-5, the colour of the resulting material, coupled with some limited characterisational analysis, partly supports the notion of $(SN)_x$ formation, induced through ionic interaction of the framework Na^+ cation with the chloride moiety of the thiazyl unit. Such effects would not be promoted in silicalite-1, however, as the framework itself remains uncharged, being composed solely of silicon and oxygen.

Upon exposure to NSCl vapour for *ca* 10 mins, the silicalite-1 sample took on an intense yellow/green colouration, indicative of NSCl itself, that remained even after 1 hour. In a similar manner to the ZSM-5 reaction (see section 5.3.1), exposure of the resulting product to atmospheric conditions induced visible sample decomposition; this time to a deep red/pink colour that remained for several months. Surface coating effects were again ruled out following analogous reactions using TPAF-silicalite-1, that contains bulky tetrapropylammonium fluoride within the channel voids.

Attempted IR sample preparation of the yellow/green reaction product, under glove box conditions, suggested that the presence of water was responsible for the decomposition of the sample: during grinding with KBr that had been stored at 90°C, the sample turned pink, indicating trace amounts of water within the KBr matrix were catalysing the decomposition, presumably through water uptake into partially occluded zeolite channels. Repeated IR sample preparation, this time ensuring both the KBr and the die itself were dried at 300°C for 24 hours, resulted in the formation of a pale yellow/green KBr disc whose spectrum was obtained as quickly as possible. The IR data, although limited due to the broad silicate stretches that dominate the analysis window, highlighted the presence of a sharp peak at 1258 cm^{-1}, which coincides with that expected for HNSO.[215]

It is believed, therefore, that owing primarily to the nature of the vapour phase species (NSCl) and the colour of the final silicalite-1 product (yellow/green), that NSCl monomer is readily occluded within the vacant pores of the zeolite. Following exposure to atmospheric conditions, even in the limited time required to obtain IR data, hydrolysis of the reactive monomer, attributable to molecular sieve type action of silicalite-1, results in the production of HNSO. Interestingly, the IR spectrum provides no indication into the presence of SO_2 or NH_3 within the sample matrix: an observation often encountered during the decomposition of NSCl (see Equation 10). Raman analysis did not provide any useful insight relating to the nature of the occluded species as a sufficient background noise to sample ratio could not be established using the sealed tube technique employed to store and analyse the samples.

The laboratory synthesis of stable zeolite based materials adopting red colouration is still very much desired.[226, 227] Conventional methodologies that give way to such pigments in plastics or ceramics often rely on the use of toxic chemicals that damage the environment when the material is made or destroyed (cadmium based salts, for example).[228-231] The apparent prolonged stability (> 6 months) of the red silicalite-1 product, following its exposure to air, is thought to be the result of polymeric formation and stabilisation of $(HNSO)_x$ within the silicalite-1 channels. Spontaneous polymerisation of the HNSO monomer is well documented and occurs readily upon condensation of the former. Analogous reaction sequence is plausible within the MFI silicalite framework following decomposition of NSCl, to HNSO, and in turn polymerisation to $(HNSO)_x$.

5.3.3. Other Zeolite Materials

The use of larger pore aperture zeolites was also investigated and typical findings indicated that guest occlusion was not favourable. The larger channel diameter of materials such as faujasite (7.4 x 7.4 Å pore diameter) and Linde Type L (7.1 x 7.1 Å pore diameter), although readily allowing the potential NSCl guest molecule to enter, also facilitate diffusion out of the zeolite framework, thereby inhibiting occlusion. Conversely, and to be expected, the use of zeolite materials with smaller pore apertures did not provide any signs of NSCl interaction. The reduced channel diameter of $AlPO_4$-18 (3.8 x 3.8 Å pore diameter), for example, hinders the uptake of NSCl, due to size exclusion principles.

5.4. Fingerprint Visualisation

The affinity of S_2N_2 and $(SN)_x$ for latent fingerprint residues has been well discussed in Chapter 3. In both instances, volatile S-N compounds are used as 'screening' vapours and their selective deposition across latent components leads to distinctive visualisation of the fingerprint ridge pattern. Accordingly, the subliminal nature of $(NSCl)_3$ and its relative ease of synthesis, allowed similar studies to be readily investigated.

The exposure of a variety of fingerprint contaminated substrates to NSCl vapour, generated *in situ* using similar methods to that described in Figure 99, resulted in the successful detection of latent prints on two exclusive surfaces: aluminium foil and paper. In the case of the former, the fingerprint ridge pattern is visualised through a black coloured deposit that selectively targets the latent residue (see Figure 102(a)).

Uncontaminated areas of the foil sample remain largely unchanged. The unusual colour of the enhanced prints (initially expected to be yellow, owing to the colour of $(NSCl)_3$ itself) may be suggestive of NSCl decomposition following contact with aluminium (forming $AlCl_3$, as indicated *via* powder XRD on aged samples), thereby affording a reactive thiazyl moiety that is able to polymerise accordingly.

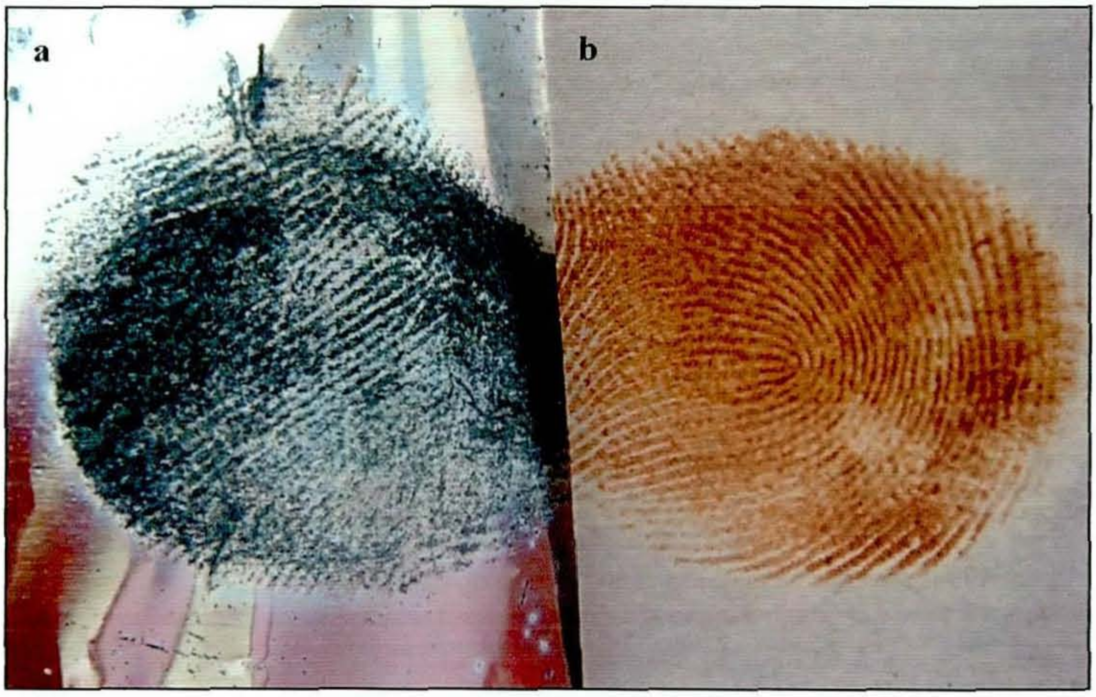

Figure 102 – ***Latent fingerprints on (a) aluminium foil and (b) paper, enhanced following exposure to NSCl vapour.***

Conversely, paper samples, deliberately loaded with fingermarks, responded differently to saturation under an NSCl atmosphere and presented themselves as dark orange/brown coloured ridge patterns (see Figure 102(b)). The colour of these enhanced latent prints is likely to be the result of $(NSCl)_3$ moisture sensitivity. It is well known that in moist conditions, such as those resulting from the deposition of a 'sweaty' fingerprint impression on a porous paper surface, $(NSCl)_3$ readily hydrolyses, turning dark brown in colour.[232]

NSCl vapour exposure to both plastic and glass contaminated substrates afforded few identifiable fingerprint marks, and the quality of the ridge pattern in terms of resolution and distribution did not compare favourably to results obtained from both S_2N_2 or $(SN)_x$ routes. Moreover, the stability of the enhanced latent prints was found to be far inferior to those enhanced with $(SN)_x$. Exposure of 'problematic' surface types (fabrics, for example), and previously wetted exhibits, did not allow successful print identification.

Despite providing an intriguing alternative fingerprint detection technique, the use of $(NSCl)_3$ was only viable at imaging latent deposits on paper and foil surfaces. It is thought that the high affinity of $(NSCl)_3$ for the fatty components in, for example, vacuum grease, is also responsible for random fingerprint enhancement; whereby sebaceous contamination within some latent deposits has the capacity to adhere the NSCl vapour, and in turn visualise the fingerprint.

6. Experimental

Unless otherwise stated, all sulfur-nitrogen species were prepared under an inert atmosphere, using standard Schlenk-line techniques,[233] and stored under nitrogen. All solvents were purchased from Aldrich, Lancaster, Alfa or Fisher, and deoxygenated prior to use, where appropriate. Diethyl ether (Et_2O), toluene (C_7H_8) and tetrahydrofuran (THF, $(CH_2)_4O$) were distilled over sodium wire, whilst dichloromethane (CH_2Cl_2) and acetonitrile (CH_3CN) were distilled from calcium hydride; all under an atmosphere of nitrogen.

The compounds $(EtO)_2SeO$,[19] $[Se_3N_2Cl]Cl$,[234] $Pt(PPh_3)_3$,[235] $PdCl_2(COD)$,[236] $[Pd_2Cl_6][PPh_4]_2$,[203] $[Pt(\mu\text{-}Cl)Cl(PPhMe_2)]_2$,[237] $[1,2(PhS)_2(\mu\text{-}N)C_6H_4][BPh_4]$,[238] $PdCl_2(MeCN)_2$,[239] $PtCl_2(PhCN)_2$,[239] Li-A (BW),[240] Linde Type A,[240] Linde Type L,[240] Boehmite,[241] NaBr Sodalite,[240] Faujasite,[240] $AlPO_4$-18,[240] [18]aneO_5S, [18]aneO_4S_2, [12]aneO_3S, [9]aneO_2S[242] and Li-TCNQ[243] were all prepared according to known literature methods, as stated. All other common reagents were purchased directly from Aldrich, Lancaster, Alfa or Fisher, and used as received, unless otherwise stated. Any materials prepared using an adaptation or modification of known routes are described in detail, and referenced accordingly.

All NMR spectra were recorded in $CDCl_3$ or using a C_6D_6 insert, unless otherwise stated. ^1H NMR spectra were recorded on a Bruker Advance US 400 MHz FT spectrometer, with chemical shifts in ppm (δ) referenced against an external tetramethylsilane, $SiMe_4$, standard. Similarly, $^{31}P\{^1H\}$ NMR were recorded using a Bruker Advance US 400 MHz FT spectrometer operating at 161.9755 MHz for phosphorus, with chemical shifts in ppm relative to an 85% H_3PO_4 standard. Solid-state NMR spectra were recorded using a Bruker Advance 500 MHz spectrometer, fitted with a 4 mm BBO HX MAS probe, using $SiMe_4$ and adamantane as reference standards for ^{29}Si and ^{13}C, respectively.

Infrared spectra were typically recorded as KBr disks using a Specac 15 Ton manual press and Perkin-Elmer System 2000 Fourier-Transform spectrometer, typically in the range 4000 – 300 cm^{-1}. Where stated however, nujol mulls between NaCl plates were obtained and run on the same spectrometer. Raman analysis (conducted at Loughborough University, Physics Department) was performed on neat samples using a Jobin Yvon Horiba LabRam HR800, fitted with a HeNe internal laser operating at a power output of 20 mW, polarised 500:1, with a wavelength of 632.817 nm. Powder X-ray diffraction data were primarily obtained using a Bruker D8 Advance powder diffractometer, fitted with a sealed copper X-ray source and Ge single crystal 110 monochromator, aligned for $K_{\alpha 1}$ radiation, with a fixed wavelength of 1.5406 Å, and PSD detector. Variable temperature powder X-ray diffraction data were obtained with the addition of an Anton Parr HTK 1200 heating stage. A Philips Xpert powder diffractometer, operating with Cu-K_{α} radiation, fitted with a scintillation counter, was occasionally used as an alternative. Elemental microanalyses were performed by Loughborough University Analytical Service, within the Department of Chemistry, using a Perkin-Elmer 2400 CHN elemental analyser or Exeter Analytical Inc. CE-440 elemental analyser.

Single crystal X-ray crystallography measurements were obtained using a Bruker AXS SMART 1000 CCD area-detector, fitted with a sealed-tube, graphite monochromated Mo-K_{α} radiation source. Cell parameters were refined from the observed (ω) angles of all strong reflections in each data set. Intensities were corrected semi-empirically for absorption, based on symmetry-equivalent and repeated reflections. All structures were refined on F^2 values for all unique data by full-matrix least-squares using the computational program, SHELXTL. Where deemed necessary, high flux synchrotron radiation crystallography was performed at Daresbury Laboratories, and the structures refined using identical methodologies and software.

Scanning Electron Microscopy (SEM) was conducted on neat samples, mounted to adhesive carbon discs and gold coated prior to examination. Images were obtained using a Carl Zeiss 1530 field emission instrument fitted with an EDAX Phoenix EDX system, detected *via* Everhart-Thornley or in-lens methods.

Safety Note: In the pure form, S_4N_4, Se_4N_4 and S_2N_2 are pernicious contact and friction sensitive explosives, the latter having been reported to spontaneously detonate at ambient temperatures.[244, 245] Although this problem was not encountered, all work involving the aforementioned compounds was performed using appropriate blast screening, Kevlar arm gators, and puncture resistant gloves. The use of metal spatulas was prohibited, and rapid heating of any nitride approached with caution. It was ensured that no such compound was stored, in mass, within a confined environment.

6.1. Synthesis of tetrasulfur tetranitride, S_4N_4

Sulfur (I) chloride, S_2Cl_2, (50.0 cm^3, 84.00 g, 0.62 moles) and dry carbon tetrachloride (1400 cm^3) were placed into a two litre, three-necked, round-bottomed flask (RBF). A paddle stirrer was inserted through the main neck (middle) of the flask, an open-end gas inlet tube inserted through another neck, and another open-end gas inlet tube was inserted through the remaining neck (see Figure 17).

While the mixture was stirred briskly (*ca.* 500 rpm), a steady stream of chlorine gas was passed directly into the solution, until a distinct green layer of chlorine was clearly visible in the headspace, over the solution (also ensuring the colour of the solution changed from yellow to a more orange-red). The flow of chlorine was then stopped and the gas delivery tube connected to a nitrogen supply. Nitrogen gas was then passed both directly through the solution, and through the headspace immediately above the solution, to remove as much excess chlorine gas as possible. This was done in order to help eliminate the risk of NCl_3 formation: a highly pernicious explosive liquid.

The gas delivery tube was then connected to an ammonia gas source. The round-bottomed flask was immersed to the level of the carbon tetrachloride solution in a water/ice bath, and ammonia gas was passed through the stirred solution. The ammonia gas was passed as rapidly as possible without causing material to splash from the flask, or allowing the temperature to rise above 50°C.

It became necessary to replace some solvent (*ca.* 400 cm^3) as an appreciable volume of carbon tetrachloride was lost during the passage of ammonia. Considerable amounts of ammonium chloride, NH_4Cl, coated all parts of the apparatus as the reaction progressed, and several transient colour changes were evident.

After approximately 3 hours, the reaction mixture was golden-poppy in colour. At this point, *ca.* 2 cm^3 of the reaction mixture was withdrawn, using a pipette, and shaken with distilled water (10 cm^3) in a small sample vial. The pH of the aqueous extract was assessed using pH paper and found to be greater than 8. Consequently, the flow of ammonia was ceased.

The reaction mixture was carefully filtered, under vacuum, on a large Buchner funnel. The damp solid material collected was vigorously slurried with de-ionised water (1000 cm^3) for 5-10 minutes and the remaining undissolved solid allowed to dry, in air, for 2 days. When dry, the crude material was cautiously re-crystallised from dry, hot toluene (90°C, *ca.* 250 cm^3) to increase purity and remove sulfur. The orange crystalline product was dried in air, on filter paper, and stored in small portions (*ca.* 2 g) in separate sample vials. Numerous syntheses were found to afford approximately 16 g (*ca.* 67%) of S_4N_4. *Anal.* Calcd. for S_4N_4: N = 30.41%; Found: N = 30.28%. IR: υ 925, 719, 696, 557, 552, 347 cm^{-1}. R_f = 0.19.

6.2. *Synthesis of S_4N_4 via stoichiometric quantisation*

(See also Figure 19)

An ammonia purged 250 cm^3 RBF (A) was back-filled with dry ammonia and sealed using a closed B24 tap adapter (1), attached to a length of Perspex tubing and another B24 tap adapter (2), that was left open. In a separate 250 cm^3 RBF (B), S_2Cl_2 (0.337 cm^3, 4.19 mmol) was dissolved in dried, de-gassed toluene (15 cm^3). Chlorine gas was then bubbled through the solution until a distinct green layer could be seen in the headspace, affording SCl_2. After purging with nitrogen gas, flask (B) was sealed using Tap (2) and the solution frozen following submergence in a liquid nitrogen bath. Flask (B), and the connecting tubing leading to Tap (1), was then placed under vacuum. With the liquid nitrogen trap in place, Tap (1) was opened allowing the ammonia gas to enter flask (B). The liquid nitrogen trap was removed and, as the reaction mixture warmed to ambient, gentle stirring was ensued. The reaction was left for 24 hours, before the mixture was doubly filtered through celite and evaporated to dryness, affording a dark red oil and an orange crystalline solid. The mixture was then dissolved in dichloromethane (20 cm^3) and again filtered through celite. After reducing the volume of the filtrate to *ca.* 5 cm^3, it was passed down a Bio-Beads Gel Permeation Column. The collected fractions were analysed *via* Thin Layer Chromatography (TLC), and slowly allowed to evaporate to dryness. Following manual separation and collection of the orange S_4N_4 crystals, they were pumped on for 24 hours to remove any trace amounts of solvent. Yield = 0.058 g, 34.38%. IR: υ 927, 720, 696, 557, 551, 344 cm^{-1}. $R_f = 0.19$.

6.3. *Synthesis of tetrapropylammonium-ZSM-5, TPA-ZSM-5*

Silicic acid, (4.00 g, 0.0666 moles) sodium hydroxide (1.00 g, 0.0250 moles) and tetrapropylammonium bromide (2.00 g, 7.51 mmol) were added to a 100 cm^3 beaker. With gentle stirring, distilled water (10 cm^3) was then added to the mixture and *n*-propylamine (2.0 cm^3, 0.0243 moles) added dropwise, to the resulting slurry. Separately, aluminium sulfate (0.501 g, 1.46 mmol) was dissolved in distilled water (2.0 cm^3) to which concentrated sulfuric acid (0.10 cm^3, 18.4 M) was added. The aluminium sulfate solution was then slowly added to the silicate solution and the total volume made up to 50 cm^3 with distilled water. After thorough mixing to homogenise the mixture (*ca.* 1 hour), it was transferred between two stainless steel autoclave 15 cm^3 Teflon containers. The Teflon cups were then placed into stainless steel autoclaves (hydrothermal bombs), and crystallisation carried out in a thermostatically controlled oven, at 160°C, for 48 hours.

After allowing the autoclaves to cool to room temperature, the mixture was filtered, under vacuum, and washed with distilled water (4 x 100 cm^3). The product, TPA-ZSM-5, was dried *in vacuo*, and then at 110°C for 16 hours, before being stored in a vacuum desiccator. Yield = 1.485 g. IR: υ 3462 (b), 2985, 2883, 1043 (b), 792, 669, 553 (b), 426 (b) cm^{-1}. Raman: 746, 770, 1038, 1099, 1334, 1451, 2745 (b), 2880, 2933, 2976 cm^{-1}. *Anal.* Calcd. for $(NBu_4)_{1.1}$-$Al_{1.1}Si_{94.9}O_{192}$: C = 2.41%, H = 0.47%, N = 0.23%; Found: C = 2.38%, H = 0.54%, N = 0.20%.

6.4. *Synthesis of sodium-ZSM-5, Na-ZSM-5*

TPA-ZSM-5 (typically *ca.* 0.500 g, 0.0837 mmol) was placed into an alumina crucible and transferred to a thermostatically controlled box furnace, at 500°C, for a minimum of 4 hours. It was ensured that adequate calcination time was allowed to guarantee complete removal of organic content (assessed by the initial onset and complete removal of a brown/grey deposit). The product, Na-ZSM-5, was then allowed to cool to room temperature and stored in a vacuum desiccator. IR: υ 1630, 1400, 1221, 1094, 799, 626, 541, 445 cm^{-1}. IR: υ 1638 (b), 1084 (b), 798, 671, 622, 549 (b), 429 (b) cm^{-1}. Raman: No Raman active moiety. *Anal.* Calcd. for $Na_{1.1}$-$Al_{1.1}Si_{94.9}O_{192}$: C = 0.00%, H = 0.00%, N = 0.00%; Found: C = 0.03%, H = 0.21%, N = 0.06%.

6.5. *Ion-exchange synthesis of protonated ZSM-5, H-ZSM-5*

An ammonium sulfate solution (250 cm^3, 1 mol dm^{-3}) was prepared and added to Na-ZSM-5 (typically *ca.* 0.500 g, 0.0863 mmol), in a beaker, so that 10 cm^3/g of zeolite was obtained. The mixture was stirred for 15 minutes and then filtered under vacuum. The solid material was then transferred back to the beaker and further ammonium sulfate solution (ensuring 10 cm^3/g) was added. Similarly, this mixture was allowed to stir for 15 minutes before being filtered. The solid was then washed with distilled water until the filtrate was free of SO_4^{2-} (*ca.* 150 cm^3), as determined with barium chloride solution. The solid product, ammonium-ZSM-5, NH_4-ZSM-5, was dried at 120°C for 30 minutes before being placed in a thermostatically controlled box furnace, at 500°C, for a minimum of 12 hours. The resulting product, H-ZSM-5, was allowed to cool to room temperature before being stored in a vacuum desiccator. IR: υ 1630, 1400, 1221, 1094, 799, 701, 626, 541, 445 cm^{-1}. Raman: No Raman active moiety. *Anal.* Calcd. for $H_{1.1}$-$Al_{1.1}Si_{94.9}O_{192}$: C = 0.00%, H = 0.02%, N = 0.00%; Found: C = 0.08%, H = 0.19%, N = 0.00%

6.6. Attempts to prepare macroscopic ZSM-5 single crystals

Sodium aluminate (42 wt. % Al_2O_2, 35 wt. % Na_2O, 0.319 g, 3.892 mmol) and sodium hydroxide (0.944 g, 0.0236 moles) were dissolved in distilled water (8 cm^3). Tetrapropylammonium bromide (6.300 g, 0.0237 moles) was added to the solution and stirred until dissolved. Separately, Ludox (40%, 5.7225 g, 4.40 cm^3, 0.0293 moles) was heated to *ca.* 80°C and then added to the solution. The resulting viscous gel was stirred vigorously for 5 mins before being transferred to a Teflon cup. Crystallisation was carried out in a stainless steel autoclave, at 175°C, for 8 days. The autoclave was then cooled at a rate of 0.1°C min^{-1}, the resulting product collected *via* vacuum filtration and washed with distilled water (200 cm^3), before being dried for 16 hours at 110°C. The product adopted a microscopic crystalline form with glimmering facets. Yield = 0.749 g.

6.7. Reactions of ZSM-5 with S_4N_4

6.7.1. Superheated toluene

H-ZSM-5 (0.050 g, 0.00867 mmol) and S_4N_4 (0.011 g, 0.0597 mmol) were both added to a de-gassed Young's tube. Dried, de-gassed toluene (8 cm^3) was then added to the mixture and gentle stirring ensured all the S_4N_4 had dissolved. The Young's tube was sealed and immersed into an oil bath at 140°C for approximately 2 hours. After allowing the reaction mixture to cool, the mother liquor was carefully decanted (using a pipette) and the dark beige/tan coloured precipitate washed with further aliquots of toluene (2 x 5 cm^3), to remove all S_4N_4 residues. The remaining solid was dried, under reduced pressure. IR: υ 3656, 3453 (b), 1637, 1225, 1096 (vb), 798, 707, 622, 547, 451 cm^{-1}. *Anal.* Calcd. for S_4N_4-$H_{1.1}Al_{1.1}Si_{94.9}O_{192}$: C = 0.00%, H = 0.02%, N = 0.94%; Found: C = 4.88%, H = 0.84%, N = 1.39%. Slight variations to the above procedure were also investigated, where temperatures were lowered to 90°C and raised to 160°C, and reaction times decreased to 30 mins and increased to 6 hours.

6.7.2. Solid-state grinding

H-ZSM-5 (0.030 g, 0.00520 mmol) was layered on top of S_4N_4 (0.032 g, 0.174 mmol) and slowly mixed together until homogenised. The mixture was then carefully ground for 5 mins and washed with dried CH_2Cl_2 (*ca.* 30 cm^3), affording a fine, pale orange/yellow powder. No visible change occurred after leaving the mixture in air over prolonged periods of time. Separately, H-ZSM-5 (0.030 g, 0.00520 mmol) was again ground with S_4N_4 (0.030 g, 0.163 mmol), as above, and placed into a Schlenk tube. The mixture was placed under dynamic vacuum for 24 hours before being washed with dried CH_2Cl_2 (*ca.* 30 cm^3). No visible difference between the two samples could be seen. IR: υ 3448 (b), 1629, 1402, 1222, 1097 (vb), 929, 799, 728, 705, 621, 583, 547, 450 cm^{-1}. *Anal.* Calcd. for S_4N_4-$H_{1.1}Al_{1.1}Si_{94.9}O_{192}$: C = 0.00%, H = 0.02%, N = 0.94%; Found: C = 0.33%, H = 0.51%, N = 2.74%.

Another powdered mixture was obtained, as detailed above, and the Schlenk immersed *ca.* one inch into an oil bath, at 90°C. A constant dynamic vacuum was maintained and various reactions allowed to progress for 15 mins, 30 mins, 2 hours, 6 hours and 24 hours. The resulting products at the bottom of the Schlenk were carefully recovered after removing the crystalline S_4N_4 sublimate, deposited above the level of the oil bath, and stored under nitrogen. Reference standards were obtained following identical treatment of both S_4N_4 (0.0504 g, 0.273 mmol) and H-ZSM-5 (0.0499 g, 0.00865 mmol) starting materials.

6.7.3. Frit vapour diffusion

(see also Figure 21)

H-ZSM-5 (0.302 g, 0.0524 mmol) was carefully placed onto the frit of a filter stick (porosity rating 3, frit diameter = 4 cm), ensuring that a thin layer covered its surface. S_4N_4 (0.100 g, 0.543 mmol) was placed directly into the bulb of a Viking adapter and the joint well greased before connecting it to the filter stick. An empty Viking adapter was placed at the top of the filter stick (greased and fitted with a PTFE sleeve to allow ease of release) to create a sealed system. The system was then placed under high dynamic vacuum (*ca.* 0.1 mbar Hg) on a Schlenk line, before being immersed into a temperature regulated oil bath at 90°C.

The glassware was immersed to a depth approximately 1 cm above the surface of the frit. Small aliquots of the sample (the zeolite that had reacted with the S_4N_4) were removed from the system at set time intervals (1, 2, 4, 6, 7, and 12 hours) and stored in small sample vials, under nitrogen. The reaction was left until all the S_4N_4 in the Viking adapter had been spent. This was deemed to have occurred by the time the 12 hour sample was taken.

Anal. Found:	1 hour	C = 1.11%	H = 0.76%	N = 0.72%
	2 hours	C = 0.67%	H = 0.67%	N = 1.36%
	4 hours	C = 1.71%	H = 0.74%	N = 2.38%
	6 hours	C = 0.32%	H = 0.57%	N = 2.48%
	7 hours	C = 0.36%	H = 0.62%	N = 2.73%
	12 hours	C = 0.36%	H = 0.57%	N = 2.32%

In the case of Na-ZSM-5, analogous reactions afforded products similar in appearance to that of the H-ZSM-5 variant.

Anal. Found:	1 hour	C = 0.87%	H = 0.24%	N = 0.58%
	2 hours	C = 0.71%	H = 0.20%	N = 1.12%
	4 hours	C = 1.10%	H = 0.32%	N = 2.15%
	6 hours	C = 0.49%	H = 0.37%	N = 2.48%
	7 hours	C = 0.28%	H = 0.41%	N = 2.72%
	12 hours	C = 0.30%	H = 0.39%	N = 2.33%

When using TPA-ZSM-5, instead of either H-ZSM-5 or Na-ZSM-5, no obvious reaction occurred.

6.8. Attempted synthesis of Se_4N_4 within Na-ZSM-5 channels

Diethylselenite, $(EtO)_2SeO$, (*ca.* 2 cm^3, 0.0108 moles) was placed into a Schlenk tube and dried, de-gassed toluene (10 cm^3) added. To this solution, Na-ZSM-5 (0.0701 g, 0.0121 mmol) was added and the suspension stirred for *ca.* 2 hours, under an atmosphere of nitrogen. NH_3 gas was then carefully bubbled through the mixture at a slow-moderate rate for 2.5 hours and the red precipitate then allowed to settle. The almost colourless mother liquor was removed, *via* pipette, and the remaining solid washed with dried diethyl ether (3 x 5 cm^3). The solid was then washed with de-ionised water (2 x 5 cm^3), followed by methanol (3 x 5 cm^3) and finally diethyl ether (3 x 5 cm^3). The salmon-red coloured product was allowed to dry in air before being analysed under microscope.

6.9. Reactions of carbon nanotubes with S_4N_4

6.9.1. In solution at room temperature

S_4N_4 (0.010 g, 0.0543 mmol) was placed into a large sample vial and dissolved in dried dichloromethane (10 cm^3). A yellow solution resulted. Multi-walled carbon nanotubes (110 – 170 nm diameter, 5 - 9 μm length) (0.011 g, 0.916 mmol) were then added to the solution. The sample vial was sealed and the reaction allowed to stir for 24 hours. The yellow-orange mother liquor was carefully removed with the use of a pipette and the resulting black solid was further washed with dry dichloromethane (3 x 10 cm^3), until the washings ran clear. The product was dried, under reduced pressure. *Anal.* Found: C = 99.08%, H = 0.14%, N = 0.37%. IR: no visible bands.

6.9.2. Superheated dichloromethane

Multi-walled carbon nanotubes (110 – 170 nm diameter, 5 - 9 μ length) (0.010 g, 0.836 mmol) were added to a Young's tube and pumped on for 5 minutes. S_4N_4 (0.012 g, 0.0651 mmol) was dissolved in dried, de-gassed dichloromethane (12 cm^3).

After back-filling the Young's tube with nitrogen, the S_4N_4 solution was added *via* syringe.

It was ensured that at least two inches of headspace remained in the Young's tube, in order to accommodate for pressure changes during the reaction. The Young's tube was then sealed and lowered into an oil bath at 90°C, ensuring that the majority of the solvent was below the level of the oil.

The reaction was left for 4 hours, and then allowed to cool to room temperature. The orange coloured mother liquor was carefully removed with the use of a pipette and the remaining black solid washed with dichloromethane (2 x 10 cm^3) until the filtrate ran clear. The final product was dried under reduced pressure. Yield = 0.0107 g. IR: no visible bands. *Anal.* Found: C = 99.82%, H = 0.10%, N = 0.00%.

A similar reaction, replacing dichloromethane with toluene and using a temperature of 140°C was also conducted, affording similar results.

6.9.3. Frit vapour diffusion

Multi-walled carbon nanotubes (110 – 170 nm diameter, 5 - 9 μ length) (0.0303 g, 2.52 mmol) were placed onto the frit of a small filter stick (porosity rating 3, frit diameter = 2 cm), ensuring that its surface was well covered. S_4N_4 (0.0498 g, 0.270 mmol) was placed into the bulb of a Viking adapter and the joint well greased before connecting it to the filter stick. An inverted Schlenk tube was placed at the top of the filter stick to allow vacuum/nitrogen control.

The system was then placed under high dynamic vacuum, before being immersed into an oil bath at 90°C. The glassware was lowered to a depth approximately 3 cm above the surface of the frit.

The reaction was left until all the S_4N_4 in the Viking adapter had been spent (*ca.* 18 hours). After removing the deposited S_4N_4 sublimate, the black product on the frit surface was tapped out and stored in a large sample vial. IR: υ 801 cm^{-1} (vacuum grease impurity). IR: no visible bands. *Anal.* Found: C = 99.76%, H = 0.19%, N = 0.00%.

6.10. Other S_4N_4 vapour diffusion reactions

6.10.1. With $Li_4Al_4Si_4O_{16}$, Li-A (BW)

Li-A (BW) (0.1002 g, 0.1987 mmol) was layered evenly over the frit of a small filter stick (porosity rating 1, frit diameter = 2 cm). S_4N_4 (0.0499 g, 0.2708 mmol) was placed into the bulb of a Viking adapter and connected to the filter stick. An inverted Schlenk tube was placed at the top of the filter stick to allow vacuum/nitrogen control. The system was placed under high dynamic vacuum, before being immersed to a level *ca.* 3 cm above the frit surface, in an oil bath at 90°C. The reaction was left until all S_4N_4 had been spent (*ca.* 6 hours). The Li-A (BW) did not appear to undergo any visible reaction.

6.10.2. With EGS-SOD

EGS-SOD (as prepared in Section 6.13) (0.100 g, 0.128 mmol) was dried at 105°C for 8 hours before being evenly layered over the frit of a filter stick (porosity rating 1, frit diameter = 2 cm). S_4N_4 (0.051 g, 0.277 mmol) was placed into the bulb of a Viking adapter and connected to the filter stick. Similarly to Section 6.10.1, sublimation of the S_4N_4 occurred over *ca.* 5 hours. No visible reaction appeared to have taken place.

6.10.3. With Linde Type A

Linde Type A (0.104 g, 0.0610 mmol) was dried at 110°C for 16 hours before being evenly layered over the frit of a filter stick (porosity rating 1, frit diameter = 2 cm). S_4N_4 (0.050 g, 0.271 mmol) was placed into the bulb of a Viking adapter and connected to the filter stick. Similarly to Section 6.10.1 and 6.10.2, sublimation of the S_4N_4 occurred over *ca.* 5 hours. The initial white colour of the Linde Type A material changed to a pale yellow/orange during the course of the reaction. The product was washed with dried, de-gassed dichloromethane (2 x 20 cm^3). IR: υ 3441 (b), 1648 (b), 1461, 1236 (b), 1000 (vb), 668, 560 (b), 463, 381 cm^{-1}. *Anal.* Calcd. for S_4N_4-$Na_{12}[(AlO_2)_{12}(SiO_2)_{12}]$: C = 0.00%, H = 0.00%, N = 2.97%; *Anal.* Found: C = 0.14%, H = 0.82%, N = 1.55%.

6.11. Synthesis of disulfur dinitride, S_2N_2, and poly(sulfur nitride), $(SN)_x$

(see also Figure 22)

In a typical experiment, the apparatus (as shown in Figure 22) was charged with S_4N_4 (0.700 g, 3.80 mmol) (A) and silver wool (C) (1.000 g, 9.27 mmol, 99.9+% grade). With Taps 1 and 2 closed, the remainder of the system was evacuated for approximately 2 hours to *ca.* 10^{-5} torr (*via* Tap 3) before the experiment was allowed to commence. The temperature of the heating tape (0.5 m, Isopad S45 tape with an Isopad ML10 variable thermal control unit) surrounding the silver wool was raised to approximately 300°C and left for several minutes before a thermostatically controlled oil bath set at 90 – 100°C was raised to immerse the RBF (A) containing the S_4N_4 (N.B. a minimum gap of approximately 0.5 cm between the top of the oil bath and the start of the heating tape was ensured). A liquid nitrogen trap was then placed around the collection vessel (D), and topped up as required.

The reaction was maintained until no S_4N_4 remained, approximately 3-6 hours. S_2N_2, formed as clear/white crystals within the collection vessel. For solid-state conversion to the polymer, all taps were closed (1-4) and the liquid nitrogen trap removed. The system was left under static vacuum for a minimum of 3 days.

Once the polymerisation was complete, the system was back-filled with nitrogen and dis-assembled to leave only the collection vessel D as a Schlenk-type flask. With a constant stream of nitrogen passing through the system, the blue-black polymer was washed, *in situ*, with dried, de-gassed dichloromethane until all washings ran clear (*ca.* 4 x 100 cm^3). The dichloromethane washings were removed via careful canulation. The resulting pure polymer was carefully dried under reduced pressure, and stored under nitrogen. A typical synthesis yields between 0.3 and 0.4 g of $(SN)_x$. IR: υ 1005 (2 x 501), 687 (SN), 630 (SN), 501 (SN), 281 (SN) cm^{-1}. Raman: 505 (vb), 636 (b), 658 (vb), 815 (b), 869 (vb), 1049 cm^{-1}. *Anal.* Calcd. for $(SN)_x$: N = 30.40%; Found: N = 29.68%.

Time resolved powder XRD experiments were run on pure samples of $(SN)_x$ to monitor its decomposition in air at room temperature, over time. The initial XRD pattern of the sample was obtained and the sample left in the flat plate sample holder and re-run at varying time intervals, spanning 15 days (see Section 5.1.3).

6.12. Reactions of poly(sulfur nitride), $(SN)_x$

6.12.1. With $[Pt(\mu\text{-}Cl)Cl(PPhMe_2)]_2$

$[Pt(\mu\text{-}Cl)Cl(PPhMe_2)]_2$ (0.0684 g, 0.0847 mmol) was added to a back-filled Schlenk, under nitrogen. Dried, de-gassed dichloromethane (10 cm^3) was added to the Schlenk and gentle stirring ensured complete dissolution of the platinum dimer. $(SN)_x$ (0.0078 g, 0.1693 mmol) was then carefully added to the pale yellow solution. The mixture was left stirring for 3 hours, before an *in situ* $^{31}P\{^1H\}$NMR was ascertained: δ -18.21 ($[Pt(\mu\text{-}Cl)Cl(PPhMe_2)]_2$), -19.57 ppm. $^1J(Pt\text{-}P_C)$ 3931 Hz, $^nJ(Pt\text{-}P_X)$ 1469 Hz. After 24 hours, the deep red solution was evaporated down to *ca.* 3 cm^3 and dried, de-gassed diethyl ether (25 cm^3) added. A flocculent pale red/pink precipitate deposited. The product was dried under reduced pressure.

An analogous reaction using $[Pt(\mu\text{-}Cl)Cl(PPhMe_2)]_2$ (0.0428 g, 0.0530 mmol) and $(SN)_x$ (0.0195 g, 0.4233 mmol) was similarly attempted. After filtering through celite, the reaction filtrate was separated *via* a Bio-beads Gel Permeation Column and $^{31}P\{^1H\}$NMR ascertained: δ -21.13 ($Pt(S_2N_2H)Cl(PMe_2Ph)$), -9.24 ppm ($PtCl_2(S_4N_4)PMe_2Ph$). $^1J(Pt\text{-}P)$ 3403 Hz, $^1J(Pt\text{-}P)$ 2117 Hz.

6.12.2. With tris(triphenylphosphine) platinum(0), $Pt(PPh_3)_3$

$(SN)_x$ (0.0041 g, 0.0890 mmol) was transferred to a de-gassed Schlenk tube, under nitrogen. $Pt(PPh_3)_3$ (0.0176 g, 0.0445 mmol) was weighed out as quickly as possible and added to the Schlenk. After evacuation and back-filling of the Schlenk, dried, de-gassed dichloromethane (8 cm^3) was slowly added, affording a yellow solution with insoluble $(SN)_x$. After 4 hours of stirring, the remaining insoluble $(SN)_x$ was removed *via* filtration through celite, under nitrogen, on a filter stick. The dark orange solution was evaporated to *ca.* 2 cm^3 before dried, de-gassed diethyl ether (25 cm^3) was added. The flocculent pale yellow/orange precipitate was removed *via* filtration. $^{31}P\{^1H\}$NMR: δ 43.32 (Ph_3PS), 23.49 - 23.63 (d, P-Pt-S), 11.27-11.42 ppm (d, P-Pt-N). $^1J(Pt-P_S)$ 2827 Hz, $^2J(P_S-P_N)$ 23 Hz, $^1J(Pt-P_N)$ 2995 Hz, $^2J(P_N-P_S)$ 23 Hz.

6.12.3. With $PdCl_2(MeCN)_2$

$(SN)_x$ (0.0044 g, 0.0955 mmol) and $PdCl_2(MeCN)_2$ (0.0250 g, 0.0738 mmol) were added to a large back-filled Schlenk tube, under nitrogen. Dried dichloromethane (10 cm^3) was added and the mixture stirred. The solution darkened in colour and a brown-red insoluble precipitate resulted after approximately 3 hours. IR: υ 3450 (b), 3187, 2988, 2923, 2365, 2334, 2304, 1624 (b), 1402, 1354, 1261, 1190 (b), 1106, 1056, 1021, 879 (b), 806, 690, 599, 536, 446, 410, 362 cm^{-1}.

Another reaction was attempted, this time using a static-type system (not stirred). As above, $(SN)_x$ (0.0046 g, 0.0998 mmol) and $PdCl_2(MeCN)_2$ (0.0250 g, 0.0738 mmol) were added to a large sample vial with dried dichloromethane (10 cm^3). The reaction mixture was left to stand, with no stirring, for 4 days. The dark orange mother liquor was removed *via* pipette, affording a crystalline looking solid at the bottom of the sample vial.

6.12.4. With $PtCl_2(PhCN)_2$

$(SN)_x$ (0.0036 g, 0.0781 mmol) was placed into a large sample vial. To this, $PtCl_2(PhCN)_2$ (0.0369 g, 0.0781 mmol), dissolved in dried dichloromethane (10 cm^3), was added. The suspension was stirred for 24 hours before filtering. The remaining insoluble, amorphous brown solid washed with dichloromethane (5 cm^3) and the dark orange filtrate evaporated to dryness under reduced pressure. IR (filtrate): υ 927, 718, 696, 558, 552, 347 cm^{-1}. $R_f = 0.18$.

6.12.5. With anhydrous $CuCl_2$

$(SN)_x$ (0.0102 g, 0.2214 mmol) and anhydrous $CuCl_2$ (0.0146 g, 0.1085 mmol) were added to a back-filled Schlenk, under nitrogen. Dried, de-gassed acetonitrile (7 cm^3) was added, and the mixture stirred briskly for *ca.* 2 minutes. The reaction was allowed to stand for 7-14 days before the orange coloured mother liquor was removed *via* pipette. Colourless flat sided crystallites were evident under microscopic examination.

6.12.6. With $[Pd_2Cl_6][PPh_4]_2$

$[Pd_2Cl_6][PPh_4]_2$ (0.0500 g, 0.0654 mmol) and $(SN)_x$ (0.0241 g, 0.5231 mmol) were placed into a back-filled Young's tube, under nitrogen, and dried, de-gassed dichloromethane (15 cm^3) added. With stirring, the suspension was superheated to 90°C, for 2.5 hours, with the aid of an oil bath. After cooling to room temperature, the mixture was filtered through celite and the deep red filtrate reduced in volume to *ca.* 3 cm^3. Diethyl ether vapour diffusion and hexane layering crystallisations were attempted and the former afforded red-brown needles were found to not diffract appropriately. IR: υ 3448 (b), 3058, 1585, 1482, 1436, 1336, 1314, 1256, 1185, 1164, 1108, 1043, 996, 854, 756, 722, 690, 615, 525, 454, 367, 318 cm^{-1}.

6.12.7. With $PdCl_2(COD)$

$PdCl_2(COD)$ (0.0483 g, 0.1693 mmol) and $(SN)_x$ (0.0078 g, 0.1693 mmol) were added to a de-gassed Schlenk tube, under nitrogen. Dried, de-gassed dichloromethane (10 cm^3) was added and the mixture stirred for 24 hours. No visible reaction was deemed to have occurred up to this point.

6.12.8. With gaseous ammonia

$(SN)_x$ (*ca.* 0.080 g, 1.736 mmol) was placed along the length of a Schlenk (1), evacuated, and left under a static vacuum. Another Schlenk (2), previously purged and back-filled with NH_3 gas, was connected to the main arm of (1), *via* a small length of vacuum tubing. The tap on (1) was opened to allow the NH_3 gas to enter and react with the $(SN)_x$. After an hour, (1) was isolated, purged with nitrogen, placed under a static vacuum and (2) re-filled with NH_3 gas. The tap on (1) was then opened again. The setup was left for 1 day before being pumped on for 24 hours. IR: υ 1400, 1228, 1050, 1018, 926, 727, 698, 603, 548, 342 cm^{-1}.

6.13. Synthesis of ethylene glycol silica sodalite, EGS-SOD

With stirring, finely powdered NaOH (0.5000 g, 0.0125 moles) was dissolved in ethylene glycol (27.89 cm^3, 0.5000 moles) over 1 hour. Fumed silica, SiO_2, (1.502 g, 0.0250 moles, 0.007 μ particle size) was added to the solution and stirred until homogenised (*ca.* 1 hour). The white slurry was transferred between three Teflon cups and crystallisation of the reaction mixture gel was carried out in stainless steel autoclaves, under autogenous pressure, at 180°C, in a thermostatically controlled oven, for 3 days. Programmed ramped cooling (0.1°C min^{-1}, 180 to 30°C) followed by washing with distilled water (3 x 200 cm^3) and drying, *in vacuo*, proceeded by 16 hours at 110°C, afforded colourless/white microscopic crystals (cubooctahedra). Typical yield = 0.908 g (87%). IR: υ 3448 (b), 2971, 2883, 2363, 2345, 1637 (b), 1523 (b), 1116, 1001, 870, 773, 458, 419 cm^{-1}. Raman: 454, 877, 1036, 1076, 1219, 1461, 2880, 2939, 2969, 3616 (vb) cm^{-1}. *Anal.* Calcd. For $Si_{12}O_{24}{\cdot}C_2H_4(OH)_2$:

C = 2.84%, H = 0.72%, N = 0.00%; Found: C = 2.60%, H = 1.01%, N = 0.00%. ^{29}Si MAS NMR: δ -122.47 ppm (CP-MAS).

6.14. *Synthesis of cubic silica sodalite*

A sample of EGS-SOD (*ca.* 0.200 g, 0.255 mmol) was transferred to an alumina combustion boat, placed into a tube furnace and the entire system purged with nitrogen gas (*ca.* 30 mins). The sample was then steadily heated from room temperature to 680°C, at a rate of 1°C min^{-1}, under the nitrogen atmosphere, and maintained at this temperature for a further 7 days. The sample was then cooled back to room temperature, at a rate of 0.1°C min^{-1}, to afford a grey coloured product. IR: υ 2363, 2345, 1647 (b), 1523 (b), 1103, 1005, 790, 602, 458, 431 cm^{-1}. Raman: No Raman active moieties. *Anal.* Calcd. for $Si_{12}O_{24}$: C = 0.00%, H = 0.00%, N = 0.00%; Found: C = 0.03%, H = 0.02%, N = 0.00 %. ^{29}Si MAS NMR: δ -117.53 ppm (DP-MAS {^{1}H}).

6.15. *Synthesis of rhombohedral silica sodalite*

A sample of carbon coated cubic silica sodalite (*ca.* 0.200 g, 0.277 mmol) was similarly transferred to an alumina combustion boat, placed into a tube furnace and the entire system purged with oxygen gas (*ca.* 30 mins). The sample was steadily heated from room temperature to 680°C, at a rate of 1°C min^{-1}, under the oxygen atmosphere, and maintained at this temperature for a further 7-14 days. The sample was then cooled back to room temperature, at a rate of 0.1°C min^{-1}, to afford a white product. IR: υ 1101, 1004, 791, 612, 601, 459, 428, 359 cm^{-1}. Raman: 187 (b), 264, 367, 416, 466 cm^{-1}. *Anal.* Calcd. for $Si_{12}O_{24}$: C = 0.00%, H = 0.00%, N = 0.00%; Found: C = 0.01%, H = 0.03%, N = 0.00%. ^{29}Si MAS NMR: δ -117.42 ppm (DP-MAS).

6.16. Synthesis of mordenite

With stirring, NaOH (0.760 g, 0.019 moles) was dissolved in distilled water (5 cm^3). Sodium aluminate (0.572 g, 6.978 mmol) was then added and stirred until fully homogenised. Distilled water (25.80 cm^3) and fumed silica (3.928 g, 0.0653 moles, 7 μ particle size) were added and the reaction mixture stirred for 30 minutes before being transferred between three Teflon cups. Crystallisation of the product was carried out in stainless steel autoclaves, under autogenous pressure, at 170°C, in a thermostatically controlled oven for 24 hours. The product was recovered by vacuum filtration and washed with distilled water (2 x 50 cm^3), until the aqueous filtrate had a pH <10. The product was dried in an oven at 110°C for 24 hours. Yield = 1.861 g.

6.17. Synthesis of nepheline

A sample of kaolin (*ca.* 0.400 g, 1.549 mmol) was transferred to an alumina combustion boat and heated in a box furnace at 900°C for 24 hours. Following steady cooling to room temperature, the product, primarily nepheline with some quartz and alumina impurity, was stored in a vacuum desiccator. IR: υ 3508 (b), 2335, 1090, 979 (vb), 685 (b), 651, 469 (b), 436 cm^{-1}.

6.18. Synthesis of silicalite-1

Tetrapropylammonium bromide (0.426 g, 1.600 mmol) and vacuum dried ammonium fluoride, NH_4F, (0.0296 g, 0.799 mmol) were dissolved in distilled water (7.20 cm^3). To this solution, fumed silica (1.201 g, 19.99 mmol, 0.0007 μm particle size) was added and manually stirred with a glass rod. The resulting gel was extremely thick and required further dilution with distilled water (*ca.* 3 cm^3) before complete homogenation was achieved. The mixture was transferred into a Teflon cup and crystallisation carried out in a stainless steel autoclave, at 200°C, for 15 days. After allowing the product to cool, it was collected *via* vacuum filtration, washed with distilled water (*ca.* 200 cm^3) and dried at 110°C for 16 hours. The final product,

$Si_{96}O_{192}[(C_3H_7)_4N]_4F_4$, was stored in a vacuum desiccator. Yield = 1.0255 g (85%). *Anal.* Calcd. for $Si_{96}O_{192}[(C_3H_7)_4N]_4F_4$: C = 8.76%, H = 1.72%, N = 0.85%; Found: C = 7.82%, H = 1.26%, N = 0.70%. IR: υ 3458 (b), 2984, 1637, 1473, 1229, 1110 (vb), 795, 700, 629, 570, 543, 523, 448 cm^{-1}. Removal of the tetrapropylammonium fluoride moiety from the zeolite was readily achieved through calcination of a sample (*ca.* 0.200 g, 0.030 mmol) in a box furnace at 500°C for 24 hours. IR: υ 1229, 1110 (vb), 800, 731, 686, 629, 548, 453 (b) cm^{-1}. Raman: No Raman active moieties. *Anal.* Calcd. for $Si_{96}O_{192}$: C = 0.00%, H = 0.00%, N = 0.00%; Found: C = 0.00%, H = 0.00%, N = 0.01%.

6.19. Synthesis of cancrinite

Sodium hydroxide (14.40 g, 0.360 moles) was dissolved in distilled water (45 cm^3), to which kaolin (0.50 g, 1.937 mmol) and sodium hydrogen carbonate (1.70 g, 0.020 moles) were added. The mixture was stirred until homogenous (*ca.* 10 mins) and transferred between three Teflon cups. Crystallisation was carried out in stainless steel autoclaves, at 200°C, for 48 hours. After allowing the product to cool to room temperature, it was collected *via* vacuum filtration and washed with distilled water (2 x 200 cm^3) to remove residual hydroxide, as tested with pH paper. The product, $Na_{7.6}(Al_6Si_6O_{24})(HCO_3)_{1.2}(CO_3)_{0.2}(H_2O)_{2.2}$, was dried at 110°C for 16 hours. Yield = 0.295 g (51%). *Anal.* Calcd. for $Na_{7.6}(Al_6Si_6O_{24})(HCO_3)_{1.2}(CO_3)_{0.2}(H_2O)_{2.2}$: C = 1.66%, H = 0.34%, N = 0.00%; Found: C = 1.27%, H = 0.45%, N = 0.00%. The carbonate template was readily removed from the product through calcination of the entire sample in a box furnace at 600°C for 24 hours. IR: υ 1442 (b), 1110, 955 (b), 742, 686, 621, 571, 484, 420 cm^{-1}.

6.20. Synthesis of SAPO-5

Boehmite nanoplates (2.3017 g, 0.0384 mmol) were added to an acidified water solution (2.28 cm^3 85 wt. % H_3PO_4 in 13.75 cm^3 H_2O) and stirred until homogenous (*ca.* 20 mins). Separately, Ludox (40 wt. %, 0.77 cm^3, 0.4004 moles) and tri-*n*-propylamine (6.51 cm^3, 0.0345 moles) were mixed and then added to the acidified boehmite mixture. The resulting white gel was stirred for *ca.* 20 mins before being transferred between two Teflon cups. Crystallisation was carried out in stainless steel autoclaves, at 200°C, for 24 hours. After allowing the product to cool to room temperature, it was collected *via* vacuum filtration, washed with distilled water (3 x 100 cm^3) and dried at 120°C for 16 hours. Yield = 0.97 g. IR: υ 3455 (b), 1638, 1224, 1117 (vb), 739, 703, 630, 556, 468 cm^{-1}. The propylamine was removed from the product following ramped calcination of a sample (*ca.* 0.200 g, 0.135 mmol) in a box furnace, from 25 to 600°C over 6 hours, at a rate of 10°C min^{-1}.

6.21. *Synthesis of $AlPO_4$-5*

Aluminium hydroxide, $Al(OH)_3$, (0.463g, 5.936 mmol) was dissolved in distilled water (49.94 cm^3) and triethanolamine (0.55 cm^3, 4.144 mmol) added to the solution. After stirring for *ca.* 10 mins, orthophosphoric acid (0.38 cm^3, 85 wt/%) was added dropwise to the solution to afford a slightly more viscous gel. This gel mixture was transferred between four Teflon cups and crystallisation was carried out in stainless steel autoclaves, at 200°C, for 11 hours. The product was allowed to cool to room temperature before being collected, *via* vacuum filtration, washed with distilled water (*ca.* 200 cm^3) and dried at 110°C for 16 hours. *Anal.* Calcd. for $(C_6H_{15}NO_3)(Al_{12}P_{12}O_{48})$: C = 4.47%, H = 0.94%, N = 0.87%; *Anal.* Found: C = 4.81%, H = 1.28%, N = 0.96%. Removal of the triethanolamine moiety was achieved through calcination of the sample (*ca.* 0.500 g, 0.342 mmol) at 500°C for 16 hours. Yield = 0.456 g. *Anal.* Calcd. for $Al_{12}P_{12}O_{48}$: C = 0.00%, H = 0.00%, N = 0.00%; *Anal.* Found: C = 0.03%, H = 0.00%, N = 0.01%. IR: υ 1127, 730, 711, 624, 494 cm^{-1}. IR: υ 1630 (b), 1129, 1083, 1041, 919 (b), 821 (b), 702, 662, 617, 560, 510, 455 (b) cm^{-1}.

6.22. Synthesis of hydroxysodalite, hydrosodalite and variations thereof

In portions (*ca.* 1 g), sodium hydroxide (9.60 g total, 0.240 moles) was dissolved in distilled water (15 cm^3) to afford a 16 M NaOH solution. To this, kaolin (1.00 g, 3.874 mmol) was added, and stirred until homogenous (*ca.* 30 mins). The cream coloured mixture was transferred between two Teflon cups (with *ca.* 70% filling of the void volume) and crystallisation achieved in stainless steel autoclaves, at 220°C, for 24 hours. The product, sodium-hydroxysodalite, $Na_8[AlSiO_4]_6[OH]_2$, was collected *via* vacuum filtration, washed with distilled water (100 cm^3) and dried at 70°C for 24 hours. A typical synthesis provided *ca.* 0.80 g of product. *Anal.* Calcd. for $Na_8[AlSiO_4]_6[OH]_2{\cdot}2H_20$: H = 0.62%; Found: H = 0.74%.

Sodium-hydroxysodalite (2.00 g, 2.145 mmol) was then refluxed in distilled water (60 cm^3) at 110°C for 48 hours. The product, sodium-hydrosodalite, $Na_6[AlSiO_4]_6{\cdot}8H_2O$, was collected and dried in an analogous manner to hydroxysodalite. Yield = 1.84 g. *Anal.* Calcd. for $Na_6[AlSiO_4]_6{\cdot}6H_2O$: H = 1.26%; Found: H = 1.23%.

Sodium-hydrosodalite (1.50 g, 1.541 mmol) was refluxed in an aqueous $LiNO_3$ solution (2 M, 60 cm^3) at 110°C for 48 hours. The resulting product, $Li_6[AlSiO_4]_6{\cdot}8H_2O$, was collected as previously mentioned and dried at 70°C for 48 hours. Yield = 1.27 g (72%). *Anal.* Calcd. for $Li_6[AlSiO_4]_6{\cdot}6H_2O$: H = 1.40%; Found: H = 1.20%. Subsequent loss of the water molecules was achieved through heating of lithium-hydrosodalite at increased temperatures (> 250°C) to afford lithium sodalite, $Li_6[AlSiO_4]_6$ (Li-SOD). *Anal.* Calcd. for $Li_6[AlSiO_4]_6$: H = 0.00%; Found: H = 0.30%.

6.23. Reactions of disulfur dinitride, S_2N_2

(see also Figure 22)

Freshly generated S_2N_2 was prepared as detailed in Section 6.11 (excluding the storage of the collection vessel at room temperature, under static vacuum for 3 days to induce polymerisation). Following conversion of all the S_4N_4, the oil bath was removed but heating of the silver wool continued for a further 5 mins. Following this time, the temperature of the heating tape was steadily reduced and the tape removed. With Tap 4 closed, a small round-bottomed Schlenk flask/tube (B), containing the reagent(s) of interest, was attached. Tap 1 was then opened, allowing (B) under dynamic vacuum. After removing the liquid nitrogen trap from around D, Tap 3 was then closed, creating a static vacuum throughout the system. Upon warming, the volatile S_2N_2 species was then able to diffuse into flask (B) and react with the compound of interest. Faster reaction time between the compound of interest and the S_2N_2 can be achieved by adding a small vial containing the former to the main flask (D) containing the S_2N_2, and sealing the system under vacuum as before (N.B. though this brings about a faster conversion it proves harder to avoid contamination of the target sample with this technique).

Further apparatus modification, where side-arm (B) and Tap 1 were replaced with a large B34 joint and Viking adaptor, allowed physically larger samples to interact with S_2N_2 vapour.

Numerous different reagents and sample materials/substrates were reacted and exposed to S_2N_2 vapour. These were namely:

- TPA-ZSM-5, Na-ZSM-5, H-ZSM-5
- Kaolinite, Mica, Nepheline, Mordenite, Silicalite-1
- Linde Type A, Cancrinite, NaBr Sodalite, NaCl Sodalite, Nosean
- $AlPO_4$-5, SAPO-5, Linde Type L, Faujasite
- $AlPO_4$-18, Li-A (BW)
- Silica sodalite (EGS-SOD, cubic S-SOD, rhombohedral S-SOD)
- Multi-walled carbon nanotubes

- α-cyclodextrin
- Dibenzo-24-crown-8
- [18]aneO_5S, [18]aneO_4S_2, [14]aneS_4, [12]aneO_3S, [9]aneO_2S
- Deoxyribonucleic acid (DNA), sodium salt
- Inkjet printed artifacts
- Contact surfaces from inkjet printed artifacts
- Fingerprint contaminated surfaces
- Indentation surfaces

In most reactions, each of the reagents were left in side-arm (B) overnight, for a minimum of 16 hours, before being removed and generally stored under nitrogen. S_2N_2 vapour interaction with both inkjet ink residues and fingerprint contaminated surfaces had slightly different protocols (see Section 6.24).

Where necessary, the reaction product was washed with dried, de-gassed dichloromethane (*ca.* 3 x 35 cm^3), until washings ran clear. The product was then pumped on to remove any residual dichloromethane and stored under nitrogen.

In some cases, Powder XRD, IR, Raman and Mass Spectroscopy (MS) data were obtained from the reaction products.

6.24. Disulfur dinitride interaction with inkjet ink and fingerprint contaminated media

For fingerprint detection attempts, all sample surfaces were contaminated with fingermarks from various individuals. For inkjet ink enhancement or ink transfer detection attempts, images/script were printed onto paper (Epson Stylus Photo R26 inkjet printer), allowed to dry and then placed in contact with the appropriate media. Contact between the two surfaces was initially ensured through use of a paperweight. In such cases all contact surfaces and fingerprint contaminated surfaces were visibly image free prior to S_2N_2 exposure.

The target samples (inkjet or fingerprint), on their varying media, were placed in the side-arm (B) of the setup (see Figure 22). Upon warming, and following identical procedures to Section 6.23, the volatile S_2N_2 vapour was then able to diffuse over the sample(s). In the case of fingerprint contaminated samples, a faint red colouration was noted along the ridges of the latent print within just a few minutes of exposure. Further exposure for *ca.* 1-3 hours allowed for full 'development' of the print as dark blue/black polymer. In the case of inkjet traces, a longer exposure time was required, with samples typically left overnight under the vacuum/S_2N_2 atmosphere. In most instances, following sample removal from the apparatus, it was not deemed necessary to remove minor S_4N_4 trace impurities with dichloromethane, prior to storage under nitrogen. Raman: 506 (vb), 639 (b), 691 (vb), 872 (vb), 974, 1064 cm^{-1}.

6.25. Spot testing: disulfur dinitride interaction with pertinent residues

Various substances were spotted onto plain paper with the use of a TLC spotter, in a tabular configuration. Each sample received 6 overlaying spots per segment and all solvents/liquids allowed to dry for 48 hours before introduction and exposure to the S_2N_2 vapour. The concentrations of each sample were as close to a saturated solution as possible.

Each spot test was repeated three times in an identical manner. The samples investigated using this method involved: oleic acid, L-alanine (in water), capric acid (in ethanol), NaCl (in water), ethylene glycol, propan-2-ol, mineral oil, hydroxyl methyl resin (in ethanol), 2-pyrrolidinone, triisopropanolamine and tri(propylene glycol) methyl ether. Subsequent reactions looked at solvent systems including: diethyl ether, ethanol, dichloromethane, toluene, acetone and hexane.

Positive results were determined by preferential blue/black colouration over the spotted test area, with significant background-to-sample clarity. Intense positive results were exhibited by: oleic acid, capric acid, mineral oil, 2-pyrrolidinone and triisopropanolamine. Less intense, but significant, positive results were seen in L-alanine, ethylene glycol, ethanol, dichloromethane and acetone samples.

6.26. Thin Layer Chromatography of inkjet ink and subsequent exposure to S_2N_2 vapour

Neat inkjet ink (from Epson Stylus Photo R26 inkjet printer) was spotted onto silica coated TLC plates (3 drops per plate). After allowing the atmosphere surrounding the TLC plates to obtain a degree of solvent saturation, the TLC plates were run with eluent mixtures of varying composition, until good separation was achieved. The most suitable eluent appeared to be a 5:1:2 ratio of butanol:ethanol:water, respectively. Although some separated spots appeared visible without the use of alternative illumination, short wave UV irradiation revealed 5 main spots: yellow ($R_f = 0.708$), pale yellow ($R_f = 0.662$), orange ($R_f = 0.615$), bright yellow ($R_f = 0.585$) and dark grey ($R_f = 0.115$).

After placing the well resolved TLC plate under vacuum for 24 hours to remove all solvent traces, the plate was exposed to freshly generated S_2N_2 vapour in a similar fashion to that described in Section 6.23. Favourable blue-black colouration was most prominent over the yellow and orange spots, but all spots showed good affinity for $(SN)_x$ growth

6.27. Latent fingerprint development directly from $(SN)_x$

(see also Figure 58)

$(SN)_x$ (*ca.* 0.050 g, 1.085 mmol) was placed into the base of the sublimation apparatus (as shown in Figure 58), under nitrogen. As outlined in Section 6.24, various fingerprint contaminated surfaces were obtained. In each case, the contaminated sample was wrapped around the cold finger, using either rubber band fastenings or adhesive tape, ensuring the majority of the substrate was in direct contact with the cold finger itself. After placing the system under high dynamic vacuum, and filling the cold finger with ice, the sublimation apparatus was lowered into an oil bath at 130-140°C, to a level *ca.* 1 cm below the cold finger. Dependent upon the sample in question, dark blue/black colouration across the fingerprint ridges was typically noticed within several minutes. Extended exposure times were found to often 'overload' the substrate and in fact reduce the clarity of the visualised fingerprint; hence, removal of the $(SN)_x$ enhanced fingerprint sample was judged 'per substrate' (commonly 2-5 mins). Raman (5 second acquisition cycles): 506 (vb), 636 (b), 660 (vb), 815 (b), 873 (vb), 1049 $cm^{-1}cm^{-1}$.

6.28. *Synthesis of Na-ZSM-5-$(SN)_x$*

As detailed in Section 6.23, exposure of Na-ZSM-5 to S_2N_2 vapour was achieved *via* introduction of the former to side-arm (B) (see Figure 22). When Na-ZSM-5 (0.1023 g, 0.0150 mmol) was added to a parafilm coated, pre-weighed sample vial, exposed to S_2N_2 vapour for 16 hours, and re-weighed following removal of the parafilm coating, its mass increased to 0.1347 g (i.e. + 0.0324 g). After washing with dried, de-gassed dichloromethane on a centrifuge (3750 rpm for 4 minutes x 6 runs) until the washings ran clear (*ca.* 50 cm^3), the dark blue/black solid was dried under reduced pressure and the filtrate evaporated to dryness in a pre-weighed flask. The flask was then re-weighed to calculate the mass of S_4N_4 impurity: 0.0207 g. Re-weighing of the blue/black solid product also confirmed a mass loss of 0.0207 g. Thus, the final product, named Na-ZSM-5-$(SN)_x$, experienced a mass increase of 0.0117 g. Yield = 0.1140 g. IR: υ 1630, 1400, 1221, 1094, 799, 701, 626, 541, 445 cm^{-1}. Raman: 1129, 965, 681, 525, 353 cm^{-1}. *Anal.* Found: C = 0.10%, H = 0.74%, N = 4.36%.

6.29. *Reactions of Na-ZSM-5-$(SN)_x$*

6.29.1. Calcination

Na-ZSM-5-$(SN)_x$ (0.0500 g, 0.00734 mmol) was placed in an alumina combustion boat and transferred to a thermostatically controlled box furnace at 500°C. The sample was left for 24 hours before being allowed to cool to ambient temperature. A white solid, Na-ZSM-5, was afforded. Yield = 0.0441 g. IR: υ 1630, 1400, 1221, 1094, 799, 626, 541, 445 cm^{-1}. $Na_{1.1}$-$Al_{1.1}Si_{94.9}O_{192}$: C = 0.00%, H = 0.00%, N = 0.00%; Found: C = 0.03%, H = 0.21%, N = 0.06%; Found: C = 0.00%, H = 0.14%, N = 0.03%.

6.29.2. With $Pt(PPh_3)_3$

Na-ZSM-5-$(SN)_x$ (0.0200 g, 0.00294 mmol) and $Pt(PPh_3)_3$ (0.0050 g, 0.00509 mmol) were added to a de-gassed Schlenk tube and back-filled with nitrogen. Dried, de-gassed dichloromethane (8 cm^3) was added and gentle stirring ensured all the $Pt(PPh_3)_3$ had dissolved. The reaction was left stirring for 4 days before the visibly unchanged blue-black solid was collected following removal of the mother liquor *via* pipette and washing with dichloromethane (2 x 5 cm^3). IR: υ 1630, 1398, 1221, 1092, 799, 701, 626, 540, 445 cm^{-1}. Raman: 1129, 966, 681, 525, 353 cm^{-1}. *Anal.* Assumed for Na-ZSM-5-$(SN)_x$: C = 0.10%, H = 0.74%, N = 4.36%.; Found: C = 0.16%, H = 0.71%, N = 4.22%.

6.29.3. With ammonia solution

Na-ZSM-5-$(SN)_x$ (*ca.* 0.0200 g, 0.00294 mmol) was placed in a large sample vial. With gentle stirring, concentrated ammonia solution (3 cm^3, 5 M) was added dropwise. The suspension was stirred and no obvious decolourisation was evident after *ca.* 1 hour. Following 24 hours, however, a white solid and yellow solution remained. The solid was isolated following vacuum filtration, washed with ammonia solution (2 x 2 cm^3, 5 M) and dried *in vacuo*. IR: υ 1632, 1401, 1221, 1093, 799, 626, 541, 444 cm^{-1}.

6.30. Synthesis of $(SN)_x$-S-SOD

A sample of rhombohedral S-SOD was dried at 150° for 4 days. This sample (*ca.* 0.050 g, 0.069 mmol) was then introduced to the S_2N_2 setup, as detailed in

Section 6.23, to side-arm (B) (see Figure 22). After *ca.* 10 mins, under the S_2N_2/static vacuum atmosphere, the sodalite sample adopted a rusty red/brown colour which, over the next 30 mins, darkened to a dark blue/black. The sample was exposed to the S_2N_2 vapour for *ca.* 16 hours, before being removed and washed with dried, de-gassed dichloromethane (3 x 25 cm^3), until the washings ran clear. The final dark blue/black solid, named $(SN)_x$-S-SOD, was dried under reduced pressure and stored under nitrogen. IR: υ 1103, 1026, 795, 709 (S-N), 610, 455 cm^{-1}. Raman: 466, 504, 639 (b), 861 (vb), 1016 (b), 1201 (b) cm^{-1}. *Anal.* Found: C = 0.03%, H = 0.00%, N = 1.36%.

6.31. Reaction of sublimed $(SN)_x$ with Na-ZSM-5

Dried Na-ZSM-5 (0.100 g, 0.0173 mmol) was layered over the frit of a small filter stick (porosity rating 0, frit diameter = 2 cm), ensuring that its surface was well covered. $(SN)_x$ (0.020 g, 0.434 mmol) was placed into the bulb of a Viking adapter and connected to the bottom of the filter stick. With the aid of an inverted Schlenk tube at the top of the filter stick, the system was placed under high dynamic vacuum for 30 mins, before being immersed into an oil bath at 135°C, to a level *ca.* 3 cm above the surface of the frit. Yellow colouration of the Na-ZSM-5 resulted within several minutes of $(SN)_x$ sublimate exposure, which intensified to a dark yellow/mustard colour over the next 30 mins. No further changes were noted following prolonged exposure times. The product was stored in the dark, under a nitrogen atmosphere. IR: υ 3489 (b), 1632, 1229, 1104 (vb), 798, 705, 627, 586, 548, 448 cm^{-1}. Raman: 414 (b), 489 (b), 707 (b), 915, 957 cm^{-1}. *Anal.* Found: C = 0.07%, H = 0.37%, N = 1.82%.

6.32. Friedel Crafts Acylation using Na-ZSM-5

After drying at 110°C for 24 hours, Na-ZSM-5 (0.202 g, 0.0349 mmol) was placed into a 50 cm^3 RBF and excess acetyl chloride, CH_3COCl, (10 cm^3, 0.1414 moles) was added. The suspension was stirred for 16 hours and then allowed to stand for a further 5 hours. The mixture was then filtered under vacuum and the white solid dried *in vacuo*. The dry product was transferred to another flask and excess, dried toluene (10 cm^3, 0.0941 moles) added. After allowing the mixture to stir for 16 hours, and stand for a further 5 hours, the white solid was collected *via* vacuum filtration, and dried *in vacuo*. IR: υ 1215, 1053 (b), 795, 680, 621, 539, 426 (b) cm^{-1}. *Anal.* Found: C = 1.83%, H = 0.59%, N = 0.00%.

The toluene filtrate was separately reduced to dryness on a Schlenk line, without the use of external heating, and afforded a pale yellow translucent oil. ^{1}H δ(H) ppm ($CDCl_3$): δ 7.45 – 7.65 (q, AA`BB`, di-substituted phenyl ring), 2.36 ppm (toluene CH_3).

A modification to this method was conducted with all reagents *in situ*. Na-ZSM-5 (0.250 g, 0.0432 mmol), acetyl chloride (10 cm^3, 0.1414 moles) and toluene (15.02 cm^3, 0.1414 moles) were added to a 50 cm^3 RBF and left to stir for 24 hours. The solid was collected *via* vacuum filtration and washed with toluene (3 x 5 cm^3). The pale yellow solution was reduced to dryness affording a pale yellow/brown oil that provided no clear NMR spectra.

6.33. Friedel Crafts Acylation using EGS-SOD

Previously dried (110°C, 24 hours) EGS-SOD (0.100 g, 0.1277 mmol) was placed into a 100 cm^3 RBF and acetyl chloride (10 cm^3, 0.1414 moles) added. The suspension was stirred for 16 hours before dried toluene (15.02 cm^3, 0.1414 moles) was added and the mixture stirred for a further 24 hours. Dry Et_2O (*ca.* 15 cm^3) was then added, and after 5 hours stirring the mixture was filtered under vacuum. The resulting white solid was slurried with Et_2O (20 cm^3) and stirred for a further 2 hours. Following filtration, the combined filtrates were reduced to dryness affording a dark brown viscous oil. ^{1}H NMR in $CDCl_3$ provided no distinguishable spectrum: IR (white solid): υ 1052 (b), 867, 777, 606, 433 (b) cm^{-1}. *Anal.* Found: C = 2.57%, H = 1.03%, N = 0.01%.

6.34. Friedel Crafts Acylation using rhombohedral S-SOD

In a similar manner to that described in Section 6.33, rhombohedral S-SOD (0.100 g, 0.1387 mmol) was reacted with acetyl chloride (10 cm^3, 0.1414 moles) and toluene (15.02 cm^3, 0.1414 moles). The mixture was worked up accordingly and the resulting clear/yellow oil isolated. IR (white solid): υ 3489 (b), 1384, 1207, 1107, 1054, 793, 612, 600. 459, 442 cm^{-1}. *Anal.* Found: C = 1.28%, H = 0.17%.

6.35. Hydrogen storage attempts within rhombohedral S-SOD

Rhombohedral S-SOD (*ca.* 0.100 g, 0.1387 mmol) was placed into an aluminium foil boat and dried in an oven at 180°C until a constant mass was obtained using a high precision Sartorius SE2 ultra-microbalance (101.7876 mg). The boat was then placed into hydrogen purged tube furnace and dry H_2 gas allowed to pass through the system for 6 hours. The sample was then removed and quickly re-weighed as before. Yield = 101.7879 mg. *Anal.* Found: H = 0.05%.

An analogous attempt was made using elevated temperatures during H_2 exposure. Rhombohedral S-SOD (99.7451 mg) was dried as before and placed into the hydrogen purged tube furnace. The sample was exposed to dry H_2 gas for 4 hours at 250°C before being re-weighed. Yield = 99.7061 g. *Anal.* Found: H = 0.03%.

6.36. Hydrogen storage attempts within Li-SOD

In a similar method to that described in Section 6.35, Li-SOD was dried and accurately pre-weighed (103.6811 mg). The sample was placed into a hydrogen purged tube furnace and exposed to dry H_2 gas for 6 hours, before quickly being re-weighed. Typical yield = 103.5 – 103.9 mg. *Anal.* Found: H = 0 - 4%. Li-SOD (102.8873 mg) was also placed into a hydrogen purged tube furnace and exposed to dry H_2 gas for 4 hours at 250°C before being re-weighed. Typical yield = 102.1 - 105.3 mg. *Anal.* Found: H = 0 - 17%.

6.37. Hydrogen storage attempts within $(SN)_x$

A sample of $(SN)_x$ (*ca.* 0.050 g, 1.085 mmol) was placed into a Schlenk tube, evacuated and purged with dry H_2 gas for 20 mins. The Schlenk was then sealed and the $(SN)_x$ allowed to stand under the hydrogen atmosphere for 24 hours. No visible sample degradation or colour change was noticeable after this time. The sample was only removed immediately prior to elemental analysis. *Anal.* Found: H = 0.91%.

6.38. Synthesis of $[S_3N_2Cl]Cl$

Ammonium chloride (24.00 g, 0.4487 moles), sulfur monochloride, S_2Cl_2, (23.93 cm^3, 0.2991 moles) and elemental sulfur (4.80 g, 0.1497 moles) were added to a 250 cm^3 RBF. The flask was then fitted with a straight-walled air condensing column, and to this, a calcium chloride drying tube was attached. The reaction mixture was heated, without stirring, using an isomantle, or heating block, and a steady reflux rate was obtained. The reflux height was monitored and the fume cupboard sash height adjusted accordingly so that the vapour condensed *ca.* one third up the condensing column. Additional cooling was used, as required, with the aid of a gentle stream of compressed air blown across the column at a suitable location (*ca.* half way). Dark red-orange/brown crystals began to deposit over the walls of the air condenser after *ca.* 1 hour. The reaction was allowed to reflux for a further 6 hours before the condenser was quickly transferred onto a Schlenk tube, with a stream of nitrogen gas passing through it. The drying tube was removed and the product, $[S_3N_2Cl]Cl$, was scraped from the walls of the condenser and collected in the Schlenk below. The dark red crystalline product was pumped on for *ca.* 1 hour to remove any HCl, S_2Cl_2 and SCl_2 impurities, and stored under nitrogen. A typical synthesis afforded *ca.* 8-10 g (40%) of product. IR (nujol mull): υ 1014 (SN), 937 (SN), 716 (SN), 589 (δSN), 459 (SCl), 407 (SS), 384 (δSN), 348 (δSN), 281 (δSN) cm^{-1}. Melting point expected: 90-92°C. Found: 89-91°C.

6.39. Synthesis of (NSCl)$_3$

After freshly preparing a crop of [S_3N_2Cl]Cl (as detailed in Section 6.38), the air condenser, containing the former, was quickly transferred onto a Schlenk tube, with nitrogen gas passing through the entire system. Following removal of the drying tube, the condenser outlet was connected to a scrubbing unit (Dreschel bottle filled with *ca.* 150 cm^3 of water) *via* a length of tubing. With the aid of a T-piece, the flow of nitrogen gas was ceased, and chlorine gas allowed to pass through the system. Rapid reaction between Cl_2 and [S_3N_2Cl]Cl resulted, and the SCl_2 side product that formed *in situ*, allowed the product to be washed down the walls of the air condenser, into the Schlenk below. Cl_2 flow was stopped after *ca.* 10 mins when all the [S_3N_2Cl]Cl was deemed to have reacted. SCl_2 was removed following extensive pumping (*ca.* 45 mins), leaving the yellow (NSCl)$_3$ product, which was stored under nitrogen, ensuring all joints were heavily greased. Typical Yield = 4 g (59%). Raman: 318, 336, 374, 432, 485, 620 (b), 703, 707, 726, 937 (b), 1011 cm^{-1}.

6.40. Introduction of NSCl monomer to zeolite systems

(see also Figure 99)

Using the custom-made glassware, as shown in Figure 99, and with nitrogen gas passing through the Schlenk flask (A), (NSCl)$_3$ (*ca.* 0.100 g, 0.4089 mmol) was added. Separately, the adapted stopper/sample dish (B) was loaded with the dried (24 hours, 180°C) target zeolite (*ca.* 0.030 g); ensuring a thin, even distribution. With nitrogen flow through the flask (A), the stopper/sample dish (B) was inserted and a secure seal ensured. The entire system was then placed under dynamic vacuum for *ca.* 5 mins, before Tap 1 was closed (affording a static vacuum sealed system). The Schlenk RBF was then immersed, to the level of the sample dish, into an oil bath at 80-90°C.

The zeolites introduced to the resulting NSCl monomer were treated appropriately, based on initial observations:

i.) Na-ZSM-5: Pale yellow colour after < 5 mins. Proceeded to dark green and finally dark blue/black after *ca.* 1 hour. No further colour change following prolonged exposure. IR: υ 3148 (b), 3051, 1635, 1408, 1223, 1092 (b), 799, 702, 621, 544, 444 cm^{-1}. Raman: 382 (vb), 423, 470 (b), 526, 663 (b), 717 (b), 916 (b), 943, 1001 (vb) cm^{-1}. *Anal.* Found: H = 0.74%, N = 3.81%.

ii.) TPA-ZSM-5: No colour change.

iii.) Faujasite: No colour change.

iv.) $AlPO_4$-18: Pale yellow colour after *ca.* 10 mins. No further colour change following prolonged exposure. IR: υ 3387 (b), 3181 (b), 1630, 1402, 1109 (vb), 702, 635, 480 (b) cm^{-1}.

v.) TEA-$AlPO_4$-18: No colour change.

vi.) Silicalite-1: Pale brown-red colour after < 5 mins. Progressed to green-yellow after *ca.* 1 hour. No further colour change following prolonged exposure. IR: υ 3453 (b) (N-H), 3136, 2334, 1406, 1258 (HNSO), 1229, 1112, 1052, 959, 797, 702, 630, 537, 457 cm^{-1}. Raman (sealed capillary method, 10 second acquisition cycles): 550 (b), 660 (b), 792 (b), 920, 1051 (b), 1238 (vb) cm^{-1}. *Anal.* Found: H = 0.49%, N = 2.22%.

vii.) TPAF-Silicalite-1: No colour change.

All coloured products exhibited varying degrees of air sensitivity and were therefore stored under nitrogen. IR sample preparation of (i) was conducted quickly in air, or under a nitrogen atmosphere, using a glove bag. IR sample preparation of (vi) required stringent anaerobic and moisture free conditions, demanding extensive drying of all apparatus and the use of a newly re-generated glove box (see Section 5.3.2).

6.41. In situ, static vacuum interaction of $(NSCl)_3$ with Na-ZSM-5

With the apparatus setup as described in Section 6.40, and dry Na-ZSM-5 (*ca.* 0.030 g, 0.005 mmol) in the stopper/sample dish well, the system was simply left under static vacuum (no heating). Pale yellow colouration of the Na-ZSM-5 became evident after *ca.* 45 mins. The sample darkened to dark green following *ca.* 48 hours and eventually turned, and remained, dark blue/black after 1 week. IR: 3146 (b), 1631, 1407, 1222, 1090 (b), 798, 700, 621, 543, 445 cm^{-1}. Raman (10 second acquisition cycles): 377 (b), 661 (b), 712 (b), 914 (b), 1003 (b) cm^{-1}.

6.42. *Solid state interaction of $(NSCl)_3$ with Na-ZSM-5*

Under a nitrogen atmosphere (glove bag), dry Na-ZSM-5 (0.0407 g, 0.00703 mmol) and $(NSCl)_3$ (*ca.* 0.100 g, 0.409 mmol) were placed into an agate pestle and mortar. The two compounds were carefully ground together (10 mins), affording a homogenous pale blue/black powder. IR: υ 3169 (b), 3046 (b), 2007, 1764 (b), 1408, 1343, 1225, 1098 (vb), 929, 797, 701, 624, 583, 543, 504, 447 cm^{-1}. Raman (10 second acquisition cycles): 431 (vb), 524 (vb), 660 (vb), 798 (vb), 900 (vb) cm^{-1}.

6.43. *Exposure of fingerprint contaminated surfaces to NSCl*

Under nitrogen, $(NSCl)_3$ (*ca.* 0.050 g, 0.2044 mmol) was placed into a Schlenk tube. Both paper and aluminium foil fingerprint contaminated substrates were then hung, in turn, from the roof of the sealed Schlenk (typically, a length of wire attached to the sample and stuck to the base of the stopper with adhesive tape or putty) and the system placed under static vacuum. The Schlenk was then lowered into an oil bath at 80-90°C and the liberated NSCl vapour allowed to interact with the substrate. Both samples provided visibly enhanced fingerprints: blue/black in colour in the case of aluminium (Raman: 387, 472, 502, 558, 643 (b), 690 (b), 844 (vb), 1036 (vb) cm^{-1}), and tan brown in colour in the case of paper (Raman: 503, 568 (b), 623, 810 (vb), 916 (b), 1001, 1035, 1160, 1193, 1209, 1252, 1303, 1417, 1422, 1599 cm^{-1}).

6.44. *Synthesis of poly(thiazyl bromide), $(SNBr_{0.4})_x$*

In a de-gassed 100 cm^3 Schlenk RBF, under nitrogen, $(NSCl)_3$ (1.340 g, 5.479 mmol) was dissolved in dry, de-gassed dichloromethane (35 cm^3). The solution was cooled to *ca.* -60°C with the aid of an acetone/dry ice bath, and trimethylsilyl bromide,

Me_3SiBr, (2.20 cm^3, 0.01670 moles) added dropwise. The mixture was stirred for 15 mins before being allowed to warm to room temperature. The resulting dark blue/black powder was collected *via* filtration under nitrogen, on a filter stick, and washed *in situ* with dichloromethane (2 x 10 cm^3). The product, $(SNBr_{0.4})_x$, was dried under reduced pressure and stored under a nitrogen atmosphere. Yield = 0.38 g (89%). IR (nujol mull): υ 1401 (2 x 701), 1096 (463 + 635), 1019 (SN), 843 (SN), 701 (SN), 635 (SN), 463 (SN_2) cm^{-1}. *Anal.* Calcd. for $(SNBr_{0.4})_x$: N = 17.95%; Found: N = 17.27%.

6.45. *Solid-state reactions of $(SNBr_{0.4})_x$*

6.45.1. Grinding

In a glove box, $(SNBr_{0.4})_x$ (*ca.* 0.150 g, 1.922 mmol) was placed into an agate pestle and mortar, and carefully ground for 2 mins, separately in each case, with various different compounds (ensuring a ratio of 1 $(SNBr_{0.4})_x$: 0.4 reactant):

i.) $(SNBr_{0.4})_x$ + Li[TCNQ]: IR (nujol mull): υ 1400, 1320, 1181, 1104, 861, 824, 622, 474 cm^{-1}.
ii.) $(SNBr_{0.4})_x$ + Na[BF_4]: IR (nujol mull): υ 1401, 1300, 1084, 1035, 771, 621, 522, 474, 404 cm^{-1}.
iii.) $(SNBr_{0.4})_x$ + Na[BPh_4]: IR (nujol mull): υ 1479, 1427, 1391, 1311, 1255, 1184, 1152, 1129, 1068, 1028, 996, 947, 919, 868, 852, 743, 714, 626, 602, 488, 464, 405 cm^{-1}.
iv.) $(SNBr_{0.4})_x$ + NaI: IR (nujol mull): υ 1460, 1455, 1376, 1104, 844, 722, 620, 467 cm^{-1}.

All resulting samples remained dark blue/black in colour, and were stored under nitrogen, often resulting in bromine and/or iodine vapour liberation, in the case of i-iii and iv, respectively.

6.45.2. Suspension

In a similar manner to Section 6.45.1, and again under nitrogen, $(SNBr_{0.4})_x$ (*ca.* 0.150 g, 1.922 mmol) and dried, de-gassed dichloromethane (10 cm^3) were added to four Schlenk tubes. The same reactants (i-iv) were then added, individually, to one of the suspension mixtures and stirred for 24 hours. Each mixture was filtered, under vacuum, resulting in a dark blue/black powder and orange filtrate. The solids were dried, *in vacuo*, stored under nitrogen, and the filtrate allowed to evaporate to dryness. IR (filtrate): υ 925, 718, 696, 556, 552, 347 cm^{-1}. $R_f = 0.18$: shows good similarity for S_4N_4. IR analysis of each solid sample had good absorption band similarity for that recorded in Section 6.45.1. No obvious vapour liberation was observed during short term sample storage (< 3 days), however prolonged storage did afford bromine/iodine vapour residues.

6.46. Novel synthesis of powdered poly(sulfur nitride), 'ppsn'

To a dry 250 cm^3 Schlenk RBF, with a steady flow of nitrogen gas passing through it, liquid ammonia (*ca.* 10 cm^3, 0.4005 moles) was added. In small portions, freshly prepared $[S_3N_2Cl]Cl$ (1.50 g total, 3 x 0.50 g portions, 7.6878 mmol; weighed out in a glove box) was added, inducing a vigorous reaction, with effervescence. The RBF was fitted with a paraffin gas bubbler to monitor the flow of the evaporating ammonia. The reaction was stirred violently, ensuring the walls of the flask were well coated with the dark brown resulting mixture. A heat gun was used intermittently to gently warm the mixture and help remove any remaining traces of ammonia.

Once the ammonia had been removed, an orange coloured precipitate remained. The solid was carefully agitated using a glass rod, or PTFE coated spatula, to break up any large solid masses that had formed. Following removal of the paraffin bubbler and fitting of a glass stopper, the RBF was placed under high dynamic vacuum for 2-3 hours. After *ca.* 10 mins, the initial orange colour of the solid began to darken and a black product, with a lustrous shimmer under reflected light, resulted after *ca.* 90 mins. Extended pumping ensured the entire sample had been converted. The product was stored under a nitrogen atmosphere. A typical synthesis afforded *ca.* 0.600 g of crude product. IR (nujol mull): υ 1401, 1220, 1015, 928, 696, 626, 508, 289 cm^{-1}.

The crude product was washed with dry dichloromethane (*ca.* 20 cm^3), affording an orange/red filtrate that was allowed to evaporate to dryness, in air, providing an orange crystalline solid. IR: υ 927, 719, 695, 552, 347 cm^{-1}. $R_f = 0.19$. The remaining black solid was then washed quickly with distilled water (*ca.* 20 cm^3) and, again, the colourless filtrate reduced to dryness affording a white residue. IR: υ 3144, 2006, 1741, 1400, 1084, 710 cm^{-1}.

Further washing of the black product with an array of solvents (CH_2Cl_2, acetone, EtOH, MeCN, toluene, THF and Et_2O) resulted in the removal of more orange-red impurity (and decreased the impurity content as shown by IR; *vide supra*), but colourless washings were never obtained. Further purification required soxhlet extraction with dichloromethane for 16 hours: the black powder was transferred to a cellulose soxhlet extraction thimble and dry dichloromethane (*ca.* 150 cm^3) added to a 250 cm^3 RBF. The soxhlet apparatus was placed under a constant nitrogen atmosphere, using a nitrogen gas inlet/outlet bubbler, and the solvent refluxed with the aid of an isomantle. Orange residues leached from the extraction thimble over *ca.* 3 hours, before becoming paler in colour and eventually colourless after *ca.* 16 hours. The 'pure' black product was dried under reduced pressure and stored under nitrogen. IR (nujol mull): υ 1013, 801, 719, 693, 618, 511, 290 cm^{-1}. *Anal.* Calcd. for $(SN)_x$: H = 0.00%, N = 30.40%; Found: H = 1.27%, N = 27.15%.

6.47. Reaction of ppsn with ammonia gas

A sample of freshly prepared ppsn (*ca.* 0.100 g, 2.1705 mmol) was placed into a Schlenk tube, under nitrogen. The Schlenk was then slowly flushed with ammonia gas, and sealed. The black ppsn material began to adopt a tarnished appearance, with a light green surface colouration. The Schlenk was then placed under dynamic vacuum for *ca.* 20 mins and the initial black colour of the powder re-presented itself.

Repeat exposure of ppsn to NH_3 gas (< 5 times) gave similar visible changes, and pumping on the product afforded a colour change back to that indicative of the starting ppsn material. Extended NH_3/vacuum cycles resulted in irreversible discolouration, and the introduction of orange S_4N_4 deposits. IR (nujol mull): υ 1014, 925, 802, 719, 693, 618, 552, 511, 290 cm^{-1}.

6.48. *Reactions of ppsn with transition metal complexes*

Reactions between ppsn with $[Pt(\mu\text{-}Cl)Cl(PPhMe_2)]_2$, $Pt(PPh_3)_3$, $PtCl_2(PhCN)_2$, $PdCl_2(COD)$ and PPh_3 were conducted in an analogous manner to those described in Section 6.12. In most cases, reactions underwent identical colour changes and provided the same products.

6.49. *Four-point collinear conductivity probe analysis*

Both 'home-made' and commercially purchased four-point collinear conductivity probes were used to investigate conductivity/resistivity properties associated with $(SN)_x$ and its derivatives. The home-made device required the use of a potentiostat, whereas the Jandel Universal Four-Point Conductivity probe was fitted with a HM20 closed circuit resistivity test unit.

Samples that required conductivity analysis were prepared by placing *ca.* 0.080 g of sample into a die and pressing the material to obtain thin pellets/wafers. Where applicable, problems associated with pellet/wafer fragility were negated with the addition of a suitable binder, typically PVA (*ca.* 20-50 mg). Although various pressing forces were investigated, pellets were usually obtained with the application of 8 tons of pressure, for 3 mins. Pellet thickness was measured using a micrometer, and a range between 200 and 350 μm was common. Each pellet was then placed onto either the 'home-made', or Jandel, conductivity probe stages and the contact pins lowered onto the sample surface, ensuring a good contact was present. Surface level direct current conductivity measurements were obtained in a similar manner for each probe apparatus. The applied current was varied accordingly (typically *ca.* 1 μA to

5 μA), so as to induce a potential (voltage) within the scale of the detector. Samples that were tested for conductivity properties included ppsn, $(SNBr_{0.4})_x$ and zeolite matrices incorporating $(SN)_x$.

6.50. Attempted synthesis of $(SeN)_x$

With a steady flow of nitrogen gas passing through a 250 cm^3 Schlenk RBF, liquid ammonia (*ca.* 10 cm^3, 0.4005 moles) was added. In small portions, freshly prepared $[Se_3N_2Cl]Cl$ (*ca.* 1.00 g total, 2 x 0.50 g portions, 2.978 mmol; weighed out in a glove box) was added, inducing a vigorous reaction, with effervescence. The RBF was fitted with a paraffin gas bubbler to monitor the flow of the evaporating ammonia. The reaction was stirred violently, ensuring the walls of the flask were well coated with the dark red resulting mixture. A heat gun was used intermittently to gently warm the mixture and help remove any remaining traces of ammonia.

Once the ammonia had been removed, a dark red coloured precipitate remained, that was not agitated or broken up in any way. Following removal of the paraffin bubbler and fitting of a glass stopper, the RBF was placed under high dynamic vacuum for 2 hours. No colour change was evident. IR (nujol mull): υ 797, 782, 574, 533, 424, 310, 272 cm^{-1}.

7. Conclusion

The work undertaken during the course of this research has encompassed several novel areas of interest and left a number of potential avenues open for further exploration and development. An initial focus into the synthesis of polythiazyl resulted in both a new preparative route to the polymer, through reaction of $[S_3N_2Cl]Cl$ with liquid ammonia, followed by extensive vacuum treatment, as well as the design and fabrication of apparatus that safely and efficiently permitted the generation of the reactive S_2N_2 intermediate, and in turn its polymerisation to $(SN)_x$, based upon conventional methodoligies. Adaptation of the initial apparatus enabled complete conversion of the S_4N_4 starting material to be achieved in less than 4 hours, compared to 8-12 hours as originally required for the reaction. Time-resolved single crystal XRD studies provided some noteworthy evidence in support of conventional mechanistic theories of the polymerisation process. The apparent movement away from a true planar geometry, and twisting of the S-N-S bonds in adjacent S_2N_2 molecules, was visually able to provide support for the likely diradical transition state predicted during phase change.

Following the synthesis of a wide array of microporous materials, many different in both structural composition (zeolites, clathrates, lamellar solids) and pore/void diameter (*ca.* 3-20 Å), the plausible occlusion of S_2N_2 within the highly ordered vacant porous sites was readily facilitated. Successful incorporation of the S_2N_2 moiety was typically proceeded with rapid polymerisation of the former to $(SN)_x$, owing primarily to increased molecular interactions due to the spatial contrainsts within the porous system. $(SN)_x$ occlusion was found to be most viable in materials that possess a bottleneck pore/void diameter of *ca.* 4-6 Å, as a consequence of the molecular dimensions pertaining to S_2N_2. The inclusion of the conductive polythiazyl chains within such structures has proven to be the first true example of $(SN)_x$ functionalisation and a relevant example of a so-called insulated molecular wire type structure. Sublimation of $(SN)_x$ through an Na-ZSM-5 layer, however, did not afford an identical product to that seen directly from S_2N_2 exposure. Instead, a mustard yellow photochromic material resulted, which readily underwent a reversible yellow-to-red colour change and remained stable over extended storage periods.

The inclusion of other thiazyl compounds within similar frameworks was also explored, and some success at incorporating both S_4N_4 and reactive thiazyl chloride units into such hosts has been presented. Despite conclusive product identification, it appears plausible that the highly elusive NSCl unit can potentially be isolated within the pores of the silicalite-1 zeolite.

The provision of a true clathrate system, the sodalite family of minerals for example, for host-guest interaction studies with $S_2N_2/(SN)_x$ was also highly sought after. The synthesis of a template-free sodalite, however, had hitherto remained experimentally impractical because of the structure-directing role served by the guest molecules occluded within the β-cages of the sodalite framework. It was discovered, however, that through careful thermal treatment of one of the silica sodalite materials, namely EGS-SOD, the templating agent could be readily removed, thereby resulting in one of two types of pure, template-free silica sodalite, dependant upon the treatment method used. The formation of a template-free cubic S-SOD is achieved under stringent anaerobic conditions (nitrogen) and a novel rhombohedral phase can be isolated following subsequent thermal treatment under an oxygen atmosphere. Exposure of the latter to S_2N_2 indeed resulted in occlusion of $(SN)_x$, as determined *via* various spectroscopic methods. The potential for these new template-free silica sodalites to act as ideal storage materials for small molecular species is a fundamental development that should be addressed in the near future. The theoretical capacity of S-SOD to actively absorb materials such as H_2, CO_2, H_2O and NH_3 should provide a meaningful reference point for prospective solid-state storage research.

Since its discovery in the early twentieth century, and following extensive research several decades later, $(SN)_x$ was never really able to live up to its expectations in terms of functional applications. It has been found however, that aside from the diverse inclusion reactions already discussed, the polymerisation process of S_2N_2 to $(SN)_x$ can be 'catalysed' and enhanced *via* the presence of both latent fingerprint deposits and inkjet-ink residues. On the former front, the secretions from the ridge skin of the fingers and palms have shown extraordinary sensitivity towards preferential $(SN)_x$ growth, and process optimisation has since enabled fingerprints to be visualised, enhanced and photographed from a myriad of substrate media. Perhaps the most significant surface types to have proven successful include fabrics, discharged firearm casings and aqueous/organic wetted samples. Moreover, the direct sublimation of $(SN)_x$ onto previously cooled fingerprint contaminated surfaces has provided comparative results, with arguably a more facile, user-friendly oriented approach, coupled with the potential for both process scale-up and portabilisation.

In addition, the apparent nucleation and epitaxial film growth of $(SN)_x$ over specific contaminated areas (fingerprints) prompted the investigation of its affinity towards other surfaces that were impregnated with another 'contaminant'. Attention duly focussed on the interaction of the nitride with inkjet ink, and it was revealed that preferential polymer growth occurred directly over the ink-printed areas of documents/text. Further studies indicated that two main volatile components of the inkjet ink were readily able to diffuse onto/through additional contact sheets and these invisible traces were noticeably enhanced by $(SN)_x$ following S_2N_2 vapour exposure. Similar observations were not noted, however, upon direct $(SN)_x$ sublimation onto ink-transfer surfaces, though enhancement of faint ink-printed text/images was found to be plausible using this route.

The synthesis of both 'ppsn' and crystalline $(SN)_x$ also enabled reaction chemistry of the polymer to be investigated for the first time. Co-ordination reactions with various transition metal complexes were attempted and despite forming products that are similar in nature to analogous S_4N_4 reactions, the reaction pathway does not appear to follow the same route. Evidence to support the decomposition of $(SN)_x$ to S_4N_4, and subsequent reaction with the target complex, is not conclusive as many reactions were unsuccessful directly from the polymer. Direct polymer addition to a metal centre has so far been practically unachievable, with main reaction products favouring co-ordination of the S_2N_2 ligand moiety. The reaction between $(SN)_x$ and NH_3 gas provided good evidence of reversibility, following vacuum treatment, and the apparent formation of an ammonia type adduct to the thiazyl backbone. Extended NH_3 exposure, however, has been shown to induce polymer decomposition to S_4N_4.

8. References

1 W. Gregory, *J. Pharm. Chim.*, 1835, **21**, 315-318.

2 D. Clark, *J. Chem. Soc.*, 1952, 1615-1620.

3 L. Chia-Si and J. Donohue, *J. Am. Chem. Soc.*, 1944, **66**, 818-827.

4 M. M. Labes, P. Love and L. F. Nichols, *Chem. Rev.*, 1979, **79**, 1-15.

5 M. Villena-Blanco and W. L. Jolly, *Inorg. Synth.*, 1967, **9**, 98-102.

6 W. L. Jolly and M. Becke-Goehring, *Inorg. Chem.*, 1961, 76-78.

7 A. Maaninen, J. Siivari, R. S. Laitinen and T. Chivers, *Inorg. Syn.*, 2002, **33**, 196-199.

8 D. K. Padma, V. Subrahmanyabhat and A. R. Vansudevamurthy, *Inorg. Chim. Acta*, 1976, **20**, L53-L54.

9 M. Becke-Goehring, *Inorg. Syn.*, 1960, **6**, 123-126.

10 F. P. Burt, *J. Chem. Soc., Trans*, 1910, **97**, 1171-1174.

11 N. Baumann, B. Heibel, J. Jouanne, H. Keller-Rudek and A. Kubny, in *Gmelin Handbook of Inorganic Chemistry - Sulfur-Nitrogen Compounds - Part 2*, ed. K. C. Buschbeck, H. Bergmann, B. Heibel, H. Katscher, R. Keim, G. Kirschstein, D. Koschel, U. Kruerke, H. K. Kugler, E. Schleitzer-Rust, A. Slawisch, B. V. Tschirschnitz-Geibler and R. Warncke, Springer-Verlag, Berlin, 1985, 127-248.

12 T. Chivers, *A Guide to Chalcogen-Nitrogen Chemistry*, World Scientific Publishing Co., Hackensack NJ, 2004.

13 R. L. Patton and W. L. Jolly, *Inorg. Chem.*, 1969, **8**, 1389-1390.

14 R. L. Patton and W. L. Jolly, *Inorg. Chem.*, 1969, **8**, 1392-1393.

15 K. Dehnicke and U. Muller, *Transit. Metal Chem.*, 1985, **10**, 361-368.

16 J. D. Woollins, *Polyhedron*, 1987, **6**, 939-941.

17 J. M. Jolliffe, P. F. Kelly and J. D. Woollins, *J. Chem. Soc., Dalton Trans.*, 1989, 2179-2182.

18 R. Jones, P. F. Kelly, D. J. Williams and J. D. Woollins, *Polyhedron*, 1985, **4**, 1947-1950.

19 V. C. Ginn, P. F. Kelly and J. D. Woollins, *J. Chem. Soc., Dalton Trans*, 1992, **13**, 2129-2130.

20 H. Folkerts, B. Neumuller and K. Dehnicke, *Z. Anorg. Allg. Chem.*, 1994, **620**, 1011-1015.

21 J. Siivari, T. Chivers and R. S. Laitinen, *Inorg. Chem.*, 1993, **32**, 1519-1520.

22 T. M. Klapotke, in *The Chemistry of Inorganic Ring Systems*, ed. Elsevier, Elsevier, Europe, 1992, 409-427.

23 P. F. Kelly and A. M. Z. Slawin, *J. Chem. Soc., Dalton Trans,* 1996, 4029-4030.

24 P. F. Kelly and A. M. Z. Slawin, *Angew. Chem. Int. Ed.,* 1995, **34,** 1758-1759.

25 H. M. Tuononen, R. Suontamo, J. Valkonen, R. S. Laitinen and T. Chiver, *J. Phys. Chem.,* 2005, **109**, 6309-6317.

26 S. M. Aucott, D. Drennan, S. L. M. James, P. F. Kelly and A. M. Z. Slawin, *Chem. Commun.,* 2007, 3054-3056.

27 G. B. Street and R. L. Greene, *IBM J. Res. Develop.,* 1977, **21**, 99-110.

28 M. J. Cohen, A. F. Garito, A. J. Heeger, A. G. Macdiarmid, C. M. Mikulski, M. S. Saran and J. Kleppinger, *J. Am. Chem. Soc.,* 1976, **98**, 3844-3848.

29 C. M. Mikulski, P. J. Russo, M. S. Saran, A. G. Macdiarmid, A. F. Garito and A. J. Heeger, *J. Am. Chem. Soc.,* 1975, **97**, 6358-6363.

30 R. C. Mawhinney and J. D. Goddard, *J. Mol. Struc. Theochem,* 2008, **856**, 16-29.

31 R. C. Mawhinney and J. D. Goddard, *Inorg. Chem.,* 2003, **42**, 6323-6337.

32 F. A. Kennett, G. K. Maclean, J. Passmore and M. N. S. Rao, *J. Chem. Soc. Dalton,* 1982, 851-857.

33 R. L. Greene, G. B. Street and L. J. Suter, *Phys. Rev. Lett.,* 1975, **34,** 577-579.

34 J. Kondo, *Phys. Rev.,* 1968, **169**, 437-440.

35 J. Kondo, *Prog. Theor. Phys.,* 1964, **32,** 37-49.

36 V. V. Walatka, M. M. Labes and J. H. Perlstei, *Phys. Rev. Lett.,* 1973, **31**, 1139-1142.

37 C. K. Chiang, M. J. Cohen, A. F. Garito, A. J. Heeger, C. M. Mikulski and A. G. MacDiarmid, *Solid State Commun.,* 1976, **18**, 1451-1455.

38 K. Kaneto, M. Yamamoto, K. Yoshino and Y. Inuishi, *J. Phys. Soc. Jpn,* 1979, **47**, 167-175.

39 A. J. Banister and I. B. Gorrell, *Adv. Mater.,* 1998, **10**, 1415-1429.

40 W. H. G. Muller, F. Baumann, G. Dammer and L. Pintschovious, *Solid State Commun.*, 1978, **25**, 119-122.

41 R. H. Friend, D. Jerome, S. Rehmatullah and A. D. Yoffe, *J. Phys. C Solid State,* 1977, **10**, 1001-1012.

42 K. J. Dunn, F. P. Bundy and L. V. Interrante, *Physical Review B,* 1981, **23**, 106-111.

43 R. Bickford, R. L. Greene and W. D. Gill, *Phys. Rev. B,* 1978, **17**, 3525-3533.

44 W. H. Jones and R. D. Bardo, *J. Phys. Chem.*, 1993, **97**, 4974-4983.

45 R. H. Baughman, P. A. Apgar, R. R. Chance, A. G. Macdiarmid and A. F. Garito, *J. Chem. Phys.*, 1977, **66**, 401-409.

46 H. Muller, S. O. Svensson, J. Birch and A. Kvick, *Inorg. Chem.*, 1997, **36**, 1488-1494.

47 M. Boudeulle, *Acta Crys. C,* 1975, **4**, 9-13.

48 A. G. MacDiarmid, C. M. Mikulski, P. J. Russo, M. S. Saran, A. F. Garito and A. J. Heeger, *J. Chem. Soc. Chem. Comm.*, 1975, 476-477.

49 J. Gerratt, S. J. McNicholas, P. B. Karadakov, M. Sironi, M. Raimondi and D. L. Cooper, *J. Am. Chem. Soc.*, 1996, **118**, 6472-6476.

50 P. A. Cox, *The Electronic Structure and Chemistry of solids*, Oxford University Press, Oxford, 1987.

51 R. D. Smith, J. R. Wyatt, D. C. Weber, J. J. Decorpo and F. E. Saalfeld, *Inorg. Chem.*, 1978, **17**, 1639-1642.

52 C. M. Mikulski, A. G. MacDiarmid, A. F. Garito and A. J. Heeger, *Inorg. Chem.*, 1976, **15**, 2943-2945.

53 R. J. Nowak, H. B. Mark, A. G. MacDiarmid and D. Weber, *J. Chem. Soc. Chem. Comm,* 1977, 9-11.

54 A. A. Bright, M. J. Cohen, A. F. Garito, A. J. Heeger, C. M. Mikulski and A. G. Macdiarmid, *Appl. Phys. Lett.*, 1975, **26**, 612-615.

55 Asahi Chemical Industry Company Ltd., US Patent: 55137671, 1980.

56 Nippon Denso Company Ltd, US Patent: 59129261, 1984.

57 Z. Iqbal, H. D. Fair and D. S. Downs, US Patent: 4206705, 1986.

58 M. J. Cohen and J. S. Harris, *Appl. Phys. Lett.*, 1978, **33**, 812-814.

59 A. Clever and W. Muthmann, *Chem. Ber.*, 1896, **29**, 340-343.

60 C. Bernard, A. Herold, M. Lelaurain and G. Robert, *CR. Acad. Sci. C Chim.*, 1976, **283**, 625-627.

61 G. B. Street, W. D. Gill, R. H. Geiss, R. L. Greene and J. J. Mayerle, *J. Chem. Soc. Trans.*, 1977, 407-408.

62 M. Akhtar, J. Kleppinger, A. G. MacDiarmid, J. Milliken, M. J. Moran, C. K. Chiang, M. J. Cohen, A. J. Heeger and D. L. Peebles, *J. Chem. Soc. Chem. Comm.*, 1977, 473-474.

63 U. Demant and K. Dehnicke, *Z. Naturforsch. B*, 1986, **41**, 929-930.

64 Z. Iqbal, R. H. Baughman, J. Kleppinger and A. G. MacDiarmid, *Solid State Commun.*, 1978, **25**, 409-413.

65 W. D. Gill, W. Bludau, R. H. Geiss, P. M. Grant, R. L. Greene, J. J. Mayerle and G. B. Street, *Phys. Rev. Lett.*, 1977, **38**, 1305-1308.

66 J. Rouquerol, D. Avnir, C. W. Fairbridge, D. H. Everett, J. H. Haynes, N. Pernicone, J. D. F. Ramsay, K. S. W. Sing and K. K. Unger, *Pure Appl. Chem.*, 1994, **66**, 1739-1758.

67 Z. Huang, H. M. Guan, W. L. Tan, X. Y. Qiao and S. Kulprathipanja, *J. Membr. Sci.*, 2006, **276**, 260-271.

68 J. J. Jafar and P. M. Budd, *Microporous Mater.*, 1997, **12**, 305-311.

69 R. J. Argauer and G. R. Landolt, US Patent: 3702866, 1972.

70 F. A. Mumpton, *Proc. Natl. Acad. Sci.*, 1999, **96**, 3463-3470.

71 D. Arieli, D. E. W. Vaughan and D. Goldfarb, *J. Am. Chem. Soc.*, 2004, **126**, 5776-5788.

72 N. Gobeltz-Hautecoeur, A. Demortier, B. Lede, J. P. Lelieur and C. Duhayon, *Inorg. Chem.*, 2002, **41**, 2848-2854.

73 T. Guilmin and SOC PLAST ENGINEERS, *Soc. Plast. E*, 1998, **44**, 2594-2595.

74 R. J. H. Clark and D. G. Cobbold, *Inorg. Chem.*, 1978, **17**, 3169-3174.

75 P. J. Langley and J. Hulliger, *Chem. Soc. Rev.*, 1999, **28**, 279-291.

76 W. Depmeier, *Rev. Mineral Geochem.*, 2005, **57**, 203-240.

77 G. T. Kokotailo, S. L. Lawton, D. H. Olson, D. H. Olson and W. M. Meier, *Nature*, 1978, **272**, 437-438.

78 A. M. Tarditi and E. A. Lombardo, *Sep. Purif. Technol.*, 2008, **61**, 136-147.

79 M. F. Fellah and I. Onal, *Catal. Today*, 2008, **137**, 410-417.

80 J. Zalucka, P. Kozyra, M. Mitoraj, E. Broclawik and J. Datka, *Pol. J. Chem.*, 2008, **82**, 1801-1808.

81 R. J. Clark, *Inorg. Chem.*, 1983, **22**, 2766-2772.

82 M. T. Weller, *J. Chem. Soc., Dalton Trans,* 2000, 4227-4240.

83 J. C. Buhl and J. Lons, *J. Alloy. Compd.,* 1996, **235**, 41-47.

84 V. I. Srdanov, W. T. A. Harrison, T. E. Gier, G. D. Stucky, A. Popitsch, K. Gatterer, D. Markgraber and H. P. Fritzer, *J. Phys. Chem.,* 1994, **98,** 4673-4676.

85 A. Stein, G. A. Ozin, P. M. Macdonald, G. D. Stucky and R. Jelinek, *J. Am. Chem. Soc.,* 1992, **114**, 5171-5186.

86 J. C. Buhl, G. Engelhardt and J. Felsche, *Zeolites,* 1989, **9**, 40-44.

87 I. F. Chang, *J. Electrochem. Soc.,* 1974, **121**, 815-820.

88 W. Depmeier, *Acta Crystallogr. C,* 1984, **40**, 226-231.

89 D. M. Bibby and M. P. Dale, *Nature,* 1985, **317**, 157-158.

90 C. M. Braunbarth, P. Behrens, J. Felsche, G. van de Goor, G. Wildermuth and G. Engelhardt, *Zeolites,* 1996, **16**, 207-217.

91 U. Werthmann, B. Marler and H. Gies, *Micropor. Mesopor. Mat.,* 2000, **39**, 549-562.

92 C. L. Shao, X. T. Li, S. L. Qiu, F. S. Xiao, Z. T. Zhang, B. Wei, R. W. Wang and Y. Yue, *Chem. J. Chinese U.,* 1999, **20**, 1667-1670.

93 T. C. Tsai, I. Wang, C. K. Huang and S. D. Liu, *Appl. Catal A-Gen.,* 2007, **321**, 125-134.

94 J. W. Richardson, J. J. Pluth, J. V. Smith, W. J. Dytrych and D. M. Bibby, *J. Phys. Chem.,* 1988, **92**, 243-247.

95 S. B. Hong, M. A. Camblor and M. E. Davis, *J. Am. Chem. Soc.,* 1997, **119**, 761-770.

96 M. J. Murphy, G. A. Voth and A. L. R. Bug, *J. Phys. Chem. B,* 1997, **101**, 491-503.

97 S. D. Loades, S. W. Carr, D. H. Gay and A. L. Rohl, *J. Chem. Soc. Chem. Comm.,* 1994, 1369-1370.

98 J. B. Nicholas, A. J. Hopfinger, F. R. Trouw and L. E. Iton, *J. Am. Chem. Soc.,* 1991, **113**, 4792-4800.

99 K. Knorr, C. M. Braunbarth, G. van de Goor, P. Behrens, C. Griewatsch and W. Depmeier, *Solid State Commun.,* 2000, **113**, 503-507.

100 C. M. Braunbarth, P. Behrens and J. Felsche, *Solid State Ionics,* 1997, **101**, 1273-1277.

101 H. Weyl, *Symmetry*, Princeton University Press, Princeton, NJ, 1952.

102 J. C. Buhl, *React. Kinet. Catal. L.,* 1991, **43**, 577-582.

103 E. Kendrick and S. E. Dann, *J. Solid State Chem.,* 2004, **177**, 1513-1519.

104 J. Homeyer, O. Bode, C. H. Ruscher and J. Buhl, *Z. Krist. Suppl.,* 2001, **18:110**.

105 M. E. Brenchley and M. T. Weller, *Zeolites,* 1994, **14**, 682-686.

106 F. Liebau, *Micropor. Mesopor. Mat.,* 2003, **58**, 15-72.

107 M. J. Frampton and H. L. Anderson, *Angew. Chem. Int. Edit.,* 2007, **46**, 1028-1064.

108 H. W. Langmi, D. Book, A. Walton, S. R. Johnson, M. M. Al-Mamouri, J. D. Speight, P. P. Edwards, I. R. Harris and P. A. Anderson, *J. Alloy. Compd.,* 2005, **404**, 637-642.

109 J. Weitkamp, M. Fritz and S. Ernst, *Int. J. Hydrogen Energ.,* 1995, **20**, 967-970.

110 D. Fraenkel and J. Shabtai, *J. Am. Chem. Soc.,* 1977, **99**, 7074-7076.

111 A. W. C. van den Berg and C. O. Arean, *Chem. Commun.,* 2008, 668-681.

112 S. S. Han, H. Furukawa, O. M. Yaghi and W. A. Goddard, *J. Am. Chem. Soc.,* 2008. **130**, 11580-11581.

113 P. Love, G. Myer, H. I. Kao and M. M. Labes, *Ann. N. Y. Acad. Sci.*, 1977, **313**, 745-758.

114 D. J. Cardin, *Adv. Mater.,* 2002, **14**, 553-563.

115 S. M. Bleay, *Latent fingerprint detetction versus DNA analysis*, HOSDB, Sandridge, 2008.

116 C. Champod, C. Lennard, P. Margot and M. Stoilovic, *Fingerprints and Other Ridge Skin Impressions*, CRC Press, USA, 2004.

117 H. C. Lee and R. E. Gaensslen, *Advances in Fingerprint Technology*, CRC Press, Boca Raton, FL, 2001.

118 K. Bobev, *J. Forensic Ident.,* 1995, **45**, 176-183.

119 J. Deans, *Sci. Justice,* 2006, **46**, 153-168.

120 T. Kent, V. Sears, S. Hardwick, D. Hewlett and S. Walker, *Fingerprint Development Handbook*, PSDB, Heanor, Derbyshire, 2000.

121 B. E. Dalrymple, J. M. Duff and E. R. Menzel, *J. Forensic Sci.,* 1977, **22**, 106-115.

122 R. Pfister, *Fingerprint Whorld,* 1985, **10**, 64-70.

123 G. A. Johnson, C. S. Creaser and J. R. Sodeau, in *Analytical Applications of Spectroscopy 2*, ed. A. M. C. Davies and C. S. Creaser, The Royal Society of Chemistry, Cambridge, 1991, 207-212.

124 H. Fraval, A. Bennett and E. Springer, *UV detection of untreated latent fingerprints*, Israel National Police, Israel, 1996.

125 S. A. Hardwick, *User Guide to Physical Developer - a Reagent for Detecting Latent Fingerprints*, Home Office Police Scientific Development Branch, Sandridge, 1981.

126 S. Oden and B. von Hofsten, *Nature,* 1954, **173**, 449-450.

127 J. R. Morris and G. C. Goode, *Police Res. Bull.,* 1975, 45-53.

128 W. O. Jungbluth, *Fingerprint Whorld,* 1992, **18**, 26-29.

129 W. O. Jungbluth, *J. Forensic Ident.*, 1993, **43**, 226-233.

130 D. F. Hewlett and V. G. Sears, *J. Forensic Ident.,* 1997, **47**, 287-389.

131 D. F. Hewlett and V. G. Sears, *J. Forensic Ident.,* 1999, **49**, 388-396.

132 R. S. Ramotowski, A. A. Cantu, M. M. Joullie and O. Petrovskaia, *Fingerprint Whorld,* 1997, **23**, 131-140.

133 D. B. Hansen and M. M. Joullie, *Chem. Soc. Rev.,* 2005, **34**, 408-417.

134 C. A. Pounds, R. Griggs and T. Mongkolaussavaratana, *J. Forensic Sci.,* 1990, **35**, 169-175.

135 M. Stoilovic, *Forensic Sci. Int.,* 1993, **60**, 141-153.

136 R. M. Bratton and J. A. Juhala, *J. Forensic Ident.,* 1995, **45**, 169-172.

137 G. C. Saunders, *Multimetal Deposition Technique for Latent Fingerprint Development*, IAI, Pensacola, 1989.

138 G. L. Thomas, *Criminology,* 1973, **8**, 21-38.

139 G. L. Thomas, *J. Forensic Sci. Soc.,* 1975, **15**, 133-135.

140 J. D. James, C. A. Pounds and B. Wilshire, *J. Forensic Sci.,* 1991, **36**, 1368-1375.

141 J. D. James, C. A. Pounds and B. Wilshire, *J. Forensic Sci.,* 1991, **36**, 1376-1386.

142 G. S. Sodhi and J. Kaur, *Forensic Sci. Int.,* 2001, **120**, 172-176.

143 E. R. Menzel, *Proc. SPIE-Int. Soc. Opt. Eng.,* 1988, **910**, 45-51.

144 E. R. Menzel and C. E. Allred, *Proc. SPIE-Int. Soc. Opt. Eng.,* 1997, **2941**, 96-101.

145 G. C. Goode and J. R. Morris, *Latent Fingerprints: A Review of Their Origin, Composition and Methods for Detection*, 022/83, AWRE, Aldermaston, 1983.

146 E. Springer and P. Bergman, *J. Forensic Ident.,* 1995, **45**, 164-168.

147 D. E. Weaver and E. J. Clary, *J. Forensic Ident.,* 1993, **43**, 481-492.

148 J. H. Froude, *J. Forensic Ident.,* 1996, **46**, 19-31.

149 J. E. Watkin and A. H. Misner, *RCMP Gaz.,* 1990, **52**, 1-5.

150 P. Theys, Y. Turgis, A. Lepareux, G. Chevet and P. F. Ceccaldi, *Rev. Int. Pol. Crim.,* 1968, **23**, 106-108.

151 G. L. Thomas, *J. Phys. E Sci. Instrum.,* 1978, **11**, 722-731.

152 T. Kent, G. L. Thomas, T. E. Reynoldson and H. W. East, *J. Forensic Sci. Soc.,* 1976, **16**, 93-101.

153 H. Grant, E. Springer and Z. Ziv, *VMD Inhibition on Polythene Bags*, Israel National Police, Israel, 1996.

154 N. Jones, M. Stoilovic, C. J. Lennard and C. Roux, *Forensic Sci. Int.,* 2001, **115**, 73-88.

155 M. Murphy, *J. Forensic Ident.,* 1991, **41**, 318-320.

156 B. L. Wilson and V. D. McCloud, *Identification News,* 1982, **32**, 3-4.

157 R. Jelly, S. W. Lewis, C. Lennard, K. F. Lim and J. Almog, *Chem. Commun.,* 2008, 3513-3515.

158 G. S. Sodhi and J. Kaur, *Forensic Sci. Int.,* 2001, **115**, 69-71.

159 S. Morimoto, A. Kaminogo and T. Hirano, *Forensic Sci. Int.,* 1998, **97**, 101-108.

160 S. K. Bramble, *J. Forensic Sci.,* 1995, **40**, 969-975.

161 C. E. Allred, T. Lin and E. R. Menzel, *J. Forensic Sci.,* 1997, **42**, 997-1003.

162 M. Zhang, A. Becue, M. Prudent, C. Champod and H. H. Girault, *Chem. Commun.,* 2007, 3948-3950.

163 S. B. Karch and M. Peat, *Drug Abuse Handbook, 2nd Edition*, CRC Press, Boca Raton, Florida, 2007.

164 S. M. Bleay, G. Bradshaw and J. E. Moore, *Fingerprint Development and Imaging Newsletter*, 26/06, HOSDB, Sandridge, 2006.

165 H. M. Rietveld, *Acta Crystallogr.,* 1967, **22**, 151-152.

166 H. M. Rietveld, *J. Appl. Crystallogr,* 1969, **2**, 65-71.

167 J. C. Taylor, *Rietveld made easy: a practical guide to the understanding of the method and succesful phase quantifications*, Sietronics Pty Ltd, Canberra, 2001.

168 W. Depmeier, *Acta Crystallogr. B,* 1988, **44**, 201-207.

169 T. Chivers, R. T. Oakley, O. J. Scherer and G. Wolmershauser, *Inorg. Chem.,* 1981, **20**, 914-917.

170 A. W. Herlinge and T. V. Long, *Inorg. Chem.,* 1969, **8**, 2661.

171 K. L. Carter, T. A. Siddiquee, K. L. Murphy and D. W. Bennett, *Acta Crystallogr. B,* 2004, **60**, 155-162.

172 A. W. Cordes, C. G. Marcellus, M. C. Noble, R. T. Oakley and W. T. Pennington, *J. Am. Chem. Soc.,* 1983, **105**, 6008-6012.

173 O. V. Sidorenko, B. B. Zvyagin and S. V. Soboleva, *Kristallografiya,* 1975, **20**, 543-544.

174 K. Kaneto, K. Tanimura, K. Yoshino and Y. Inuishi, *Solid State Commun.,* 1977, **22**, 383-385.

175 A. J. Banister, Z. V. Hauptman, J. Passmore, C. M. Wong and P. S. White, *J. Chem. Soc., Dalton Trans,* 1986, 2371-2379.

176 D. H. Olson, G. T. Kokotailo, S. L. Lawton and W. M. Meier, *J. Phys. Chem.,* 1981, **85**, 2238-2243.

177 N. Kamiya, Y. Torii, M. Sasaki, K. Nishi and Y. Yokomori, *Z. Kristallogr.,* 2007, **222**, 551-554.

178 M. M. Labes, *Mol. Cryst. Liq. Cryst.,* 1976, **32**, 161-163.

179 M. Bellotto, A. Gualtieri, G. Artioli and S. M. Clark, *Phys. Chem. Miner.,* 1995, **22**, 207-214.

180 A. Gualtieri, M. Bellotto, G. Artioli and S. M. Clark, *Phys. Chem. Miner.,* 1995, **22**, 215-222.

181 H. Kahlert and B. Kundu, *Mater. Res. Bull.,* 1976, **11**, 967-972.

182 J. W. Bond, *J. Forensic Sci.,* 2008, **53**, 1344-1352.

183 J. W. Bond, *J. Forensic Sci.,* 2008, **53**, 812-822.

184 V. Bowman, V. Sears, H. Bandey, S. Bleay, L. Fitzgerald, A. Gibson, S. Hardwick, A. Hart, D. Hewlett, T. Kent and S. Walker, *HOSDB Fingerprint Development Handbook*, Heanor Gate Printing, Heanor, 2005.

185 D. Robertson and G. M. Pound, *Crit. Rev. Solid State,* 1973, **4**, 163-204.

186 N. J. Smith, A. Domin and L. T. Scott, *Org. Lett.,* 2008, **10**, 3493-3496.

187 N. Jones, D. Mansour, M. Stoilovic, C. Lennard and C. Roux, *Forensic Sci. Int.,* 2001, **124**, 167-177.

188 H. Qisheng, F. Shouhua and X. Ruren, *J. Chem. Soc. Chem. Comm.,* 1988, 1486-1487.

189 A. L. Spek, *Acta Crystallogr.,* 1990, **A46**, C34.

190 G. van de Goor, P. Behrens and J. Felsche, *Microporous Mater.,* 1994, **2**, 493-500.

191 C. M. B. Henderson and D. Taylor, *Spectrochim. Acta A,* 1977, **33**, 283-290.

192 D. F. Shriver and P. W. Atkins, in *Inorganic Chemistry*, ed. D. F. Shriver and P. W. Atkins, Oxford University Press, Oxford, UK, 1999, 331-372.

193 V. A. Maroni and S. J. Epperson, *Vib. Spectrosc.,* 2001, **27**, 43-51.

194 I. A. Kalinnikova, N. N. Muchaidze, A. A. Pribylov, V. V. Serpinskii and G. V. Tsitsishvili, *Encapsulation of Gases by Zeolites*, 1987.

195 D. W. Breck, *J. Chem. Educ.,* 1964, **41**, 678-689.

196 R. M. Barrer and D. E. W. Vaughan, *Trans. Faraday Soc.,* 1971, **67**, 2129-2136.

197 A. G. Wong-Foy, A. J. Matzger and O. M. Yaghi, *J. Am. Chem. Soc.,* 2006, **128**, 3494-3495.

198 V. B. Kazansky, V. Y. Borovkov, A. Serich and H. G. Karge, *Micropor. Mesopor. Mat.,* 1998, **22**, 251-259.

199 N. Baumann, B. Heibel, J. Jouanne, H. Keller-Rudek and A. Kubny, in *Gmelin Handbook of Inorganic Chemistry - Sulfur-Nitrogen Compounds - Part 2*, ed. K. C. Buschbeck, H. Bergmann, B. Heibel, H. Katscher, R. Keim, G. Kirschstein, D. Koschel, U. Kruerke, H. K. Kugler, E. Schleitzer-Rust, A. Slawisch, B. V. Tschirschnitz-Geibler and R. Warncke, Springer-Verlag, Berlin, 1985, 1-24.

200 G. Heger, S. Klein, L. Pintschovius and H. Kahlert, *J. Solid State Chem.,* 1978, **23**, 341-347.

201 J. Bojes, T. Chivers, A. W. Cordes, G. Maclean and R. T. Oakley, *Inorg. Chem.,* 1981, **20**, 16-21.

202 P. F. Kelly and J. D. Woollins, *Polyhedron,* 1989, **8**, 2907-2910.

203 V. C. Ginn, P. F. Kelly, A. M. Z. Slawin, D. J. Williams and J. D. Woollins, *J. Chem. Soc. Dalton,* 1992, **6**, 963-968.

204 M. M. Olmstead, A. S. Ginwalla, B. C. Noll, D. S. Tinti and A. L. Balch, *J. Am. Chem. Soc.,* 1996, **118**, 7737-7745.

205 U. Thewalt, *Angew. Chem. Int. Edit.,* 1976, **15**, 765-766.

206 U. Thewalt, *Z. Anorg. Allg. Chem.,* 1981, **476**, 105-108.

207 U. Thewalt, *Z. Naturforsch. B,* 1980, **35**, 855-859.

208 I. P. Parkin, J. D. Woollins and P. S. Belton, *J. Chem. Soc., Dalton Trans,* 1990, 511-517.

209 P. S. Belton, I. P. Parkin, D. J. Williams and J. D. Woollins, *J. Chem Soc. Chem. Comm.,* 1988, 1479-1480.

210 J. D. Woollins, *Inorganic Experiments,* Wiley-VCH Verlag, Weinheim, 1995.

211 W. L. Jolly, K. D. Maguire and D. Rabinovich, *Sov. Phys. Tech. Phys-U.,* 1963, **8**, 1304.

212 R. D. Smith, J. R. Wyatt, J. J. Decorpo, F. E. Saalfeld, M. J. Moran and A. G. Macdiarmid, *J. Am. Chem. Soc.,* 1977, **99**, 1726-1730.

213 R. R. Cavanagh, R. S. Altman, D. R. Herschbach and W. Klemperer, *J. Am. Chem. Soc.,* 1979, **101**, 4734-4735.

214 H. Schroder and O. Glemser, *Z. Anorg. Allg. Chem.,* 1959, **298**, 78-83.

215 E. G. Robertson and D. McNaughton, *J. Mol. Spectrosc.,* 2006, **238**, 56-63.

216 A. Muller, N. Mohan, S. J. Cyvin, N. Weinstock and O. Glemser, *J. Mol. Spectrosc.,* 1976, **59**, 161-170.

217 S. C. Peake and A. J. Downs, *J. Chem. Soc., Dalton Trans,* 1974, 859-864.

218 A. Muller, G. Nagaraja, O. Glemser, S. F. Cyvin and J. Wegener, *Spectrochim. Acta A-M,* 1967, **A23**, 2683.

219 T. Beppu, E. Hirota and Y. Morino, *J. Mol. Spectrosc.,* 1970, **36**, 386.

220 M. G. Reed and D. Y. Zhang, *J. Mol. Struct-Theochem,* 2001, **548**, 107-112.

221 M. T. Nguyen and R. Flammang, *Chem. Ber.,* 1996, **129**, 1379-1381.

222 G. Beber, J. Hanich and K. Dehnicke, *Z. Naturforsch. B,* 1985, **40**, 9-12.

223 J. Hanich and K. Dehnicke, *Z. Naturforsch. B,* 1984, **39**, 1467-1471.

224 U. Kynast and K. Dehnicke, *Z. Anorg. Allg. Chem.,* 1983, **502**, 29-34.

225 W. C. Emken and K. Hedberg, *J. Chem. Phys.,* 1973, **58**, 2195-2196.

226 L. S. Kumari, P. P. Rao and M. L. Reddy, *J. Alloy. Compd.,* 2008, **461**, 509-515.

227 M. Jansen and H. P. Letschert, *Nature,* 2000, **404**, 980-982.

228 A. Kumar and P. Pastore, *Curr. Sci.,* 2007, **93**, 818-822.

229 G. Bertin and D. Averbeck, *Biochimie,* 2006, **88**, 1549-1559.

230 A. Jensen and F. Brorasmussen, *Rev. Environ. Contam. Toxicol.,* 1992, **125**, 101-181.

231 J. L. Gabby, *Arch. Indhyg. Occ. Med.,* 1950, **1**, 677-684.

232 N. Baumann, B. Heibel, J. Jouanne, H. Keller-Rudek and A. Kubny, in *Gmelin Handbook of Inorganic Chemistry - Sulfur-Nitrogen Compounds - Part 2*, ed. K. C. Buschbeck, H. Bergmann, B. Heibel, H. Katscher, R. Keim, G. Kirschstein, D. Koschel, U. Kruerke, H. K. Kugler, E. Schleitzer-Rust, A. Slawisch, B. V. Tschirschnitz-Geibler and R. Warncke, Springer-Verlag, Berlin, 1985, 63-107.

233 C. M. Davis and K. A. Curran, *J. Chem. Educ.,* 2007, **84**, 1822-1823.

234 R. Wollert, B. Neumuller and K. Dehnicke, *Z. Anorg. Allg. Chem.,* 1992, **616**, 191.

235 R. Ugo, F. Cariati and G. Lamonica, *Inorg. Syn.,* 1990, **28**, 123-126.

236 D. Drew and J. R. Doyle, *Inorg. Syn.,* 1972, **13**, 47.

237 W. Baratta and P. S. Pregosin, *Inorg. Chim. Acta,* 1993, **209**, 85-87.

238 S. M. Aucott, M. R. Bailey, M. R. J. Elsegood, L. M. Gilby, K. E. Holmes, P. F. Kelly, M. J. Papageorgiou and S. Pedron-Haba, *New J. Chem.,* 2004, **28**, 959-966.

239 G. K. Anderson and M. Lin, *Inorg. Syn.,* 1990, **28**, 60-63.

240 C. Baerlocher, W. M. Meier and D. H. Olson, *Atlas of Zeolite Framework Types*, Elsevier, Amsterdam, 2001.

241 X. Y. Chen, H. S. Huh and S. W. Lee, *Nanotechnology,* 2007, **18**, 285608.

242 M. R. J. Elsegood, P. F. Kelly, G. Reid, A. M. Z. Slawin and P. M. Staniland, *Dalton T.,* 2008, 5076-5082.

243 L. R. Melby, R. I. Harfer, W. R. Hertler, W. Manler, R. E. Benson and W. E. Mochel, *J. Am. Chem. Soc.,* 1962, **84**, 3374.

244 M. Goehring and D. Voigt, *Naturwissenscaften,* 1953, **40**, 482.

245 M. Becke-Goehring, *Progr. Inorg. Chem.,* 1959, **1**, 207/34-217/8.

9. Appendices

9.1. *Data Tables for Crystal Structures*

Table 1. Crystal data and structure refinement for low temperature EGS-SOD.

Chemical formula	$C_2H_6O_{14}Si_6$	
Formula weight	422.61	
Temperature	150(2) K	
Radiation, wavelength	synchrotron, 0.6710 Å	
Crystal system, space group	monoclinic, $P2_1/m$	
Unit cell parameters	a = 7.387(3) Å	$\alpha = 90°$
	b = 12.492(5) Å	$\beta = 110.174(6)°$
	c = 7.546(3) Å	$\gamma = 90°$
Cell volume	653.6(5) $Å^3$	
Z	2	
Calculated density	2.147 g/cm^3	
Absorption coefficient μ	0.717 mm^{-1}	
F(000)	428	
Crystal colour and size	colourless, 0.03 × 0.03 × 0.03 mm^3	
Reflections for cell refinement	1237 (θ range 3.08 to 28.52°)	
Data collection method	Bruker APEX 2 CCD diffractometer ω rotation with narrow frames	
θ range for data collection	1.54 to 28.65°	
Index ranges	h −10 to 10, k −17 to 17, l −10 to 9	
Completeness to $\theta = 28.65°$	98.8 %	
Intensity decay	0%	
Reflections collected	5263	
Independent reflections	2057 ($R_{int} = 0.0661$)	
Reflections with $F^2>2\sigma$	1544	
Absorption correction	semi-empirical from equivalents	
Min. and max. transmission	0.979 and 0.979	
Structure solution	direct methods	
Refinement method	Full-matrix least-squares on F^2	
Weighting parameters a, b	0.0965, 0.5192	
Data / restraints / parameters	2057 / 24 / 116	
Final R indices [$F^2>2\sigma$]	R1 = 0.0615, wR2 = 0.1612	
R indices (all data)	R1 = 0.0836, wR2 = 0.1760	
Goodness-of-fit on F^2	1.062	
Largest and mean shift/su	0.000 and 0.000	
Largest diff. peak and hole	1.352 and −0.778 e $Å^{-3}$	

Table 2. Crystal data and structure refinement for room temperature EGS-SOD.

Chemical formula	$C_2H_6O_{14}Si_6$	
Formula weight	422.61	
Temperature	298(2) K	
Radiation, wavelength	synchrotron, 0.6941 Å	
Crystal system, space group	cubic, Im $\bar{3}$m	
Unit cell parameters	a = 8.903(12) Å	$\alpha = 90°$
	b = 8.903(12) Å	$\beta = 90°$
	c = 8.903(12) Å	$\gamma = 90°$
Cell volume	705.7(16) $Å^3$	
Z	2	
Calculated density	1.989 g/cm^3	
Absorption coefficient μ	0.664 mm^{-1}	
F(000)	428	
Crystal colour and size	colourless, 0.015 × 0.015 × 0.015 mm^3	
Reflections for cell refinement	711 (θ range 3.16 to 22.45°)	
Data collection method	Bruker APEX 2 CCD diffractometer ω rotation with narrow frames	
θ range for data collection	3.16 to 30.75°	
Index ranges	h −12 to 13, k −12 to 13, l −13 to 13	
Completeness to $\theta = 30.75°$	97.9 %	
Intensity decay	17%	
Reflections collected	7907	
Independent reflections	143 ($R_{int} = 0.0994$)	
Reflections with $F^2 > 2\sigma$	139	
Absorption correction	semi-empirical from equivalents	
Min. and max. transmission	0.990 and 0.990	
Structure solution	direct methods	
Refinement method	Full-matrix least-squares on F^2	
Weighting parameters a, b	0.0421, 0.0000	
Data / restraints / parameters	143 / 0 / 7	
Final R indices [$F^2 > 2\sigma$]	R1 = 0.0354, wR2 = 0.0702	
R indices (all data)	R1 = 0.0385, wR2 = 0.0713	
Goodness-of-fit on F^2	1.158	
Largest and mean shift/su	0.000 and 0.000	
Largest diff. peak and hole	0.353 and −0.569 e $Å^{-3}$	

Table 3. Crystal data and structure refinement for rhombohedral silica sodalite.

Chemical formula	O_2Si	
Formula weight	60.09	
Temperature	150(2) K	
Radiation, wavelength	Synchrotron, 0.6942 Å	
Crystal system, space group	rhombohedral, $R\bar{3}$	
Unit cell parameters	a = 12.441(2) Å	$\alpha = 90°$
	b = 12.441(2) Å	$\beta = 90°$
	c = 7.0911(12) Å	$\gamma = 120°$
Cell volume	950.5(3) Å^3	
Z	18	
Calculated density	1.890 g/cm^3	
Absorption coefficient μ	0.710 mm^{-1}	
F(000)	540	
Crystal colour and size	colourless, 0.02 × 0.02 × 0.02 mm^3	
Reflections for cell refinement	932 (θ range 3.20 to 28.50°)	
Data collection method	Bruker APEX 2 CCD diffractometer ω rotation with narrow frames	
θ range for data collection	3.20 to 29.73°	
Index ranges	h −17 to 17, k −17 to 17, l −10 to 10	
Completeness to $\theta = 29.73°$	99.7 %	
Intensity decay	4%	
Reflections collected	3601	
Independent reflections	641 ($R_{int} = 0.0423$)	
Reflections with $F^2 > 2\sigma$	579	
Absorption correction	semi-empirical from equivalents	
Min. and max. transmission	0.989 and 0.989	
Structure solution	direct methods	
Refinement method	Full-matrix least-squares on F^2	
Weighting parameters a, b	0.0789, 1.4969	
Data / restraints / parameters	641 / 0 / 29	
Final R indices [$F^2 > 2\sigma$]	R1 = 0.0456, wR2 = 0.1140	
R indices (all data)	R1 = 0.0528, wR2 = 0.1181	
Goodness-of-fit on F^2	1.063	
Largest and mean shift/su	0.000 and 0.000	
Largest diff. peak and hole	0.485 and −0.485 e Å^{-3}	

Table 4. Crystal data and structure refinement for S_4N_4.

Chemical formula	N_8S_8	
Formula weight	368.56	
Temperature	149(2) K	
Radiation, wavelength	MoKα, 0.71073 Å	
Crystal system, space group	monoclinic, P21/n	
Unit cell parameters	a = 8.6421(8) Å	α = 90°
	b = 7.0895(7) Å	β = 93.5330(10)°
	c = 8.7321(9) Å	γ = 90°
Cell volume	533.98(9) Å3	
Z	2	
Calculated density	2.292 g/cm^3	
Absorption coefficient μ	1.653 mm^{-1}	
F(000)	368	
Crystal colour and size	orange, 0.40 × 0.07 × 0.04 mm^3	
Reflections for cell refinement	3468 (θ range 3.22 to 30.04°)	
Data collection method	Bruker APEX 2 CCD diffractometer ω rotation with narrow frames	
θ range for data collection	3.22 to 30.07°	
Index ranges	h –12 to 12, k –9 to 9, l –12 to 12	
Completeness to θ = 26.00°	99.9%	
Intensity decay	0%	
Reflections collected	5940	
Independent reflections	1562 (R_{int} = 0.0180)	
Reflections with F^2>2σ	1442	
Absorption correction	semi-empirical from equivalents	
Min. and max. transmission	0.5577 and 0.9368	
Structure solution	direct methods	
Refinement method	Full-matrix least-squares on F^2	
Weighting parameters a, b	0.0216, 1.3255	
Data / restraints / parameters	1562 / 0 / 73	
Final R indices [F^2>2σ]	R1 = 0.0316, wR2 = 0.0896	
R indices (all data)	R1 = 0.0343, wR2 = 0.0906	
Goodness-of-fit on F^2	1.324	
Largest and mean shift/su	0.000 and 0.000	
Largest diff. peak and hole	0.478 and –0.358 e Å^{-3}	

Table 5. Crystal data and structure refinement for freshly prepared S_2N_2.

Chemical formula	N_2S_2	
Formula weight	92.14	
Temperature	150(2) K	
Radiation, wavelength	MoKα, 0.71073 Å	
Crystal system, space group	monoclinic, $P2_1/c$	
Unit cell parameters	a = 4.4834(5) Å	$\alpha = 90°$
	b = 3.7748(4) Å	β= 106.4120(10)°
	c = 8.4435(9) Å	$\gamma = 90°$
Cell volume	137.07(3) $Å^3$	
Z	2	
Calculated density	2.232 g/cm^3	
Absorption coefficient μ	1.610 mm^{-1}	
F(000)	92	
Crystal colour and size	gold, 0.43 × 0.25 × 0.10 mm^3	
Reflections for cell refinement	1519 (θ range 2.515 to 31.203°)	
Data collection method	Bruker APEX 2 CCD diffractometer ω rotation with narrow frames	
θ range for data collection	7.84 to 31.81°	
Index ranges	h –6 to 6, k –5 to 5, l –11 to 12	
Completeness to $\theta = 26.00°$	95.6%	
Intensity decay	0%	
Reflections collected	1415	
Independent reflections	424 ($R_{int} = 0.0148$)	
Reflections with $F^2 > 2\sigma$	423	
Absorption correction	semi-empirical from equivalents	
Min. and max. transmission	0.544 and 0.856	
Structure solution	direct methods	
Refinement method	Full-matrix least-squares on F^2	
Weighting parameters a, b	0.0256, 0.0687	
Data / restraints / parameters	424 / 0 / 19	
Final R indices [$F^2 > 2\sigma$]	R1 = 0.0183, wR2 = 0.0477	
R indices (all data)	R1 = 0.0184, wR2 = 0.0477	
Goodness-of-fit on F^2	1.079	
Largest and mean shift/su	0.000 and 0.000	
Largest diff. peak and hole	0.621 and –0.280 e $Å^{-3}$	

9.2. *Publications, Conferences and Courses*

PUBLICATIONS

- R. S. P. King, P. F. Kelly, S. E. Dann, M. R. J. Elsegood, R. J. Mortimer, *Chem. Eur. J.*, 2009, **15**, 5441-5443.

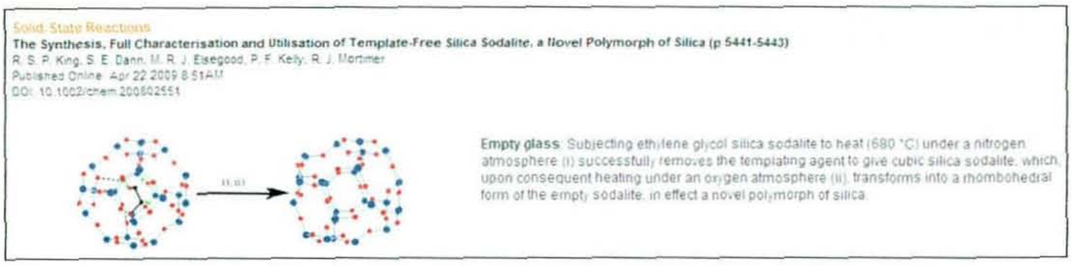
Solid State Reactions

The Synthesis, Full Characterisation and Utilisation of Template-Free Silica Sodalite, a Novel Polymorph of Silica (p 5441-5443)

R. S. P. King, S. E. Dann, M. R. J. Elsegood, P. F. Kelly, R. J. Mortimer

Published Online: Apr 22 2009 8:51AM

DOI: 10.1002/chem.200802551

Empty glass: Subjecting ethylene glycol silica sodalite to heat (680 °C) under a nitrogen atmosphere (i) successfully removes the templating agent to give cubic silica sodalite, which, upon consequent heating under an oxygen atmosphere (ii), transforms into a rhombohedral form of the empty sodalite, in effect a novel polymorph of silica.

- R. S. P. King, P. F. Kelly, R. J. Mortimer, *Chem. Commun.*, 2008, 6111-6113.


Communication

Chem. Commun., 2008, 6111 - 6113, DOI: 10.1039/b815742a

Fingerprint and inkjet-trace imaging using disulfur dinitride

Paul F. Kelly, Roberto S. P. King and Roger J. Mortimer

Exposure of fingerprints to S_2N_2 vapour results in the prints being visually imaged by polymeric $(SN)_x$ on an unprecedented range of media; in addition, the polymer forms in response to the interaction of S_2N_2 with traces of inkjet inks, for example the minute amounts left by the contact between printed paper and an envelope.

- R. S. P. King, P. F. Kelly, R. J. Mortimer, *Chemistry World*, July 2007.


Superconductivity: explosive new images

13 July 2007

UK chemists have created superconducting images, including the Chemistry World logo, on paper

- R. S. P. King, P. F. Kelly, S. E. Dann, R. J. Mortimer, *Chem. Commun.*, 2007, 4812-4814.

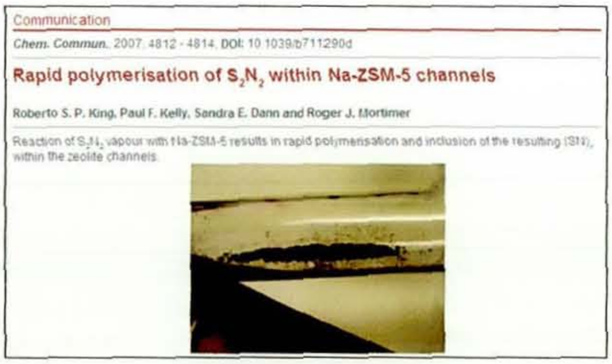
Communication

Chem. Commun., 2007, 4812 - 4814, DOI: 10.1039/b711290d

Rapid polymerisation of S_2N_2 within Na-ZSM-5 channels

Roberto S. P. King, Paul F. Kelly, Sandra E. Dann and Roger J. Mortimer

Reaction of S_2N_2 vapour with Na-ZSM-5 results in rapid polymerisation and inclusion of the resulting $(SN)_x$ within the zeolite channels.

ASSOCIATED PUBLICATIONS

S. Davey, *Nature Chemistry*, Research Highlights, October 2008. "Forensic detection: Fingerprints fixed"

A-M. Corley, *MIT in-house SCOPE magazine*, December 2008. "Making visible what is invisible"

COURSES AND CONFERENCES

Presented talk at triennial EAFS conference, Strathclyde University, September 2009.

Presented poster at 42nd IUPAC Conference, SECC, Glasgow, August 2009.

Presented talk at 42nd IUPAC Conference, SECC, Glasgow, August 2009.

Presented poster at SET for Britain 2009, House of Commons, London, March 2009.

Presented poster at RSC IRMDG/CCDG, Edinburgh University, June 2008.

Presented talk at RSC IRMDG/CCDG, Edinburgh University, June 2008.

Presented talk at RSC Dalton Division Midlands Postgraduate Symposium, Warwick University, March 2008.

Presented poster at RSC Dalton Midlands Division one day meeting, Birmingham University, September 2006.

Presented poster at IRIS Conference, Oulu, Finland, July 2006.

Attended all RSC lectures held within the department.

Teaching Skills for postgraduates and research assistants, January 2006.

Student Mentor, 2006 – 2009.

Laboratory demonstrator and tutor, 2006 – 2009.